SIMULTANEOUS BOILING AND SPREADING OF LIQUEFIED PETROLEUM GAS ON WATER

by

HSUEH-RONG CHANG

B.S., Tunghai University, Taiwan
(1974)

M.S., State University of New York at Buffalo
(1976)

SUBMITTED IN PARTIAL FULFILLMENT
OF THE REQUIREMENTS FOR THE
DEGREE OF

DOCTOR OF SCIENCE

at the

MASSACHUSETTS INSTITUTE OF TECHNOLOGY

January 1981

Signature of Author _____
Department of Chemical Engineering
January 30, 1981

Certified By _____
Professor R.C. Reid
Thesis Supervisor

Accepted by _____
Professor G.C. Williams
Chairman, Departmental Committee on Graduate Thesis

SIMULTANEOUS BOILING AND SPREADING OF LIQUEFIED PETROLEUM GAS ON WATER

by

HSUEH-RONG CHANG

Submitted to the Department of Chemical Engineering in January 1981, in partial fulfillment of the requirements for the Degree of Doctor of Science.

ABSTRACT

An experimental and theoretical investigation was carried out to study the boiling and spreading of liquid nitrogen, liquid methane and liquefied petroleum gas (LPG) on water in a one-dimensional configuration. Primary emphasis was placed on the LPG studies.

Experimental work involved the design and construction of a spill/spread/boil apparatus which permitted the measurement of spreading and local boil-off rates. With the equations of continuity and momentum transfer, a mathematical model was developed to describe the boiling-spreading phenomena of cryogens spilled on water. The model accounted for a decrease in the density of the cryogenic liquid due to bubble formation.

In the case of liquid nitrogen and liquid methane spills on water, the experimental spreading fronts were successfully simulated by assuming constant evaporation rates (40kW/m^2 and 92kW/m^2 for nitrogen and methane respectively) in the theoretical model.

The boiling and spreading rates of LPG were found to be the same as those of pure propane. An LPG spill was characterized by very rapid and violent boiling initially and highly irregular ice formation on the water surface. The measured local boil-off rates of LPG agreed reasonably well with theoretical predictions from a moving boundary heat transfer model. The spreading velocity of an LPG spill was found to be constant and determined by the size of the distributor opening. The maximum spreading distance was found to be unaffected by the spilling rate. These observations can be explained by assuming that the ice formation on the water surface controls the spreading of LPG spills. While the mathematical model did not predict the spreading front adequately, it predicted the maximum spreading distance reasonably well.

The work described in this thesis provides a first step towards estimating the extent of hazardous spills from an LNG or LPG tanker accident.

MASSACHUSETTS
INSTITUTE OF TECHNOLOGY

DEPARTMENT OF
CHEMICAL ENGINEERING

Room number: Cambridge, Massachusetts
02139 Telephone:

January 1981

Professor George C. Newton
Secretary of the Faculty
Massachusetts Institute
of Technology
Cambridge, Massachusetts 02139

Dear Professor Newton:

In accordance with the regulations of the Faculty, I herewith submit a thesis, entitled "Simultaneous Boiling and Spreading of Liquefied Petroleum Gas on Water", in partial fulfillment of the requirements for the degree of Doctor of Science in Chemical Engineering at the Massachusetts Institute of Technology.

Respectfully submitted,

Hsueh-Rong Chang

獻給我敬愛的

父母

ACKNOWLEDGEMENTS

I would like to thank my thesis supervisor, Professor Robert C. Reid, for his excellent advice, encouragement and guidance during the course of this study. I am extremely grateful for his support and understanding during difficult moments.

I would also like to express my gratitude to Professors J.A. Fay and K.A. Smith for their helpful discussion and comments. Appreciation is also extended to the other members of my thesis committee, Professor P.S. Virk and Dr. P. Raj for their suggestions.

I also wish to thank my colleague John Sorensen at M.I.T. for his great assistance in building the experimental apparatus. I wish him good luck in his doctoral work and hope our friendship always remains strong.

I wish to also thank all my friends at M.I.T. for their help in many facets of my work and mostly for their friendship. In particular, I am indebted to Raymond Cwiklinski, who helped me through the very difficult times. His support will always be remembered. I also thank him for editing and proof-reading my thesis. I wish him all the success in life and hope our friendship last forever.

I wish to thank Sally Kreuz for typing the manuscript.

I also wish to express my appreciation to my teachers at Taiwan for their continuous encouragement.

I especially thank my parents, my brothers and sisters, and my entire family for their love, encouragement and understanding through all these years. Their support has helped make this long educational process possible and enjoyable. I would like to dedicate this work to my parents.

TABLE OF CONTENTS

LIST OF FIGURES

LIST OF TABLES

I. SUMMARY

A. THESIS OBJECTIVES

Liquefied petroleum gas (LPG) is often transported in bulk within large insulated tankers. An accidental spill of such a fluid on water could lead to a serious hazard since LPG boils well below ambient water temperature and forms a combustible (and, possibly, an explosive) cloud.

LPG consists primarily of propane with some ethane and butane. When brought in contact with water, LPG vaporizes very rapidly and forms a flammable cloud which is more dense than air and is not readily dispersed. A serious accident is conceivable if the cloud contacts an ignition source. Evaluating the potential hazards from accidents in marine transportation requires reliable data of boil-off rates and spreading rates for LPG spills on water.

Previous experimental work was limited to LPG spills on confined water surfaces. It was not known whether the evaporation rates measured in the confined area experiments were applicable to unconfined spills where boiling and spreading occur simultaneously. No experiments had been reported which determined such rates for LPG spills. It was the objective of the present work to measure experimentally the simultaneous boiling and spreading rates for LPG spilled on a water surface. A model was developed which described the boiling/spreading phenomena of LNG and LPG spills on water. Finally, a better understanding of the fundamentals and mechanism of LPG spills on water was also an important objective of this thesis.

B. RELEVANT PREVIOUS WORK

Reid and Smith (1978) conducted spills of propane and LPG on water in an adiabatic calorimeter, placed on a load cell to record the mass of the sys-

tem continuously. For a rapid spill of propane or LPG, the initial boiling rate was found to be extremely fast and ice formation took place almost instantaneously on the water surface. Within a few seconds, the water surface was covered by a rough ice sheet, the boiling rate dropped to a smaller value, and the vaporization then could be well described by a moving boundary model (Eckert and Drake (1975)). The boiling rates of LPG were found to be the same as those of pure propane.

Very few experiments have been conducted which examine simultaneous boiling and spreading rates for any volatile cryogen. Burgess et al. (1970) used an overhead camera to study LNG spills from a point source onto an open pond. The spreading rate was reported to be constant (0.38 m/s). The boiling rate was assumed to be the same for both confined and unconfined spills and equal to 92 kW/m^2. The time (τ) required to evaporate an initial quantity V_o of LNG and the corresponding pool diameter (d_{max}) were estimated by

$$\tau = 24.9\ V_o^{1/3} \quad (V_o \text{ in } m^3,\ \tau \text{ is s}) \qquad \text{(I-1)}$$

$$d_{max} = 19.0\ V_o^{1/3}\ (m) \qquad \text{(I-2)}$$

By examining Burgess' spreading data, in general, the relationship of constant spreading rate was obeyed in the early part of the tests, but later the spreading rate decreased.

Boyle and Kneebone (1973) made three spills of LNG on a pond and measured the pool diameter when the pool began to break up into discrete patches. The spreading rate was reported to be constant during a test, but, unexpectedly, it decreased as the amount of LPG spilled increased. The thickness of LNG at pool break-up was found to be 1.8 mm. The boiling rate was calculated from the experimentally observed time for pool break-up (corresponding to the thickness of

1.8 mm) and equalled 15 kW/m^2.

Boyle and Kneebone claimed that in a spreading situation, ice did not form and boiling rates should be lower than those for confined spills.

Other studies of boiling and spreading of cryogenic liquids on water have been theoretical and based predominantly upon studies of non-volatile oil spills on water.

Hoult (1972b) coupled the evaporation and spreading rates of LNG to predict the maximum pool radius and the time for complete vaporization for LNG spilled on open water. By assuming that the heat used to evaporate LNG came from freezing of the water and neglecting the volume loss of LNG during spreading Hoult obtained the following expressions for τ (the time for complete vaporization) and r_{max} (maximum pool radius at time τ):

$$\tau = 27.8\ V_o^{1/3} \quad (V_o \text{ in } m^3, \tau \text{ in s}) \qquad \text{(I-3)}$$

$$r_{max} = 8.1\ V_o^{5/12} \text{ (m)} \qquad \text{(I-4)}$$

In Hoult's analysis, the sensible cooling of ice and water were neglected. The only thermal resistance was within the ice layer, no surface resistance from the initial film boiling of LNG was considered.

Fay (1973) improved Hoult's model by accounting for the sensible heat of ice subcooled below the freezing temperature and obtained the following expressions for τ and r_{max} for LNG spills:

$$\tau = 9.8\ V_o^{1/3} \quad (V_o \text{ in } m^3, \tau \text{ in s}) \qquad \text{(I-5)}$$

$$r_{max} = 5.8\ V_o^{5/12} \text{ (m)} \qquad \text{(I-6)}$$

By equating the gravitational spreading force to the inertial resistance

force, using a constant heat flux ($\dot{q}$) and mean thickness approximation, Raj and Kalelkar (1973) developed a model to predict the maximum pool radius and the time required to evaporate an initial spilled volume V_o:

$$\tau = 1.67 \left[\frac{\rho_L^2 \, \Delta H_v^2 \, V_o}{g\Delta \dot{q}^2}\right]^{1/4} \qquad \text{(I-7)}$$

$$r_{max} = \left[\frac{\rho_L^2 \, \Delta H_v^2 \, g\Delta \, V_o^3}{\dot{q}^2}\right]^{1/8} \qquad \text{(I-8)}$$

where ρ_L is the cryogen density, ΔH_v is the heat of vaporization, g is the gravitational acceleration, and Δ is the ratio of the density difference between water and cryogen to the density of water.

With $\dot{q}$ = 92 kW/m^2, for LNG:

$$\tau = 21.0 \, V_o^{1/4} \quad (V_o \text{ in } m^3, \tau \text{ in s}) \qquad \text{(I-9)}$$

$$r_{max} = 8.7 \, V_o^{3/8} \quad (m) \qquad \text{(I-10)}$$

Using the same assumptions as those for radial spreading, Raj (1977) developed a one-dimensional boiling/spreading model in which the spreading distance (x) as a function of time (t) can be expressed as follows:

$$x = 1.39 \left[\frac{g\Delta \, V_o \, t^2}{w}\right]^{1/3} + 0.097 \left[\frac{\dot{q}}{\rho_L \, \Delta H_v}\right] \left[\frac{(g\Delta)^2 \, wt^7}{V_o}\right]^{1/3} \qquad \text{(I-11)}$$

Where w is the width of spreading channel.

The time for complete vaporization (t_e) and the corresponding maximum spreading distance (x_e) are given by

$$t_e = 1.09 \left[\frac{(V_o/w)^2}{g\Delta \, (\dot{q}/\rho_L \, \Delta H_v)^3}\right]^{1/5} \qquad \text{(I-12)}$$

$$x_e = 1.59 \left[\frac{g\Delta\ (V_o/w)^3}{(\dot{q}/\rho\Delta H_v)^2} \right]^{1/5} \qquad \text{(I-13)}$$

Muscari (1974) proposed a numerical model to describe the radial spreading and boiling process for instantaneous spills of cryogens on water. He assumed the gravity force balanced the inertia of spreading fluid and the leading edge was considered as an intrusion. By assuming a constant boil-off rate, Muscari solved the conservation equations of continuity and momentum numerically and was able to predict the thickness profile of the spreading cryogen and the path of the spreading-front as well as the trailing-edge. The maximum pool radius and the time for complete vaporization for a given quantity V_o are expressed as:

$$\tau = 0.80 \left[\frac{\rho_L^{\ 2}\ \Delta H_v^{\ 2}\ V_o}{g\Delta\ \dot{q}^2} \right]^{1/4} \qquad \text{(I-14)}$$

$$r_{max} = 1.23 \left[\frac{\rho_L^{\ 2}\ \Delta H_v^{\ 2}\ g\Delta\ V_o^{\ 3}}{\dot{q}^2} \right]^{1/8} \qquad \text{(I-15)}$$

By accounting for the evaporation of cryogen during spreading, Otterman applied the radial spread law of oil spills, with the initial spilled volume divided by 2 for LNG spills. Assuming a constant heat flux, Otterman obtained the following expressions for τ and r_{max}:

$$\tau = 0.75 \left[\frac{\rho_L^{\ 2}\ \Delta H_v^{\ 2}\ V_o}{g\Delta\ \dot{q}^2} \right]^{1/4} \qquad \text{(I-16)}$$

$$r_{max} = 0.82 \left[\frac{\rho_L^{\ 2}\ \Delta H_v^{\ 2}\ g\Delta\ V_o^{\ 3}}{\dot{q}^2} \right]^{1/8} \qquad \text{(I-17)}$$

In Table I-1, the predicted values of τ and r_{max} from these various models are compared with the experimental data of Boyle and Kneebone. Note the poor

TABLE I-1

Boyle's Data Compared with Predictions from Various Models
For LNG Spills in a Radial Configuration

Spill Size, $2.24 \times 10^{-2} m^3$	Boyle (Experimental)	Burgess	Hoult	Fay	Muscari	Raj	Otterman
Pool Diameter at Break up, m	3.96	5.36	3.33	2.38	5.14	4.18	3.42
Time to Evaporate Completely, s	24.	7.0	7.8	2.5	9.8	8.1	11.6
Spill Size, $4.48 \times 10^{-2} m^3$							
Pool Diameter at Break-up, m	5.64	6.75	4.44	3.18	6.68	5.43	4.43
Time to Evaporate Completely, s	33.	8.8	9.9	3.1	11.6	9.7	13.8
Spill Size, $8.97 \times 10^{-2} m^3$							
Pool Diameter at Break up, m	7.32	8.5	5.93	4.25	8.66	7.04	5.75
Time to Evaporate Completely, s	35.	11.1	12.4	3.9	13.8	11.5	16.4

agreement for different analyses. Fay's model gives much smaller value of τ and r_{max} than those predicted by the others. This is because in his analysis, Fay assumed that the energy to evaporate LNG comes from freezing of the water and the sensible heat released as ice cools below its freezing point. He also neglected the surface resistance to boiling due to the initial vapor film formation at the LNG-water interface and the resulting lower heat transfer rate. The maximum pool diameters predicted on the basis of Raj and Kalelkar's model are in good agreement with Boyle's data. The values of τ predicted from the models mentioned above are much lower than experimental results. This is not unexpected because all the models (except Muscari's) assume that the circular area uniformly covered with LNG continues to increase as long as any liquid cryogen remains. However, Boyle and Kneebone observed that the LNG pools broke up into discontinuous areas before complete vaporization. Using a "continuous pool" assumption for the LNG layer therefore results in underestimating the time for complete vaporization because the cryogen-water contact area is overestimated.

In summary, few experiments have been conducted to examine the simultaneous boiling and spreading of LNG on water. The available data do not agree well with the theories that have been proposed. For LPG, essentially no research had been done to describe the boiling and spreading phenomena following a spill on water.

C. EXPERIMENTAL

The experimental apparatus was designed for the study of the boiling and spreading of cryogenic liquids spilled on water in a one-dimensional configuration. A schematic representation of the apparatus is given in Figure I-1. The equipment consists of six major parts: (1) the liquefaction station, (2) the cryogen distributor, (d) a water trough, (4) the vapor sampling stations, (5)

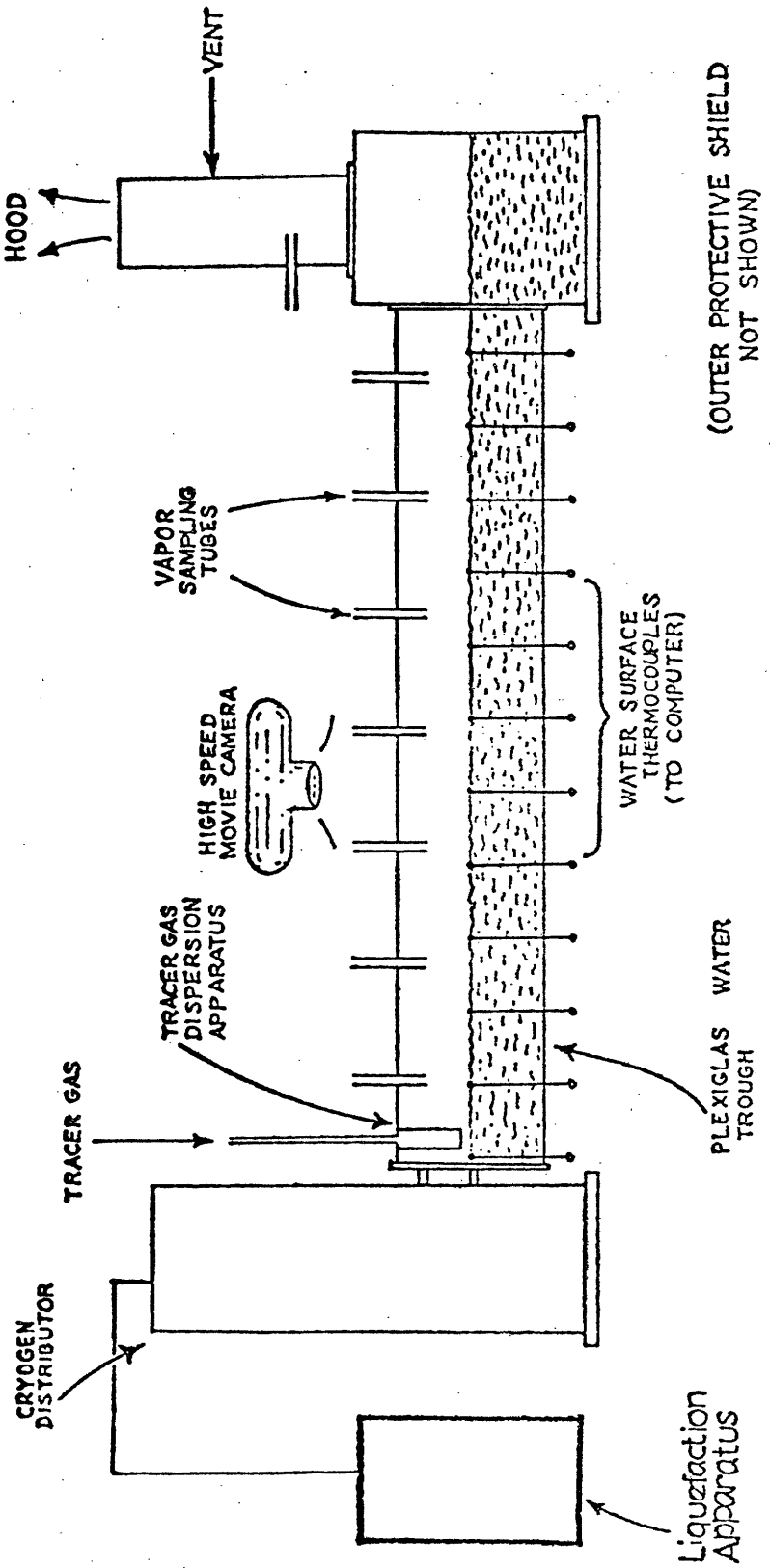

FIGURE I-1: SCHEMATIC OF SPILL/SPREAD/BOIL APPARATUS

the hood connection, and (6) a safety shield.

The cryogenic liquids were prepared in the liquefaction station by cooling the cryogen gases below their boiling points with liquid nitrogen. After a sufficient quantity has been prepared, as indicated by the weight change of the gas cylinder, the cryogen liquid was delivered from the liquefaction station to the cryogen distributor by pressurizing the liquefaction station with helium gas.

The cryogen distributor employs a spring-loaded piston which, upon release, will open a side port through which the cryogen can be delivered rapidly onto the water surface without severe disruption of the water surface. A programmable sequencer was used to release the distributor piston at a pre-selected time. The distributor was fabricated from Lexan polycarbonate resin to permit visual observation of the cryogen level. The dimensions of the distributor are 17.8 cm O.D. x ~ 60 cm in height. The maximum liquid capacity of the distributor is ~ 3 liters. Upon full downward displacement of the piston, the effective cross-sectional flow area through the side port is ~ 48 cm^2.

The simultaneous boiling and spreading experiments were conducted in a long, narrow water trough. The trough consisted of Plexiglas tubing and was half filled with water. A set of liquid-thermocouples placed on the water surface indicated the passage of the cryogen. Vapor temperatures were monitored by a set of vapor-thermocouples introduced through the top of the spill tube. The thermocouple out-puts were fed directly into a NOVA-840 Real Time Computer.

The local boil-off rates of cryogen spreading on water were estimated in an indirect manner. A tracer gas, CO_2, was injected continuously and evenly at steady state into the system through a gas dispersion apparatus. Vapor samples were collected at several locations along the water trough during the experiment. A gas chromatograph was used to analyze the vapor samples. The temperatures and compositions of vapor samples provided the necessary informa-

tion to determine the mass boiled off as a function of time and position.

Eight sampling stations were used to collect vapor samples at specified times during the experiment; each sampling station was able to collect six different samples. Figure I-2, is a transverse view of one sample station. The sampling bulbs were initially purged and pressurized with argon gas. The operation of the sample intake was controlled automatically by the sequencer.

The envolved cryogen vapor and tracer gas were ducted to the hood.

A high speed carmera was used to record the movement of the cryogen over the water surface.

D. DATA ANALYSIS TO DETERMINE LOCAL BOIL-OFF RATES

The differential mass balances for tracer gas and hydrocarbon cryogen vapor can be expressed as follows:

$$\frac{\partial C_T}{\partial t} = - \frac{\partial (UC_T)}{\partial x} \qquad \text{(I-18)}$$

$$\frac{\partial C_{HC}}{\partial t} = - \frac{\partial (UC_{HC})}{\partial x} + \left(\frac{w}{A}\right) \dot{M} \qquad \text{(I-19)}$$

where C_T and C_{HC} are the molar concentrations of tracer gas and cryogen vapor respectively. U is the vapor velocity. $\dot{M}$ is the local mass boil-off rate (moles per unit area). w is the width of the water trough.

Vapor temperature measurements were used to calculate the molar density (C) of the vapor with the equation of state:

$$C = \frac{P}{ZRT} \qquad \text{(I-20)}$$

where P = pressure, 1 bar

Z = compressibility factor

R = universal gas constant, 83.14 bar-cm^3/mol-K

T = vapor temperature, K

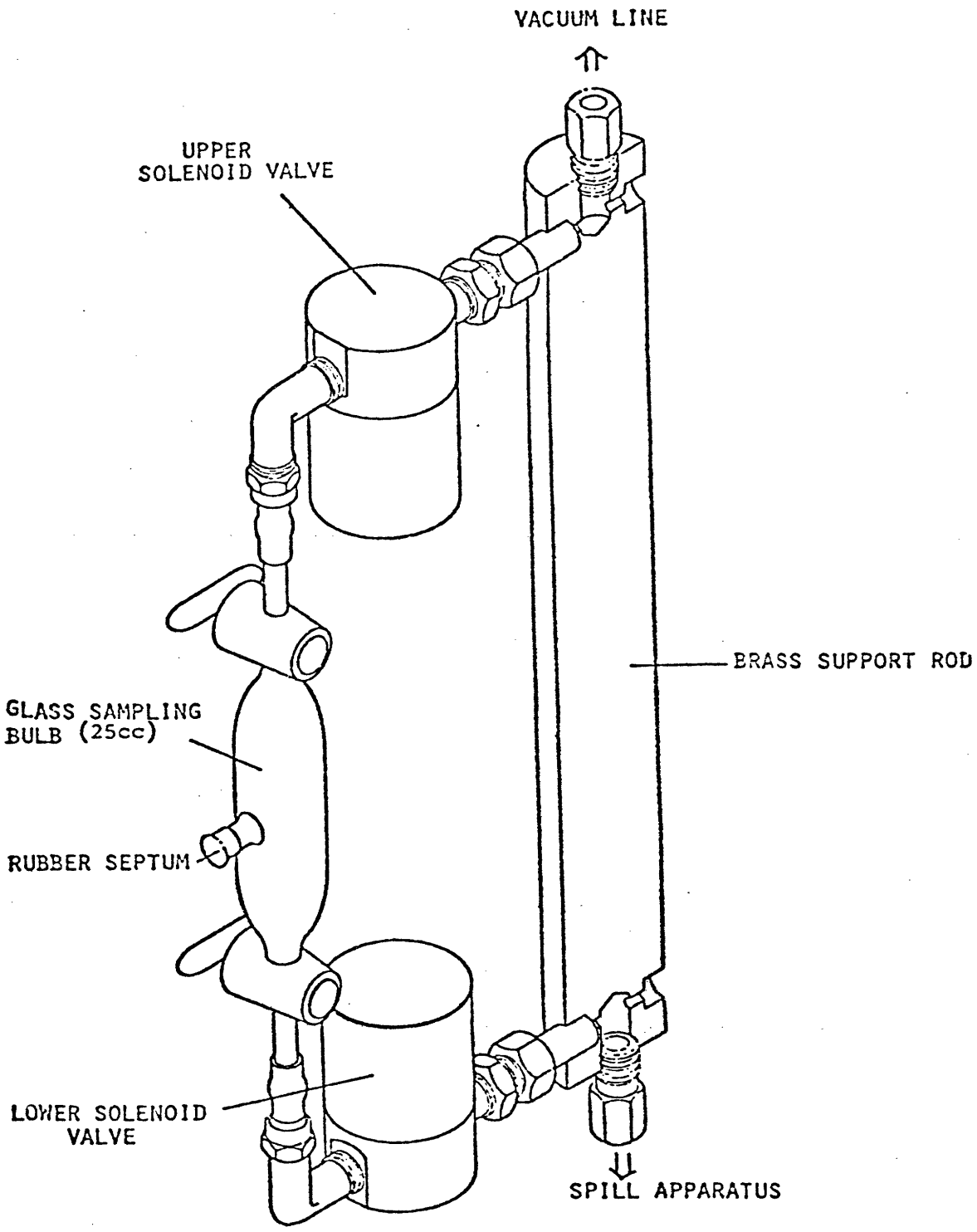

FIGURE I-2: ISOMETRIC CUT-AWAY VIEW OF VAPOR SAMPLING STATION

The concentrations of tracer gas (C_T) and cryogen vapor (C_{HC}) were estimated by vapor sample analyses:

$$C_T = x_T \cdot C \tag{I-21}$$

$$C_{HC} = C - C_T \tag{I-22}$$

where x_T = mole fraction of the tracer gas.

A numerical finite difference technique was used to evaluate the gas velocity (U) and local boil-off rates ($\dot{M}$).

$$\frac{(C_T)_{i+1,\,j} - (C_T)_{i,\,j}}{t_{i+1} - t_i} = -\left[\frac{(UC_T)_{i+1,\,j} - (UC_T)_{i+1,\,j-1}}{x_j - x_{j-i}}\right] \tag{I-23}$$

$$\frac{(C_{HC})_{i+1,\,j} - (C_{HC})_{i,\,j}}{t_{i+1} - t_i} = -\left[\frac{(UC_{HC})_{i+1,\,j} - (UC_{HC})_{i+1,\,j-1}}{x_j - x_{j-1}}\right] + \left(\frac{W}{A}\right)\dot{M}_{i+1,j} \tag{I-24}$$

i is the ith time interval and j is the jth space interval. $\dot{M}_{i+1,\,j}$ is the local mass boil-off rate at jth spatial point and (i+1)th instant in time.

The algorithm began with the known velocity at j = 0 (x=0). Equation (I-23) was used to solve for the gas velocity $U_{i+1,\,j}$, which was then substituted into equation (I-24) to yield the local boil-off rate $M_{i+j,\,j}$.

E. ONE-DIMENSIONAL BOILING/SPREADING MODEL FOR INSTANTANEOUS SPILLS OF CRYOGENIC LIQUIDS ON WATER

The spreading mechanics of cryogenic liquids on water is similar in many respects to that of non-volatile liquids on water. The major distinction between these two processes is the evaporative mass loss of cryogen during the spreading.

Fay (1969) used an order-of-magnitude analysis to identify three principle flow regimes through which a spreading oil film passes: the first is the grav-

ity-inertia regime, the second is the gravity-viscous regime and the third is the surface tension-viscous regime. For cryogen spilled on water, only the physics of the first regime is important. Before the second or third regime becomes established, most of the cryogen has evaporated.

Assuming the density of the cryogen (ρ) is constant and the cryogen is in hydrostatic equilibrium in the vertical direction, neglecting the acceleration across the thickness (h) of the cryogen layer, the equations of continuity and momentum transfer in one-dimensional configuration can be expressed as:

$$\frac{\partial h}{\partial t} + \frac{\partial}{\partial x}(hU) + \frac{\dot{m}}{\rho} = 0 \qquad \text{(I-25)}$$

$$\frac{\partial U}{\partial t} + U\frac{\partial U}{\partial x} + \Delta g \frac{\partial h}{\partial x} = 0 \qquad \text{(I-26)}$$

where x is the spreading direction and t is time. U is the spreading velocity and $\dot{m}$ is the local mass boil-off rate per unit area (it can be a function of both x and t). Δ is defined as $(\rho_{water} - \rho)/\rho_{water}$ and g is the gravitational acceleration.

The boundary conditions are:

at the leading edge: $$U_{LE} = [\lambda \Delta g\, h_{LE}]^{1/2} \qquad \text{(I-27)}$$

at the origin of the spill: $$U_{x=0} = 0 \qquad \text{(I-28)}$$

where λ is experimentally determined and equal to 1.64.

The initial condition is evaluated at a time very close to the start of the spill when the amount of cryogen evaporated is very small so that the spill process can be adequately described by Hoult's (1972a) analytical solution for oil spills on water, which is expressed as:

$$= \left[g\Delta V t^2\right]^{1/3}$$

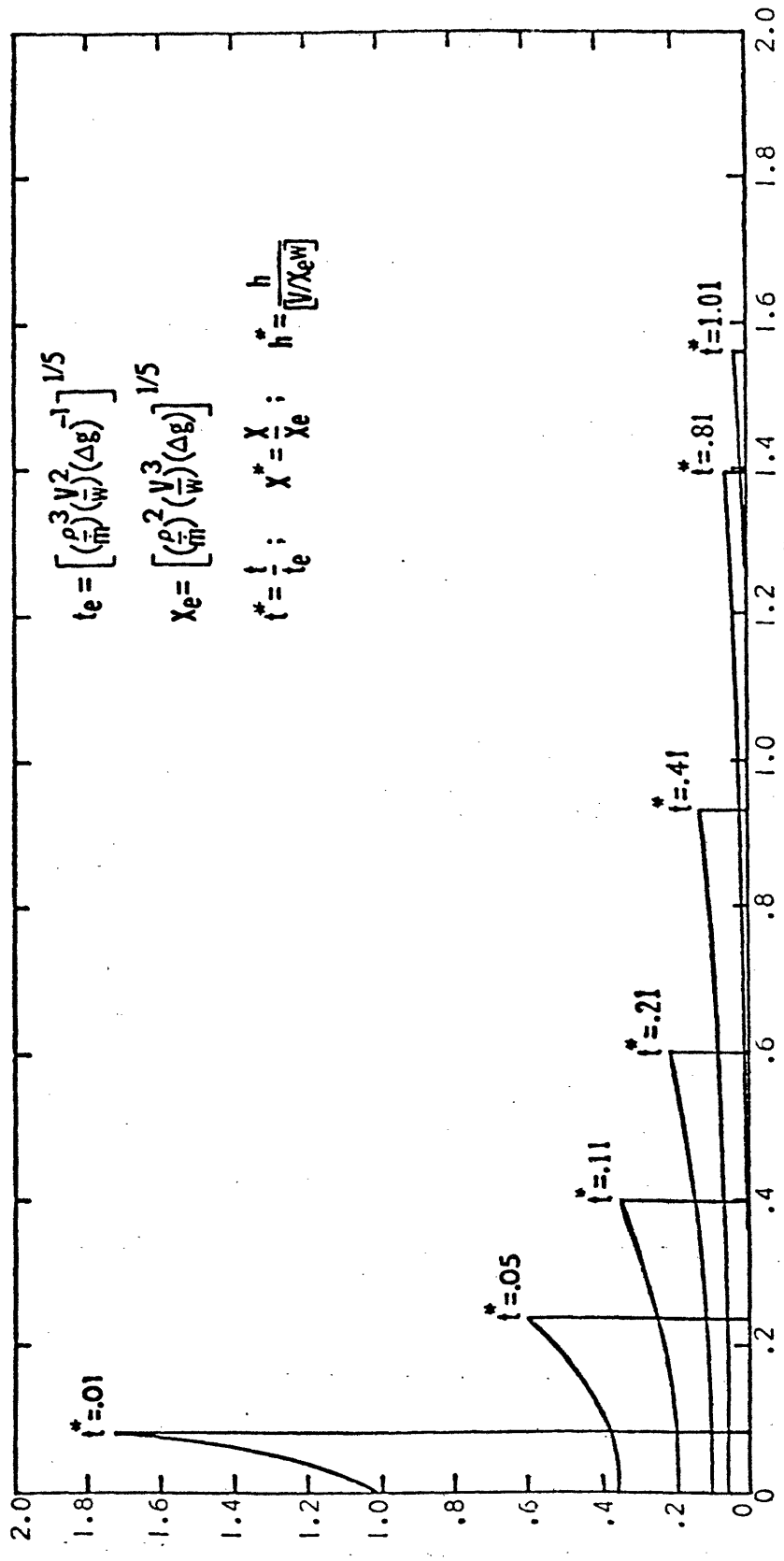

FIGURE 1-3: DIMENSIONLESS THICKNESS PROFILE PREDICTED BY THE NUMERICAL MODEL FOR THE CASE OF CONSTANT HEAT FLUX.

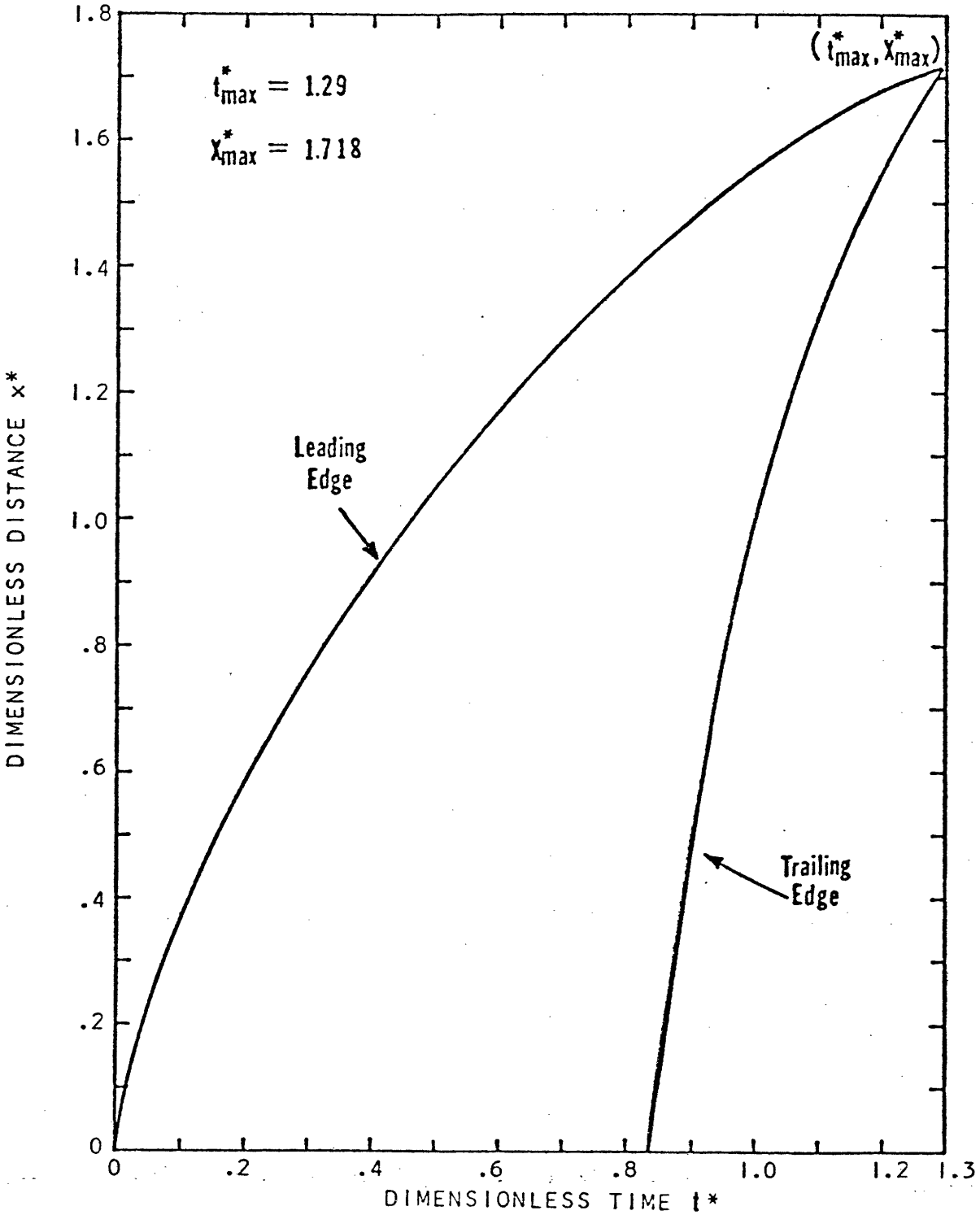

FIGURE 1-4: PATHS OF THE LEADING AND TRAILING EDGES PREDICTED BY THE NUMERICAL MODEL FOR THE CASE OF CONSTANT HEAT FLUX.

where

$$n = \left[\frac{4}{9\lambda} - \frac{2}{27}\right]^{-1/3} \qquad \text{(I-30)}$$

A numerical technique called "the method of characteristics" was used to solve equations (I-25) and (I-26) and U and h as functions of x and t were determined.

For the case of constant boil-off rate (per unit area), the theoretical thickness profile of the spreading fluid (in dimensionless form) is shown in Figure I-3; the spreading front is thicker and the tail thins out towards the spill origin. As the cryogen continues to evaporate, a trailing edge begins to appear at x = 0 and moves toward the spreading front. The numerical model predicts the paths of the leading-edge and trailing-edge, as shown in Figure I-4. The intersection of these two paths determines the time for complete vaporization and the maximum spreading distance.

As a cryogenic liquid spills on an unconfined water surface, boiling and spreading occur simultaneously. The bubbles of the evaporated cryogen rising through the liquid reduce the effective density of liquid cryogen layer. The reduction in density can be estimated using the average bubble rising velocity (U_{av}) and volumetric flux ($\dot{V}$):

$$\rho_{effective} = \rho_L \left(1 - \frac{\dot{V}}{U_{av}}\right) \qquad \text{(I-31)}$$

The bubble rising velocity is a function of the bubble size. For nitrogen and methane, the average bubble rising velocity was estimated to be 24 cm/sec. In the case of propane, U_{av} was estimated to be 26 cm/sec.

F. EXPERIMENTAL RESULTS

Spills of n-pentane were made and the spreading front was recorded as a

function of time. Similarly, spills were carried out with liquid nitrogen and methane. Pure liquid propane, binary mixtures of ethane-propane and propane-n-butane, and ternary mixtures of ethane-propane-n-butane were spilled on water and the spreading rates and local boil-off rates were measured.

Pentane Spills

Several pentane spill experiments were conducted to determine the value of λ in the leading-edge boundary condition (equation (I-27)). Figure I-5 presents the experimental results for pentane spills of various volumes. The value of n in equation (I-29) was found to be 1.72. λ was then obtained from equation (I-30) and equalled 1.64.

Nitrogen and Methane Spills

The spreading curves for liquid nitrogen and methane as functions of time are shown in Figure I-6. During the spreading of nitrogen or methane, the cryogen is thicker near the leading edge and becomes thinner in the tail. This general shape persists until almost the end of the spreading process when most of the cryogen has evaporated. A layer of ice forms on the water surface downstream of the cryogen distributor during the experiment. In the vicinity of the cryogen distributor, no ice formation was observed.

Propane Spills

Propane boils very rapidly from its initial contact with water. Highly irregular ice forms quickly (~ 1 s). The boiling rate then drops to considerably lower values. This can be seen in Figures I-7 and I-8, where triangles represent data from a pure propane spill. The spreading distance as a function of time is shown in Figure I-9; the discontinuity is due to an "ice dam" formation, which hinders the spreading of cryogen. For the same volume spilled, the maximum spreading distance for propane is much smaller than for nitrogen or methane.

LPG Spills

The spreading data of ethane-propane, propane-n- butane, and ethane-propane-

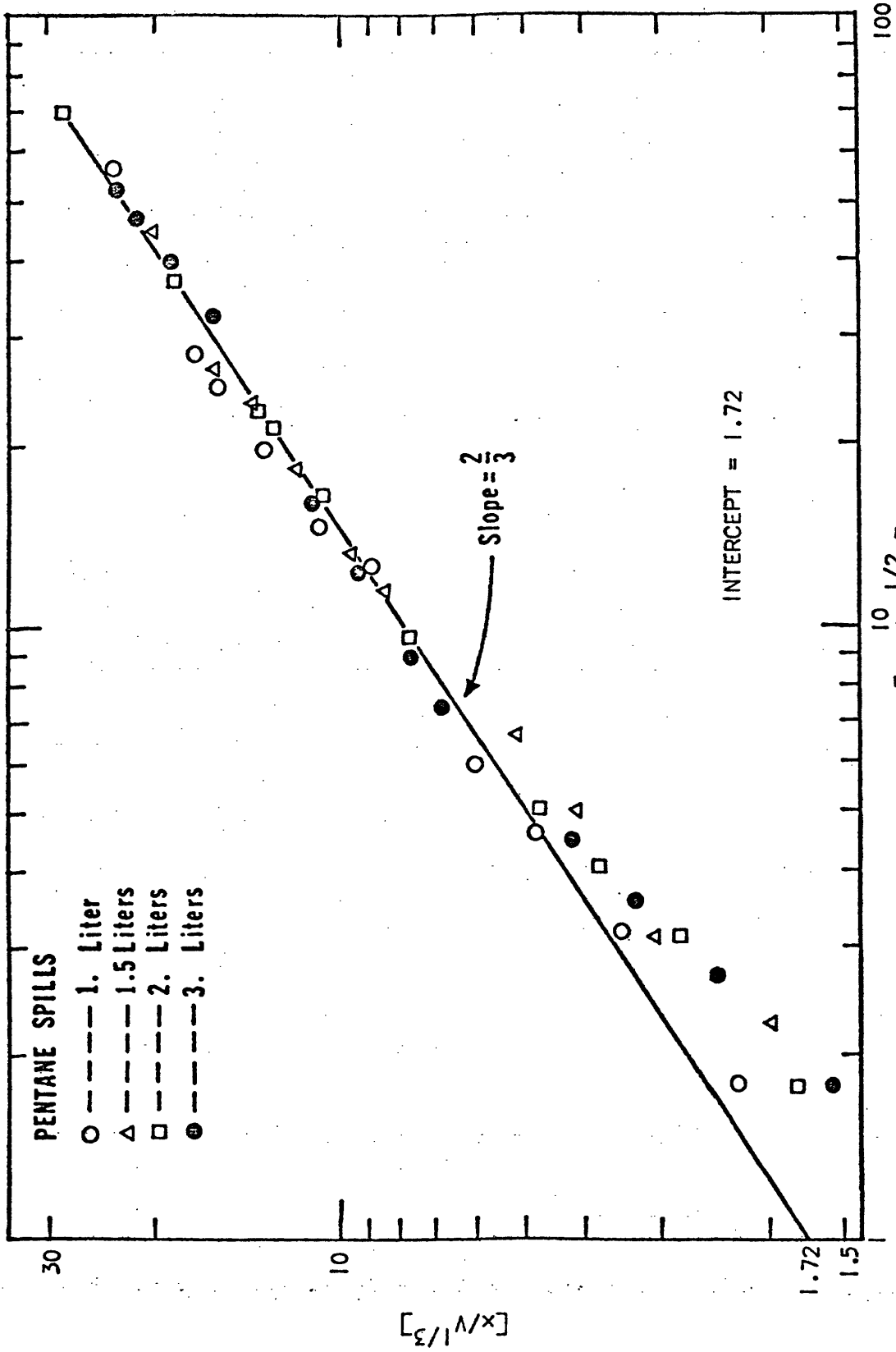

FIGURE 1-5: DIMENSIONLESS CORRELATION OF SPREADING DISTANCE WITH TIME FOR PENTANE SPILLS.

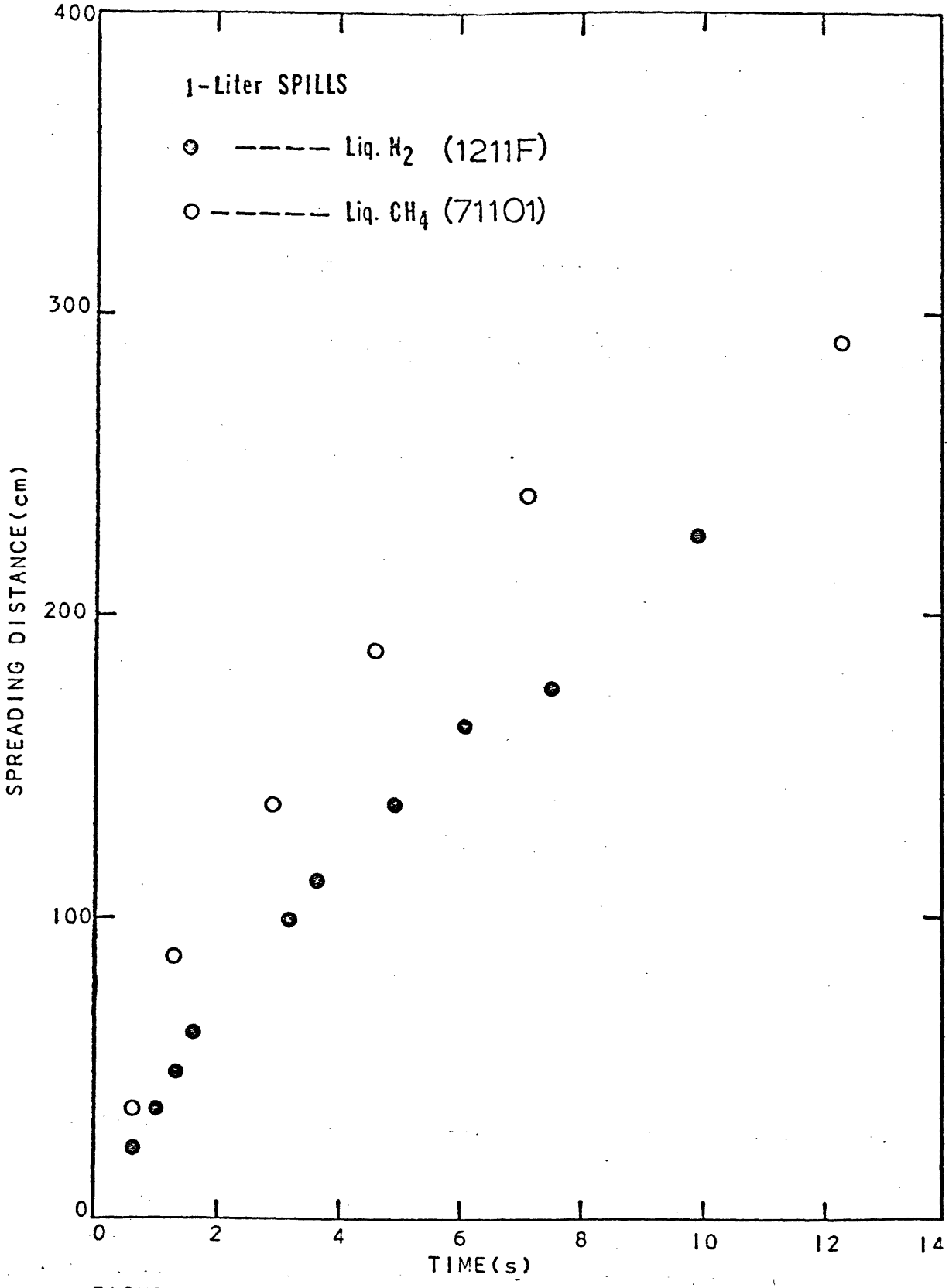

FIGURE I-6: SPREADING DISTANCE AS A FUNCTION OF TIME FOR LIQUID NITROGEN AND METHANE SPILLS

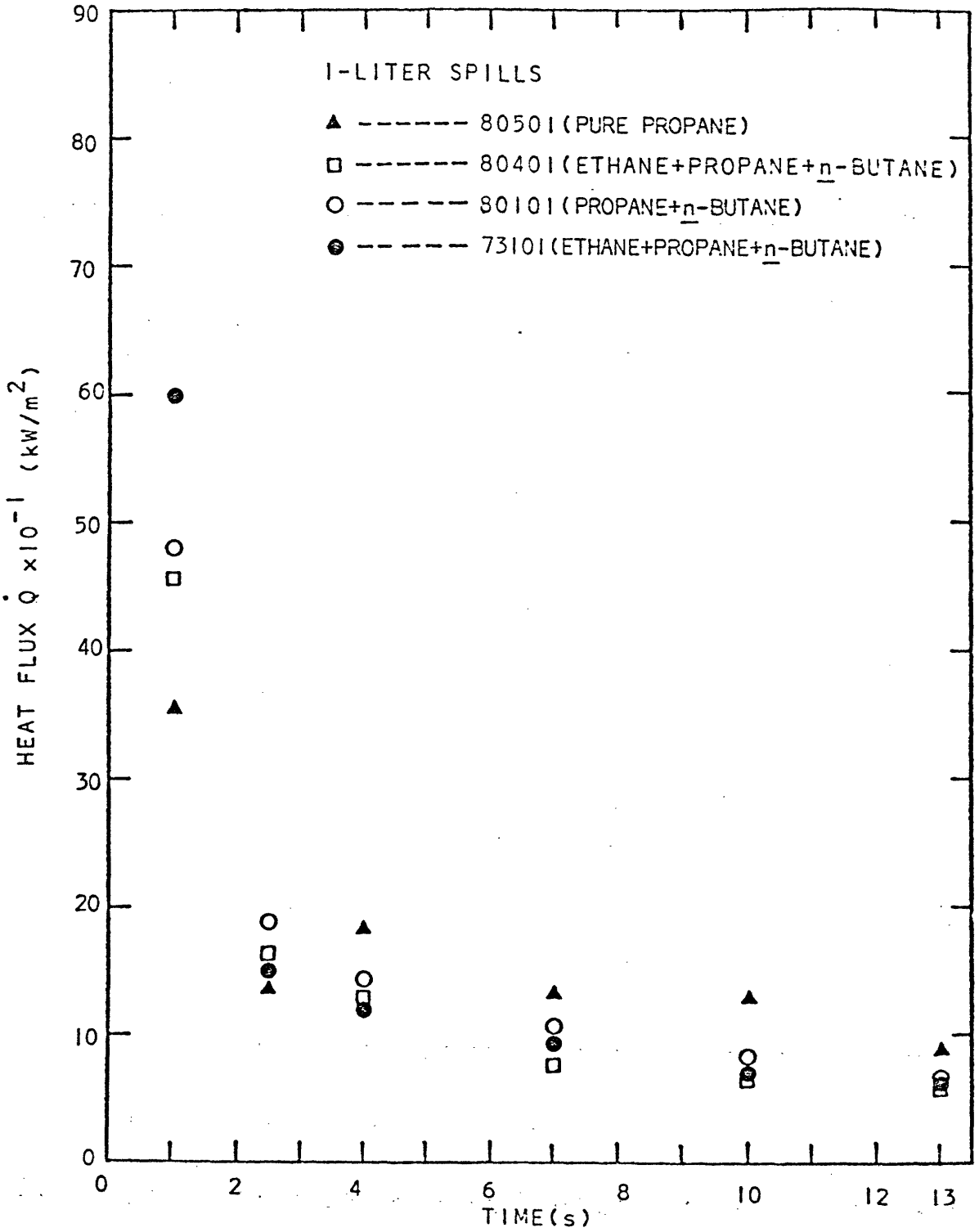

FIGURE I-7: LOCAL BOIL-OFF RATE AS A FUNCTION OF TIME FOR PROPANE AND LPG SPILLS AT THE FIRST SAMPLING STATION.

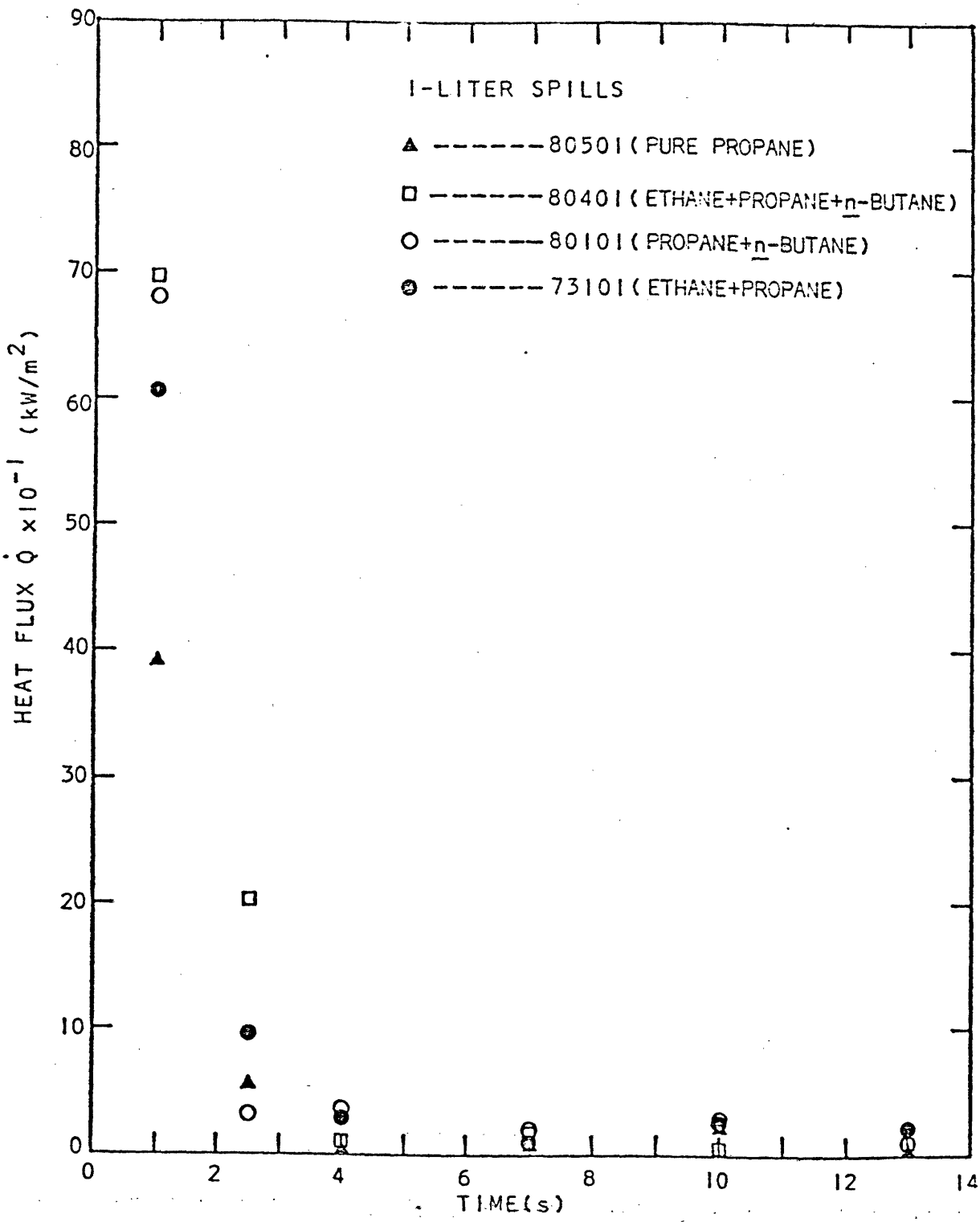

FIGURE 1-8: LOCAL BOIL-OFF RATE AS A FUNCTION OF TIME FOR PROPANE AND LPG SPILLS AT THE SECOND SAMPLING STATION.

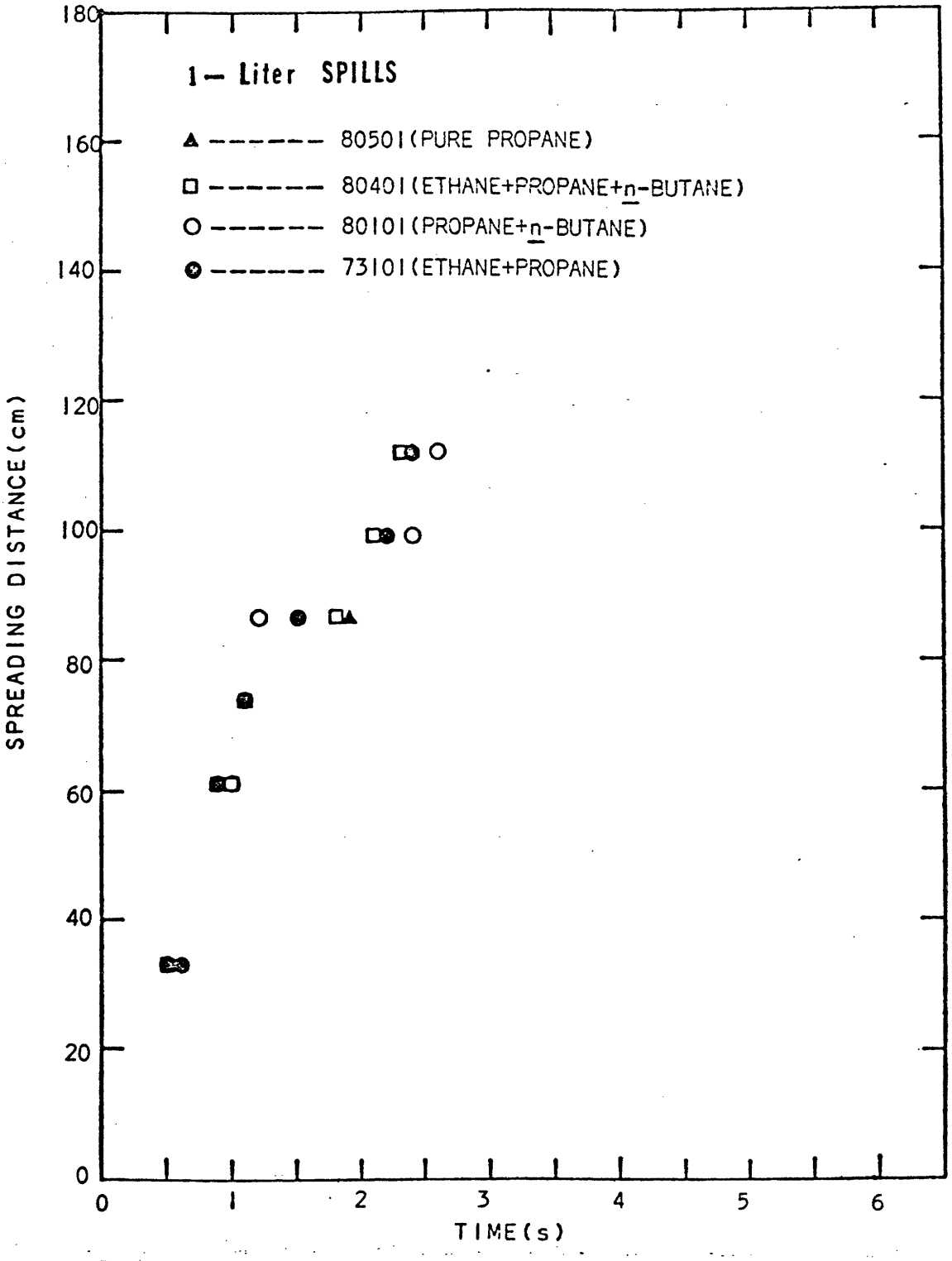

FIGURE 1-9: SPREADING DISTANCE AS A FUNCTION OF TIME FOR PROPANE AND LPG SPILLS.

n-butane mixtures are also presented in Figure I-9. In Figures I-7 and I-8, the boil-off rates for the mixtures are similar to the case of pure propane, the initial boil-off rate being very high and then decreasing very rapidly. The ice forms very quickly and is rough and irregular.

G. DISCUSSION

Nitrogen and Methane Spills

In Figure I-10, the experimental spreading data for liquid nitrogen and methane spills are compared to the values predicted by the numerical model described earlier. The boil-off rates of nitrogen and methane are assumed constant and selected to be 40 and 92 kW/m^2 respectively. The effective densities of nitrogen and methane are then calculated using equation (I-31) and equal to 0.66 and 0.254 g/cm^3 respectively (the normal densities of liquid nitrogen and methane at their boiling points, 77K and 111K, are 0.8 and 0.425 g/cm^3). These effective densities are used in the numerical analysis. Good agreement is obtained between the experimental data and the predicted values. For nitrogen and methane spreading on water, the leading-edge is thicker than the tail. This is consistent with theoretical predictions (see Figure I-3). The model also predicts the trailing edge where the cryogen has completely evaporated and the water surface is cryogen free. The trailing edge starts at the distributor and moves towards spreading front. The intersection of the leading edge and trailing edge determines the maximum spreading distance and the time for complete vaporization. The numerical model gives reasonable predictions of the maximum spreading distance for nitrogen and methane spills, as shown in Table I-2.

The close agreement between the experimental data and the predicted values, using an assumed constant heat flux for nitrogen or methane, proves the validity of the assumption. It is concluded that the numerical model successfully de-

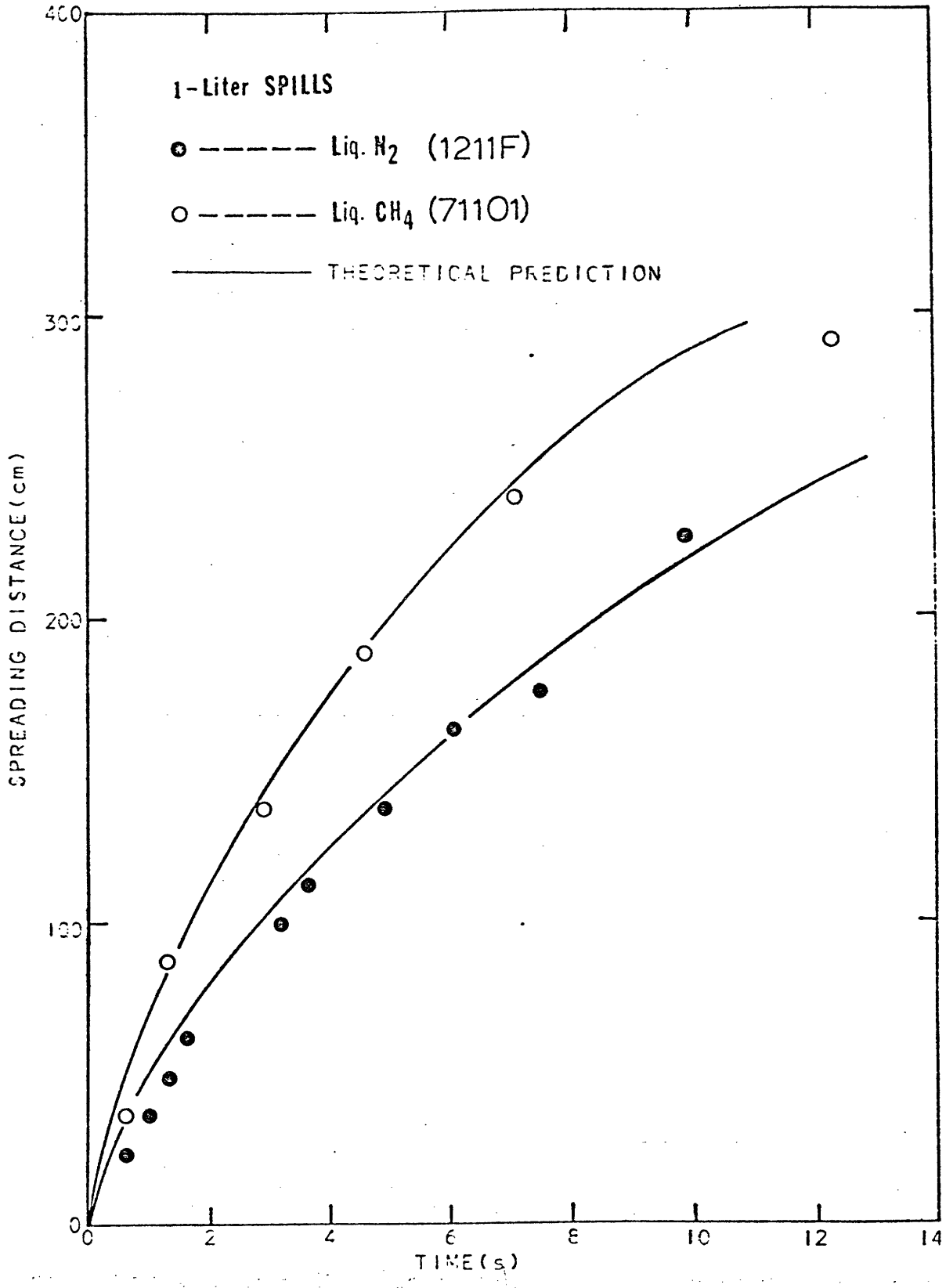

FIGURE I-10: SPREADING CURVES FOR LIQUID NITROGEN AND METHANE SPILLS. EXPERIMENTAL DATA AND NUMERICAL PREDICTIONS COMPARED.

TABLE I-2

Maximum Spreading Distance for Liquid Nitrogen and Methane Spills

Volume Spilled	Maximum Spreading Distance (cm) Nitrogen Experiment	Nitrogen Theory	Maximum Spreading Distance (cm) Methane Experiment	Methane Theory
0.5 liter	226	193	229	197
0.75 liter	---	246	279	251
1.0 liter	310	293	317	298
1.5 liters	*	374	*	380
2.0 liters	*	444	*	452

* The length of the spill apparatus is 360 cm.

scribes the boiling and spreading phenomena for nitrogen and methane spills on water (at least for this size spill).

Propane and LPG Spills

For propane or LPG spills on water, violent and rapid boiling occurs immediately upon contact. The water surface near the distributor opening is severely agitated. It is very difficult to define the true area of contact between cryogen and water at this point. Rough ice forms on the water surface very quickly (~ 1 s). From this point, heat transfer is controlled by the conduction through the ice and water; the boiling rate decreases further with time as the ice layer grows thicker. The local boiling behavior can then be reasonably well described by a moving boundary heat transfer model (Eckert and Drake (1975)). This model leads to the conclusion that the local heat flux is inversely proportional to the square root of the corrected time, t_{c_i}:

$$\dot{Q}_i = \varepsilon\, t_{c_i}^{-1/2} = 154\, t_{c_i}^{-1/2} \ (kW/m^2) \qquad (I\text{-}32)$$

where t_{c_i} is defined as :

$$t_{c_i} = t_i - t_\delta \qquad (s)$$

ε is a function of the physical properties of ice and is evaluated at an average temperature between the freezing point of water and the boiling point of LPG. t_δ represents the time associated with the initial ill-defined boiling phase before the formation of an ice layer. The value of t_δ has been chosen equal to one second but numerical tests have shown that variations in t_δ (0.5 - 1.5 sec) do not affect the predicted results. t_i is the time ellapsed after the initial contact of water with cryogen at a position x_i where the heat flux is $\dot{Q}_i$.

Predictions from equation (I-32) are compared with experimental data in

Figures I-11 and I-12. Theory and experiment agree reasonably well for the first sampling station. The values of the heat flux obtained from the second station are below the predicted values. The explanation for this is that propane or LPG initially evaporates very fast and there is not enough cryogen to cover evenly the entire surface area between the first and second sampling stations ($\dot{Q}$ estimated by the data analysis scheme is the average heat flux between the sampling stations).

Figures I-11 and I-12 also show that the addition of small amounts of ethane and (or) n-butane to propane has no effect on its boiling rates. This is the same as the conclusion obtained from LPG spills on confined water surfaces.

The numerical model mentioned earlier can also be used to simulate the boiling-spreading process for LPG, assuming a boiling rate that changes with time according to the following equation:

$$\dot{Q}_i = \varepsilon_o \qquad 0 \leq t_i \leq 1.0 \text{ s}$$

$$\dot{Q}_i = \varepsilon \, (t_i - t_o)^{-1/2} \qquad t_i > 1.0 \text{ s} \tag{I-33}$$

where $\dot{Q}_i$ is in kW/m^2 and

$$t_o = t_\delta - \left(\frac{\varepsilon}{\varepsilon_o}\right)^2 \quad (s)$$

Equation (I-33) attempts to account for the high evaporation rate ε_o, observed in the first second of contact between water and cryogen; the value of ε_o is selected to be 10^3 kW/m^2 which is about the same as the average value of the heat fluxes obtained from various propane and LPG spills at the first second after LPG contacts the water surface.

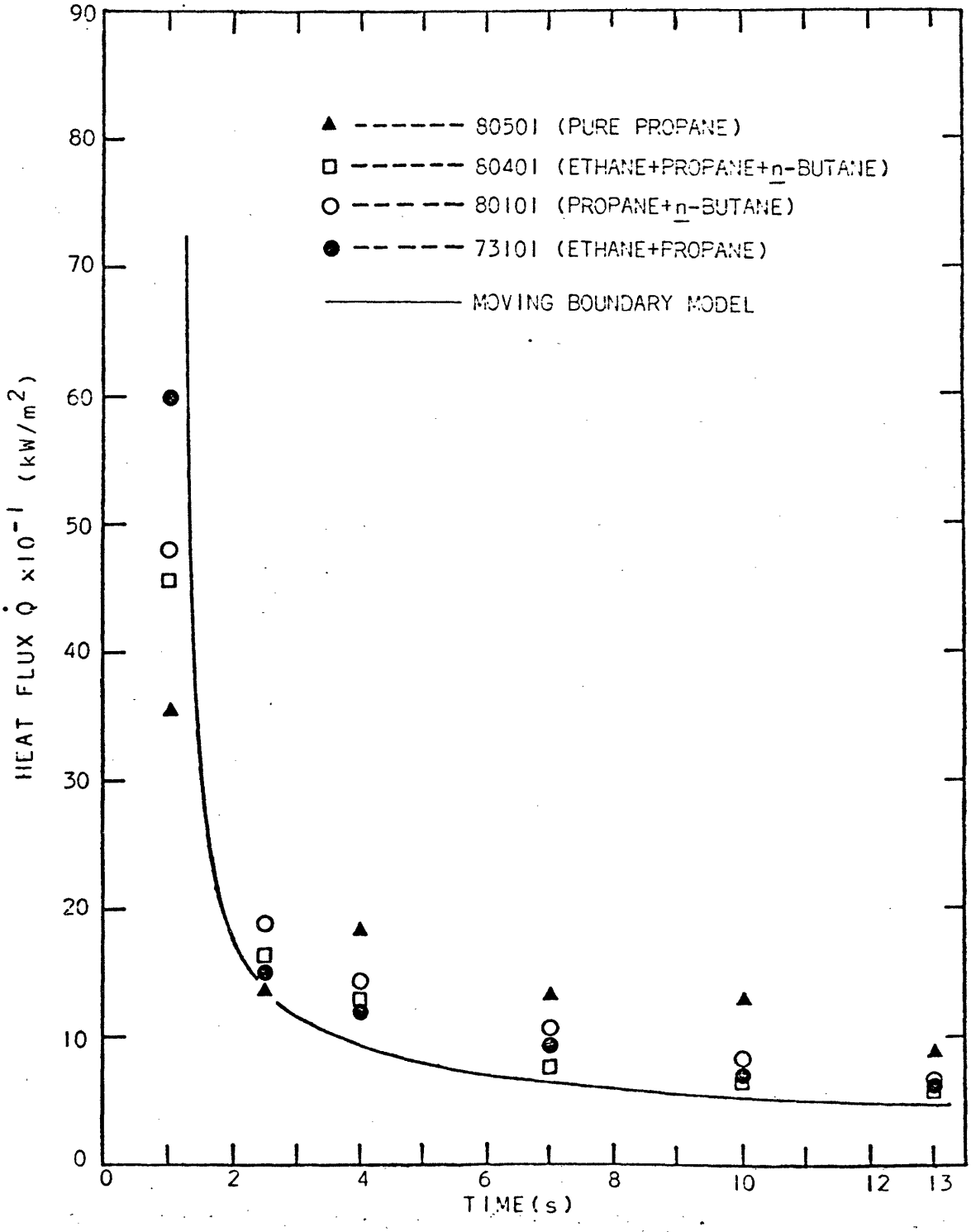

FIGURE I-11: LOCAL BOIL-OFF RATE CURVES FOR PROPANE AND LPG SPILLS AT THE FIRST SAMPLING STATION. EXPERIMENTAL DATA COMPARED WITH PREDICTIONS FROM MOVING BOUNDARY MODEL.

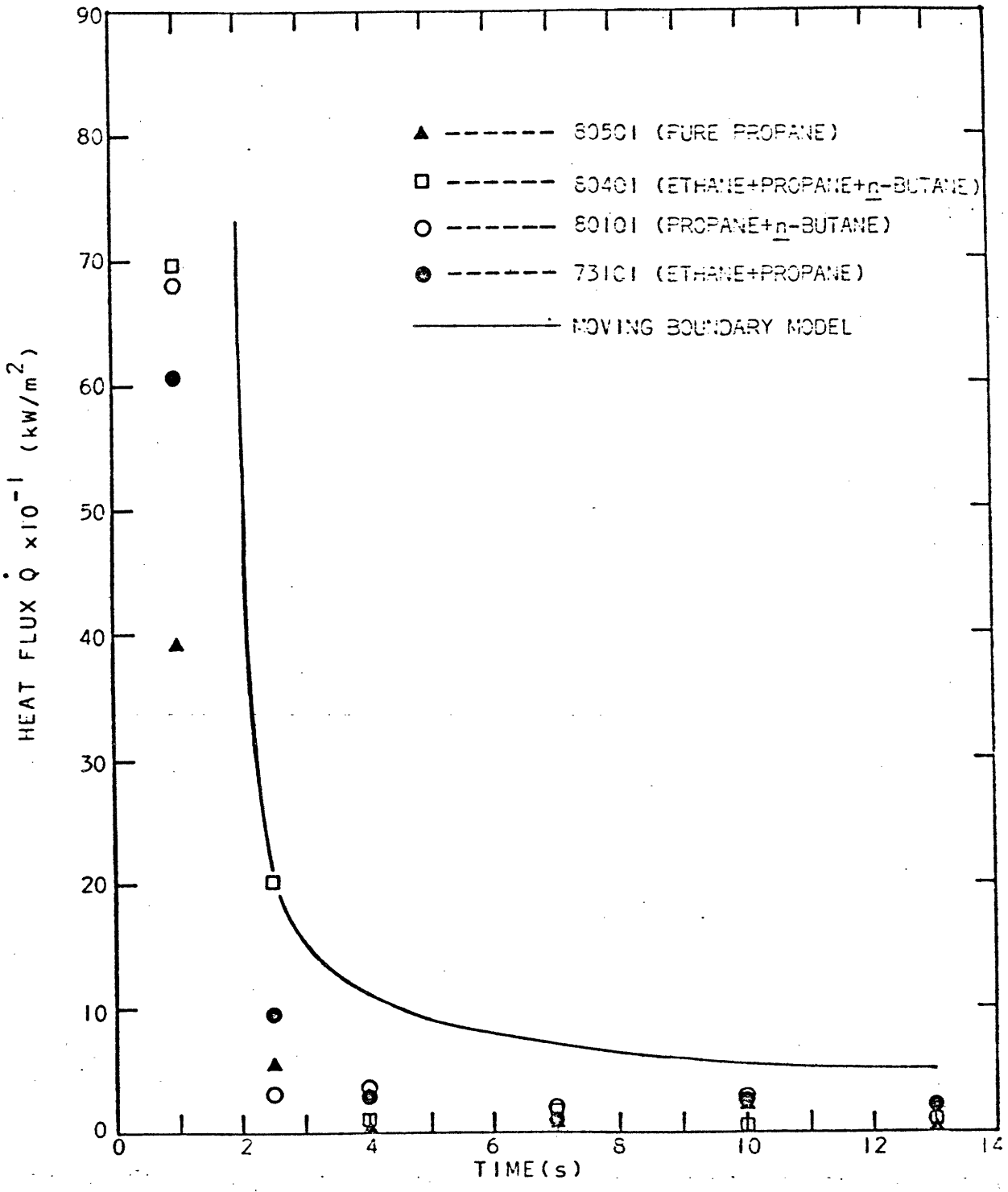

FIGURE I-12: LOCAL BOIL-OFF RATE CURVES FOR PROPANE AND LPG SPILLS AT THE SECOND SAMPLING STATION. EXPERIMENTAL DATA COMPARED WITH PREDICTIONS FROM MOVING BOUNDARY MODEL.

The effective density of LPG is set equal to 0.3 g/cm^3, using an average evaporation rate (per unit area) for the first 13 seconds after LPG contacts water and an average bubble rising velocity, 26 cm/s.

The predicted spreading curve as a function of time is compared to the experimental data in Figure I-13. The model does not accurately predict the spreading front position. The highly irregular ice formed in LPG spills is very difficult to characterize, and its effect on hindering the spreading of cryogen cannot be adequately accounted for in the theory. Figure I-13 also shows that the composition of LPG has little effect on its spreading process. Therefore, it is concluded that the boiling-spreading process for LPG spills is independent of its composition.

The predicted values of the maximum spreading distance and the experimental data are given in Table I-3. Close agreement is observed.

In Table I-4, maximum spreading distances for methane and propane spills are compared; methane spreads over a much larger area than propane (LPG) for the same volume spilled.

H. CONCLUSIONS

1. An apparatus was designed and constructed to monitor the spreading of a boiling liquid on water. The apparatus allows measurement of vapor temperatures and compositions. These data can be used to infer liquid vaporization rates.

2. For liquid nitrogen and methane spills, film boiling occurs initially upon contact with water. Ice forms on the water surface during the spreading. Before an ice layer appears, most of the cryogen was evaporated. Because there is little ice growth before most of the liquid nitrogen or methane has evaporated, their boiling rates were found to be nearly constant. This conclusion would not be valid for a large spill.

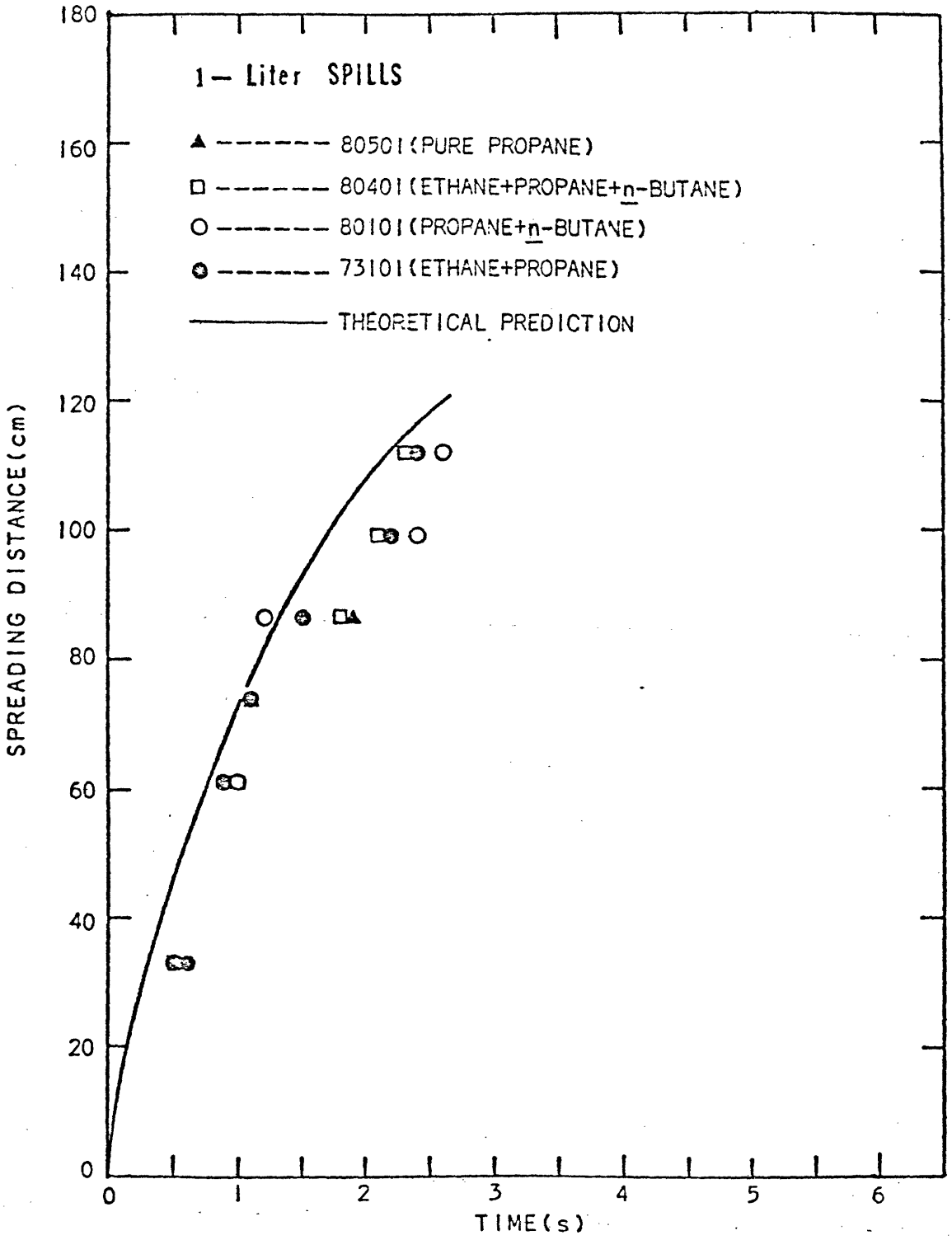

FIGURE 1-13: SPREADING CURVES FOR PROPANE AND LPG SPILLS. EXPERIMENTAL DATA AND NUMERICAL PREDICTIONS COMPARED.

TABLE I-3

Maximum Spreading Distance for Propane and LPG Spills

Volume Spilled	Maximum Spreading Distance (cm) Experiment	Theory
0.5 liter	68	79
0.75 liter	90	101
1.0 liter	110	120
1.5 liters	150	153
2.0 liters	163	182

TABLE I-4

*Maximum Spreading Distance for Methane and LPG Spills

Volume Spilles	Maximum Spreading Distance (cm) Methane	LPG
0.5 liter	229	68
0.75 liter	279	90
1.0 liter	317	110
1.5 liters	380**	150
2.0 liters	452**	163

* Experimental Data

** Theoretical Prediction

3. Liquid nitrogen and methane exhibit similar thickness profiles during spreading, that is, the spreading front is thickest and the profile thins out toward the spill origin.

4. The bubbles of evaporated cryogen entrained in the liquid affect the spreading of cryogen on water. The bubbles alter the effective density of the cryogen layer and this effect has been accounted for in the model development.

5. A numerical technique using the method of characteristics has been developed that successfully describes the boiling-spreading phenomena for liquid nitrogen and methane spills on water. The model provides information of the maximum spreading distance and the time for complete vaporization for various quantities spilled.

6. For liquid propane or LPG spills, nucleate boiling occurs upon initial contact with water. Highly irregular ice forms very quickly and the local boil-off rates monotonically decrease with time. A moving boundary heat transfer model can adequately describe the boiling phenomena. This is consistent with earlier observations made for propane or LPG spilled on confined water surfaces.

7. For LPG mixture spills, fractionation occurs with the more volatile components vaporizing preferentially.

8. Addition of small quantities of ethane or n-butane to propane has little effect on the boiling process. This was also the case in confined propane and LPG spills.

9. Propane or LPG does not spread in a manner similar to liquid nitrogen or methane. The formation of a rough ice layer hinders the spreading of propane and LPG and the spreading was found to be linear with respect to time.

10. The composition of LPG has essentially no effect on the spreading phenomena. Pure propane will simulate actual LPG behavior. The same conclusion

was obtained in confined LPG spill experiments.

11. Irregular ice formations in LPG spills are difficult to characterize and their effect on hindering the spreading of LPG cannot be adequately accounted for in the theory. The numerical model does not adequately describe the boiling-spreading phenomena for LPG spills.

12. In an industrial accident, it is expected that LNG will spread over a much larger area than LPG for the same volume spills. In this case, the formation of an ice layer beneath the cryogen may lead to much lower evaporation rates.

12. The high-speed motion picture photographic study improved the understanding of cryogen movements, ice formation and bubble growth in the boiling/spreading process.

The work described in this thesis provides a first step towards estimating the extent of hazardous spills from an LNG or LPG tanker accident.

II. INTRODUCTION

A. THESIS OBJECTIVES

Liquefied petroleum gas (LPG) is often transported as bulk cargoes in large insulated tankers. The safety record for ships carrying LPG is generally excellent. However, there would be a serious risk from any accidental spill. This is because LPG boils well below ambient water temperatures and will form a combustible (and, possibly, an explosive) cloud that is dense and not readily dispersed. The capacity of many of the existing tankers is very large and, in the event of a serious tanker accident, very large vapor clouds could be found.

Normally LPG consists largely of propane with some ethane and butane. When in contact with water, LPG vaporizes rapidly. A serious accident could occur if the cloud contacts an ignition source before dispersing. Evaluating the potential hazards from accidents in the marine transportation requires reliable data of boil-off rates and spreading rates for LPG on water.

Previous work dealt with LPG spills on water surfaces of limited area. The results of these studies have been summarized by Reid and Smith (1978). Their key conclusion was that LPG boiled in the nucleate boiling regime upon contacting water with very rapid ice formation. Heat transfer rates were then limited by conduction across the growing ice shield. Before the formation of ice, the method of spilling the LPG strongly influenced the boiling rate.

However, these conclusions are limited because rarely would one expect a spill of LPG to occur in the confined area. The more usual case would involve simultaneous boiling and spreading. No experiments had been reported which determined such rates for LPG spills. It was not known whether the heat fluxes measured in the confined area experiments were applicable to unconfined

spills. Current analyses of the boiling/spreading process for any volatile cryogen are almost completely theoretical and assume that the boiling rate per unit area is independent of time. No experiments had been reported to refute or substantiate this assumption. It was the objective of the present work to measure experimentally the simultaneous boiling and spreading rates for LPG spilled onto a water surface. Furthermore, a mathematical model was to be developed to describe the boiling/spreading phenomena of LNG and LPG spilled on water. Finally, a better understanding of the fundamentals and mechanism of LPG spilled on water was also an important objective of this thesis.

B. RELEVANT PREVIOUS WORK

The transient boiling of a volatile liquid on the surface of a hotter immiscible liquid has received relatively little attention compared to the more common phenomenon of boiling on a heated solid surface. The former is less readily characterized in a quantitative manner as the hot surface is mobile and capable of internal heat transfer not only by conduction but by convection as well. Furthermore, if the volatile liquid boils at a temperature below the freezing point of the hot liquid, it is possible for a solid phase to form at the interface and extend into the hot liquid. Finally, any spill of a cryogenic liquid on water will lead to a highly transient situation where rapid variations in the heat flux are possible.

Regimes of Boiling

Heat transfer to boiling liquids is a convection process involving a change in phase from liquid to gas. The phenomena of boiling heat transfer are considerably more complex than those of convection without phase change. There are various distinct regimes of boiling in which the heat-transfer mechanisms differ radically.

To illustrate the different boiling regimes, consider a simple system consisting of an electrically heated horizontal wire submerged in a pool of liquid at saturation temperature. Figure II-1 shows the characteristic variation of heat flux with temperature difference (Rohsenow and Choi, 1961). As the heating surface temperature is raised above the saturation temperature, convection currents circulate the slightly superheated liquid and evaporation takes place at the free liquid surface. The heat transfer mechanism in this process is single-phase natural convection; only liquid is in contact with the heating surface.

As the temperature of the heating surface is further increased, a point A is reached where vapor bubbles form on the heating surface at a number of nucleation sites or cavities. At first the vapor bubbles are small and condense before reaching the free liquid surface. As the temperature is raised further, larger and more numerous bubbles are formed and succeed in rising to the free liquid surface. This is called nucleate boiling. In this regime, bubbles transport the latent heat of the phase change and also agitate the liquid near the heating surface. Moreover, as the bubbles become detached from the heating surface, they drag a mass of superheated liquid from the layer adjacent to the heating surface into the core of the stream. This produces an intensive macroscopic transport of heat from the heating surface into the bulk of the boiling liquid. As a result, the nucleate boiling regime is characterized by high heat transfer rates for small temperature differences.

The heat flux in nucleate boiling regime cannot be increased indefinitely as the temperature difference increases further. When the heating surface temperature is raised to a point where the heat flux reaches a maximum (point B), the bubble concentration becomes very high and vapor forms an unstable film covering the heating surface. Under the action of circulation currents, this

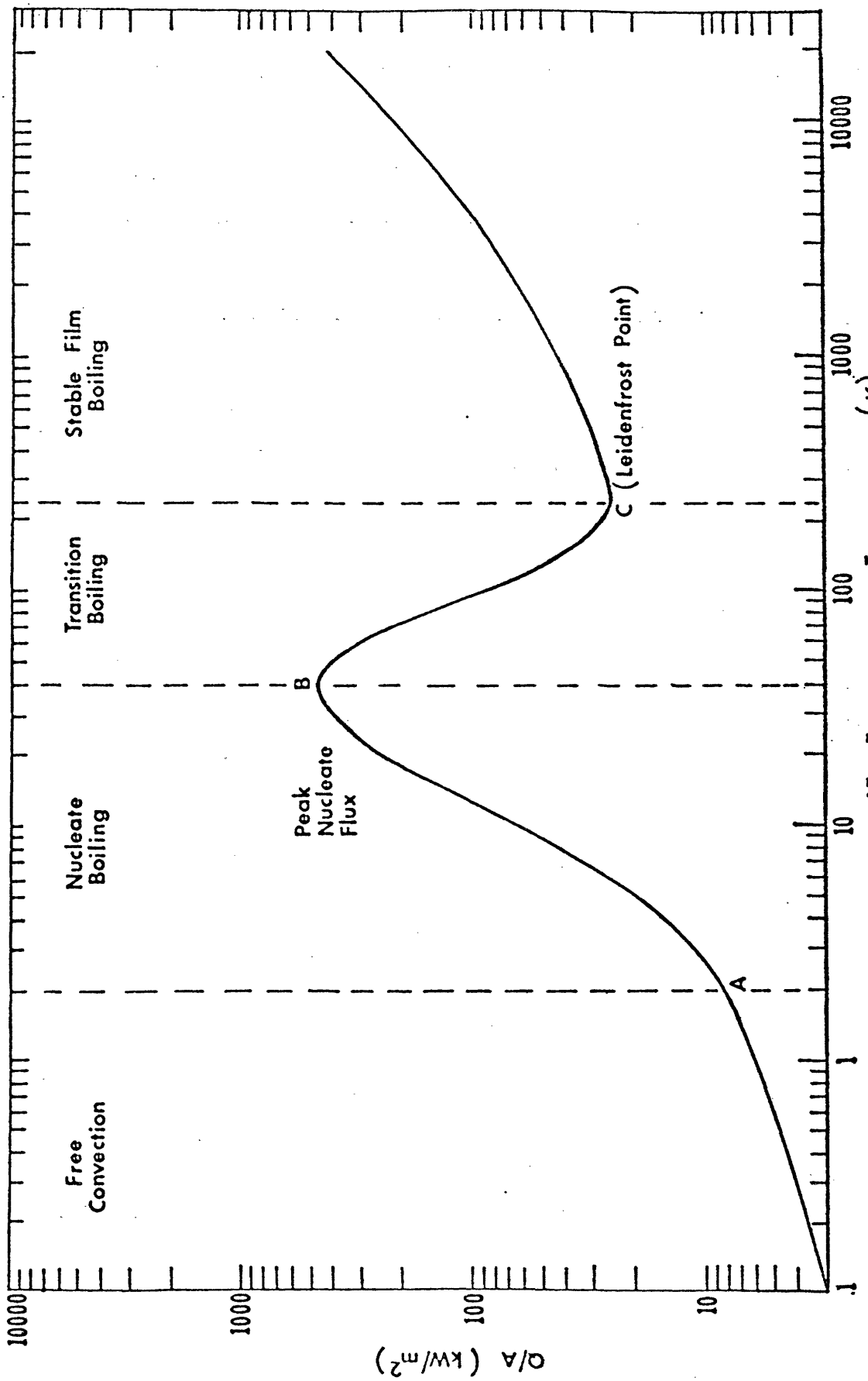

FIGURE II-1: REGIMES OF BOILING

vapor film collapses and reforms rapidly. Beyond the peak of the curve is the transition boiling regime. The presence of the vapor film over the hot surface provides additional resistance to heat transfer and reduces the heat transfer rate.

Increasing the heating surface temperature past point C leads to a stable vapor film on the heating surface. This is called the stable film boiling regime. Heat is transferred through the vapor film to the liquid. Large bubbles originate at the outer upper surface of the vapor film and consequently any nucleation sites on the heating surface are ineffective. The low thermal conductivity of the vapor film produces the low heat transfer rate observed in the film boiling regime.

Further increases in the temperature of the heating surface results in correspondingly higher heat transfer rates because of thermal radiation. The lowest temperature capable of maintaining a stable vapor film is called the Leidenfrost point.

Effect of Surface Roughness on Boiling Heat Transfer

Investigations of the effect of surface roughness on the boiling characteristics (by Corty and Foust (1955) and Berenson (1962)) show that not only the positions of the nucleate boiling curves but also their slopes vary with roughness. Figure II-2 shows that the nucleate boiling regime is expanded and the transition boiling regime compressed for very smooth heating surfaces. This is because for a smooth surface, there is a smaller number of nucleation sites (or cavities) on which the vapor bubbles can form. Therefore, the temperature difference required to produce a given heat flux is increased. Berenson pointed out that the film boiling regime and the Leidenfrost temperature are, however, not greatly affected provided that the roughness height is less than the film thickness. This can be explained by noting that in the film boiling regime, the heat is transferred by conduction through a vapor film,

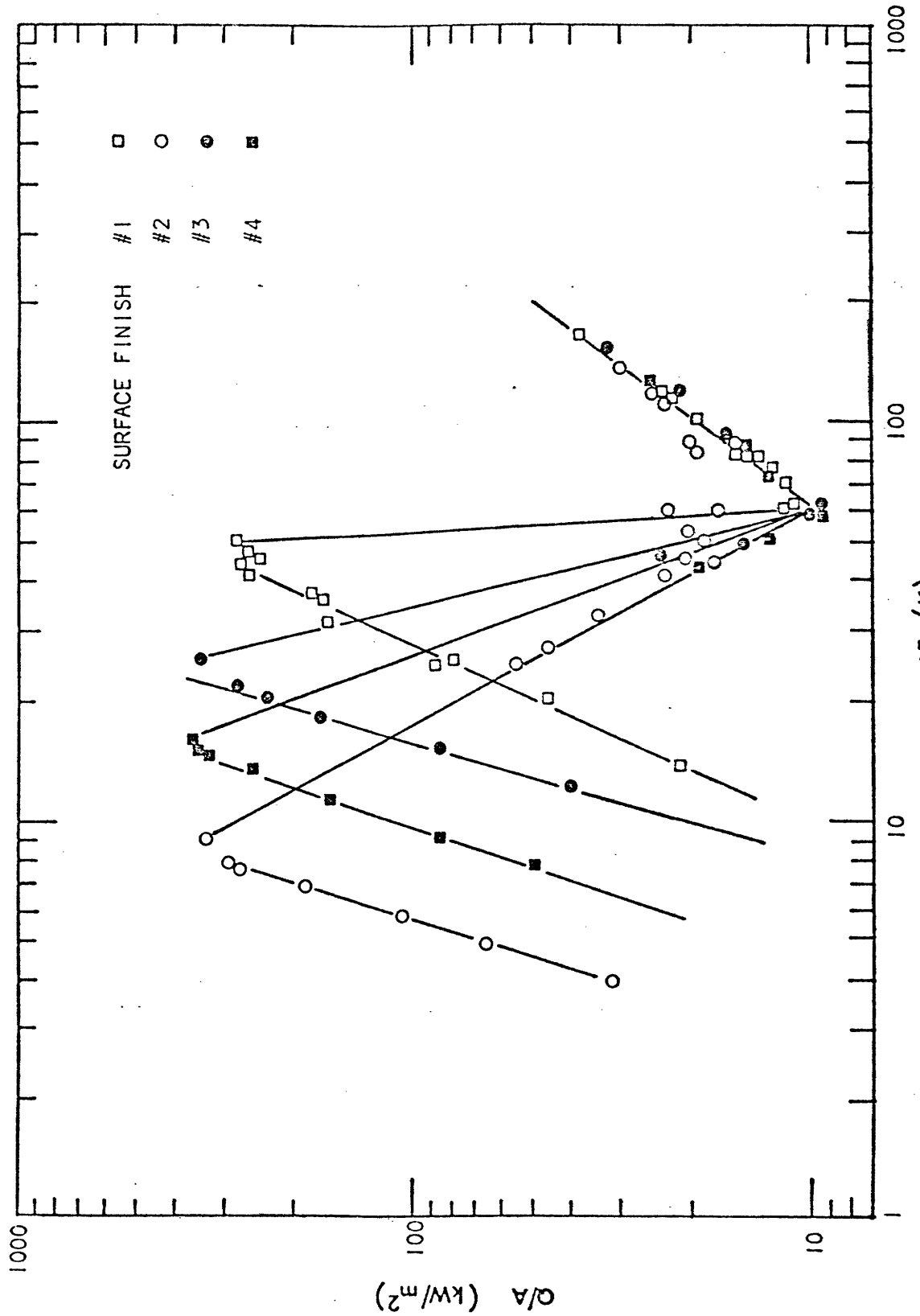

FIGURE II-2: EFFECT OF SURFACE ROUGHNESS ON BOILING CHARACTERISTICS FOR PENTANE BOILING ON A HORIZONTAL COPPER SURFACE (BERENSON, 1962).

which covers the heating surface. The bubbles originate on the upper surface of the vapor film and the surface characteristics do not have influence on the heat transfer process. Berenson also emphasized that the significant roughness parameter with regard to nucleate boiling was the number of cavities of appropriate size, not any general indicator of surface quality such as the root-mean-square (r.m.s.) roughness. It was also noted that surface material do affect nucleate boiling.

Boiling of Cryogenic Liquids on Solid Surfaces

The heat transfer to boiling cryogenic liquids has applications in the cooling of nuclear reactors, rocket engines and in many industrial processes. These applications motivated the study of the heat transfer properties of cryogenic fluid. The discussion here will be restricted to liquid nitrogen and light hydrocarbon liquids.

Park and his co-workers (1966) studied the nucleate and film boiling of nitrogen and methane at elevated pressures. The experiments were conducted on a horizontal gold-plated cylinder under steady state conditions. The nitrogen boiling data of Park et al. at atmospheric pressure are compared with those reported by Kosky and Lyon (1968), Bewilogua et al. (1975) and Ackermann et al. (1976) in Figure II-3. Kosky and Lyon's experiments were performed on a flat, horizontal, platinum-plated surface. Bewilogua et al. used a horizontal copper disk as the heating surface. Ackermann et al. carried out their experiments on a horizontal cylinder of an unidentified material.

It can be inferred from Figure II-3 that the geometry and the material of the heating surface affect the nucleate boiling heat fluxes for nitrogen. However, the maximum heat flux of nitrogen at atmospheric pressure is about the same (between 140 and 220 kW/m^2) in all the investigations grouped in Figure II-3. Only two groups of investigators, Park et al. and Ackermann et al., covered the film boiling regime and both used a horizontal cylindrical configuration.

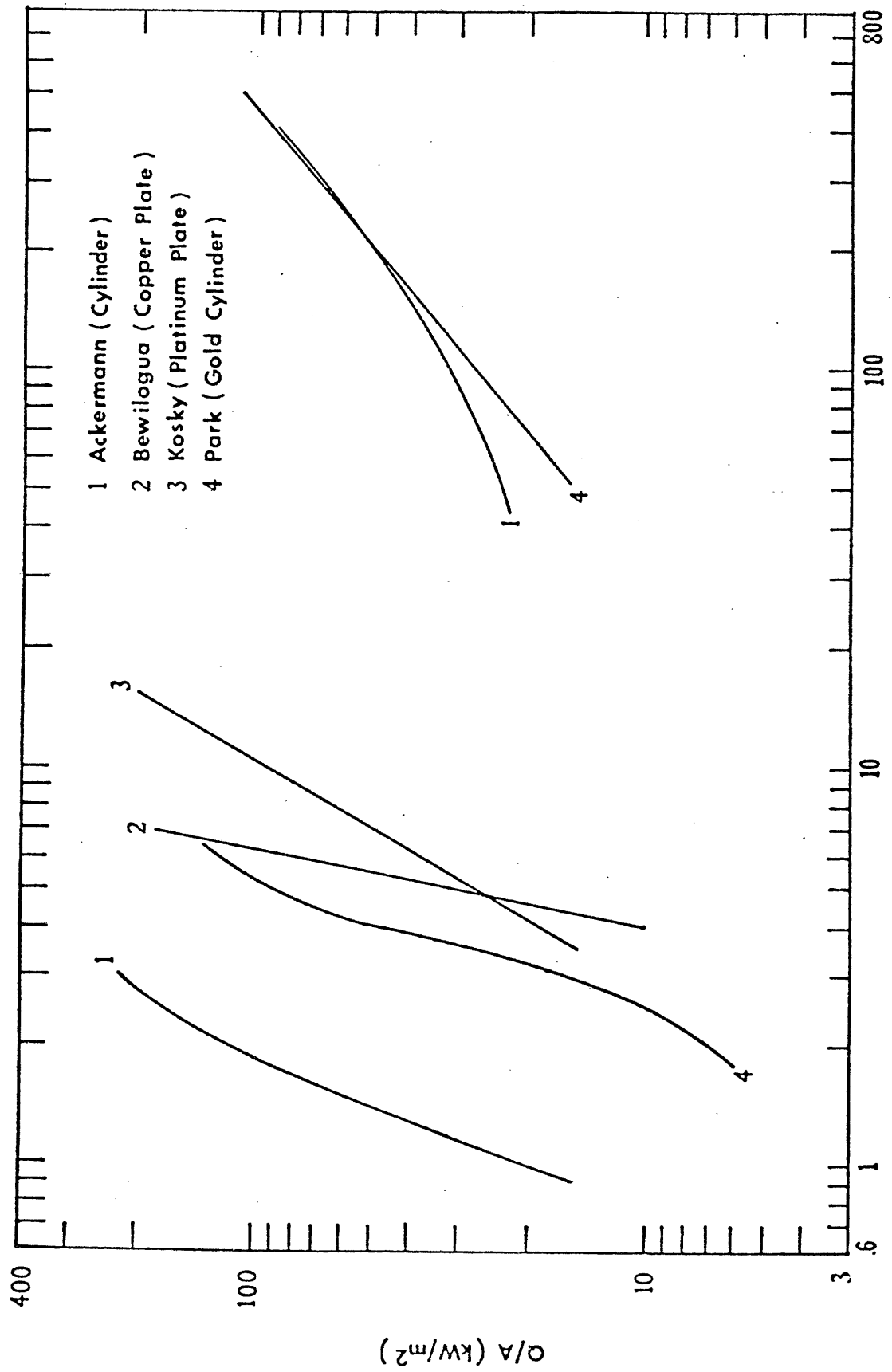

FIGURE II-3: BOILING OF LIQUID NITROGEN ON SOLID SURFACES AT ATMOSPHERIC PRESSURE.

The film-boiling data are consistent and the Leidenfrost heat flux for nitrogen at atmospheric pressure is between 16 and 23 kW/m^2 corresponding to a ΔT of ~47K.

Kosky and Lyon also studied the boiling of methane on the same platinum-plated surface used for the boiling of nitrogen. Moreover, Sciance et al. (1967a) investigated the pool boiling of methane on a gold-plated horizontal cylinder and Ackermann et al. (1976) used a horizontal cylinder as the heating surface. Figure II-4 shows their data at atmospheric pressure. Significant scattering among the results of different investigators is observed. As seen in this figure, the maximum nucleate boiling heat flux for methane is between 215 and 265 kW/m^2 corresponding to a ΔT between 16 and 20K. The Leidenfrost temperature is about 70K.

Sciance et al. (1967b) studied the nucleate boiling of ethane, propane and n-butane on a horizontal gold-plated cylinder. Wright and Colver (1971) studied ethane-ethylene systems on the same heating element used by Sciance et al.. Sliepcevich et al. (1968) presented the film boiling data of ethane. The corresponding boiling curves for ethane at atmospheric pressure are shown in Figure II-5. The nucleate-boiling data are consistent and the maximum nucleate boiling heat flux is approximately 220 kW/m^2, corresponding to a ΔT between 20 and 28K.

Brown (1967) investigated the nucleate and film boiling of liquefied natural gas (LNG) and liquefied petroleum gas (LPG) at various pressures on the same heating element used by Sciance et al.. In Figure II-6, the LNG data are compared to those reported by Sciance et al. for pure methane at atmospheric pressure. LNG exhibits higher nucleate fluxes than methane at the same ΔT while there is little difference in the film boiling curves for the two. These results imply that nucleate boiling behavior is strongly concentration dependent.

Brown also obtained the maximum nucleate heat fluxes for LNG and LPG. The peak nucleate heat flux of LNG was more than twice the value for methane, and

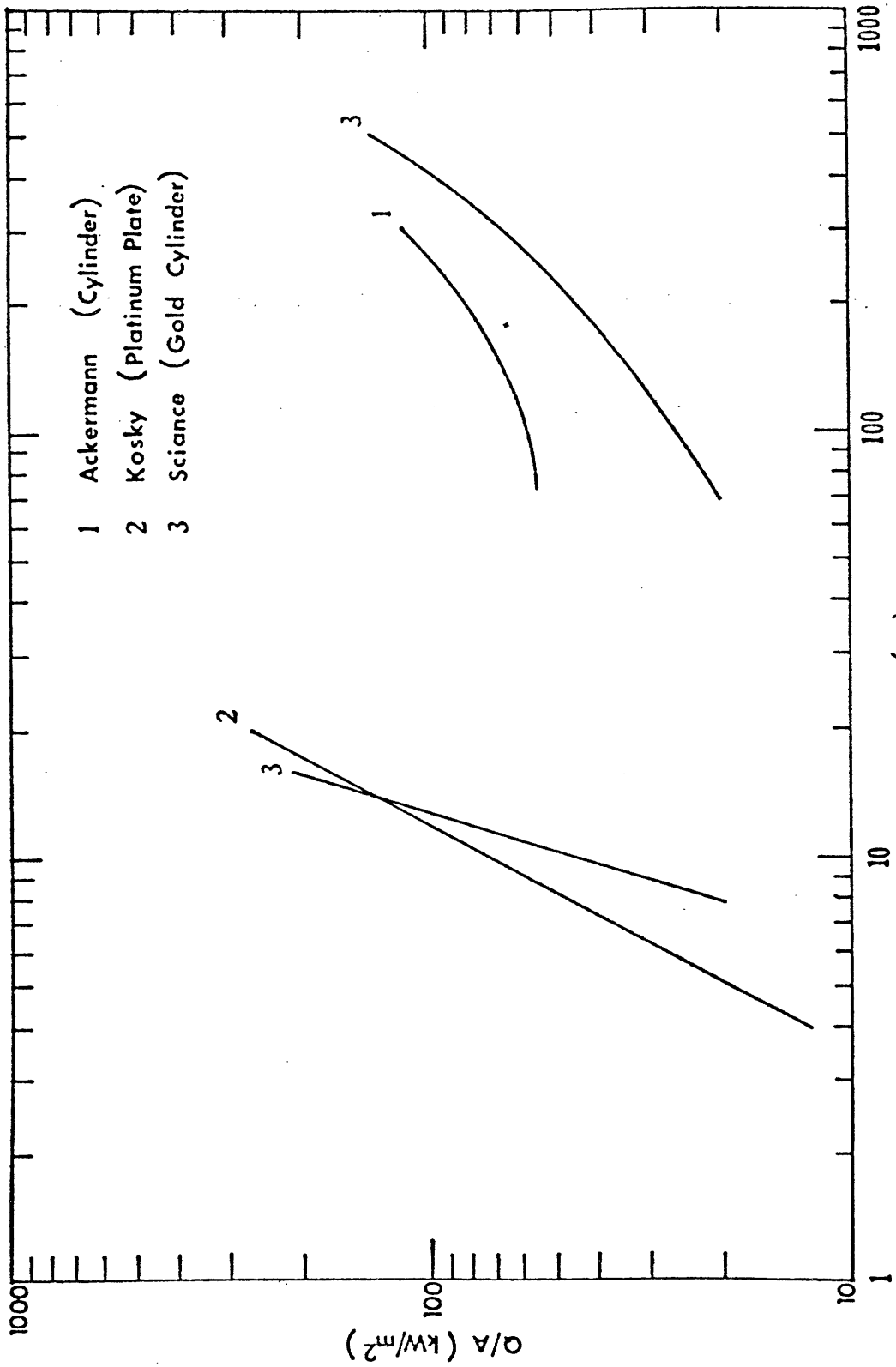

FIGURE II-4: BOILING OF LIQUID METHANE ON SOLID SURFACES AT ATMOSPHERIC PRESSURE.

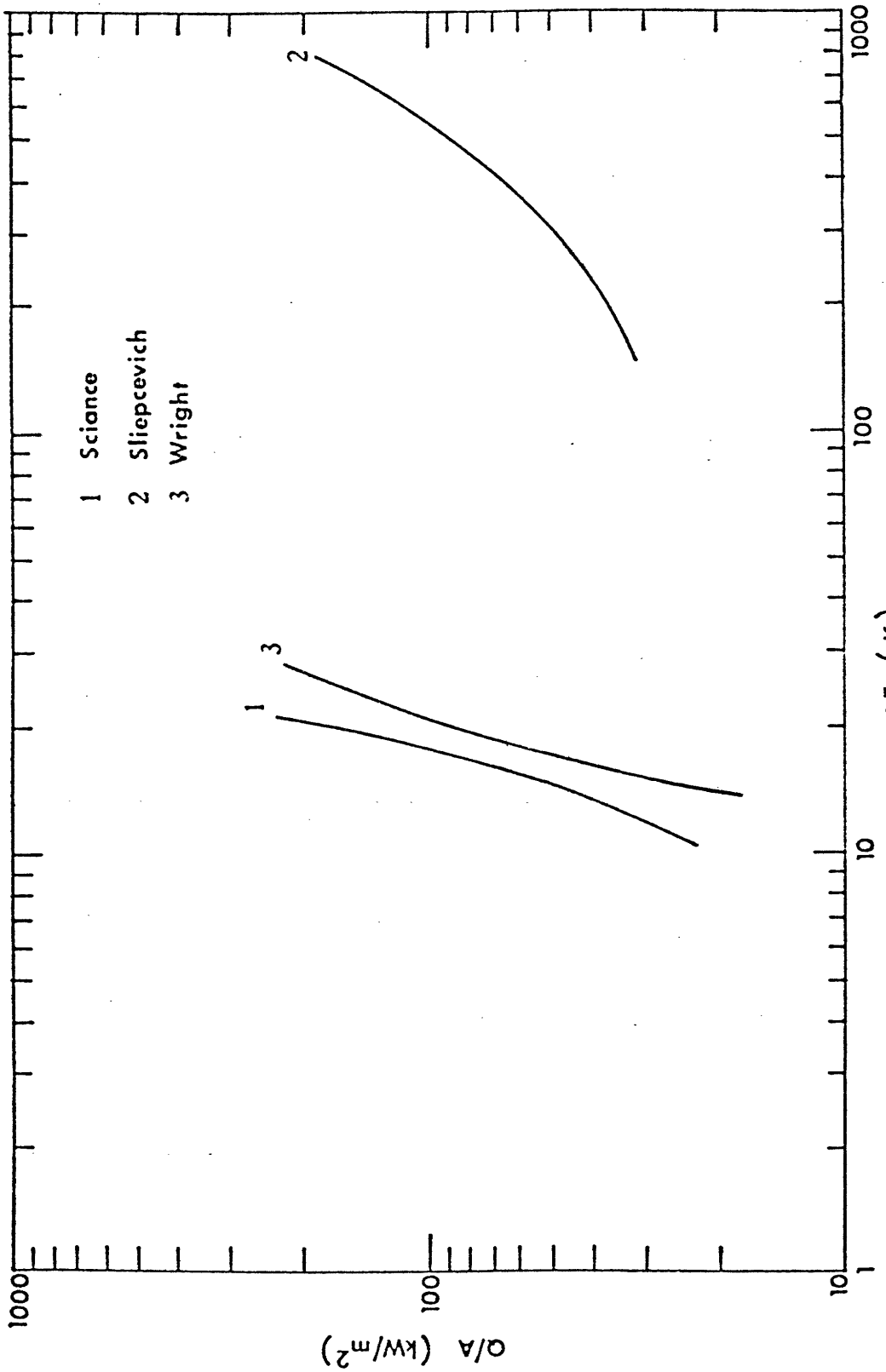

FIGURE II-5: BOILING OF LIQUID ETHANE ON A COLD PLATED SURFACE AT ATMOSPHERIC PRESSURE.

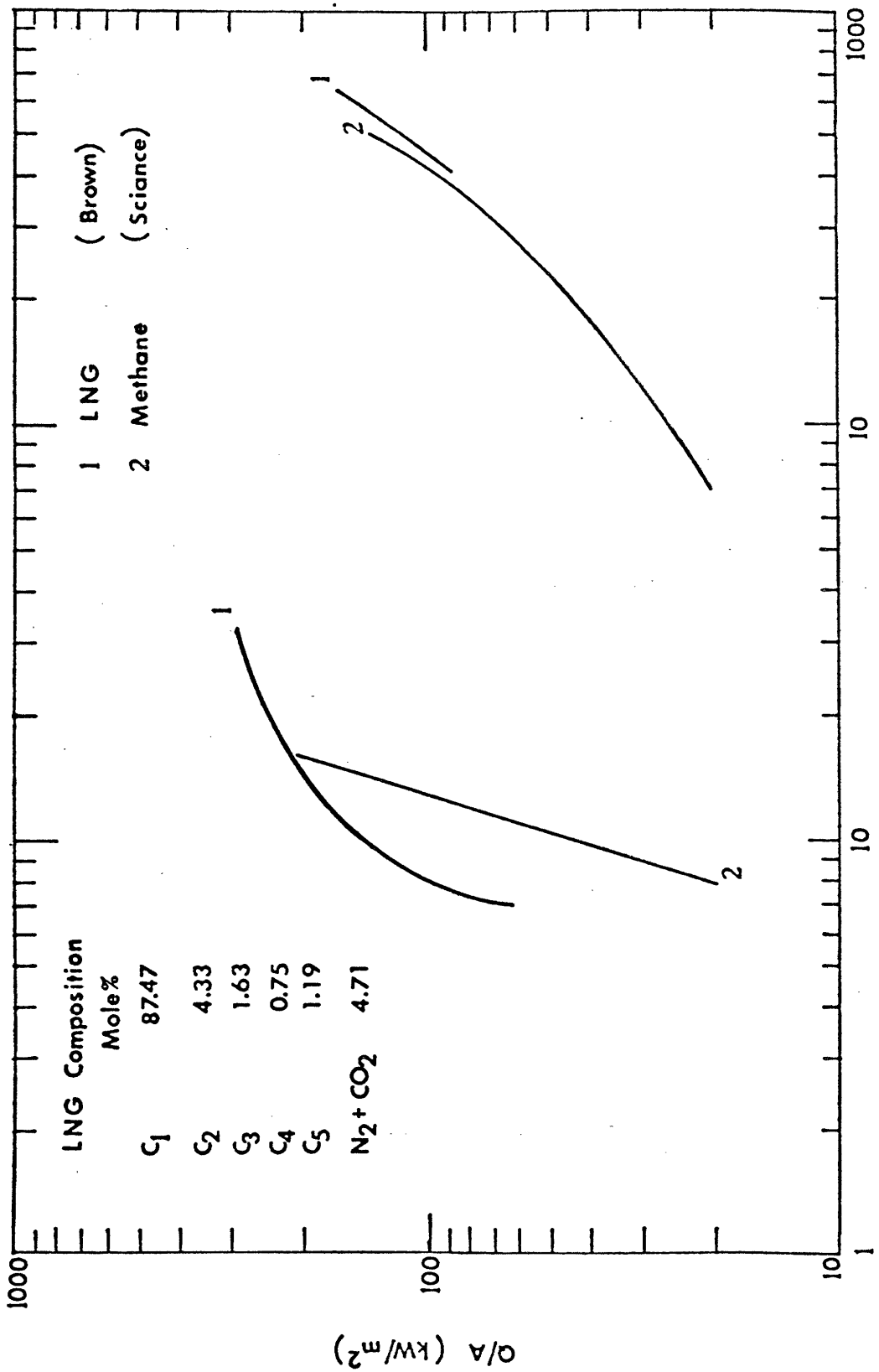

FIGURE 11-6: BOILING OF LNG AND METHANE ON A GOLD PLATED SURFACE AT ATMOSPHERIC PRESSURE.

maximum heat flux for LPG was only slightly higher than that of pure propane. Similar results were obtained where LNG and LPG boiled on water instead of a solid surface (see Drake et al. (1975); Reid and Smith (1978)).

The study of LNG boiling on typical dike floor materials was conducted by Reid and Wang (1978). Experiments were performed using Styrofoam boxes filled with various test substrates such as concretes, soil, sand, polyurethane, and corrugated aluminum. The test box with the substrate in place was set upon a load cell and the weight of the system was recorded. For all the results except those obtained from corrugated aluminum, the boiling rates could be correlated with a one-dimensional heat transfer model which contains a single characterizing parameter for the substrate. According to this model, the controlling step in heat transfer is the conduction in the substrate and the theory predicts that the mass of LNG boiled off is proportional to square root of time. Figure II-7 shows the good agreement between theory and experiments for LNG boiled on insulated concretes. The boiling rate data of LNG on corrugated aluminum over soil were found to be lower than the others.

Boiling of Cryogenic Liquids on Water

The current increase in marine transportation of cryogens motivated the study of cryogenic liquids boiling on water so as to assess the safety of such transportation. To date, only a few studies have been made.

Burgess et al. (1970, 1972) conducted several preliminary tests where liquid nitrogen, methane and LNG were boiling on a water surface. Spills were made in both the confined and unconfined modes.

Confined spills were carried out in an aquarium placed on a load cell, and the continuous mass change was recorded during vaporization. It was found that for the first 20-40 seconds, the boiling rate of LNG was relatively constant with a rather high average value of 0.18 kg/m^2-s. The corresponding heat flux

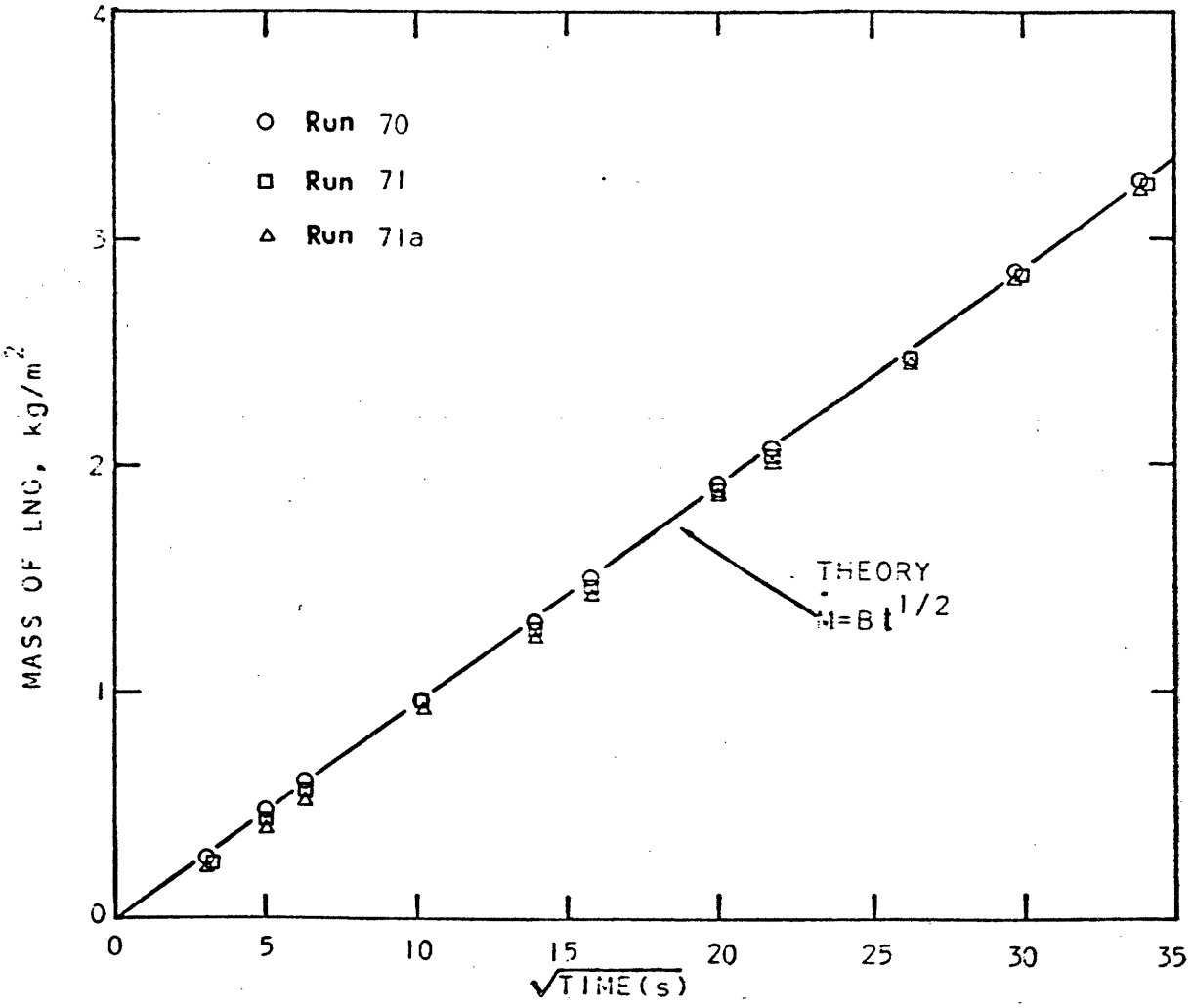

FIGURE 11-7: EXPERIMENTAL BOIL-OFF DATA FOR LNG ON INSULATED CONCRETE(REID AND WANG, 1978).

calculated based on the heat of vaporization of pure methane was 92 kW/m^2. This rate decreased after an ice layer formed on the water surface. LNG was also observed to foam on water.

The aquarium was later replaced by a polystyrene ice chest (1972). LNG spills using this chest yielded a heat flux of about 77 kW/m^2. No explanation was given for the difference between this value and the value of 92 kW/m^2 obtained in 1970.

Similar confined spills using pure liquid methane showed that the boiling rate increased with time and with the quantity spilled. For LNG the vaporization rate was independent of the amount spilled.

Confined spills of liquid nitrogen revealed a heat flux of 32 kW/m^2, much lower than that for LNG. Although ice was also formed in the nitrogen spills, its formation was slower than for LNG. No foaming was observed in the nitrogen spills.

Liquid nitrogen boiling on water yielded results (~32 kW/m^2) close to those reported for boiling on solids (~25 kW/m^2 by Merte and Clark (1964)). However, LNG and methane experiments gave boiling heat fluxes (~80 kW/m^2) which were much larger than the corresponding values for boiling on solids (~37 kW/m^2 by Sciance et al. (1967)). Explaining this large difference involved postulating a chemical interaction between the hydrocarbon and water and that hydrate formation was taking place. An aluminum sheet was placed on the top of the water thus eliminating the possibility of any direct water-cryogen interaction. The heat flux of LNG decreased from 77 to 36 kW/m^2. For liquid methane it decreased from 82 to 25 kW/m^2. Finally, for liquid nitrogen, the heat flux decreased from 32 to 26 kW/m^2

Hydrate formation could have been inhibited by the aluminum sheet if the hydrate indeed forms when hydrocarbons are spilled on water. However, Burgess et al. measured the rates of formation of methane hydrate and concluded that

the hydration rate was too low to account for the large difference in heat fluxes of methane boiling on water and on an aluminum sheet.

For LNG or methane spills on water, film and perhaps transition boiling first occur due to the large initial temperature difference. As patches of ice form and cool, nucleate boiling becomes the likely heat transfer mechanism. For liquid nitrogen, heat transfer occurs by film boiling. As Berenson (1962) observed, the microstructure of the surface is not important for film boiling but it has a strong effect on nucleate or transition boiling. This explains why the boiling rate of nitrogen with an aluminum sheet placed on the water surface was not greatly different than that from spilling directly. The slightly larger value of 32 kW/m^2 for liquid nitrogen on water is probably due to the agitation of water and its mixing with nitrogen.

Boyle and Kneebone (1973) carried out a few tests where LNG was spilled on sea water contained in basins of 0.37 m^2 and 0.84 m^2 in area, placed on a load cell. The boil-off rates were observed to increase with time until reaching a maximum at the point of "pool break-up". At this point the amount of LNG was no longer sufficient to cover completely the water surface. The thickness of LNG layer at pool break-up point was found to be about 1.8 mm.

The explanation regarding Boyle and Keenbone's observation that the boiling rate of LNG on water increased with time involved the change of heat transfer mechanism from film boiling to nucleate boiling. This occurred as the water surface became progressively covered with ice and the fraction of heavy hydrocarbons increased.

Boyle and Kneebone also noted that an increase in the initial quantity of LNG spilled (per unit area) is reflected by an increase in the boil-off rate. Decreasing the initial water temperature increased the evaporation rate significantly. The boiling rate was strongly dependent upon the chemical composition of LNG. However, the work reported by Boyleand Kneebone is of a preliminary

nature. Their results are of limited significance because the quantity spilled was often insufficient to cover the water surface with a continuous film.

Drake et al. (1975) investigated the transient boiling of liquid nitrogen, methane, ethane and LNG on water. A well-insulated triple-wall container was used in the experiments. It was placed on a load cell to measure continuously the mass of the system. The water temperature and vapor temperature were recorded during the experiments by thermocouples. The initial water temperature was varied from 6 to 60°C and the quantity spilled ranged from about 2 to over 10 kg/m^2.

Table II-1 presents the experimental results by Drake et al.. It was observed that water temperatures a few mm below the interface changed little in all tests, but ice formed rapidly. The initial water temperature had little effect on the boil-off rates for all cases. For liquid nitrogen, the boiling rate was very sensitive to the initial quantity spilled. Nitrogen vapors were quite superheated. For large spills, the degree of superheat was 40-50°C but for small spills, it increased to 90-100°C.

Liquid methane and liquid ethane did not show sensitivity of the boiling rate to the initial mass spilled. Some superheat was noted in the vapor for methane spills but this decreased appreciably with the larger spill tests. In case of ethane, essentially no superheat was noted in the vapor. The vapor superheat information implies that liquid nitrogen and methane initially film boil on water whereas liquid ethane nucleate boils. This is further supported by the more rapid ice formation observed for ethane spills.

The boiling rates of nitrogen were lower than those observed for methane which in turn were lower than those for ethane. The boil-off rate of methane increased continuously with time. For ethane, initially the evaporation rate increased until a coherent ice crust formed and then the heat flux decreased significantly.

TABLE II-1

DRAKE et al.'s RESULTS FOR BOILING OF CRYOGENIC LIQUIDS ON WATER

MATERIAL	NITROGEN	METHANE	ETHANE	LNG (1)*	LNG (2)**
Heat Flux High	50	90	120	120	150
$\dot{Q}$ (KW/m^2) Low	20	40	30	50	50
Effect on $\dot{Q}$ due to an increase in:					
Water Temperature	same	same	same	same	--
Cryogen Mass	up	same	same	up	up
Time	down	up	up down after ice formation	up	up
Foaming?	no	no	no	yes	yes
Vapor Superheat?	40-100 K	10-30 K	--	5-10 K	5-10 K

* LNG Composition: C_1 = 98.2%, C_2 = 1.6%, C_3 = 0.11%, C_4 = 0.07%

** LNG Composition: C_1 = 89.4%, C_2 = 8.2%, C_3 = 2.0%, C_4 = 0.4%

Addition of small amounts of heavier hydrocarbons increased the boiling rate of methane significantly, as shown in Figure II-8.

Two ranges of LNG composition were studies. For both ranges the boiling rates of LNG increased with time and significant foaming occurred. Figure II-9 indicates that increasing the fraction of heavy hydrocarbons has the same effect of enhancing the vaporization rate of LNG.

Dincer et al. (1977) investigated the effect of the initial water temperature on the boiling rate of liquid nitrogen and methane. The experimental apparatus was the same used by Drake et al. except for minor modifications.

The boil-off rates for liquid nitrogen and methane agreed well with those reported by Drake et al.. The initial water temperature had no effect on the vaporization rates in either case. However, there was a significant difference in the pattern of water temperatures depending upon the initial water temperature.

In experiments where the initial water temperature was below 20°C, coherent ice formed almost immediately on the surface and the water temperature beneath this ice sheet changed little during the test. When the initial water temperature exceeded 25°C, the surface ice still formed but quite slowly. The water temperature in all locations decreased uniformly, although the largest decrease always occurred in the immediate vincinity of the interface.

From their experiments, Dincer et al. concluded that at low initial water temperatures, heat transfer to the cryogen occurred through a growing ice shield with little effect on the underlying water. On the other hand, if the water was initially warm, ice formed more slowly and cool surface water convectively descended and mixed thoroughly with the bulk water phase.

Reid and Smith (1978) conducted spills of liquid propane, ethane, n-butane and LPG on water in an adiabatic calorimeter. The boiling rate was measured as a function of time. For a rapid spill of propane or LPG on water, the cryo-

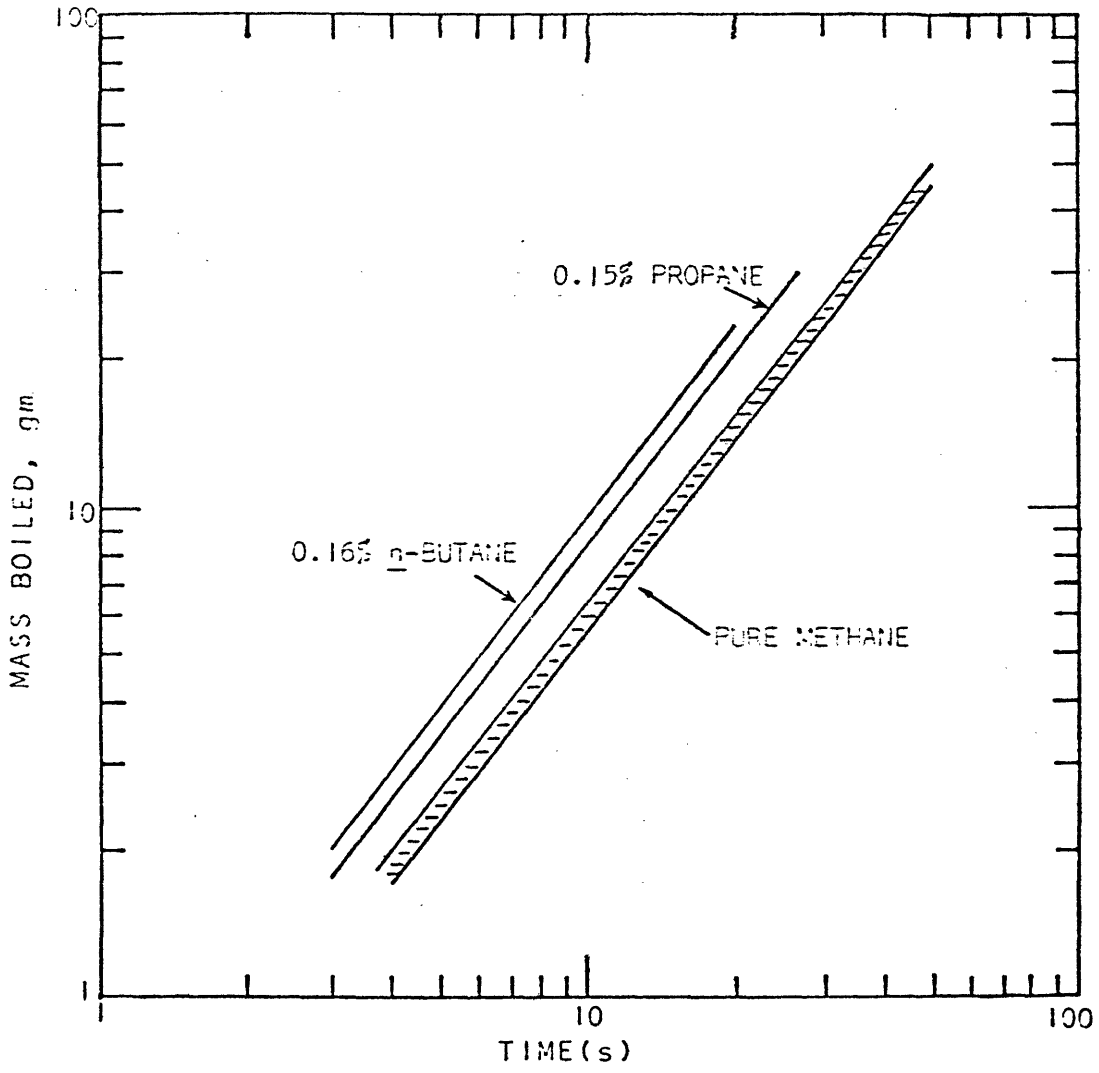

FIGURE II-8: BOILING OF METHANE MIXED WITH TRACE HEAVIER HYDROCARBONS ON WATER(DRAKE et al.,1975).

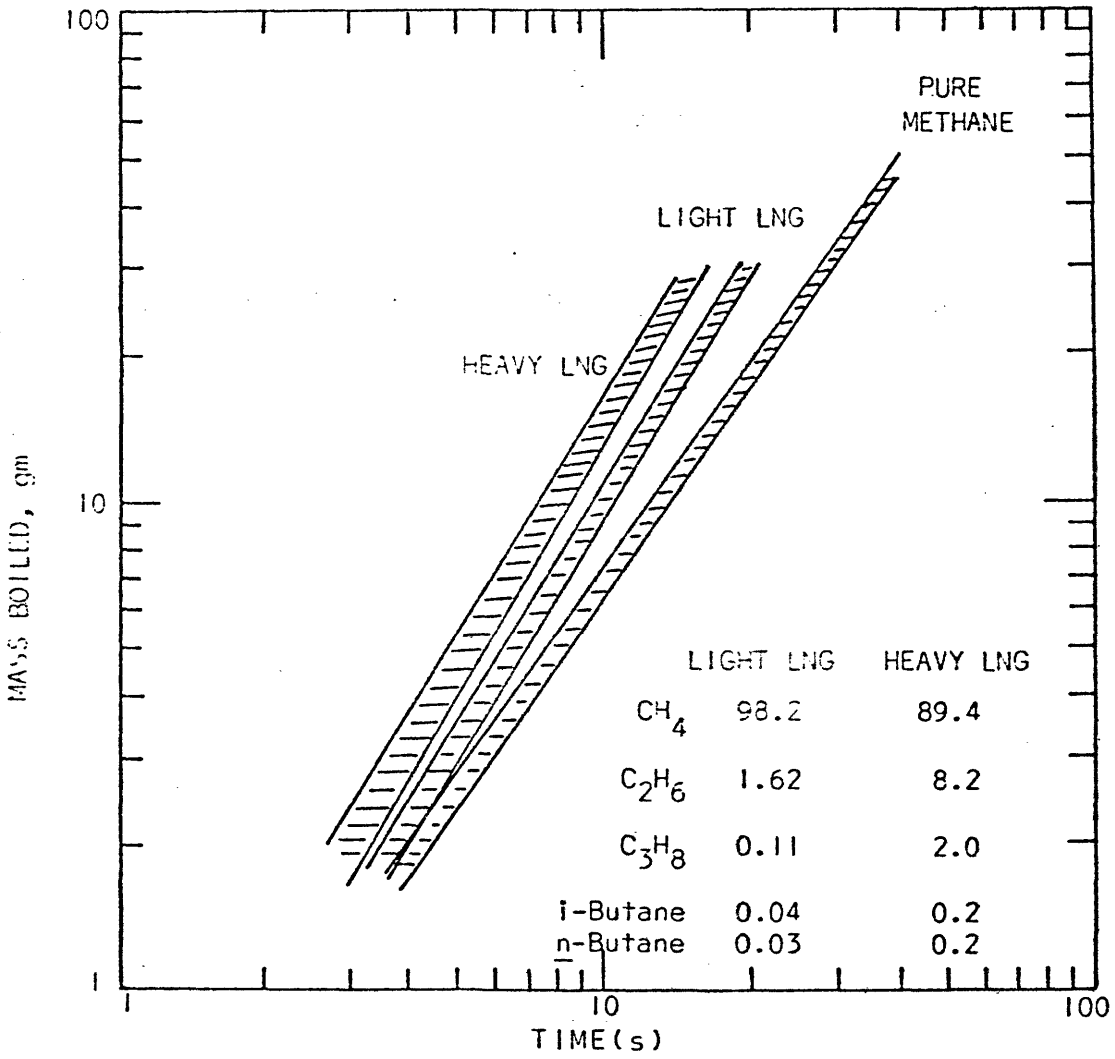

FIGURE II-9: EFFECT OF COMPOSITION ON THE BOILING HEAT TRANSFER OF LNG ON WATER(DRAKE et al.,1975).

gen boiled violently and rapidly for a very short period following the spill. The water surface was severely agitated and ice formed almost instantaneously on the surface. Within a few seconds, the water surface was covered by a rough ice sheet. From this time on, heat transfer became controlled by conduction through the ice and the boiling rate decreased as the ice grew thicker. The boiling at this stage could be described by a moving-boundary heat-transfer model. According to this model, the boil-off rate was inversely proportional to the square root of corrected time $(t - \tau^*)$, where τ^* is a time of the order of 2-4 seconds, associated with the initial, ill-defined boiling phase before ice formation. A detailed description of this model is give in Appendix-I. The translation of heat flux into mass boiled off yielded a linar relationship between the mass boiled off and $(t - \tau^*)^{1/2}$. Figure II-10 shows the agreement between theory and experiment.

For a slow (about 5 seconds duration) and smooth spill of propane or LPG on water, the initial violence is absent with little impacting force. The boiling behavior can be described by the moving boundary model with the value of τ^* equal to zero. A reasonable agreement between model and experiment is noted in Figure II-11.

Reid and Smith showed that the addition of small amounts of ethane or n-butane to propane had no observable effect on the boiling rate of propane. This result contrasts with that observed for LNG which showed strong composition dependence.

Opschoor (1977) modelled the evaporation of LNG on water in both confined and unconfined modes. By assuming that the energy to vaporize the LNG came from freezing water and cooling the ice below the freezing temperature, Opschoor obtained the following equation for the evaporation rate of LNG spilled on a confined ice surface:

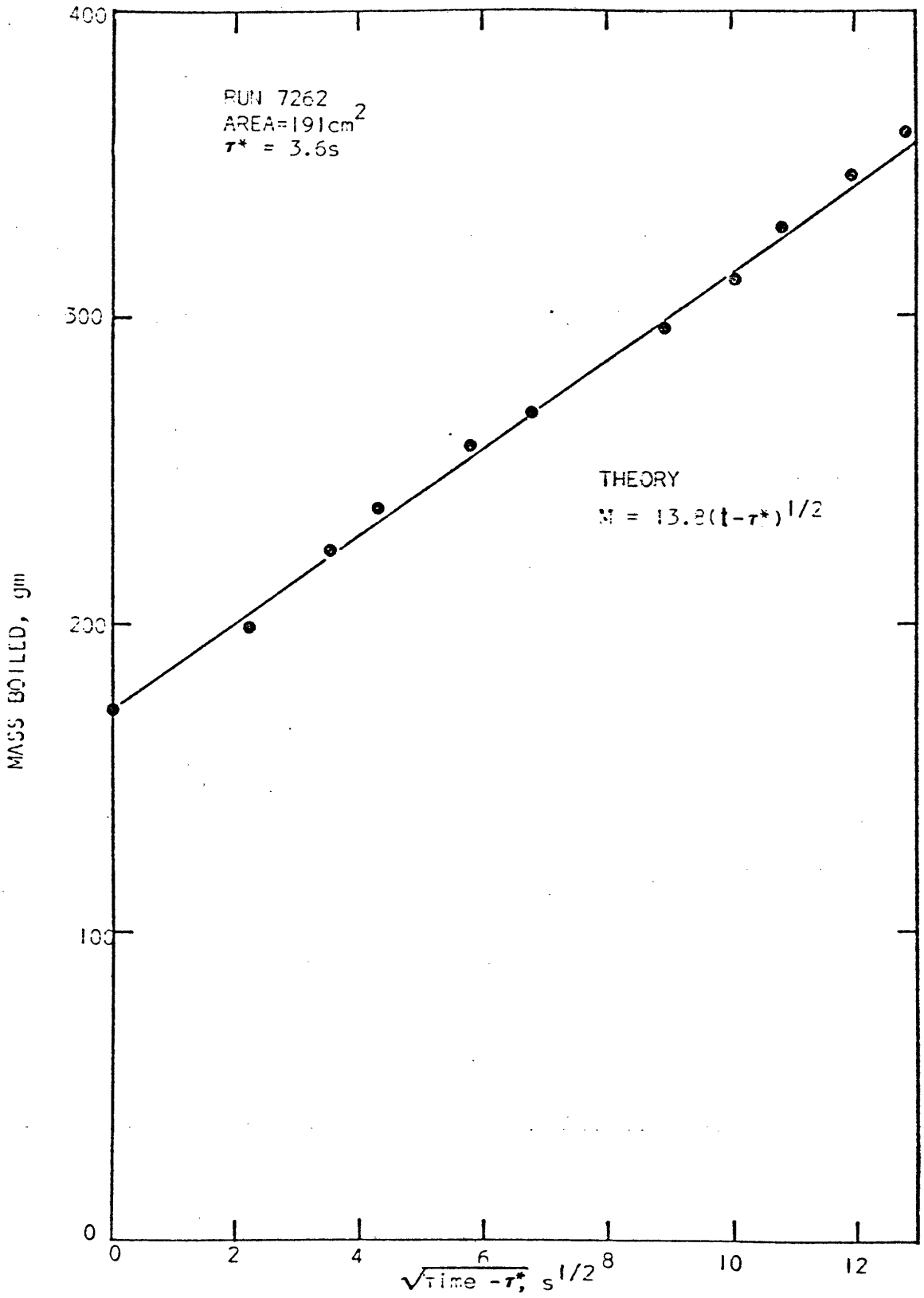

FIGURE II-10: BOIL-OFF DATA FOR A PROPANE SPILL ON 22°C WATER (REID AND SMITH, 1978).

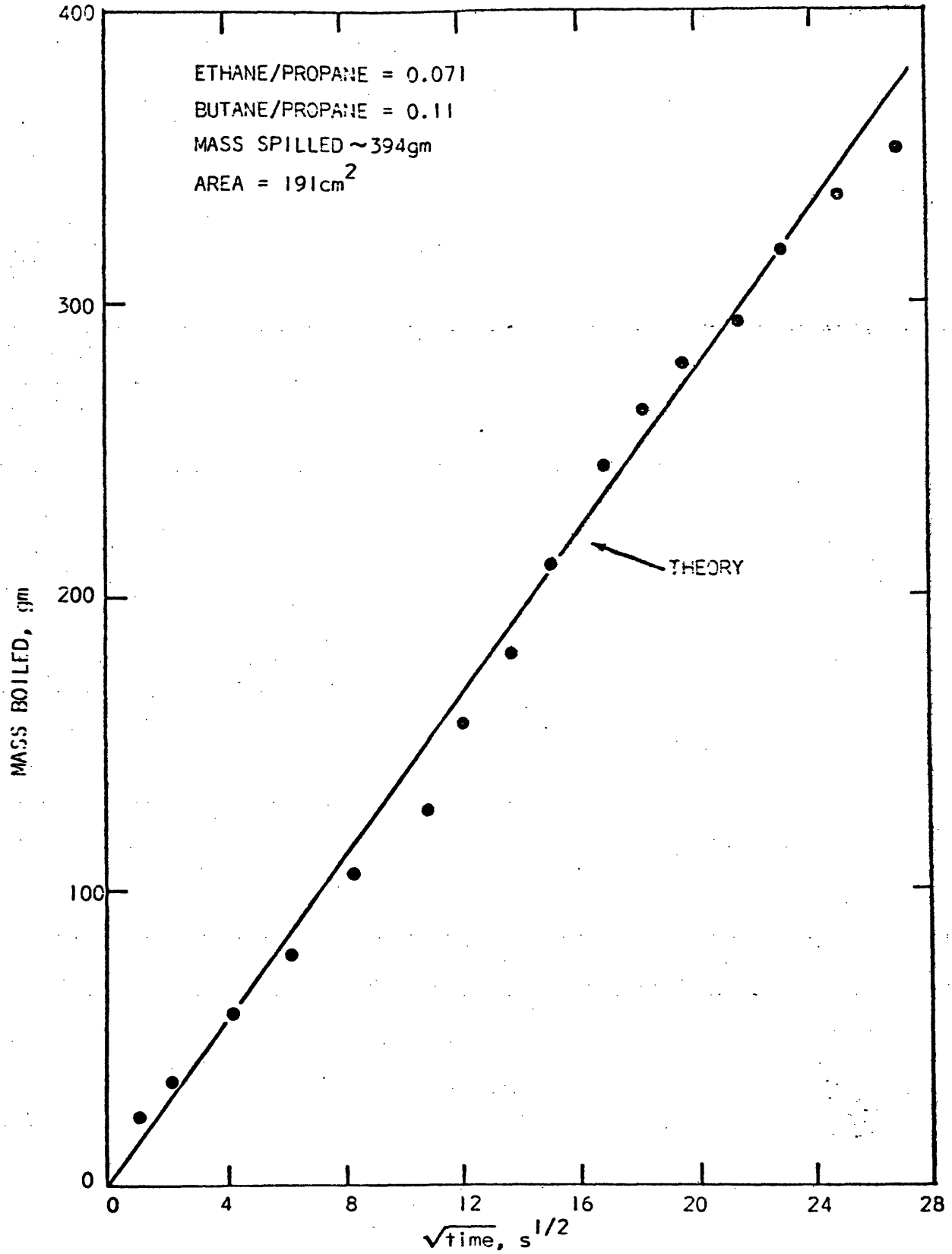

FIGURE II-11: BOIL-OFF DATA FOR AN LPG SPILL ON WATER WITH A SLOW SPILL(REID AND SMITH, 1978)

$$\dot{m} / A = 0.517\ t^{-1/2}\ (kg/m^2s) \qquad (II\text{-}1)$$

Opschoor indicated that an ice layer formed on the water surface about 20 seconds after the start of the spill. Equation (II-1) applies only for the period after ice has formed. To arrive at a method for calculating the, evaporation rate for the entire boiling process, Opschoor examined the data reported by Boyle and Kneebone (1973) and proposed the following equation for estimating the boiling rate for the initial period before ice formation:

$$\dot{m} / A = 0.008\ t\ (kg/m^2s) \qquad 0 \leq t \leq 25\ sec \qquad (II\text{-}2)$$

The values of the coefficients in these two equations were determined by the best least-squared-error fit for two sets of experimental data; they have no theoretical justification. Although Opschoor recognized that film boiling occurred initially and that the LNG saturation temperature would increase as methane evaporates preferentially, he was unable to incorporate these effects in his model.

Valencia and Reid (1979) studied the compositional effect on the boiling rates of LNG spilled on a confined water surface. The experiments were conducted in an adiabatic calorimeter placed on a load cell. Similar to the results obtained by Drake et al. (1975), Valencia and Reid observed that increasing the concentration of heavier hydrocarbons resulted in higher boiling rates for LNG. The evaporation rate of LNG varied with its composition, water temperature, as well as with the condition of the water surface. The authors proposed a qualitative theory to explain the effect of hydrocarbon composition on the boiling rates of LNG spilled on water.

LNG film boils immediately after contacting water and vapor bubbles begin to form. The bubbles consist almost entirely of methane due to the large difference in the volatility of methane compared to ethane or propane. The re-

maining hydrocarbon liquid therfore becomes enriched with the less volatile components. At the lower portion of the bubble, the concentrations of ethane and propane increase with a concomitant decrease in pressure. Liquid flow occurs and the vapor film collapses near the base and the buoyant bubbles carries the methane-depleted liquid in its wake while fresh LNG replaces it at the hot surface. The cycle is then repeated. Therefore the heat transfer rates increase near the interface, small bubbles are produced and ice forms more rapidly. With ice, the surface temperature drops and eventually nucleate boiling results. Because of the increasing thermal resistance from the growing ice shield, boiling rates eventually decrease. This theory offers a plausible mechanism to explain the significant increase in the initial vaporization rate of LNG as the concentration of the heavy hydrocarbons increases.

Valencia and Reid employed these qualitative concepts coupled with a vapor-liquid equilibrium theory, which tracks the changes in LNG composition and temperature to develop a quantitative model to predict the boil-off rates for LNG spilled on water. Good agreement was obtained between theory and experiment with the use of a single adjustable parameter that is related to the initial LNG composition.

A summary of the information on the boiling of methane and LNG on water is given in Tables II-2 and II-3. In the case of methane, the boiling rate increases with time and is independent of the initial water temperature. Drake and Valencia calimed that the initial quantity of methane spilled did not affect the evaporation rate whereas Burgess reported an increase in heat flux with the amount spilled. No foaming has been observed by either group. Drake and Valencia noted that the evaporated methane was superheated, but the degree of superheat decreased as the quantity of liquid methane spilled increased.

The disagreement becomes more apparent when LNG mixtures are considered.

TABLE II-2

BOILING OF LIQUID METHANE ON WATER

Investigator		Burgess	Drake	Valencia
$\dot{Q}$ (Kw/m^2)	High	82	90	120
	Low	51	40	25
Effect on $\dot{Q}$ due to an increase in:				
Water Temperature		--	same	same
Cryogen Mass		up	same	same
Time		up	up	down, up after collapse of vapor film
Foaming?		--	no	no
Vapor Superheat?			0-10 K(>5.0kg/m^2) 10-30 K(<5.0kg/m^2)	0-5 K(>5.0kg/m^2) 10-20K(<5.0kg/m^2)

TABLE II-3

BOILING OF LNG ON WATER

Investigator		Burgess		Boyle	Drake		Valencia	
$\dot{Q}$ (Kw/m^2)	High		153	100	120	150	190	
	Low	(92)	(77)		50	50	25	
	(Ave)							
LNG Composition	C_1	94.5	92.0	94.7	98.2	89.4	82.9	84.9
	C_2	3.4	6.3	4.5	1.6	8.2	10.1	10.1
	C_3	0.9	0.1	0.1	0.11	2.0	7.0	5.0
	C_4			0.2	0.07	0.4		
	other	1.2	1.6	0.5				
Effect on $\dot{Q}$ due to an increase in: Water Temperature		-------		down	same		-----	
Cryogen Mass		same		up	up		up	
Time		same down after ice formation		up, down after pool break up	up		up, down after ice formation	
Foaming?		yes		----	yes		yes	
Vapor Superheat?		---		-----	5-10 K		no	

Boyle showed that the boil-off rate of LNG decreased with the initial water temperature, while Drake reported no change. The vaporization rate was sensitive to the quantity spilled and increases with time; Burgess is the only investigator that disagreed with this statement. A maximum has been observed for the boiling rate's variation with time. Boyle believed it to occur at the time of LNG pool break-up, Burgess and Valencia thought the maximum occurred after ice formation, and Drake observed no maximum. Evaporation of LNG is a complicated phenomenon in which composition plays an important role. The reported heat fluxes range from 25 to 190 kW/m^2.

Spreading of Non-Volatile Liquids on Water

Few studies of oil spreading on water have been conducted with the goal of providing information to evaluate the effects of marine oil transportation accidents.

Fay (1969, 1971) identified four basic forces that either cause or retard spreading in the physical process of oil moving over an undisturbed water surface. The force of gravity acts downward and causes a sidewise spreading motion of a floating oil film by creating an unbalanced pressure distribution in the pool of oil and the surrounding water. This force is proportional to the oil layer thickness and its gradient as well as the density difference between oil and water. As the oil film spreads and becomes thinner, the gravity force diminishes. At the front edge of the expanding oil slick an imbalance exists between the surface tension at the water-air interface and the sum of surface tensions at the oil-air and oil-water interfaces. The net difference is a force which acts at the edge of the oil film, pulling it outwards. This spreading force is independent of the oil film thickness and does not decrease as the oil film thins out. Eventually, for very thin slicks, the surface tension force will become the predominant spreading force.

These spreading forces are counterbalanced by the inertia of the oil film

and a frictional drag force from the water below the oil slick. The inertia of the oil phase decreases with time because the oil layer becomes thinner as it spreads, but the inertia of the viscous layer of water below the oil increases with time as its thickness grows. Consequently, the viscous retardation eventually outweighs the inertial resistance of the oil layer itself.

Fay (1969) used an order-of magnitude analysis to recognize three principle flow regimes through which the spreading oil film passes. The first regime occurs at short times: the spreading rate is controlled by a balance of gravity and inertial forces. The second regime occurs later when the oil slick has become thinner. The viscous drag replaces the inertial force as the predominant retarding force, while the gravitational force continues to be more important than the surface-tension driving force. In this regime the spreading rate depends on a balance of the gravity and viscous forces. The third regime becomes important at very late times when the spreading of the very thin oil slick is promoted by the surface tension force and retarded by the viscous force.

The following discussion will be restricted to the regime of interest in this work, i.e., the gravity-inertia regime.

Fannelop and Waldman (1972) theoretically analyzed the dynamics of oil slicks on calm water. They neglected the vertical acceleration and assumed that the oil was in hydrostatic equilibrium in the vertical direction. In the gravity-inertia regime, the gravitational force balances the inertia of the oil. Assuming the oil density is constant, the conservation of mass and the equation of motion for a one-dimensional configuration are expressed as follows:

$$\frac{\partial h}{\partial t} + \frac{\partial}{\partial x}(hU) = 0 \qquad \text{(II-3)}$$

$$\frac{\partial U}{\partial t} + U\frac{\partial U}{\partial x} = -g\Delta\frac{\partial h}{\partial x} \qquad \text{(II-4)}$$

where x is the spreading direction and Δ is defined as $(\rho_{water}-\rho_{oil})/\rho_{water}$. U is the spreading velocity of the oil in x-direction, h is the oil thickness and g is the gravitational acceleration. Fannelop and Waldman assumed that the velocity of the leading edge of the oil was analogous to a wave speed in gas-dynamic theory:

$$U_{LE} = [g \Delta h_{LE}]^{1/2} \qquad \text{(II-5)}$$

Integrating equations (II-3) and (II-4) yields the following relation for the one-dimensional spreading of oil slicks on water. The equation gives the spreading distance as a function of time for an instantaneous spill.

$$x = 1.39 \left[\frac{g \Delta V t^2}{w}\right]^{1/3} \qquad \text{(II-6)}$$

where V is the oil volume and w is the width of the channel.

Fay (1971) commented upon Fannelop and Waldman's theory and argued that the oil leading edge was an intrusion. According to von Karman's (1940) famous calculation, the velocity of the leading edge should be:

$$U_{LE} = [2 g \Delta \bar{h}]^{1/2} \qquad \text{(II-7)}$$

where $\bar{h}$ is the thickness of the oil some distance from the leading edge. In Fay's treatment of the oil slick equation (II-7) was used for predicting the velocity of the leading edge, except $\bar{h}$ was replaced with h_{LE}, the thickness of the oil at the leading edge.

Benjamin (1968) has shown that a steady-state intrusion does not take place, so that a speed between $[g\Delta h_{LE}]^{1/2}$ and $[2g\Delta h_{LE}]^{1/2}$ for leading edge is possible.

Hoult (1972a) proposed that the leading-edge boundary condition should be:

$$U_{LE} = [\lambda\, g\, \Delta\, h_{LE}]^{1/2} \qquad \text{(II-8)}$$

and considered λ as experimentally determinable. Using Fannelop and Waldman's assumptions and applying a similarity transformation to solve equations (II-3) and (II-4), Hoult obtained a spreading law similar to Fannelop and Waldman's except the coefficient η is undetermined but can be related to λ.

$$x = \eta \left[\frac{g\, \Delta\, Vt^2}{w}\right]^{1/3} \qquad \text{(II-9)}$$

where

$$\eta = \left[\frac{4}{9\lambda} - \frac{2}{27}\right]^{-1/3} \qquad \text{(II-10)}$$

If Fay's leading-edge boundary condition ($\lambda = 2$) was used, the value of η should be equal to 1.89 instead of 1.57 reported in Hoult's paper. Hoult also derived the following equation which predicts the thickness profile of the oil during spreading:

$$\frac{h(x, t)}{h(0, t)} = 1 + \frac{\left[\frac{4}{9\lambda} - \frac{2}{27}\right]^{2/3} \xi^2}{\left[\frac{4}{9\lambda} - \frac{1}{9}\right]} \qquad \text{(II-11)}$$

where

$$\xi = x \left[\frac{g\, \Delta\, Vt^2}{w}\right]^{-1/3} \qquad \text{(II-12)}$$

Figure II-12 shows that the theoretical thickness profile rises smoothly from the origin to the spreading front, using Fay's leading-edge boundary condition.

Experimental studies of the gravity-inertia spreading regime in a one-

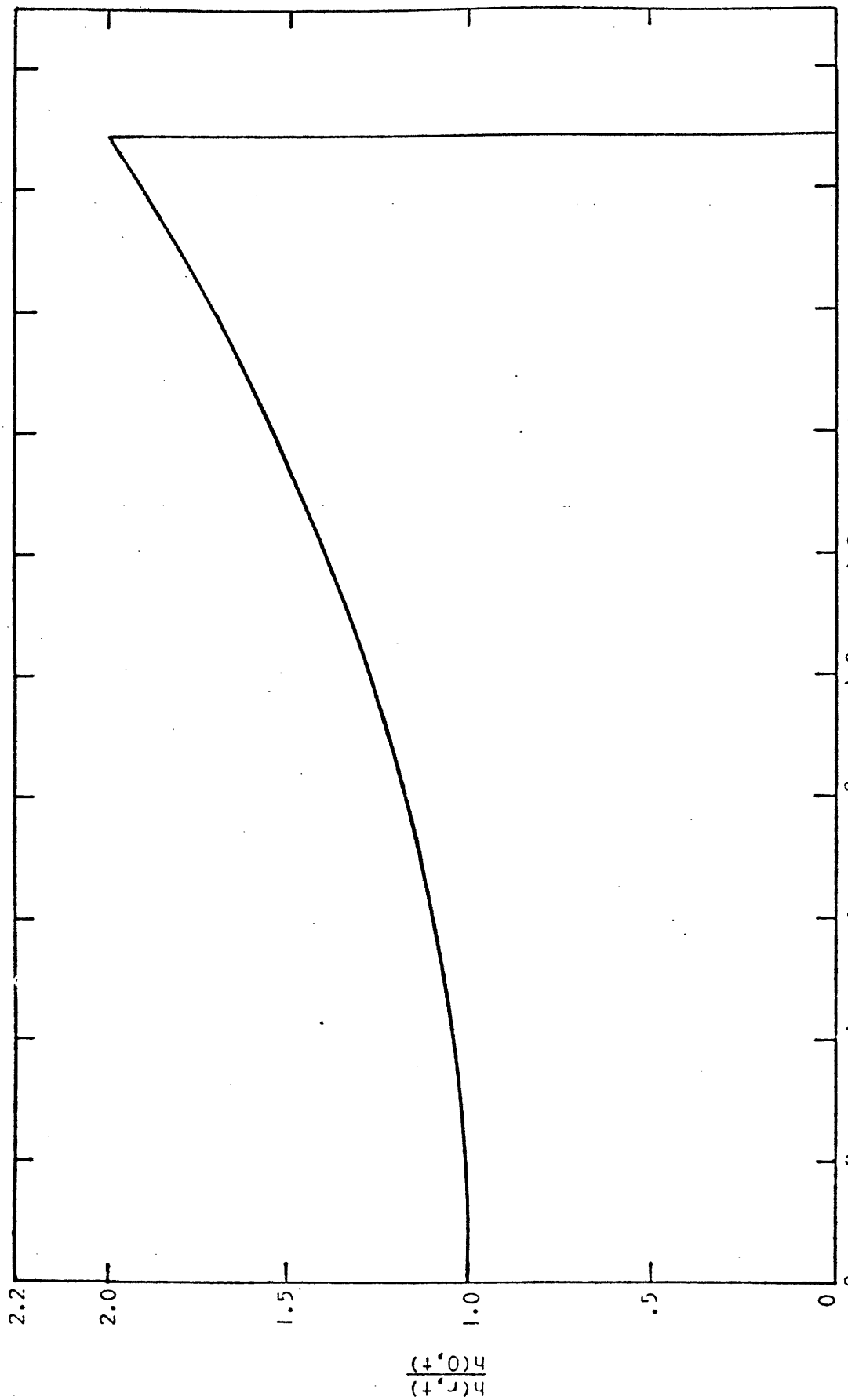

FIGURE 11-12: THEORETICAL THICKNESS PROFILE IN THE GRAVITY-INERTIA REGIME FOR A NON-VOLATILE LIQUID SPILLED ON WATER(ONE-DIMENSIONAL CONFIGURATION)(HOULT,1972a).

dimensional configuration were conducted by Suchon (1970). The experimental apparatus was a plexiglass tank 2 feet wide, 7 feet long and 1 foot deep. Typical experimental results are plotted in Figure II-13. Hoult's theory agrees well with the experiments. The value of the intercept is equal to 1.6, which is taken as η in equation (II-9), and the corresponding λ can therefore be evaluated indirectly as 1.40 from equation (II-10). Furthermore, Suchon's photographic study of the leading edge of the oil slick shows that the oil slick is thickest at the spreading front and thins out toward the spill origin; this profile is consistent with Hoult's theory.

Boiling and Spreading of Cryogenic Liquids on Water

Instantaneous Spills

A review of the literature indicates that few experiments have examined simultaneous boiling and spreading rates for any volatile cryogen. Burgess et al. (1970) used an overhead camera to study LNG spills from a point source onto an open pond and reported that LNG spread with a constant radial velocity of 0.38 m/s. Figure II-14 presents the pool diameter as a function of time for several LNG spills on water. In general the relationship of constant spreading rate was obeyed in the early part of the tests but later the spreading rate decreased.

In Burgess et al.'s analysis, with the radial spread velocity u, the pool diameter d and the corresponding area A are given by

$$d = 2ut \qquad \text{(II-13)}$$

$$A = \frac{\pi d^2}{4} = \pi(ut)^2 \qquad \text{(II-14)}$$

Assuming a constant heat flux $\dot{q}$, the volume of LNG evaporated at time τ is

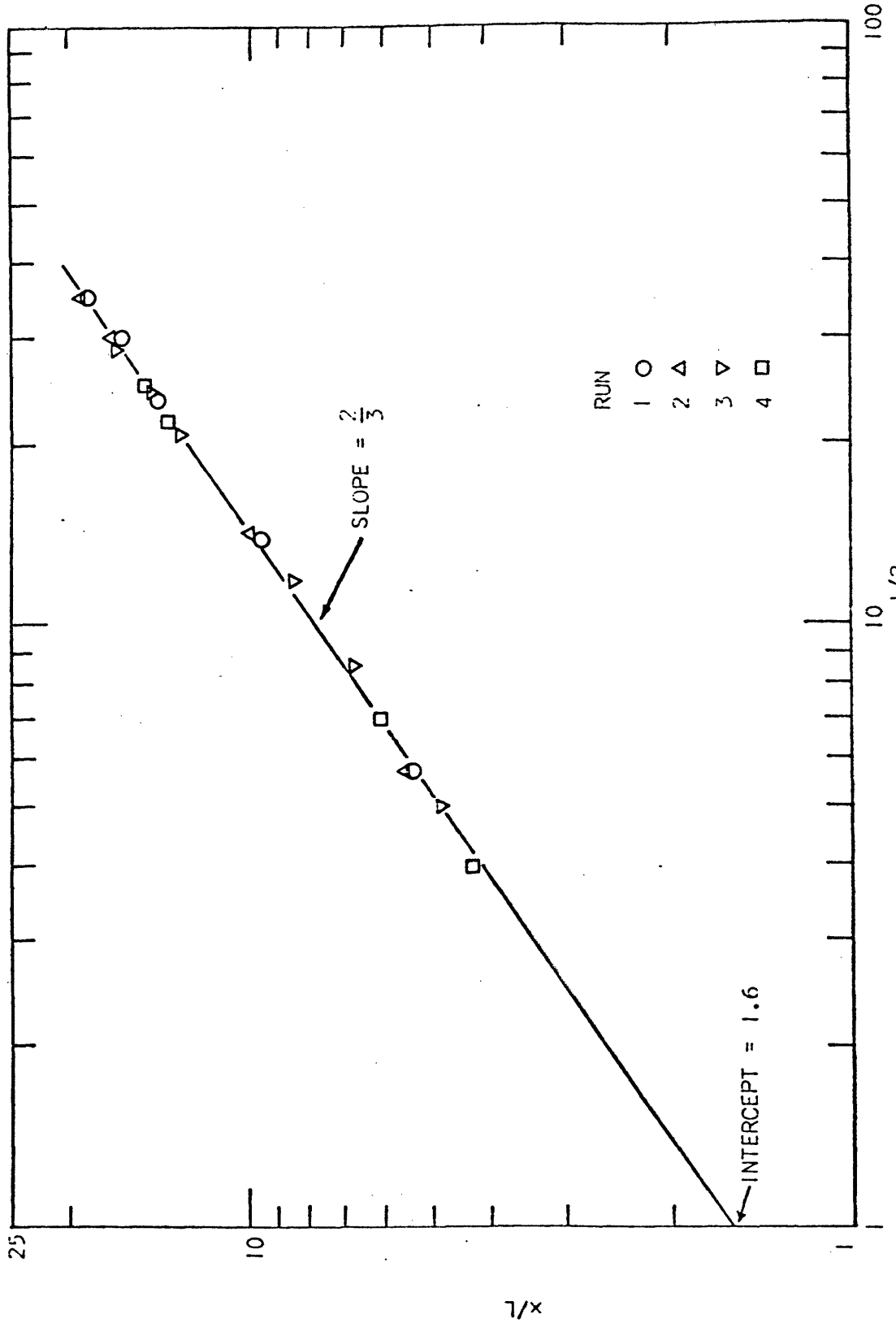

FIGURE II-13: DIMENSIONLESS CORRELATION OF SPREADING DISTANCE AS A FUNCTION OF TIME FOR THE ONE-DIMENSIONAL SPREADING OF OIL ON WATER IN THE GRAVITY-INERTIA REGIME (SUCHON, 1970).

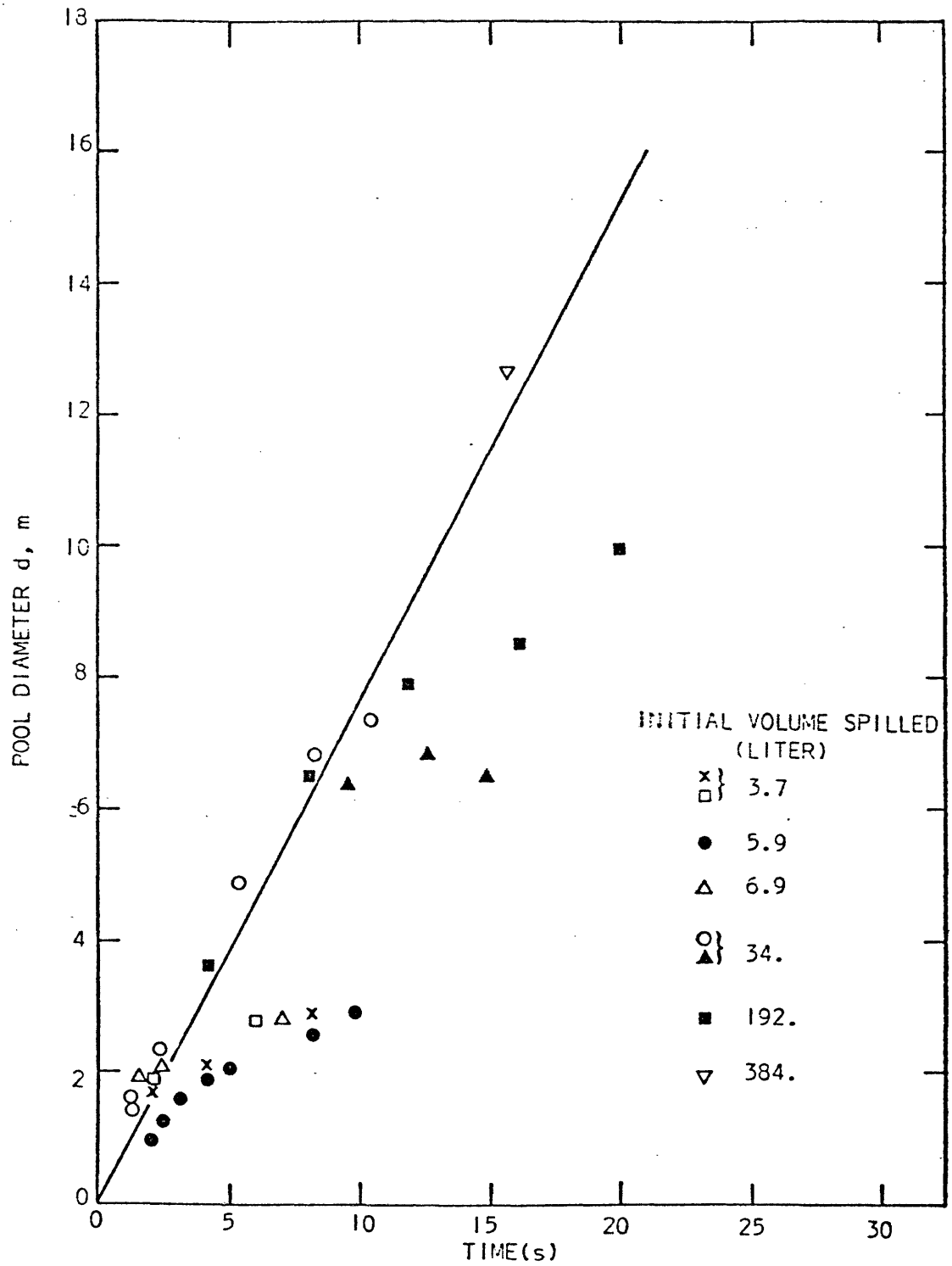

FIGURE II-14: POOL DIAMETER AS A FUNCTION OF TIME FOR LNG SPILLS ON WATER(BURGESS et al.,1970).

$$V = \int_0^{\tau} \left[\frac{\dot{q}A}{\Delta H_v \rho_L}\right] dt = \left(\frac{\pi}{3}\right)\left[\frac{\dot{q} u^2 t^3}{\Delta H_v \rho_L}\right] \qquad \text{(II-15)}$$

where ρ_L is the density of LNG and ΔH_v is its heat of vaporization. The time required to evaporate an initial quantity V_o is

$$\tau = \left[\frac{3 \Delta H_v \rho_L V_o}{\pi \dot{q} u^2}\right]^{1/3} \qquad \text{(II-16)}$$

Burgess et al. used $\dot{q} = 92$ kW/m^2 (obtained from confined LNG spills). With $\rho_L = 425$ kg/m^3, $\Delta H_v = 511$ kJ/kg, and u = 0.38 m/sec, equation (II-16) yields

$$\tau = 24.9\ V_o^{1/3} \quad (V_o \text{ in } m^3, \tau \text{ in sec}) \qquad \text{(II-17)}$$

The maximum pool diameter d_{max} is then obtained by combining equations (II-13) and (II-17), yielding

$$d_{max} = 19.0\ V_o^{1/3} \text{ (m)} \qquad \text{(II-18)}$$

Boyle and Kneebone (1973) made three spills of LNG on a pond and measured the pool diameter at the instant of time when the pool began to break up into descrete patches. Their data are given in Table II-4. Note that the spreading rate decreases as the initial quantity of LNG spilled increases. This is inconsistent with the findings of Burgess et al., who claim the spreading rate is constant and independent of the amount spilled.

Boyle and Kneebone claimed that, when the thickness of LNG decreases to approximately 1.8 mm, there is no longer a coherent LNG layer and discrete patches of LNG spontaneously form. With this assumption, they computed the required average evaporation rate necessary to produce this layer thickness at the experimentally observed time for pool break-up. The evaporation rate was equal to

TABLE II-4

Boyle and Kneebone Boil/Spread Data for LNG

Spill Size, m^3	2.24×10^{-2}	4.48×10^{-2}	8.97×10^{-2}
Pool Diameter at Break up, m	3.96	5.64	7.32
Time to Pool Break-up, s	2.75	4.5	9.5
Time to Complete Evaporation, s	24.	33.	35.
Average Spreading Rate, m/s	1.43	1.25	0.76

15 kW/m^2, a value significantly below that suggested by Burgess et al. (92 kW/m^2).

Boyle and Kneebone also claimed that in a spreading situation, ice did not form and boiling rates should be quite low compared to that for confined area spills. Recall that in confined area spills ice quickly develops and most boiling occurs in the nucleate boiling regime on a thin ice crust.

Other studies of boiling and spreading of cryogenic liquids on water have been theoretical and based predominantly upon studies of non-volatile oil spilled on water.

Hoult (1972b) coupled the evaporation and spreading rates of LNG and was able to predict the maximum pool diameter and the time required for complete vaporization for LNG spilled on open water. By assuming that the heat used to evaporate the LNG comes from freezing of the water and the ice temperature varies linearly across the ice layer from the LNG boiling temperature (T_b) at the top to the water freezing temperature (T_f) at the bottom, Hoult obtains the following expression for the ice thickness δ:

$$\delta = \left[\frac{2\, k_i\, \Delta T\, t}{\rho_i\, \Delta H_f}\right]^{1/2} \qquad \text{(II-19)}$$

where $\Delta T = T_f - T_b$, and k_i is the thermal conductivity, ΔH_f the heat of fusion and ρ_i the density of ice. Hoult neglects the volume loss of LNG from vaporization while it spreads and decribes the spreading of LNG with the radial spread law for an instantaneous spill of oil on water by Fannelop and Waldman (1972):

$$r = [g\, \Delta\, V_o\, t^2]^{1/4} \qquad \text{(II-20)}$$

where $\Delta = (\rho_{H_2O} - \rho_{LNG})/\rho_{H_2O}$ and V_o is the initial spilled volume of LNG.

By equating the heat required to evaporate the LNG to that removed from

the ice, Hoult obtains (after neglecting the variation of ice thickness with radial distance) the following expression for τ, the time required to evaporate the initial quantity V_o of LNG:

$$\tau = 0.77 \left[\frac{\rho_L^2 \, \Delta H_v \, V_o}{g\Delta \, \rho_i \, k_i \, \Delta H_f \, \Delta T} \right]^{1/3} \qquad \text{(II-21)}$$

The physical constants of ice are evaluated at an average temperature of $(T_b + T_f)/2$. Substituting the various physical constants into equation (II-21) one obtains

$$\tau = 27.8 \, V_o^{1/3} \quad (V_o \text{ in } m^3, \tau \text{ in sec}) \qquad \text{(II-22)}$$

The maximum pool radius is obtained by combining equations (II-20 and (II-22), yielding

$$r_{max} = 8.1 \, V_o^{5/12} \quad (m) \qquad \text{(II-23)}$$

Hoult's model ingnores the effect of evaporation on the spreading of LNG. This yields an overestimate of the maximum spill radius. Moreover, the sensible cooling of ice and water under the ice is also neglected. In Hoult's analysis, the only thermal resistance is within the ice layer. No surface resistance due to initial film boiling is considered. Consequently, Hoult underestimates the time required to completely vaporize the LNG spilled on water.

Fay (1973) improved Hoult's model by accounting for the sensible heat when the ice is cooled below the freezing temperature. The thickness of the ice layer at time t is given by

$$\delta = \left[\frac{2 \, k_i \, \Delta T \, t}{\rho_i \, \Delta H_f + \frac{1}{2} \rho_i \, c_i \, \Delta T} \right]^{1/2} \qquad \text{(II-24)}$$

where c_i is the heat capacity of ice. Note that the first term in the denominator represents the heat release due to phase change while the second term represents the loss by the ice as it cools.

Fay assumes the thickness (h) of LNG layer is uniform and models the leading edge of LNG as an intrusion. Consequently, for a

$$\frac{dr}{dt} = [2\ g\ \Delta\ h]^{1/2} \qquad \text{(II-25)}$$

where

$$h = \frac{V}{\pi r^2} \qquad \text{(II-26)}$$

combining:

$$\frac{dr}{dt} = \left[\frac{2\ g\ \Delta\ V}{\pi r^2}\right]^{1/2} \qquad \text{(II-27)}$$

Neglecting the volume change from evaporation as LNG spreads, Fay obtains

$$r = \left[\frac{8}{\pi}\ g\ \Delta\ Vt^2\right]^{1/4} \qquad \text{(II-28)}$$

by integrating equation (II-27).

If the heat removed from ice equals that required to evaporate the LNG, the time for the volume V_o of LNG to completely vaporize, τ, is expressed by

$$\tau = \left[\frac{\rho_L^{\,2}\ \Delta H_v^{\,2}\ V_o}{16\pi\ g\Delta\ \rho_i\ k_i\ \Delta T\ (\Delta H_f + \frac{1}{2} c_i\ \Delta T)}\right]^{1/3} \qquad \text{(II-29)}$$

Substituting the physical constants into equation (II-29), Fay obtains

$$\tau = 8.8\ V_o^{1/3}\ (V_o \text{ in } m^3, \tau \text{ in sec}) \qquad \text{(II-30)}$$

The maximum pool radius is given by

$$r_{max} = 5.8\ V_o^{5/12} \quad (m) \qquad \text{(II-31)}$$

Fay's model suffers from the same shortcomings of Hoult's model except that the sensible heat of cooling the ice has been included. It is because of this assumption, that Fay's analysis predicts smaller ice growth and consequently, shorter times required for complete vaporization and a smaller extent of spreading than does Hoult.

For instantaneous spills, Raj and Kalelkar (1973) have obtained an expression for the radial spreading rate of LNG by equating the gravitational spreading force F_{gr} to the inertial resistance force F_i:

$$F_{gr} = \pi\ r\ h^2\ \rho_L\ g\Delta \qquad \text{(II-32)}$$

$$F_i = -\ k\ (\pi\ r^2\ h\ \rho_L)\frac{d^2r}{dt^2} \qquad \text{(II-33)}$$

h is the mean thickness of LNG at time t and ρ_L is assumed constant. The authors used the factor k in equation (II-33) to account for the fact that the inertia of the entire LNG layer is a fraction k of the inertia of the total mass, if the entire mass were being accelerated at the leading edge acceleration d^2r/dt^2. They assume that k remains the same at all times.

Equating F_{gr} and F_i, Raj and Kalelkar obtain the spreading law:

$$h = -\ k\left[\frac{\rho_L}{g\Delta}\right] r\ \frac{d^2r}{dt^2} \qquad \text{(II-34)}$$

They also account for vaporization of the LNG with the following mass conservation equation:

$$V = V_o - \left(\frac{\pi}{\rho_L}\right)\int_o^t \left(\frac{\dot{q}}{\Delta H_v}\right) r^2 dt \qquad \text{(II-35)}$$

and

$$V = \pi r^2 h \qquad \text{(II-36)}$$

where $\dot{q}$ is the boiling heat flux (assumed constant).

Solving equations (II-34) through (II-36) yields a third order non-linear differential equation. Because of the unknown value of k, four boundary conditions are required to specify the solution. The only boundary condition specified by Raj and Kalelkar is that $V = V_o$ at $t = 0$. The remaining three constants are obtained by forcing their solution (for the case $\dot{q} = 0$) to be identical to that of Fannelop and Waldman. Raj and Kalelkar obtained the following equations for the time, τ, for complete evaporation of LNG and the maximum radius of spill at τ:

$$\tau = 0.67 \left[\frac{\rho_L^2 \, \Delta H_v^2 \, V_o}{g \, \Delta \, \dot{q}^2} \right]^{1/4} \qquad \text{(II-37)}$$

and

$$r_{max} = \left[\frac{\rho_L^2 \, \Delta H_v^2 \, g \, \Delta \, V_o^3}{\dot{q}^2} \right]^{1/8} \qquad \text{(II-38)}$$

with $\dot{q} = 92 \text{ kW/m}^2$, for LNG

$$\tau = 21. \, V_o^{1/4} \quad (V_o \text{ in } m^3, \tau \text{ in sec}) \qquad \text{(II-39)}$$

$$r_{max} = 8.7 \, V_o^{3/8} \quad \text{(m)} \qquad \text{(II-40)}$$

Using the same assumptions as those for radial spreading, Raj (1977) developed a boiling-spreading model for instantaneous spills of cryogen on water in a one-dimensional configuration. Since there is no analytical solution to the second order non-linear differential equation which describes this system,

Raj used a first-order perturbation approximation to obtain an analytical expression for the spreading distance x as a function of time t.

$$x = 1.39\left[\frac{g\,\Delta\,V_o\,t^2}{w}\right]^{1/3} + 0.097\left[\frac{\dot{q}}{\rho_L\,\Delta H_v}\right]\left[\frac{(g\Delta)^2\,wt^7}{V_o}\right]^{1/3} \qquad \text{(II-41)}$$

where w is the width of the channel. The time for complete vaporization t_e and the maximum spreading distance x_e for the one-dimensional configuration are given by

$$t_e = 1.09\left[\frac{\left(\frac{V_o}{w}\right)^2}{g\Delta\left(\frac{\dot{q}}{\rho_L\,\Delta H_v}\right)^3}\right]^{1/5} \qquad \text{(II-42)}$$

and

$$x_e = 1.59\left[\frac{g\Delta\left(\frac{V_o}{w}\right)^3}{\left(\frac{\dot{q}}{\rho_L\,\Delta H_v}\right)^2}\right]^{1/5} \qquad \text{(II-43)}$$

Muscari (1974) proposed a numerical model to describe the boiling and spreading process for cryogens spilled on water. In his analysis, it is assumed that hydrostatic equilibrium is established in the vertical direction and the boiling heat flux is constant. For an instantaneous spill in a radial configuration, the conservation equations for mass and monentum follow:

$$\frac{\partial h}{\partial t} + \frac{1}{r}\frac{\partial}{\partial r}(rhU) = -\frac{\dot{q}}{\rho_L \Delta H_v} \qquad \text{(II-44)}$$

$$\frac{\partial U}{\partial t} + U\frac{\partial U}{\partial r} = -g\Delta\frac{\partial h}{\partial r} \qquad \text{(II-45)}$$

where h is the thickness of the cryogen and U is the spreading velocity. Muscari considered the leading edge of the cryogen as an intrusion and used the

the following equation for the leading-edge boundary condition:

$$U_{LE} = (2\ g\ \Delta\ h_{LE})^{1/2} \qquad \text{(II-24)}$$

As the initial condition Muscari applied Hoult's (1972a) oil spill theory at a very small time (t).

A numerical technique called "the method of characteristics" was used to solve equations (II-44) and (II-45). Muscari theoretically predicted the thickness profile for the cryogen at various times during spreading. Figure II-15 shows the thickness profile in dimensionless form. The expression for the dimensionless thickness, radius and time are given in the figure. As seen in this figure, the leading edge is thicker and thins out towards the center of the pool. As the cryogen continues to evaporate, the center part soon becomes cryogen free and a trailing edge appears and moves outward. This is consistent with May and Perumal's (1975) reports that LNG pool break-up starts at the center and the last material to evaporate is a ring at the leading edge.

Muscari's analysis gives predictions for both the spreading-front path and the trailing-edge path, shown in Figure II-16. The intersection of the spreading-front path and the trailing-edge path, determines the time for complete vaporization and the maximum spreading radius, which can be expressed by the following equations:

$$\tau = 0.80 \left[\frac{\rho_L^{\ 2}\ \Delta H_v^{\ 2}\ V_o}{g\ \Delta\ \dot{q}^2}\right]^{1/2} \qquad \text{(II-46)}$$

$$r_{max} = 1.23 \left[\frac{\rho_L^{\ 2}\ \Delta H_v^{\ 2}\ g\Delta\ V_o^{\ 3}}{\dot{q}^2}\right]^{1/8} \qquad \text{(II-47)}$$

Compared to equations (II-37) and (II-38), equations (II-46) and (II-47) predict higher values of τ and r_{max} than those found by Raj and Kalelkar's model.

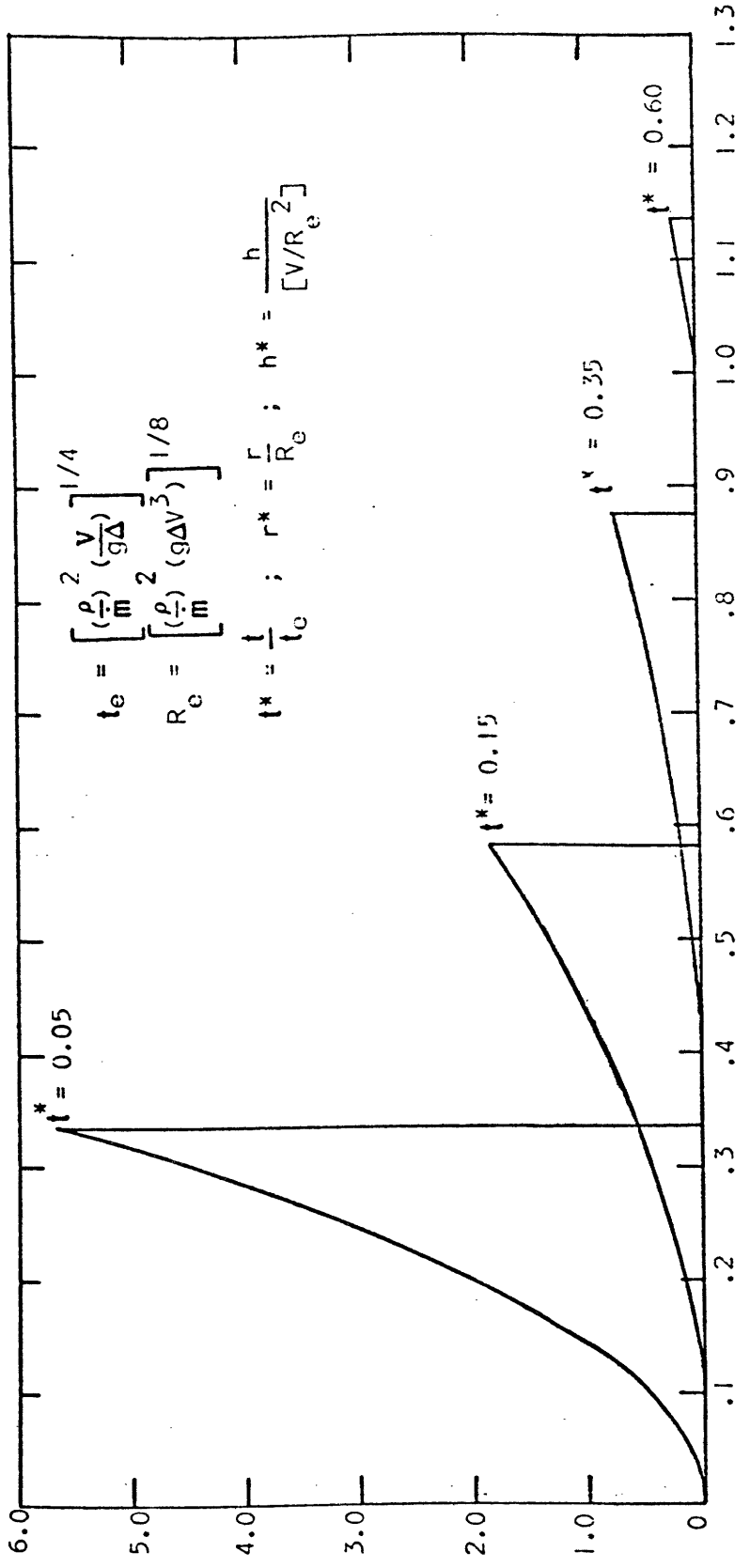

FIGURE 11-15: THEORETICAL DIMENSIONLESS THICKNESS PROFILE FOR A CRYOGENIC LIQUID SPILLED ON WATER IN A RADIAL CONFIGURATION. CONSTANT BOILING RATE PER UNIT AREA ASSUMED (MUSCARI, 1974).

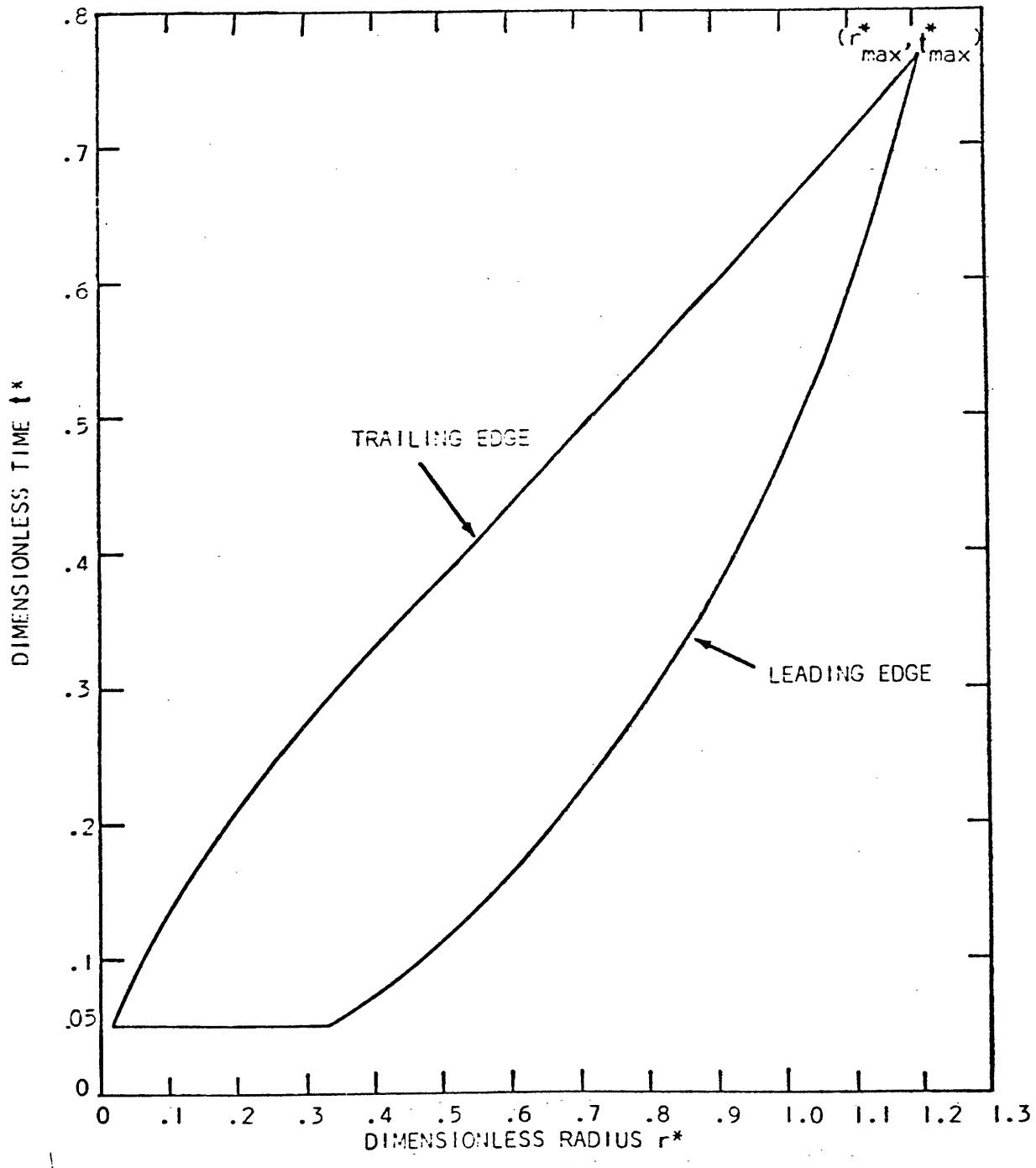

FIGURE II-16: PATHS OF THE LEADING AND TRAILING EDGES FOR A CRYOGENIC LIQUID SPILLED ON WATER IN A RADIAL CONFIGURATION. CONSTANT HEAT FLUX ASSUMED(MUSCARI, 1974).

However, the theoretical thickness profile predicted by Muscari's analysis gives zero thickness at the center of the pool at all times. This is not physically realistic in the initial stage.

Otterman (1975) has reviewed various models for instantaneous spills of cryogen on water. Essentially, all the models are based upon derivations which assume gravity forces cause spreading and are opposed by inertial forces. In such cases, without evaporation, the spread law is

$$r = [g \Delta V_o t^2]^{1/4} \qquad \text{(II-20)}$$

By accounting for the evaporation of cryogen during spreading, Otterman assumed that the average volume during the process can be approximated by $V_o/2$ which should be used in equation (II-20) instead of the initial spilled volume V_o. With a constant heat flux $\dot{q}$, Otterman equated the time integral of the boiling heat flux to the quantity spilled and obtained the following expression for τ, the time for complete evaporation:

$$\tau = 0.95 \left[\frac{\rho_L^2 \Delta H_v^2 V_o}{g \Delta \dot{q}^2} \right]^{1/4} \qquad \text{(II-48)}$$

Sustituting into equation (II-19), one obtains

$$r_{max} = 0.82 \left[\frac{\rho_L^2 \Delta H_v^2 g \Delta V_o^3}{\dot{q}^2} \right]^{1/8} \qquad \text{(II-49)}$$

Compared to equation (II-46), equation (II-48) predicts an even higher value of τ but the value of r_{max} predicted by Otterman's model is much lower than those by Raj and Kalelkar and Muscari.

In Table II-5, the predicted values of τ and r_{max} from various models are compared with the experimental data of Boyle and Kneebone (1973). Note the poor agreement for the different analyses. Fay's model gives much smaller values

TABLE II-5

Boyle's data and Predictions from Various Models for Spills of LNG in a Radial Configuration

Spill size, 2.24×10^{-2} m^3	Boyle	Burgess	Hoult	Fay	Muscari	Raj	Otterman
Pool Diameter at Break-up, m	3.96	5.36	3.33	2.38	5.14	4.18	3.42
Time to Evaporate Completely, s	24.	7.0	7.8	2.5	9.8	8.1	11.6
Spill Size, 4.48×10^{-2} m^3							
Pool Diameter at Break-up, m	5.64	6.75	4.44	3.18	6.68	5.43	4.43
Time to Evaporate Completely, s	33.	8.8	9.9	3.1	11.6	9.7	13.8
Spill Size, 8.97×10^{-2} m^3							
Pool Diameter at Break-up, m	7.32	8.5	5.93	4.25	8.66	7.04	5.75
Time to Evaporate Completely, s	35.	11.1	12.4	3.9	13.8	11.5	16.4

of τ and r_{max} then those predicted by the others. This is not surprising since in Fay's ice analysis, he neglects the surface resistance to boiling which is important in the early portion of the boiling process of LNG on water. This is when the heat transfer rate is much lower because it is in the film boiling regime. It is interesting to note that analyses of Hoult and Otterman yield almost identical predictions for the maximum pool radius. Hoult assumes the LNG volume does not change during spreading and the heat used to evaporate LNG comes from freezing the water while Otterman uses an average volume assumption with a constant boiling rate. However, this agreement is fortuitous. The maximum pool diameters predicted on the basis of Raj and Kalelkar's model are in good agreement with Boyle's data. The values of τ predicted from the models discussed above are much lower than the experimental results. This is not unexpected because all the models (except Muscari's) assume that the circular area uniformly covered with LNG continues to increase as long as any liquid cryogen remains. However, Boyle and Kneebone observed that the LNG pools broke up into discontinuous areas before complete evaporation. Using a "continuous pool" assumption for the LNG layer therefore results in underestimating the time for complete vaporization because the cryogen-water interfacial area is overestimated.

Continuous Spills

In cases where the discharge of cryogen is not instantaneous but persists for a long period of time, the spill is referred to as continuous. Otterman (1975) obtains an expression for the maximum radius of a continuous spill of cryogen by equating the spill rate $\dot{R}$ to the evaporating rate, assuming a constant heat flux,

$$r_{max} = \left[\frac{\rho_L \, \Delta H_v \, \dot{R}}{\pi \dot{q}}\right]^{1/2} \qquad \text{(II-50)}$$

For an initial quantity V_o of cryogen continuously released over a period (t) of time at a constant spill rate V_o/t, the maximum spreading radius is then

$$r_{max} = \left[\frac{\rho_L \Delta H_v}{\pi \dot{q}}\right]^{1/2} \left(\frac{V_o}{t}\right)^{1/2} \qquad \text{(II-51)}$$

The maximum spreading radius for a continuous spill varies inversely with the square root of time. Since the instantaneous spill is a special case of continuous spill (with infinite spill rate), the maximum radius attained in the instantaneous spill is the maximum for any continuous spill. The maximum pool radius for an instantaneous cryogen spill on water is expressed by (Otterman)

$$r_{max} = 0.82 \left[\frac{\rho_L^2 \Delta H_v^2 g \Delta V_o^3}{\dot{q}}\right]^{1/8} \qquad \text{(II-49)}$$

By equating equation (II-49) to (II-51), one obtains the following equation which can be used as a criterion for classifying continuous and instantaneous spills of the same quantity of cryogen:

$$t_{cr} = 0.69 \left[\frac{\rho_L^2 \Delta H_v^2 V_o}{g \Delta \dot{q}^2}\right]^{1/8} \qquad \text{(II-52)}$$

If the duration of a spill is longer than t_{cr}, the spill should be modeled as a continuous spill. If the spill time is shorter than t_{cr}, the spill can be considered instantaneous.

As indicated in equation (II-52), t_{cr} is a function of the boiling rate $\dot{q}$; t_{cr} increases as $\dot{q}$ decreases. For LNG, with $\dot{q} = 92\ kW/m^2$,

$$t_{cr} = 3.86\ V_o^{1/8} \quad (V_o \text{ in } m^3,\ t_{cr} \text{ in sec}) \qquad \text{(II-53)}$$

For example, for a LNG spill of $V_o = 10^3$ liters, t_{cr} is equal to 3.86 sec. If the duration of the spill is 4 seconds, the spill is classified as a continuous spill.

Georgakis et al. (1978) proposed a model for a non-instantaneous spill of a liquid fuel on water that could result from a collision and rupture of a ship's fuel tank.

As mentioned previously, in the prior analyses of instantaneous spills, the shape of the spill was taken to be circular. The spill area then depends only on the spill volume, not on geometrical characteristics of the ruptured tank or on the hole size and location of the tank.

Georgakis and his co-workers accounted for these effects and presented a model which predicted the time variation of the shape of the liquid fuel spill on water. Instead of the circular shape from an instantaneous spill, the predicted shapes of the hole spills are long and narrow. Their maximum spill area are significantly less than that predicted for an instantaneous spill, of the same fuel volume and so is the time to attain the maximum area.

However, the author's derivation assumes that hydrostatic equilibrium is established in the vertical direction as the fuel leaves the tank and that the displaced water travels with the same velocity as the fuel. The authors did not account for the balance between inertial and gravitational forces on the fluid elements once these fuel elements leave the source of the spill. Physically the velocity of the fuel-water interface should be the same as the fuel velocity, but the velocity of the displaced water can not be expected to be the same as the fuel. In spite of the assumptions and limitations of this model, it does provide a somewhat more realistic basis for an actual spill.

In summary, few experiments have been conducted to examine the simultaneous boiling and spreading of LNG on water. The available data do not agree well with the theories that have been proposed. For LPG, essentially no research has been done to describe the boiling and spreading phenomena following a spill on water.

III. EXPERIMENTAL

A. SPILL/SPREAD/BOIL APPARATUS

The experimental apparatus was designed to study the boiling and spreading of cryogenic liquids spilled on water. A one-dimensional apparatus was used.

A schematic representation of the apparatus is given in Figure III-1 while Figure III-2 is an actual photograph. The equipment consists of six major parts: (1) the liquefaction station, (2) the cryogen distributor, (3) a water trough, (4) the vapor sampling stations, (5) the hood connection, and (6) a safety shield. A detailed description of each part of the apparatus follows.

1. Liquefaction Station

Figure III-3 depicts the liquefaction station. This apparatus was fabricated from 15cm (nominal 6 inch) diameter, Schedule 10, #304 stainless steel pipe, providing strength at very low temperatures. It consists of a cylindrical pipe, 15.2cm in length, welded at each end to dished caps. The total internal capacity is approximately 6.5 liters.

The helium gas and light hydrocarbon gases flow into the vessel through 0.635cm (1/4 inch) O.D. seamless 304 stainless steel tubing. The helium has two-fold function: 1) flushing out the air in the vessel before liquefying hydrocarbon gases and 2) pressurizing the vessel to deliver the condensed hydrocarbon.

A length of 0.953cm (3/8 inch) O.D. stainless steel tubing has been vertically installed with its end 1.27 cm above the bottom of the vessel. This lines serves to transfer the hydrocarbon condensate to the cryogen distributor.

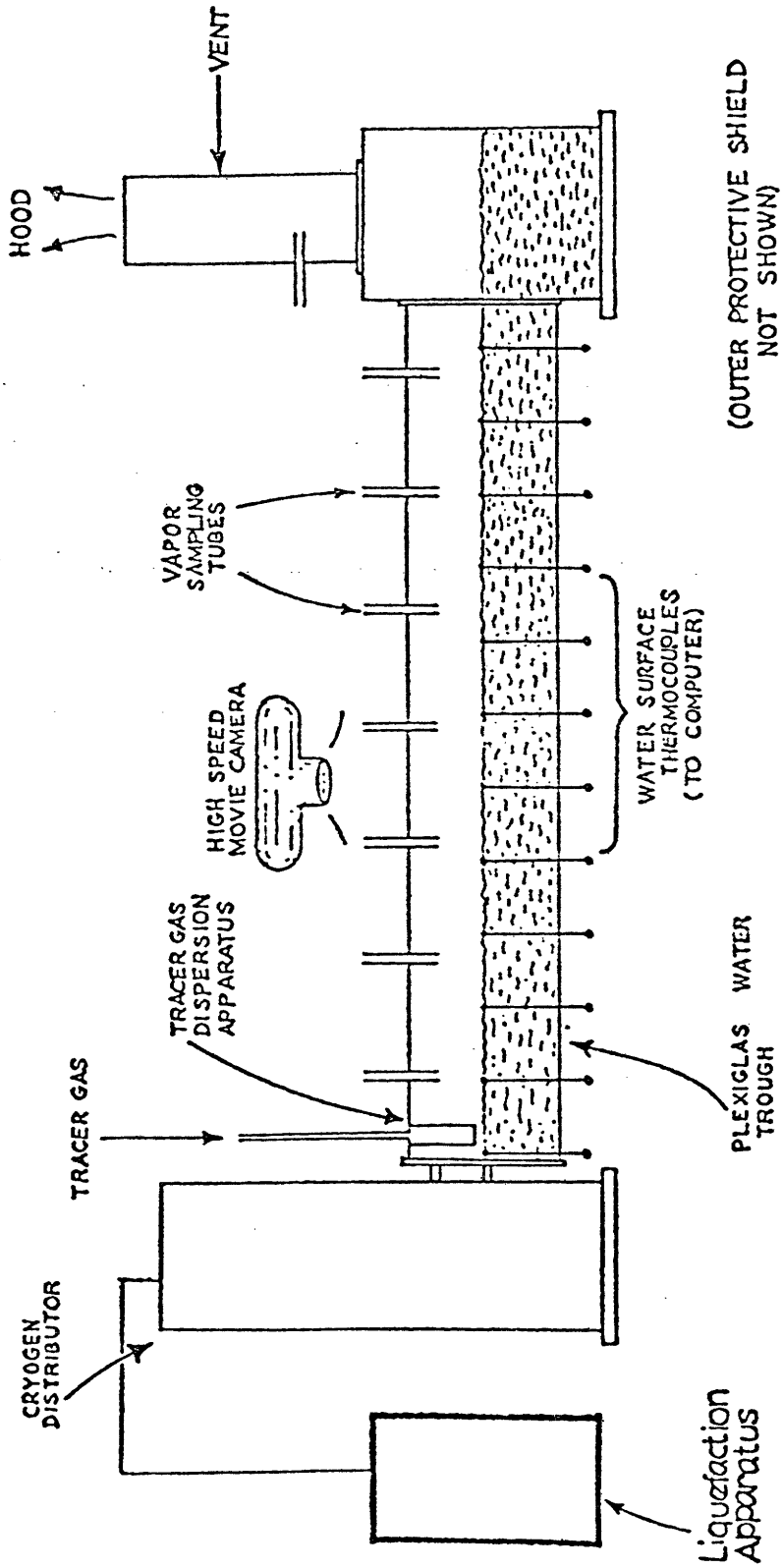

FIGURE III-1: SCHEMATIC OF SPILL/SPREAD/BOIL APPARATUS

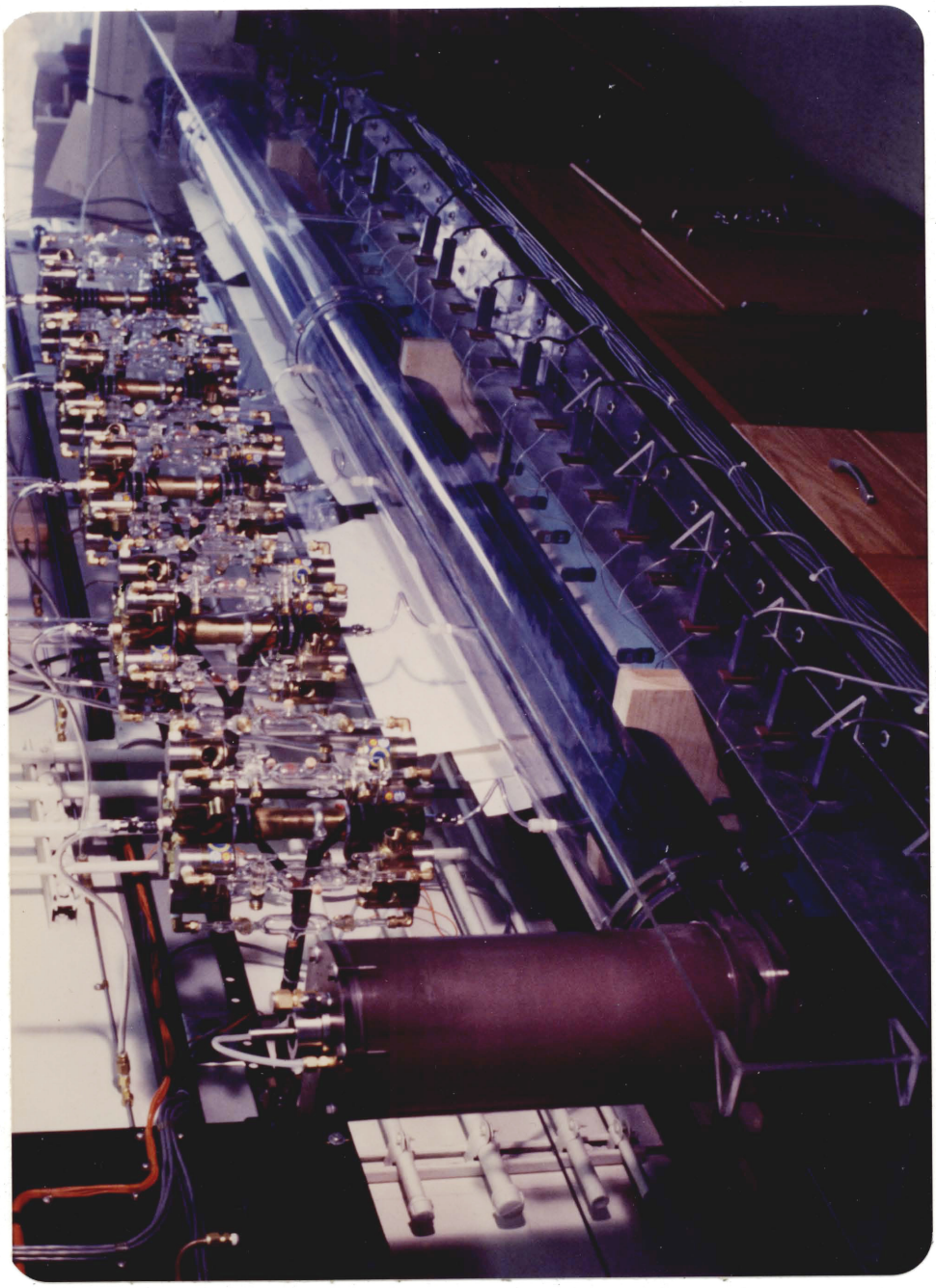

FIGURE III-2: A PHOTOGRAPH OF THE SPILL/SPREAD/BOIL APPARATUS

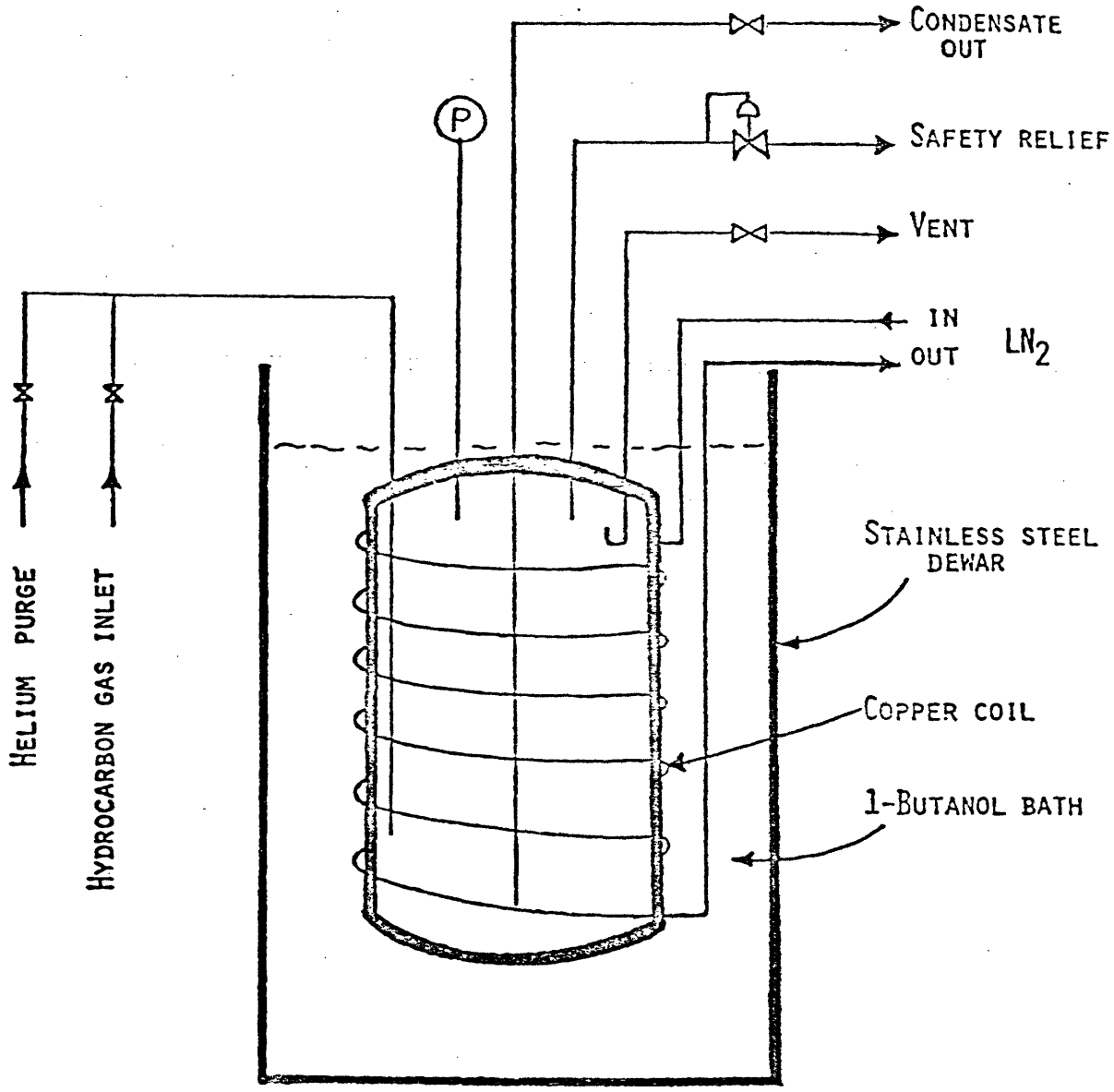

FIGURE III-3: SCHEMATIC OF LIQUEFACTION APPARATUS

valve in the line. The valve has a stainless steel ball/trim and Teflon seals to allow operation at very low temperatures. A pressure gauge (labeled "P" in Figure III-3) indicates the internal pressure of the vessel. In the case that an uncontrollable pressure increase occurs inside the liquefier, a safety release valve (wrapped with an electric heating tape to prevent freezing) will open. The relief valve is spring loaded with Teflon seats, and is set for a release pressure of approximately 3.7 bars.

Two chromel-constantan thermocouples are externally silver soldered the opposite sides of the vessel. Around the vessel is wrapped approximately 18 meters of 0.635cm (1/4 inch) copper tubing. The entire unit is placed on an aluminum stand inside a large stainless steel Dewar. The Dewar is filled with n-butanol that serves as a heat transfer medium. Liquid nitrogen evaporating within the copper coils lowers the temperature of the liquefaction unit. The nitrogen flow rate is limited by the need to maintain complete vaporization of the liquid N_2. The temperatures of the liquefaction unit, measured by the wall thermocouples, are maintained at various level, depending on the hydrocarbon gas which is liquefied, by adjusting the flow rate of liquid nitrogen (and therefore the rate of liquefaction) inside the vessel.

2. Cryogen Distributor

The cryogenic liquids prepared in the liquefaction station are delivered to the cryogen distributor prior to the spill. A simple pouring of large quantities of cryogen at the end of the water trough is not feasible because it would cause a severe disruption of the water surface producing undesirable wave motions withing the tube. The cryogen distributor has been designed to minimize these effects. A transverse view of the distributor is shown in Figure III-4.

The distributor employs a spring-loaded piston with a Teflon-encapsulated

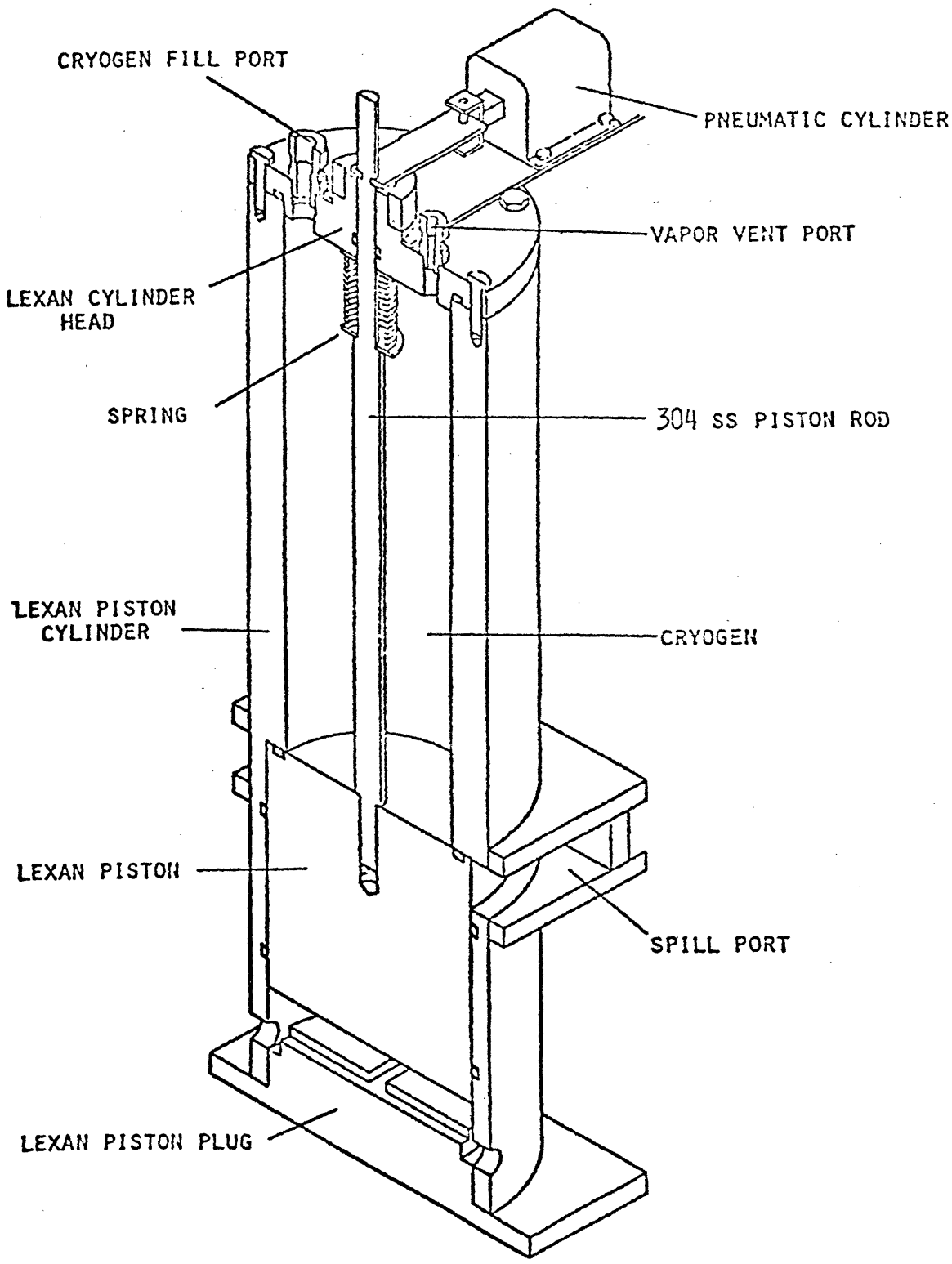

FIGURE III-4: TRANSVERSE VIEW OF CRYOGEN DISTRIBUTOR

spring seal on the groove of piston surface. When the piston shaft is lifted and held in place by a retaining latch, a cylindrical void in the distributor is sealed at the bottom by the piston. The void in the distributor can hold approximately 3.5 liters of cryogen. The release of the latch releases the piston shaft and allows the piston to fall, opening a side port through which the cryogen can flow onto the water surface.

The piston cylinder is fabricated from nearly transparent Lexan polycarbonate resin to permit visual observation of the cryogen level. A series of calibration lines have been marked on the distributor at 0.5-liter intervals to aid in the determination of the quantity of cryogen delivered. The dimensions of the piston cylinder are 17.8cm O.D. x 61.cm in height. Upon full downward displacement of the piston, the maximum cross-sectional flow area of the rectangular side port is about $48cm^2$. This side port area is adjustable and in the LPG spills, it is changed to check the size effect on the spill phenomena.

A nitrogen-driven pneumatic cylinder shifts the latch on the piston shaft. This frees the spring-loaded piston and initiates the cryogen delivery. The nitrogen flow is regulated by a three-way solenoid valve actuated by a programmable sequencer (Texas Instruments 5TI-102 series), thus providing automatic release of the piston at the appropriate time during the experiment.

The build-up of pressure inside the distributor before an experimental run is prevented by venting the distributor to the hood and allowing the boil-off vapor to escape. This vent line is closed by a sequencer-controlled solenoid valve after the piston is released.

3. Water Trough

Simultaneous boiling and spreading tests are conducted in a long, narrow water trough. The trough consists of a plexiglas tube that has a 17.8cm

O.D., 16.5cm I.D., and is approximately 4 m long. It is half filled with water. Water, cryogen, and vapor temperatures are monitored by a set of chromel-constantan thermocouples fabricated from 76μm wires. Seven vapor-thermocouples enter through the top of the water trough and are placed at 50cm intervals along the length of the tube. The first vapor thermocouple is placed 25 cm from the cryogen distributor. An eighth vapor-thermocouple is placed in the chimney which is the gas vent leading to the hood.

A total of twenty-seven liquid-thermocouples are introduced through the bottom of the water trough and are located at the water surface to indicate the passage of cryogen. These thermocouples are placed at 12.7cm intervals along the length of the trough. The first thermocouple is located next to the side port of the cryogen distributor to mark the beginning of the spill.

The thermocouple out-puts are fed directly into a NOVA-840 Real Time Computer (Data General Corp.) for data sampling, storage and analysis. This computer can simultaneously sample sixteen channels at intervals of 100 ms.

Initial tests of the apparatus showed that spilling large quantities of liquid onto the water creates a large wave which, when reflected off the far end of the apparatus, interferes with the spreading. A wave damping system has been therefore installed at the far end of the water trough. It consists of a pile of stainless steel wool coarsely packed into a square box attached to the exit end of the water trough. The steel wool was found to be effective in absorbing and dissipating the energy of water waves.

A high speed camera has also been used to record the movement of cryogen over the water surface.

The local boil-off rates of cryogen spreading on water are estimated in an indirect manner. A tracer gas, carbon dioxide, is injected continuously at steady rate into the system through a gas dispersion apparatus, shown in

Figure III-5. The dispersion apparatus is located next to cryogen distributor and distributes the tracer gas evenly above the water surface inside the tube. Vapor samples are taken at several locations along the tube during the experiment. A temperature-programmable gas chromatograph is used to analyze the vapor samples. The temperatures and compositions of vapor samples provide the necessary information to determine the mass boiled off as a function of time and position. The detailed data treatment will be described in a following chapter.

4. Vapor Sampling Station

Eight vapor sampling stations are positioned next to the vapor-thermocouples along the spill apparatus. Each of these stations has the capacity to collect six separate vapor samples in an array of 25 cm^3 glass sampling bulbs. Figure III-6 and III-7 show the top view and isometric cut-away view of a sampling station. Figure III-8 is an actual photograph of a sampling station. Before an experimental run, each sampling bulb is initially purged and pressurized to approximately 1.4 bars with an inert gas, argon. During the experiment, the lower solenoid valve opens just prior to sampling; expansion of the argon gas then serves to purge residual vapors from the common inlet line. The upper solenoid valve, which is connected to a vacuum line, then opens and the vapor sample is drawn into the bulb. Finally, the sampling stops with the simultaneous closing of both solenoid valves. Each complete sampling procedure takes about one second.

The actuation of solenoid valves is controlled by the programmable sequencer. A 5TI-3200 TCAM (Time/Counter Access Module) enables easy monitoring and alteration of programmed timing operations. The scan time of 8.3 ms yields an expected maximum timing error of less than 4.2 ms.

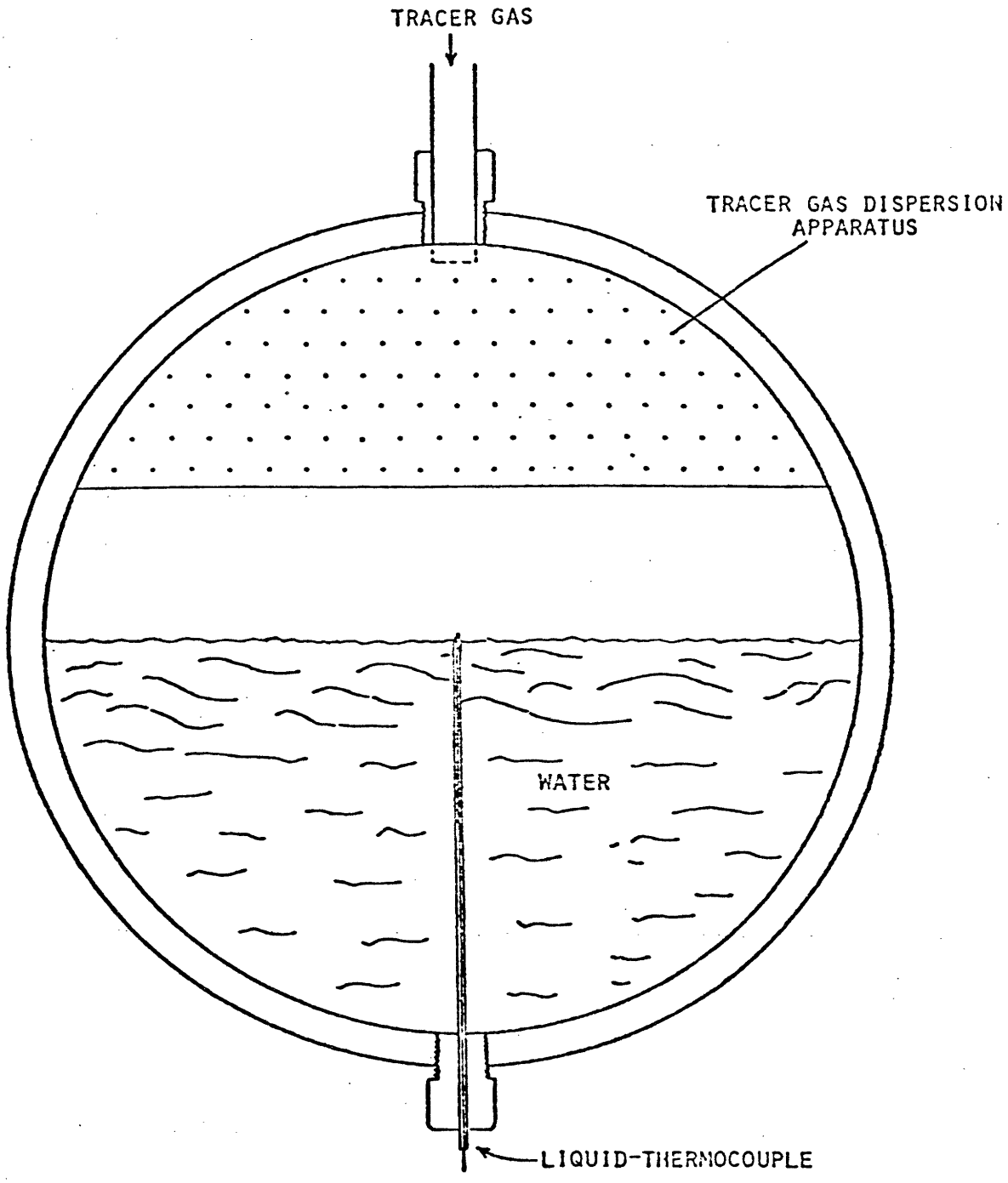

FIGURE III-5: POSITIONING OF TRACER GAS DISPERSION APPARATUS
(CROSS-SECTION VIEW)

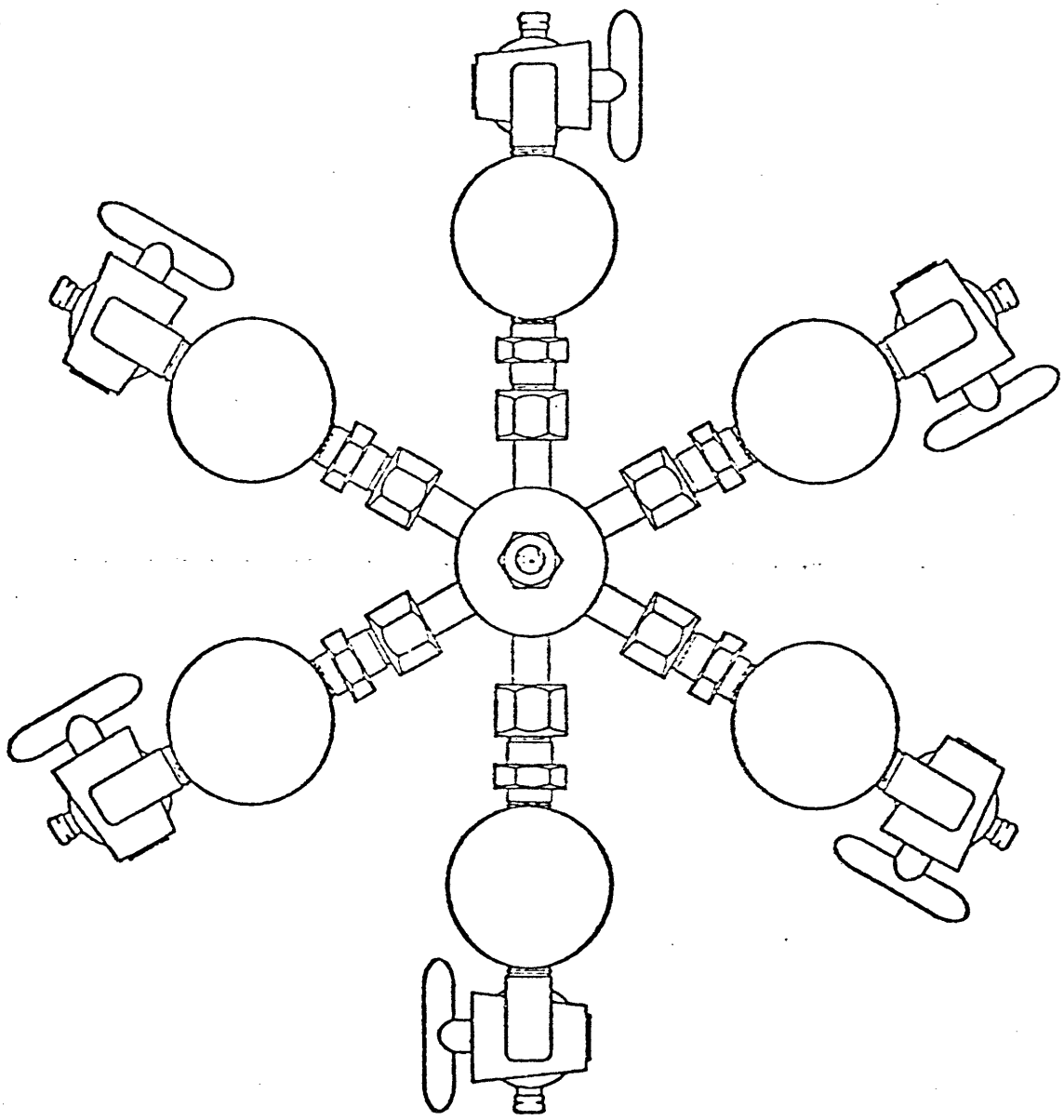

FIGURE III-6: TOP VIEW OF VAPOR SAMPLING STATION

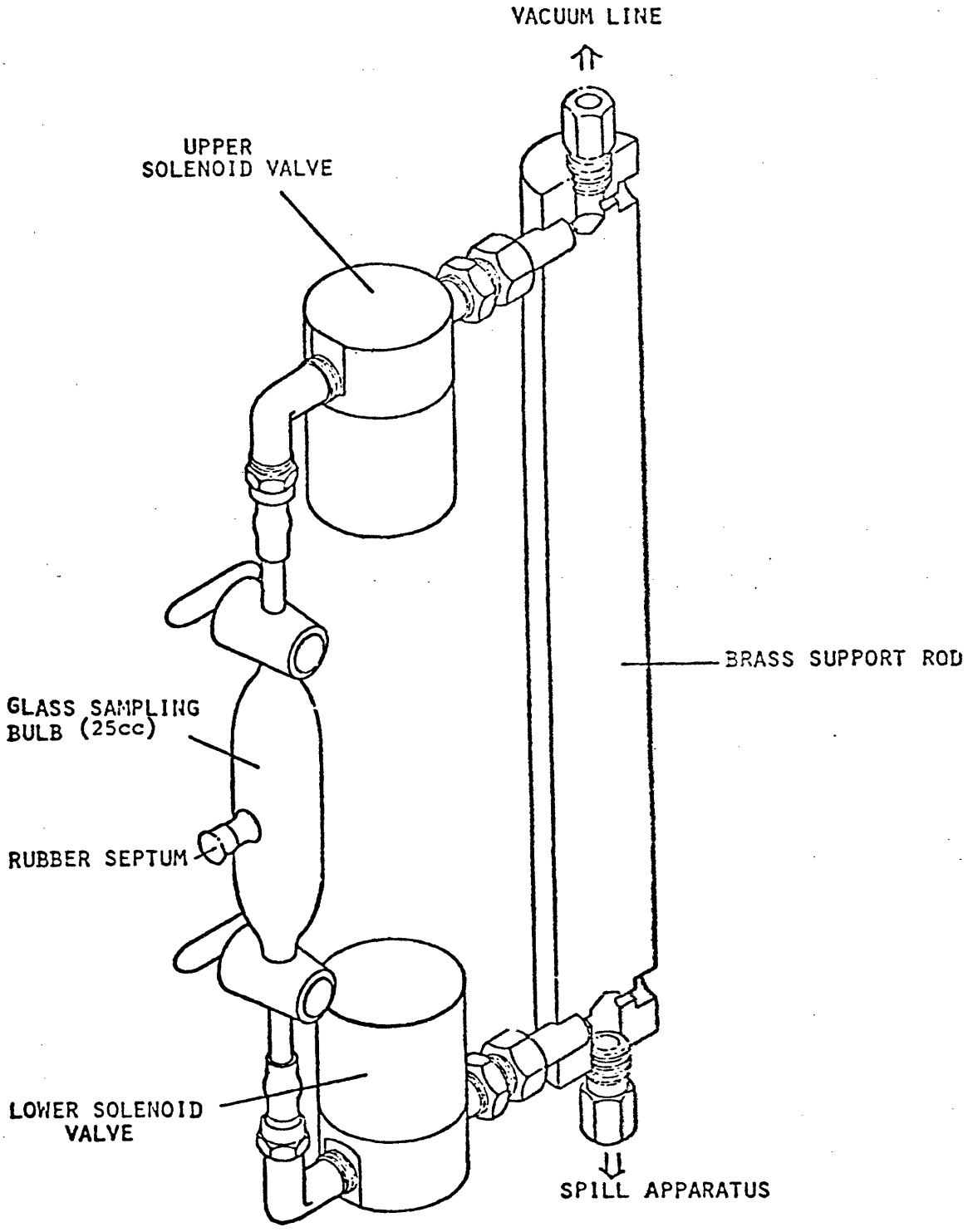

FIGURE III-7: ISOMETRIC CUT-AWAY VIEW OF VAPOR SAMPLING STATION

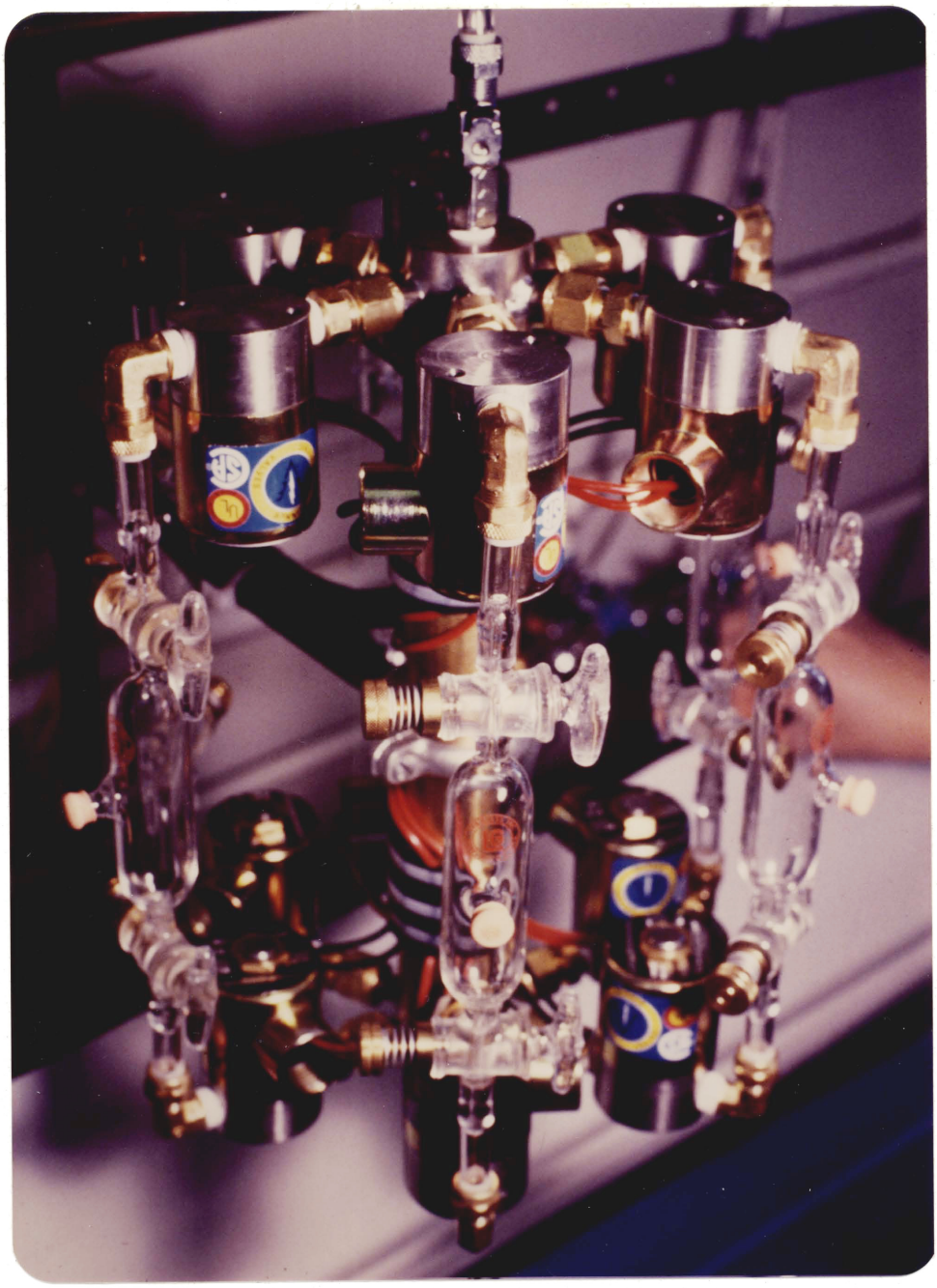

FIGURE III-8: A PHOTOGRAPH OF A VAPOR SAMPLING STATION

5. Hood Connection

The spill apparatus is connected to the hood to allow the venting of the flammable hydrocarbon gases. The hood connection pipe, fabricated from thin galvanized steel, fits around the vertical chimney of the spill apparatus. There is an annular spacing of approximately 1.27cm between the pipe and the chimney.

6. Safety Shield

For safety purposed the water trough, elevated by wooden supports, is placed within a metal U-shape container. In the event of breakage, all of the fluid would be retained. In the case of an accident, ambient air would be prevented from mixing with the light hydrocarbon gases because the entire apparatus is enclosed in a sealed plexiglas box. Nitrogen is introduced into this outer plexiglas cover to purge the surrounding space of air. Figure III-9 presents an end view of the safety shield.

B. PREPARATION OF CRYOGENS

The liquid hydrocarbons are prepared in the liquefaction station by cooling the hydrocarbon gases below their boiling points. This is accomplished by evaporating liquid nitrogen in the coils around the liquefaction vessel.

Before beginning liquefaction, the vessel is purged with helium gas to remove air. A hydrocarbon gas cylinder is then connected and gas is allowed to flow into the vessel. As liquid nitrogen starts flowing through the copper coils around the vessel, it chills the n-butanol and the liquefaction vessel. The thermocouples attached to the exterior of the vessel permit the monitoring of temperature.

As the temperature decreases further, the hydrocarbon gas begins to condense. Since methane and propane liquefy at 111.7K and 231.1K respectively

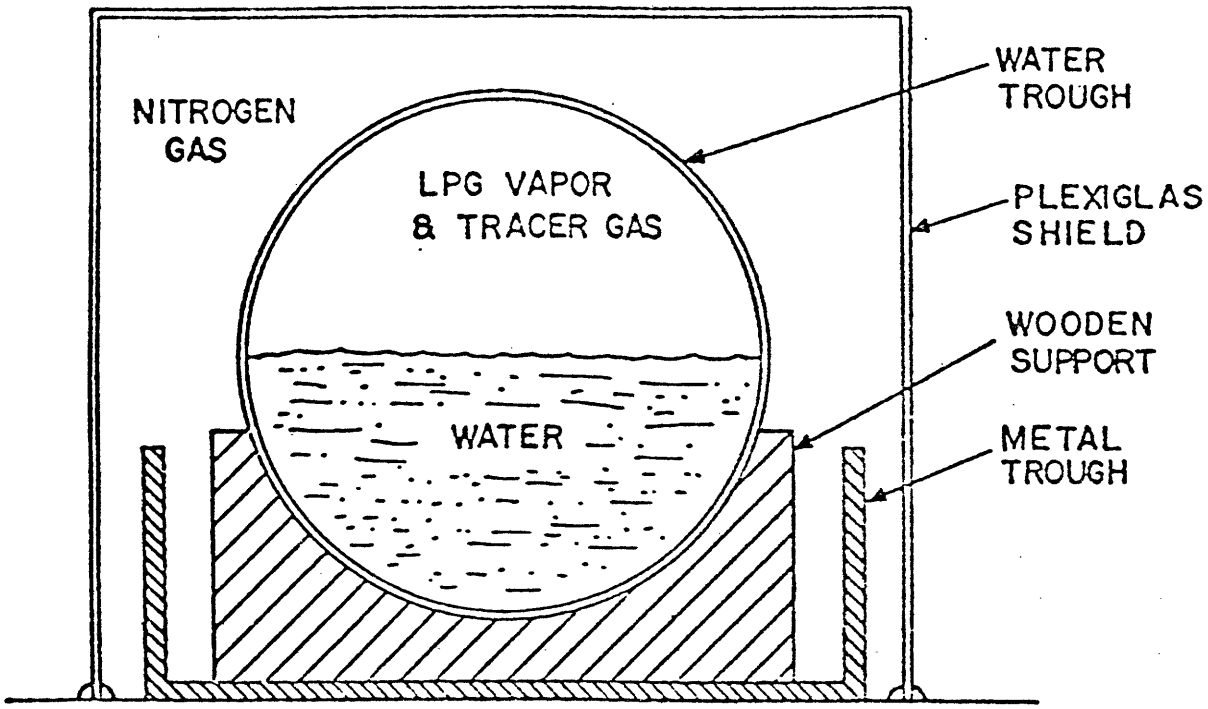

(CROSS SECTION VIEW)

FIGURE III-9: SAFETY SHIELD

(at 1 atmosphere pressure), the temperatures of the liquefaction vessel are maintained between 90K and 115K for methane and between 220K and 230K for propane by varying the flow rate of liquid nitrogen. The liquid nitrogen flow rate indirectly controls the rate of liquefaction.

The change in weight of the gas cylinder indicates the amount of liquid cryogen produced. When sufficient cryogen has been obtained, the feed of liquid nitrogen is discontinued. The cryogen is then ready for delivery to the distributor.

Matheson Ultra High Purity Grade methane and C.P. Grade methane, ethane, propane and n-butane cylinders have been used to prepare the cryogenic liquids in this work. The liquid nitrogen is supplied by the M.I.T. Cryogenic Laboratory. The purities of all the gases used in the experiment are listed in Table III-1.

Preparation of LPG mixtures requires a special prodecure. According to Porteous and Reid's (1976) prediction, the spillage of LPG on water at the ambient temperature would result in super critical explosions if the propane/ethane molar ratio is less than 0.60 and n-butane/ethane ratio less than 0.25. Therefore LPG mixtures must be carefully prepared with compositions far away from the explosive region.

Since propane-n-butane mixtures do not exhibit the super critical explosion phenomena, liquid propane is prepared first. N-butane gas is then connected to the liquefaction vessel and the desired amount is liquefied. Finally, ethane is added to the vessel, but a special caution is used to ensure that the compositions of the LPG mixtures fall within the safe region.

C. APPARATUS OPERATING PROCEDURE

Initially, the center openings of the sampling bulbs are closed with rubber septa held in place by thin wire. For each experiment new rubber

TABLE III-1

Purities of Various Cylinders

Helium	99.995	mole %
Argon	99.998	
Carbon Dioxide	99.8	
Methane	99.97	
	99.0	
Ethane	99.5	
Propane	99.4	
n-Butane	99.4	
Liquid Nitrogen	99.95	

septa are used for all sampling bulbs. Eight sampling stations are connected to an argon cylinder and separately purged with argon gas until the molar concentration of argon in each sampling station exceeds 99 percent. The gas chromatograph is used to determine this. The sampling stations are then pressurized with argon to approximately 1.4 bars. After this step, water is introduced into the water trough until the tube is half filled. The piston inside the cryogen distributor is then lifted up to block the side port. The distributor is thereby prepared to hold cryogen. Nitrogen gas is injected slowly into the safety shield to purge the surrounding space of air.

The liquefaction station is purged first with inert helium gas and then with the desired hydrocarbon gas from a weighed cylinder. After purging with the hydrocarbon gas, liquid nitrogen is allowed to flow through the copper coils around the liquefaction vessel. As the vessel temperature drops below the boiling point of the hydrocarbon gas, condensation of the hydrocarbon begins. By adjusting the flow rate of liquid nitrogen, the temperature of the liquefation station can be maintained between 90K and 115K for methane and between 220K and 230K for propane. After a sufficient quantity of cryogen has been prepared, as indicated by the weight change of the gas cylinder, the feed of liquid nitrogen is discontinued.

The next step is to prepare the Real Time Computer for collecting the temperature readings from the vapor and liquid thermocouples. A tracer gas, carbon-dioxide, is directed through the dispersion apparatus into the spill tube to purge air from the gas space above the water surface. The flow rate of the tracer gas is monitored with a four-tube flowmeter unit. A 16mm, high speed movie camera (Red Lake Model #400 HYCAM) is used to photograph the spreading in the experiment.

Before the cryogen is delivered from the liquefaction station to the cryo-

gen distributor, all the sampling stations are connected to the vacuum line. As a safety precaution the overhead lights of the room are turned off. The helium gas is then used to pressurize the liquefaction vessel and the outlet valve is opened; the desired quantity of cryogen is pressured out of the liquefaction container into the cryogen distributor.

The operation of the entire apparatus is controlled automatically by the programmable sequencer. When the sequencer is actuated the real time computer program begins to collect data. The sequencer then releases the distributor piston at a pre-selected time and the cryogen flows onto water surface. The high speed camera begins photographing 2 seconds before the release of the piston. The solenoid valve on the vent line of the cryogen distributor is closed immediately after the release of the piston. Sampling stations collect vapor samples at specified times during the experiment; each sampling station collects six samples. Afterwards the gas chromatograph is used to analyze the compositions of vapor samples. The Real Time Computer yields the temperature readings stored during the experiment.

Table III-2 presents the sample collection times for the six samples taken at each sampling station.

D. ANALYSIS OF VAPOR-SAMPLE COMPOSITIONS

A Hewlett-Packard 5734A temperature-programmable gas chromatograph is used to analyze the compositions of the vapor samples. Two 0.318 cm O.D. (1/8 inch) by 180 cm long stainless steel columns are used to separate the sample constituents. One column, packed with 13X Molecular Sieve, is used to analyze the compositions of the sampling bulbs before the experiment. The other column, packed with Porapak-Q, is used to analyze the vapor samples collected during the experiments.

TABLE III-2

Sample Collection Times

Vapor Sample	Collection Time* (sec)	Average Time (sec)
1	0.75 - 1.25	1.0
2	2.25 - 2.75	2.5
3	3.75 - 4.25	4.0
4	6.75 - 7.25	7.0
5	9.75 - 10.25	10.0
6	12.75 - 13.25	13.0

* The time zero corresponds to the release of the distributor piston.

A gas sample is removed from a sampling bulb through the rubber septum by means of a Precision Sampling-Pressure Lok-gas tight syringe and then run through either of the columns; depending on the components to be analyzed. Helium is used as the carrier gas.

After separation in the column, the sample passes through a thermal conductivity detector. The output voltage of the detector is integrated by a Hewlett-Packard 3380A Advanced Reporting Integrator. The equipment settings are given in Table III-3. Table III-4 gives the retention times for various components. The detector's output voltage versus time profile presents a peak for each component. The area under each peak is proportional to the amount of each component present in the sample. The composition of the mixtures can then be determined once the detector is calibrated for the specific response to each component.

TABLE III-3

Settings Used in Gas Chromatographic Analysis

Hewlett Packard 5734A Gas Chromatograph

Helium Flow	20 cm^3/min.
Injection Port	150°C
Detector	250°C
Detector Current	160 ma
Column A (Porapak-Q)	2 min. at 60°C, then temperature ramped at 32°C/min. until 180°C
Column B (13X Molecular Sieve)	0°C

Hewlett Packard 3380A Advanced Reporting Integrator

Report	AREA%
Attenuation	LOG
Chart	AUTO
Stop timer	10 (min.)
Slope sensitivity	0.1 mV/min.

TABLE III-4

Retention Times in Gas Chromatographic Analysis

*Oven temperature: 2 min. at 60°C, then temperature ramped 32°C until 180°C

Carbon dioxide	0.93 min.
Ethane	2.31 min.
Propane	4.48 min.
n-Butane	6.16 min.

**Oven temperature: 0°C

Argon + Oxygen	1.00 min.
Nitrogen	2.80 min.

* Porapak-Q column

**13X Molecular Sieve column

IV. DATA ANALYSIS TO DETERMINE LOCAL BOIL-OFF RATES

The local boil-off rates of LPG on water cannot be measured directly from the experimental measurement. However, the local boiling rates can be inferred indirectly from the information obtained in the experiment.

It is assumed that the tracer gas and cryogen vapor are well mixed in the vertical direction of the vapor ullage. This assumption is justified in Appendix-III. A mass balance over a differential volume element for the vapor phase (see Figure IV-1) can be written:

$$\underset{\substack{\text{(mass flowing)}\\ \text{in}}}{AUC|_x} - \underset{\substack{\text{(mass flowing)}\\ \text{out}}}{AUC|_{x+dx}} + \underset{\substack{\text{(evaporation)}\\ \text{source}}}{\dot{M}wdx} = \underset{\text{(accumulation)}}{\frac{\partial}{\partial t}(CAdx)} \qquad \text{(IV-1)}$$

where A = cross-sectional area above the water surface

U = vapor velocity

C = molar density of vapor

$\dot{M}$ = local boiling rate, moles per unit area per unit time

w = width of the water trough

Rearranging equation (IV-1), we obtain the following form:

$$\frac{\partial C}{\partial t} = -\frac{\partial (UC)}{\partial x} + \left(\frac{w}{A}\right)\dot{M} \qquad \text{(IV-2)}$$

Similarly the mass balance for tracer gas and cryogen vapor are expressed by

$$\frac{\partial C_T}{\partial t} = -\frac{\partial (UC_T)}{\partial x} \qquad \text{(IV-3)}$$

$$\frac{\partial C_{HC}}{\partial t} = -\frac{\partial (UC_{HC})}{\partial x} + \left(\frac{w}{A}\right)\dot{M} \qquad \text{(IV-4)}$$

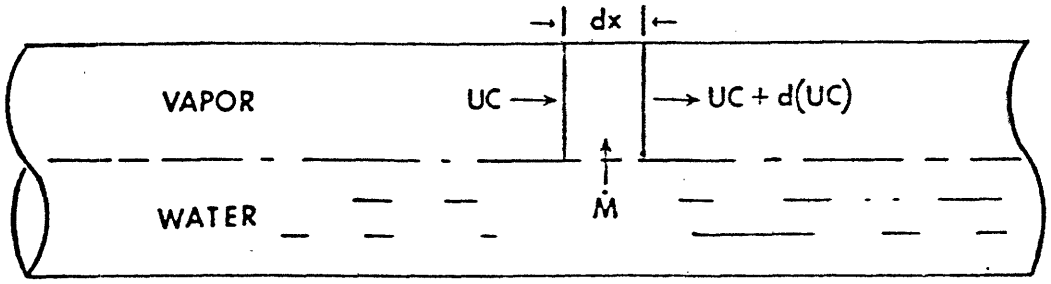

FIGURE IV-1: DIFFERENTIAL ELEMENT IN THE VAPOR PHASE ABOVE THE EVAPORATING CRYOGEN LAYER.

where C_T = molar concentration of tracer gas

C_{HC} = molar concentration of cryogen vapor

Vapor temperature measurements at various locations during the experiment can be used to calculate the molar density (C) of the vapor as functions of time and position. A equation of state of the following form is used:

$$C = \frac{P}{ZRT} \qquad \text{(IV-5)}$$

where P = pressure, 1 bar

Z = compressibility factor

R = universal gas constant, 83.14 bar-cm^3/mol-K

T = vapor temperature, K

The concentrations of tracer gas (C_T) and cryogen vapor (C_{HC}) are determined by gas chromatographic analysis of the vapor samples.

$$C_T = x_T \cdot C \qquad \text{(IV-6)}$$

$$C_{HC} = C - C_T \qquad \text{(IV-7)}$$

where x_T is the mole fraction of the tracer gas obtained from sample analysis. There are now two independent equations (IV-3) and (IV-4) and two unknowns U and $\dot{M}$. A numerical finite difference technique is used to evaluate the gas velocity and the local boil-off rates.

Writing the differential equations (IV-3) and (IV-4) in the standard finite differene form:

$$\frac{(C_T)_{i+i,\,j} - (C_T)_{i,j}}{t_{i+1} - t_i} = -\left[\frac{(UC_T)_{i+1,\,j} - (UC_T)_{i+1,\,j-1}}{x_j - x_{j-1}}\right] \qquad \text{(IV-8)}$$

$$\frac{(C_{HC})_{i+1,\,j} - (C_{HC})_{i,j}}{t_{i+1} - t_i} = -\left[\frac{(UC_{HC})_{i+1,\,j} - (UC_{HC})_{i+1,\,j-1}}{x_j - x_{j-1}}\right] + \left(\frac{W}{A}\right)\dot{M}_{i+1,\,j} \qquad \text{(IV-9)}$$

i is the ith time interval and j is the jth space interval. $\dot{M}_{i+1,\,j}$ is the local mass boil-off rate at jth spatial point and (i+1)th instant in time.

The algorithm begins with the known velocity at j = 0 (x = 0). There the velocity U is only due to the known flow rate of pure tracer gas. Equation (IV-8) can be solved for the gas velocity $U_{i+1,\,j}$. The two velocity values at the (j-i)th and jth space intervals can be substituted into equation (IV-9) to yield the local boil-off rate $\dot{M}$ at the (i+1)th time and jth position.

The units of $\dot{M}$ are moles per unit area per unit time. The values of the heat flux per unit area can be related to the molar fluxes by the following two equations for a single component cryogen and mixtures respectively.

$$\dot{Q}_{pure} = \dot{M} \cdot (mw) \cdot \Delta H_v \qquad (kW/m^2) \qquad \text{(IV-10)}$$

$$\dot{Q}_{mix} = \dot{M} \sum_i \{x_i \cdot (mw)_i \cdot (\Delta H_v)_i\} \qquad (kW/m^2) \qquad \text{(IV-11)}$$

where x_i is the mole fraction of component i estimated from the vapor sample analysis, $(mw)_i$ is its molecular weight, and $(\Delta H_v)_i$ is its heat of vaporization.

V. ONE-DIMENSIONAL BOILING/SPREADING MODEL FOR INSTANTANEOUS SPILLS OF CRYOGENIC LIQUIDS ON WATER

The spreading mechanics of cryogenic liquids on water in many respects is similar to that of non-volatile liquids on water. The major difference between these two processes is the evaporative mass loss of cryogen during the spreading.

Fay (1969) used an order-of-magnitude analysis to identify three principle flow regimes through which the spreading film passes (see Chapter II): the first is the gravity-inertia regime, the second is the gravity-viscous regime and the third is the surface tension-viscous regime. For cryogenic liquids spilled on water, only the physics of the first regime is important, where the gravity and inertial forces balance (see Appendix-IV). Before the second or third regime becomes established, most of the cryogen has evaporated.

A. FORMULATION OF THE MATHEMATICAL MODEL

For the spreading of a cryogen liquid on water in a one-dimensional configuration, assuming the density of the cryogenic liquid, ρ, is constant and neglecting the acceleration across the thickness, h, of the cryogen layer, the following form of the continuity equation is obtained (see Figure V-I):

$$\frac{\partial h}{\partial t} + \frac{\partial}{\partial x}(hU) + \frac{\dot{m}}{\rho} = 0 \qquad \text{(V-1)}$$

where x is the spreading direction, U is the spreading velocity, and $\dot{m}$ is the local mass boil-off rate per unit area. $\dot{m}$ can be a function of both x and t.

In the gravity-inertia spreading regime, the gravitational force balances the inertia of the cryogenic liquid. By assuming that the cryogen is in hydrostatic equilibrium in the vertical direction, the equation of motion takes the following form:

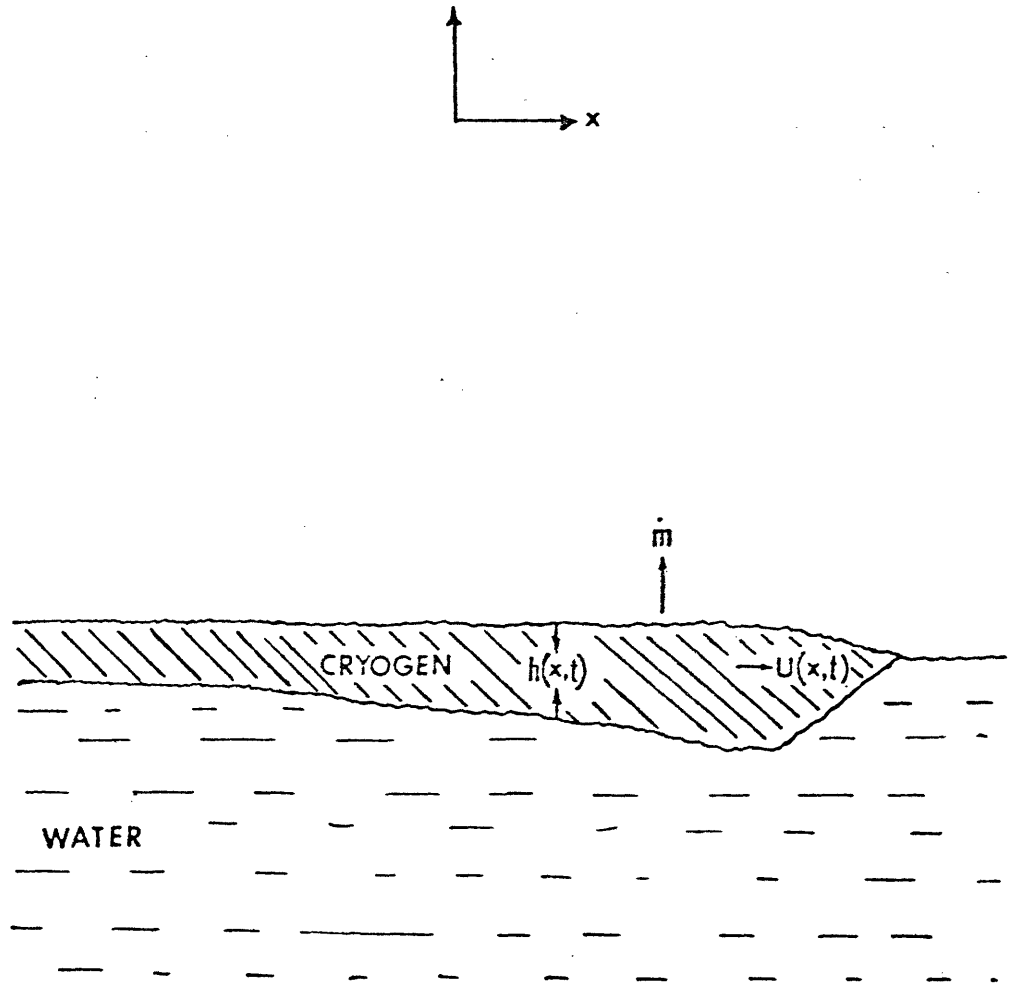

FIGURE V-1: SKETCH OF A CRYOGENIC LIQUID SPREADING ON A WATER SURFACE.

$$\frac{\partial U}{\partial t} + U \frac{\partial U}{\partial x} + g\Delta \frac{\partial h}{\partial x} = 0 \qquad \text{(V-2)}$$

where Δ is defined as the ratio of the density difference between water and the cryogenic liquid to the water density, $(\rho_w - \rho)/\rho_w$. The derivations of equations (V-1) and (V-2) are described in details in Appendix-IV.

At the leading edge, the spreading velocity of the cryogen is given by

$$U_{LE} = (\lambda g h_{LE} \Delta)^{1/2} \qquad \text{(V-3)}$$

where the value of λ is experimentally determined and equal to 1.64 (see Chapter VI).

At the origin of the spill, the potential energy of the cryogen is converted to kinetic energy. The cryogen has only vertical velocity and the horizontal component of velocity is zero. Thus

$$U_{x=0} = 0 \qquad \text{(V-4)}$$

There is no analytical solution for equations (V-1) and (V-2) (Muscari, 1974). A numerical technique called "the method of characteristics" has been used to solve these partial differential equations.

The physical model considers the entire spill process as being initiated from a point. This geometric idealization leads to unmanageable singularities in the governing equations (V-1) and (V-2) at $x = 0$ and $t = 0$. These difficulties can be avoided by initiating the spill description at a very small t as opposed to $t = 0$, where it is assumed the spill process up to that time can be described adequately by Hoult's (1972a) analytical solution for the spreading of a non-volatile liquid on water. The justification of this assumption is given in Appendix-IV.

B. DESCRIPTION OF NUMERICAL SOLUTION: THE METHOD OF CHARACTERISTICS

Definition and Derivation of the Method

Solution by the method of characteristics is widely used in the study of compressible fluid mechanics. It is a powerfull numerical technique that provides solution to any two-or three-dimensional system of pratial differential equations of the hyperbolic type. The criterion for defining this classification is described below for the case of two dependent and two independent variables.

Clear expositions of the theory with its application are described frequently and extensively in the literature (Shapiro, 1953 and Thompson, 1972). The development which follows is concerned only with the formalisms of the method as they apply to this particular system.

Since h and U are functions of x and t, the total differentials of h and U may be written as:

$$dh = \frac{\partial h}{\partial x} dx + \frac{\partial h}{\partial t} dt \qquad \text{(V-5)}$$

$$dU = \frac{\partial U}{\partial x} dx + \frac{\partial U}{\partial t} dt \qquad \text{(V-6)}$$

Equations (V-1), (V-2), (V-5) and (V-6) are rearranged in the following manner:

$$U \frac{\partial h}{\partial x} + \frac{\partial h}{\partial t} + h \frac{\partial U}{\partial x} + = -\frac{\dot{m}}{\rho}$$

$$\Delta g \frac{\partial h}{\partial x} + U \frac{\partial U}{\partial x} + \frac{\partial U}{\partial t} = 0$$

$$dx \frac{\partial h}{\partial x} + dt \frac{\partial h}{\partial t} = dh$$

$$dx \frac{\partial U}{\partial x} + dt \frac{\partial U}{\partial t} = dU$$

These equations may be considered as simultaneous linear equations in the unknowns $\frac{\partial h}{\partial x}$, $\frac{\partial h}{\partial t}$, $\frac{\partial U}{\partial x}$ and $\frac{\partial U}{\partial t}$. Since the characteristic directions depend only on the coefficients of the variables $\frac{\partial h}{\partial x}$, $\frac{\partial h}{\partial t}$, $\frac{\partial U}{\partial x}$ and $\frac{\partial U}{\partial t}$, any of these unknowns can be solved to find the characteristic directions. For instance, solving for $\frac{\partial h}{\partial x}$, one obtains, in determinant notation

$$\frac{\partial h}{\partial x} = \frac{\begin{vmatrix} -\frac{\dot{m}}{\rho} & 1 & h & 0 \\ 0 & 0 & U & 1 \\ dh & dt & 0 & 0 \\ dU & 0 & dx & dt \end{vmatrix}}{\begin{vmatrix} U & 1 & h & 0 \\ \Delta g & 0 & U & 1 \\ dx & dt & 0 & 0 \\ 0 & 0 & dx & dt \end{vmatrix}}$$

$$= \frac{(\frac{\dot{m}}{\rho})\ (Udt - dx)\ dt - (hdU - Udh - dh)\ dx}{(U^2 - \Delta gh)\ (dt)^2 - 2Udxdt + (dx)^2} \qquad \text{(V-7)}$$

In order to establish the characteristic curves on the x - t and U - h plane across which $\frac{\partial h}{\partial x}$, $\frac{\partial h}{\partial t}$, $\frac{\partial U}{\partial x}$ and $\frac{\partial U}{\partial t}$ are indeterminate, the determinants of equation (V-7) are set equal to zero.

$$\text{denominator:}\quad (U^2 - \Delta gh)\ (dt)^2 - 2Udxdt + (dx)^2 = 0 \qquad \text{(V-8)}$$

which rearranges to form the following equation:

$$(U^2 - \Delta gh)\ (\frac{dt}{dx})^2 - 2U\ (\frac{dt}{dx}) + 1 = 0 \qquad \text{(V-9)}$$

$$\text{numerator:}\quad [hdU - Udh + (\frac{\dot{m}}{\rho})\ (dx - Udt)]\ dt + dhdx = 0 \qquad \text{(V-10)}$$

leading to the following form :

$$\frac{dU}{dh} = \left(U - \frac{dx}{dt}\right) \frac{1}{h} - \frac{\dot{m}}{\rho} \left(1 - U \frac{dt}{dx}\right) \frac{1}{h} \frac{dx}{dh} \qquad \text{(V-11)}$$

Equation (V-9) is a quadratic in $(\frac{dt}{dx})$ and has the solutions with $A = U^2 - \Delta gh$, $B = U$ and $C = 1$,

$$\left(\frac{dt}{dx}\right)_I = \frac{B-\sqrt{B^2-AC}}{A} = \frac{1}{U+(\Delta gh)^{1/2}} \; ; \; \left(\frac{dt}{dx}\right)_{II} = \frac{B+\sqrt{B^2-AC}}{A} = \frac{1}{U-(\Delta gh)^{1/2}} \qquad \text{(V-12a,b)}$$

which define the characteristic directions in the x - t plane. The slopes $(dt/dx)_{I,\ II}$ are dependent on U and h.

Substitution of equations (V-12) into equation (V-11) gives the slopes of the characteristic curves in the U-h plane in terms of U, h, x and t:

$$\left(\frac{dU}{dh}\right)_I = -\left(\frac{g\Delta}{h}\right)^{1/2} - \frac{\dot{m}}{\rho} \left[1 - U \left(\frac{dt}{dx}\right)_I\right] \frac{1}{h} \frac{dx}{dh} \qquad \text{(V-13a)}$$

$$\left(\frac{dU}{dh}\right)_{II} = \left(\frac{g\Delta}{h}\right)^{1/2} - \frac{\dot{m}}{\rho} \left[1 - U \left(\frac{dt}{dx}\right)_{II}\right] \frac{1}{h} \frac{dx}{dh} \qquad \text{(V-13b)}$$

Examination of equations (V-12) shows that the differential equations (V-1) and (V-2) may be of three types, depending on the sign of $(B^2 - AC)$. These types are defined as follows:

Hyperbolic type: $(B^2 - AC)$ is positive and equation (V-9) have two distinct real roots.

Parabolic type: $(B^2 - AC)$ is zero and there is only one real root for equation (V-9).

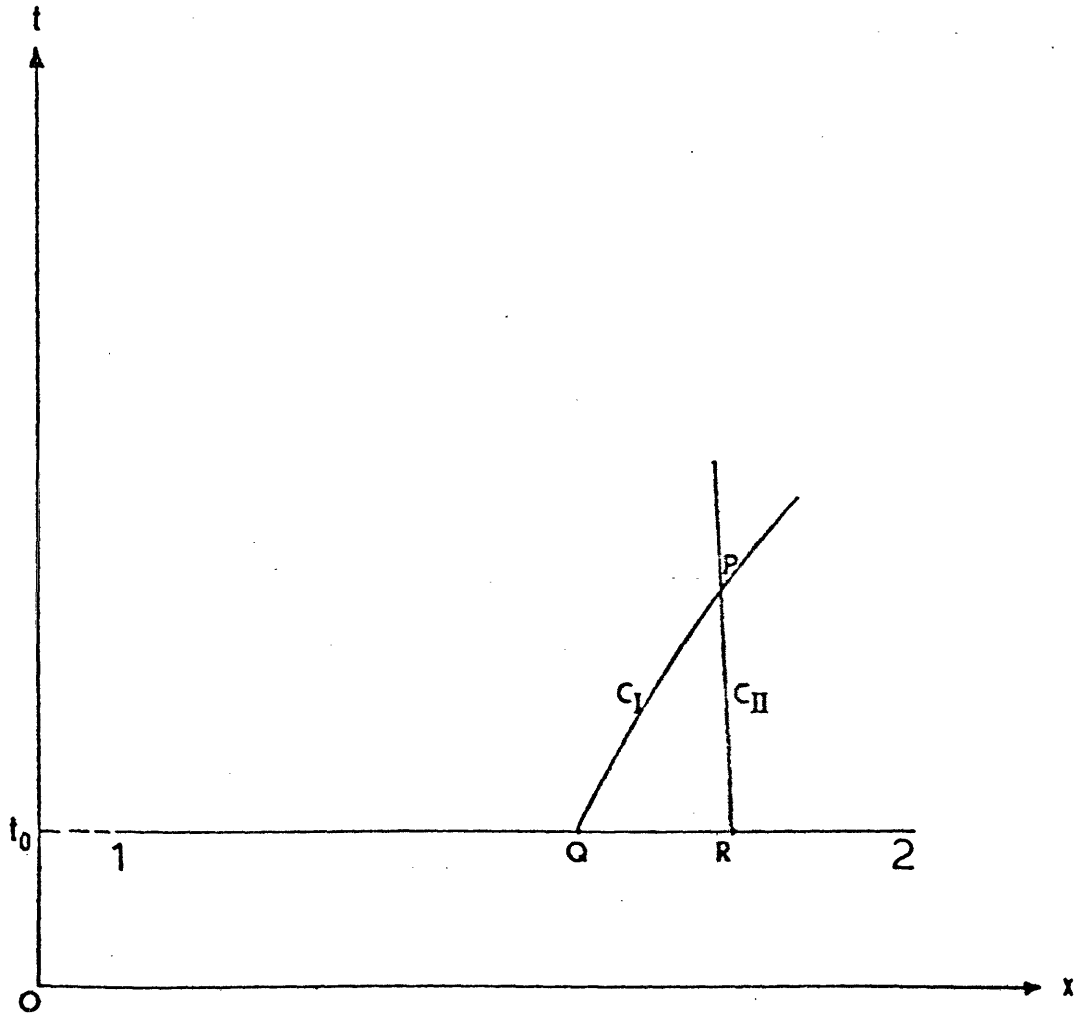

FIGURE V-2: PROGRESSION OF THE x-t CHARACTERISTIC NETWORK FROM THE INITIAL DATA LINE.

Elliptic type: $(B^2 - AC)$ is negative and equation (V-9) has no real roots.

As h is always positive, the value of $(B^2 - AC)$ is greater than zero. The system of the partial differential equations (V-1) and (V-2) is classified as hyperbolic and therefore permits solution by the method of characteristics.

Equations (V-12) and (V-13) satisfy the differential equations (V-1) and (V-s). Given suitable initial data, the characteristic curves in the x-t and U-h planes may simultaneously be constructed numerically or graphically in a stepwise fashion and the solutions of U and h can be determined as functions of x and t. The original task of solving the nonlinear partial differential equations (V-1) and (V-2) is thereby replaced by the comparatively easy task of simultaneously solving the ordinary differential equations (V-12) and (V-13).

To use the new system (equations (V-12) and (V-13)), a two dimensional plane diagram of t versus x is first constructed. On this diagram two families of characteristic curves, labeled I and II, are constructed as a result of intergrating equation (V-12), with the given initial data. The two families of curves will cross each other at a number of common mesh points. Equation (V-13a) can be integrated along the characteristic $(dU/dh)_I$ and equation (V-13b) along the characteristic $(dU/dh)_{II}$ to calculate U and h at the intersection points. The actual integrations are performed by a finite difference method on a computer.

An outline of this method, as it applies here, is described as follows: Consider figure (V-2) along the horizontal line 1-2, corresponding to the initial time, t_o, where the values of U and h are known. Let Q and R be two arbitary points on the line 1-2. Further, let P be the point of intersection of the characteristic $(dt/dx)_I$ through point Q and the characteristic $(dt/dx)_{II}$ through point R. The location of point P along with its values of U and h are

to be found.

Rearranging equations (V-13) leads to the following form:

$$\frac{d}{dx}\left[U + 2\,(\Delta gh)^{1/2}\right] = -\frac{\dot{m}}{\rho}\left(\frac{\Delta g}{h}\right)^{1/2}\left[\frac{1}{U + (\Delta gh)^{1/2}}\right] = G_{PQ} \qquad \text{(V-14a)}$$

$$\frac{d}{dx}\left[U - 2\,(\Delta gh)^{1/2}\right] = \frac{\dot{m}}{\rho}\left(\frac{\Delta g}{h}\right)^{1/2}\left[\frac{1}{U - (\Delta gh)^{1/2}}\right] = G_{PR} \qquad \text{(V-14b)}$$

Writing equations (V-14a) and (V-14b) in finite difference forms between points P and Q, and between points P and R respectively:

$$\frac{(U_P - U_Q) + 2\left[(\Delta gh)_P^{1/2} - (\Delta gh)_Q^{1/2}\right]}{x_P - x_Q} = G_{PQ} \qquad \text{(V-15a)}$$

$$\frac{(U_P - U_R) - 2\left[(\Delta gh)_P^{1/2} - (\Delta gh)_R^{1/2}\right]}{x_P - x_R} = G_{PR} \qquad \text{(V-15b)}$$

The function G_{PQ} is evaluated at both points P and Q, and then the mean of these two values is used as the value of G_{PQ} for further computation. Similarly, the function G_{PR} is evaluated at points P and R, and the mean of these two values is used as the value of G_{PR}. Solving equations (V-15a) and (V-15b) simultaneously yields the values for U_P and h_P.

The procedure to determine the values of x_P, t_P and U_P, h_P is as follows:

(i) The values of U and h at point Q are used in equation (V-12a) to compute the value of $(dt/dx)_I$ at point Q. A line with the slope $(dt/dx)_I$ is tentatively passed through point Q.

(ii) The values of U and h at point R are used in equation (V-12b) to compute the value of $(dt/dx)_{II}$ at point R. A line with the slope $(dt/dx)_{II}$ is tentatively passed through point R. The intersection with

the line drawn in step (i) provides the first estimation of x_p and t_p.

(iii) With G_{PQ} and G_{PR} evaluated at points Q and R as they apply, and using the value of x_p obtained in step (ii), the first estimation of U_p and h_p can be determined by solving simultaneously equations (V-15).

(iv) An iteration procedure is used to evaluate x_p, t_p and U_p, h_p more accurately. Starting with the tentative locations found previously, the location of point P is found more accurately by drawing the lines through points Q and R with slopes corresponding to the mean conditions between points P and Q, and between points P and R, respectively. Likewise, the values of U_p and h_p are found more accurately by evaluating G_{PQ} and G_{PR} with their respective mean conditions between the respective points. The iteration is continued until satifactory convergence (given in Appendix-IV) has been attained.

With the initial data line divided into a suitable number of discrete points, the intersections of the respective alternating I and II characteristics of these points are determined in the above fashion. The entire flow pattern in terms of velocity and thickness distribution is therefore established.

A detailed computation algorithm for this one-dimensional boiling/spreading model is given in Appendix-IV.

Solution for the Case Without Boiling

With $\dot{m} = 0$, the case is identical to the system of non-volatile liquids spreading on water. The numerical solutions of equation (V-1) and (V-2) by the method of characteristics are compared to the analytical solution of Hoult(1972a) in Figures V-3 and V-4, using the same value of $\lambda = 1.64$ in the leading-edge boundary conditions. x and t are normalized using a characteristic length x_e, taken as the length of the spill apparatus, and a characteristic time t_e, which

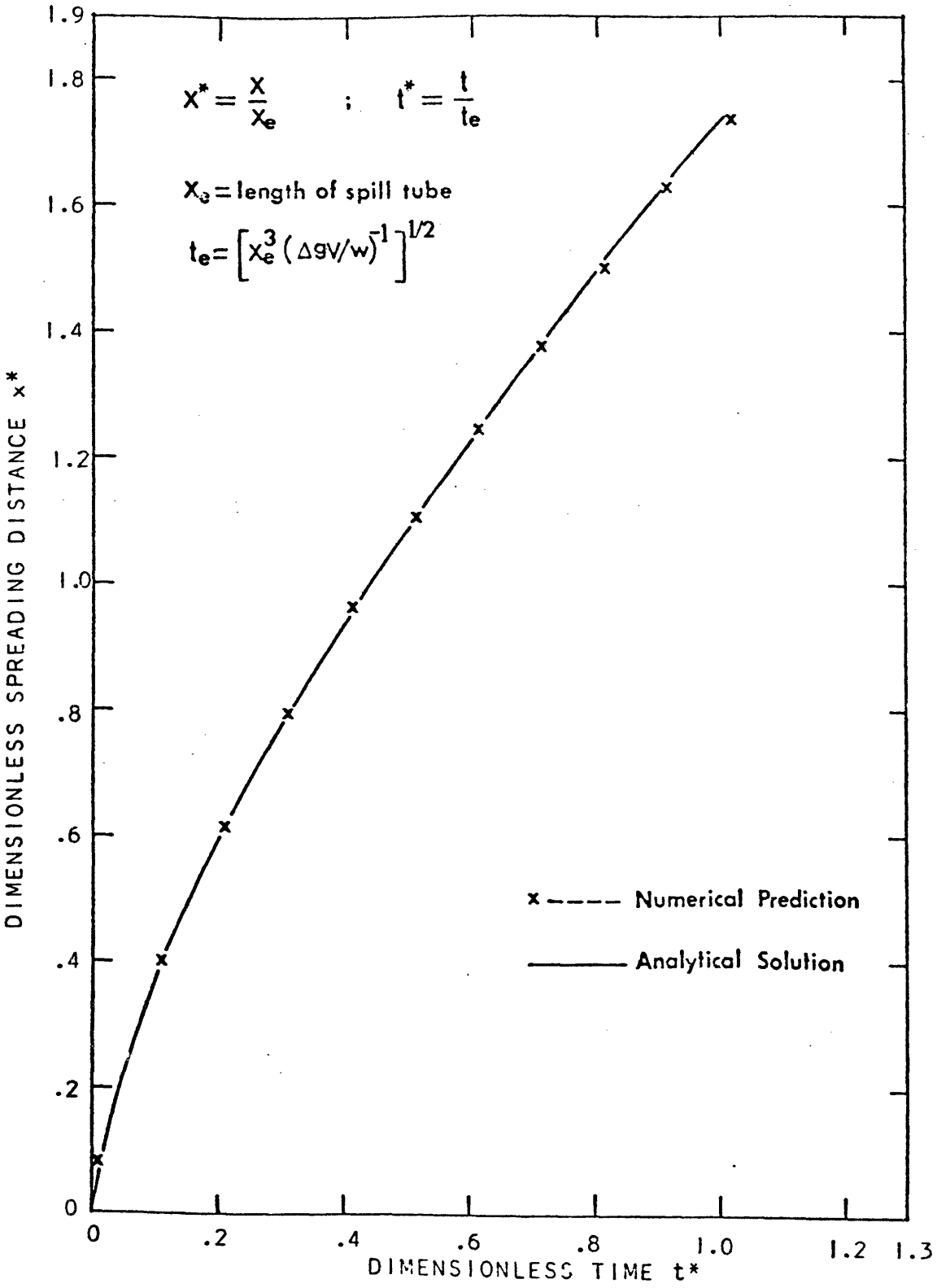

FIGURE V-3: ONE-DIMENSIONAL SPREADING CURVES IN THE GRAVITY-INERTIA REGIME FOR A NON-VOLATILE LIQUID SPILLED ON WATER. NUMERICAL PREDICTION COMPARED WITH HOULT'S(1972a) ANALYTICAL SOLUTION.

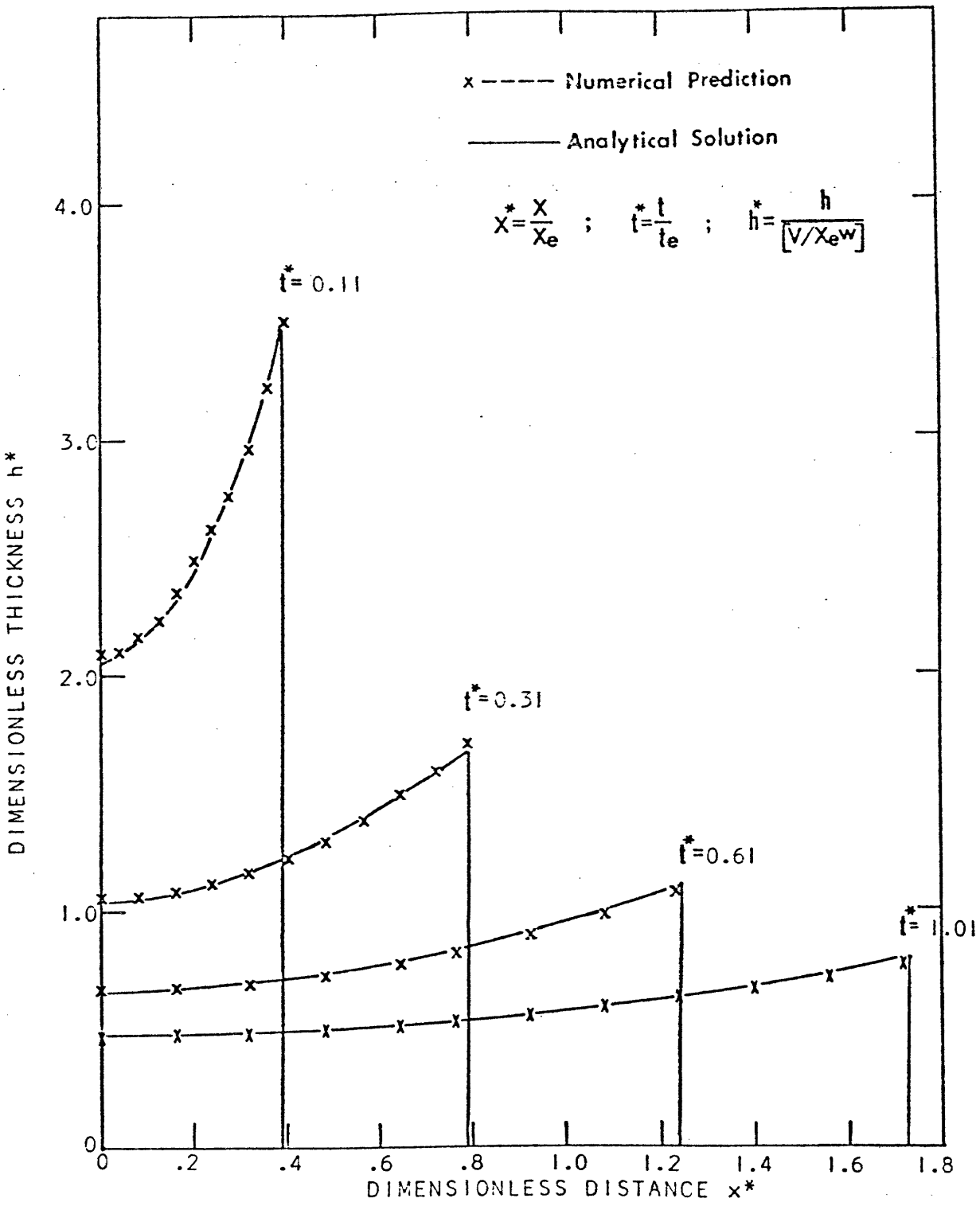

FIGURE V-4: DIMENSIONLESS THICKNESS PROFILE FOR A NON-VOLATILE LIQUID SPREADING ON WATER IN THE GRAVITY-INERTIA REGIME. NUMERICAL PREDICTION AND ANALYTICAL SOLUTION COMPARED.

is related to x_e by the following expression:

$$t_e = \left[x_e^3 \left(\frac{g\Delta V}{w}\right)^{-1} \right]^{1/2} \qquad \text{(V-16)}$$

where V is the volume spilled. The solutions from these two methods are essentially identical.

Solution for the Case with a Constant Boiling Rate Per Unit Area

Assuming $\dot{m}$ is a constant, the thickness profile of the liquid and the spreading front path in dimensionless form are shown in Figures V-5 and V-6. The explanation of characteristic length and time is given in Appendix-IV. In Figure V-5 one can see that the spreading front is thicker but thins out in the tail. This shape is similar to that observed in the case of non-volatile liquid spills. As the cryogenic liquid continues to evaporate, the tail becomes cryogen-free and a trailing edge appears and moves towards spreading front. The numerical model also predicts the trailing-edge path, as seen in Figure V-6. The intersection of the spreading-front path and trailing-edge path determines the values for the maximum spreading distance and the time for complete vaporization.

Figure V-6 also presents the prediction of the spreading-front path by Raj's (1977) one-dimensional boiling-spreading model (equation (II-41)). Raj's analysis does not predict the trailing-edge path. The numerical model predicts larger values of the maximum spreading distance and the time for complete vaporization than Raj's model.

C. ESTIMATION OF THE EFFECTIVE DENSITY OF CRYOGENIC LIQUIDS SPREADING ON WATER

When a cryogenic liquid spills on an unconfined water surface, boiling and spreading occur simultaneously. Bubbles form at the liquid cryogen-water in-

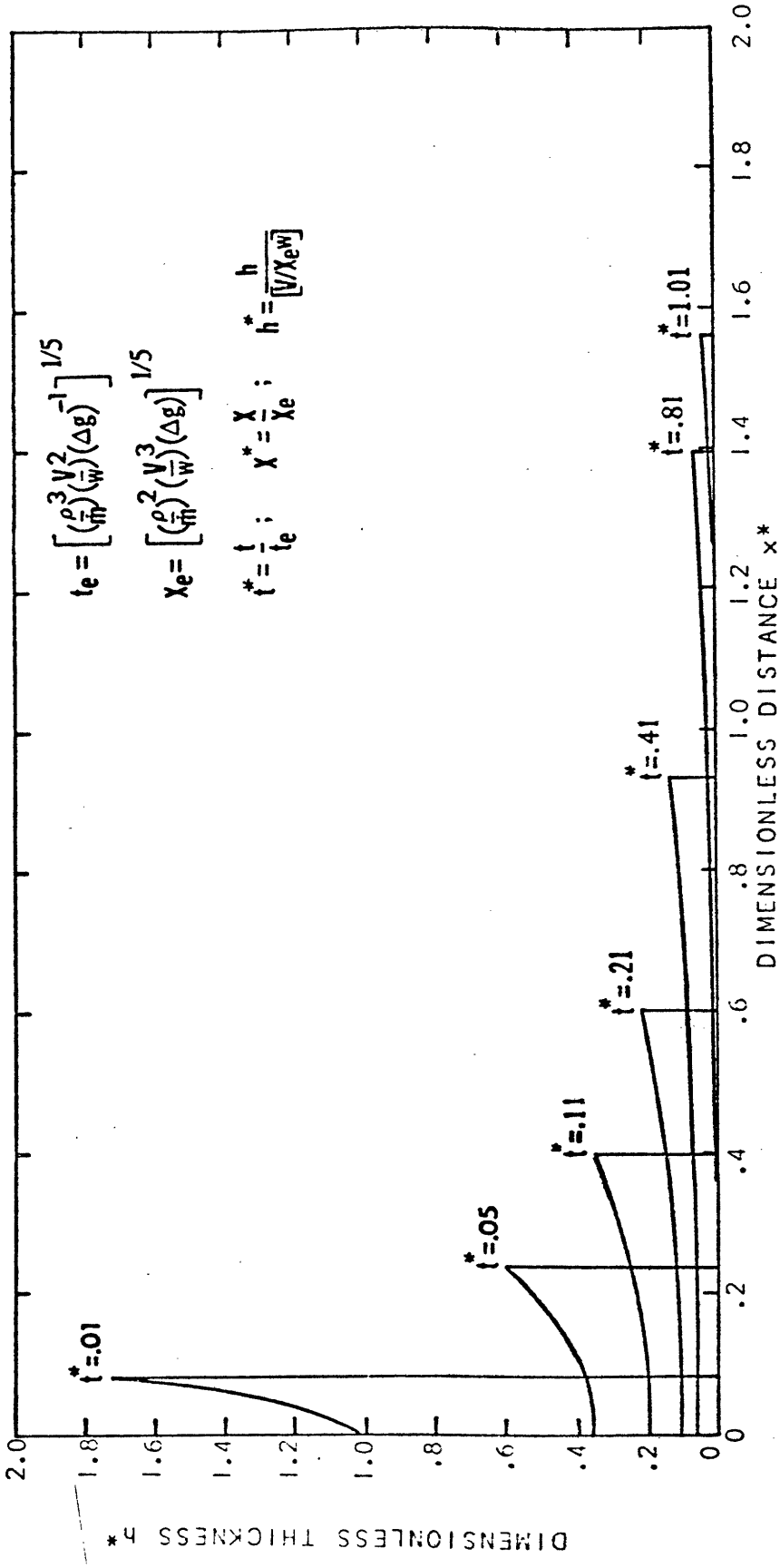

FIGURE V-5: DIMENSIONLESS THICKNESS PROFILE PREDICTED BY THE NUMERICAL MODEL FOR THE CASE OF CONSTANT HEAT FLUX.

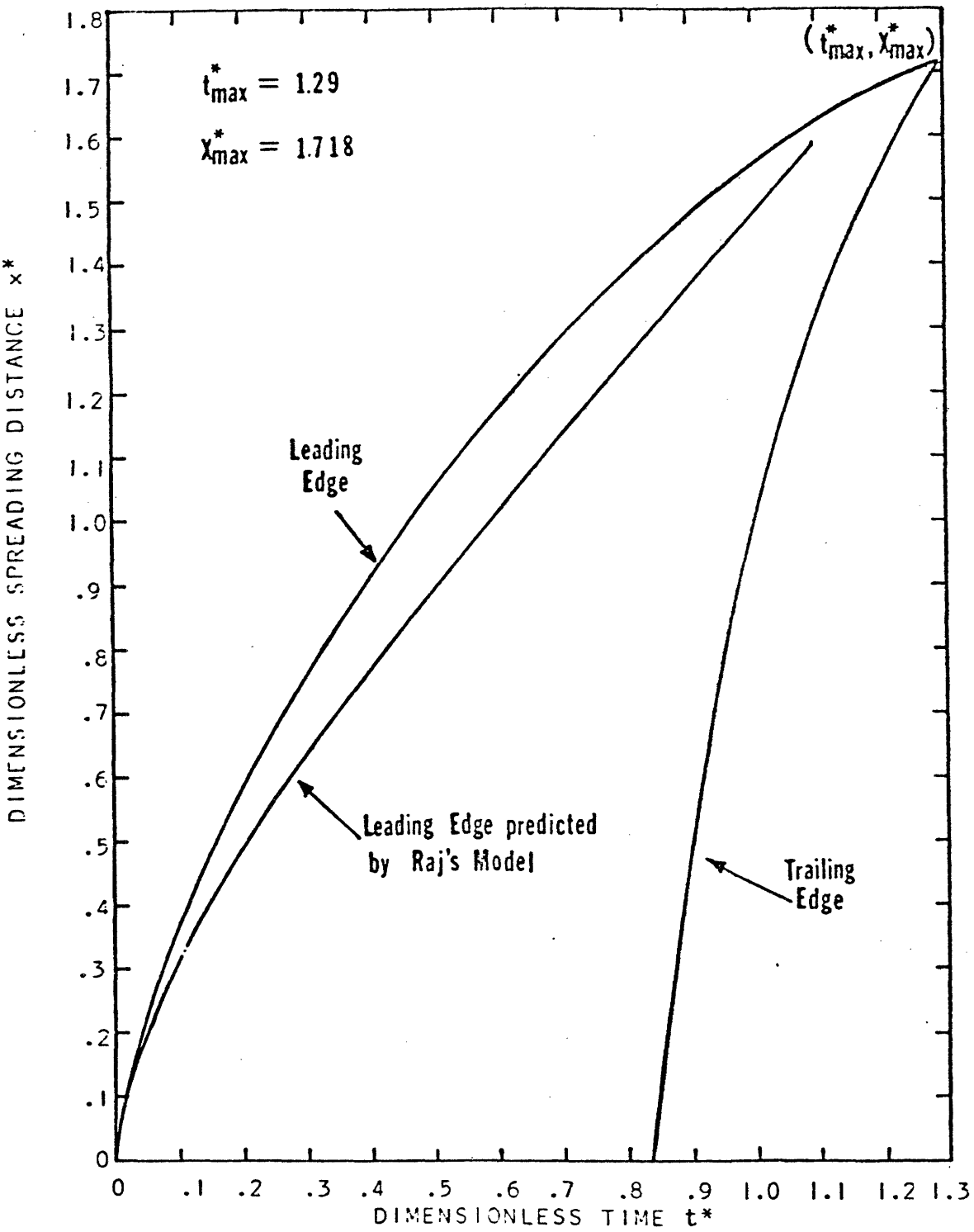

FIGURE V-6: PATHS OF THE LEADING AND TRAILING EDGES PREDICTED BY THE NUMERICAL MODEL FOR THE CASE OF CONSTANT HEAT FLUX. THE CORRESPONDING PREDICTION FROM RAJ'S MODEL ALSO SHOWN.

terface and rise through the cryogen layer toward the upper surface. The bubbles of the evaporated cryogen reduce the effective density of liquid cryogen layer and increase its height. The effect of bubbles on the spreading rate is described below, assuming a constant boil-off rate per unit area. For the case of propane an average boiling rate is used to estimate the bubble effect on the density of liquid peopane.

$\dot{q}$ is a constant heat flux through the cryogen-water interface. The vapor flux of the evaporated cryogen can be estimated from the equation of state:

$$\dot{V} = \left(\frac{\dot{q}}{\Delta H_v M}\right)\left(\frac{ZRT}{P}\right) \qquad (cm^3/cm^2\text{-}s) \qquad (V\text{-}17)$$

where $\dot{q}$ = constant heat flux, J/cm^2-s

H_v = heat of vaporization of cryogen, J/g

M = molecular weight of cryogen, g/mole

Z = compressibility factor

R = universal gas constant, 82.05 cm^3-atm/mole-K

T = temperature, K

P = pressure, atm

The velocity with which bubbles rise through a liquid is determined principally by the buoyancy force that drives the bubble upwards, and the viscous and form drag forces that tend to retard this motion. When the opposite-directional forces are equal, the bubble rises with a constant velocity.

Much theoretical work has been done on the rising velocity and shape of (insoluble)gas bubbles in liquids, and, in most cases, theory is well supported by experimental data. In general, small bubbles (below 0.2cm in diameter) behave like rigid spheres and rise through a liquid at terminal velocities that place them in the laminar-flow region. Their rising velocity may therefore be calculated from Stoke's law (Haberman and Morton, 1953). For diameters larger

than 0.2 cm the shape of the bubbles may vary from spherical to ellipsoidal. For diameters greater than 2 cm bubbles become lens-shaped and their velocity can be calculated with a reasonable degree of accuracy by using the Davis and Taylor correlation (1950). In this range of bubble sizes, the terminal velocity is independent of the properties of the liquid. The rising velocity in thin liquids for the size range 0.1 cm < d_b < 2 cm, has been reported between 20 and 30 cm/sec (Haberman and Morton, 1953; Davenport, Richardson, and Bradshaw, 1967).

There are no experimental data reported in the literature concerning the rising velocity of cryogen bubbles through cryogenic liquids. The bubble rising velocities for different cryogens are estimated with correlations obtained for other systems.

By assuming that bubbles rise at an average velocity U_{av}, the residence time, t_R, of bubbles in the cryogen layer, h, is

$$t_R = \frac{h}{U_{av}} \tag{V-18}$$

The effective density of the liquid cryogen, ρ_e, which includes the bubble effect, is expressed by the following mass-balance equation:

$$\rho_e = \frac{\rho_L V_L + \rho_V V_V}{V_t} \tag{V-19}$$

where ρ_L, V_L and ρ_V, V_V are the densities and volumes of cryogen liquid and bubbles respectively.

Substituting $V_L = V_t - V_V$ into equation (V-19), one obtains

$$\rho_e = \rho_L - \left(\frac{V_V}{V_t}\right) \rho_L + \left(\frac{V_V}{V_t}\right) \cancel{\rho_V} = \rho_L \left(1 - \frac{V_V}{V_t}\right) \tag{V-20}$$

Because the bubble density is very small relative to the liquid densitites,

the term, $(\frac{V_V}{V_t})\ \rho_V$, can be neglected. Furthermore, the volume of the bubbles in the cryogen layer can be expressed by

$$V_V = \dot{V} t_R A \qquad \text{(V-21)}$$

and the total volume is

$$V_t = hA \qquad \text{(V-22)}$$

where A is the area covered by cryogen.

Substitution of equations (V-21) and (V-22) into equation (V-20), the final form which expresses the effective density as a function of the boil-off rate and the rising velocity of the bubbles is:

$$\rho_e = \rho_L\ (1 - \frac{\dot{V}}{U_{av}}) \qquad \text{(V-23)}$$

In the development of the numerical model mentioned previously, the effective density evaluated by equation (V-23) is used instead of the density of the cryogenic liquid at its normal boiling point.

In Valencia's (1978) work, actual bubble sizes were measured for boiling methane and ethane on water in a confined system. The vapor bubbles of methane is roughly 0.3 - 0.5 cm in diameter. For ethane, the bubbles have a bimodal size distribution. Large bubbles, 0.5 ~ 1.0 cm in diameter, form initially. Later in the test the formation of the small bubbles (~ 0.2 cm) becomes predominant.

For propane (or LGP) system in the present work, a 1 cm bubble diameter was assumed. During propane and LPG spill experiments, observations near the distributor indicated the bubble diameters in the order of 1 cm.

Van Krevelen and Hoftijzer's (1956) work as reviewed in Szekeley and

Themelis's book (1971) shows that the bubble rising velocity is related to the bubble diameter. For 1 cm diameter LPG bubbles the rising velocity is 26 cm/sec which is estimated from the system with air rising in water. This is consistent with the findings of Haberman and Morton (1953) and Davenport et al. (1967). Their observation shows that the rising velocity in thin liquids for bubble sizes between 0.1 and 2 cm is between 20 and 30 cm/sec, more or less independent of the liquid system used. Van Krevelen and Hoftijzer's work also shows that the rising velocity is insensitive to bubble size for air-water system in the range of 0.2 - 0.7 cm. Consequently the exact knowledge of the bubble size within this range is not essential. A rising velocity of 24 cm/sec was assumed for methane and nitrogen bubbles (the size of nitrogen bubbles is slightly smaller than that of methane bubbles).

VI. EXPERIMENTAL RESULTS

Previous studies on the boiling of LPG on water have been conducted in confined areas without spreading. Rarely would one expect an industrial spill of LNG or LPG to occur in a confined area. The more likely case would involve simultaneous boiling and spreading. However, very few experiments have been made to determine such rates for any volatile cryogen. Until now, the analyses have been almost completely theoretical and assume that the boiling rate per unit area is independent of time. No data exists to justify this assertion. It is the purpose of the present work to obtain a better understanding of the boiling-spreading phenomena for cryogens spilled on water.

The equipment and procedure described in Chapter III were used to carry out experiments. Several pentane spills have been made to study the spreading of a non-volatile liquid on water. Pure cryogens of nitrogen, methane and propane were spilled on water to study the effect of boiling on the spreading process. Similarly, tests were conducted with binary mixtures of ethane-propane and propane-n-butane and with ternary mixtures of ethane-propane-n-butane. Finally, the effect of the area of the distributor opening on LPG spills was examined.

A. SPREADING OF NON-VOLATILE LIQUIDS ON WATER

As mentioned in the previous chapter, in order to determine the value of λ in the leading-edge boundary condition, equation (V-3), several pentane spills were made to evaluate λ experimentally. The experimental conditions for pentane spills are given in Table VI-1.

Pentane was chilled with liquid nitrogen to approximately 230K. This ensured an adequate response from the liquid-thermocouples in the water trough. Figure VI-1 is a photograph of the leading edge of pentane early in the

TABLE VI-1

Experimental Conditions for Pentane Spills

Test	Volume Spilled (liter)	Cross-Sectional Area of Distributor Opening (cm^2)
1120A	0.5	48.4
1120B	0.5	48.4
1119A	1.0	48.4
1121A	1.0	48.4
1121B	1.0	48.4
1126B	1.5	48.4
1127A	1.5	48.4
1128C	1.5	48.4
1206A	2.0	48.4
60309	2.0	48.4
1205A	3.0	48.4

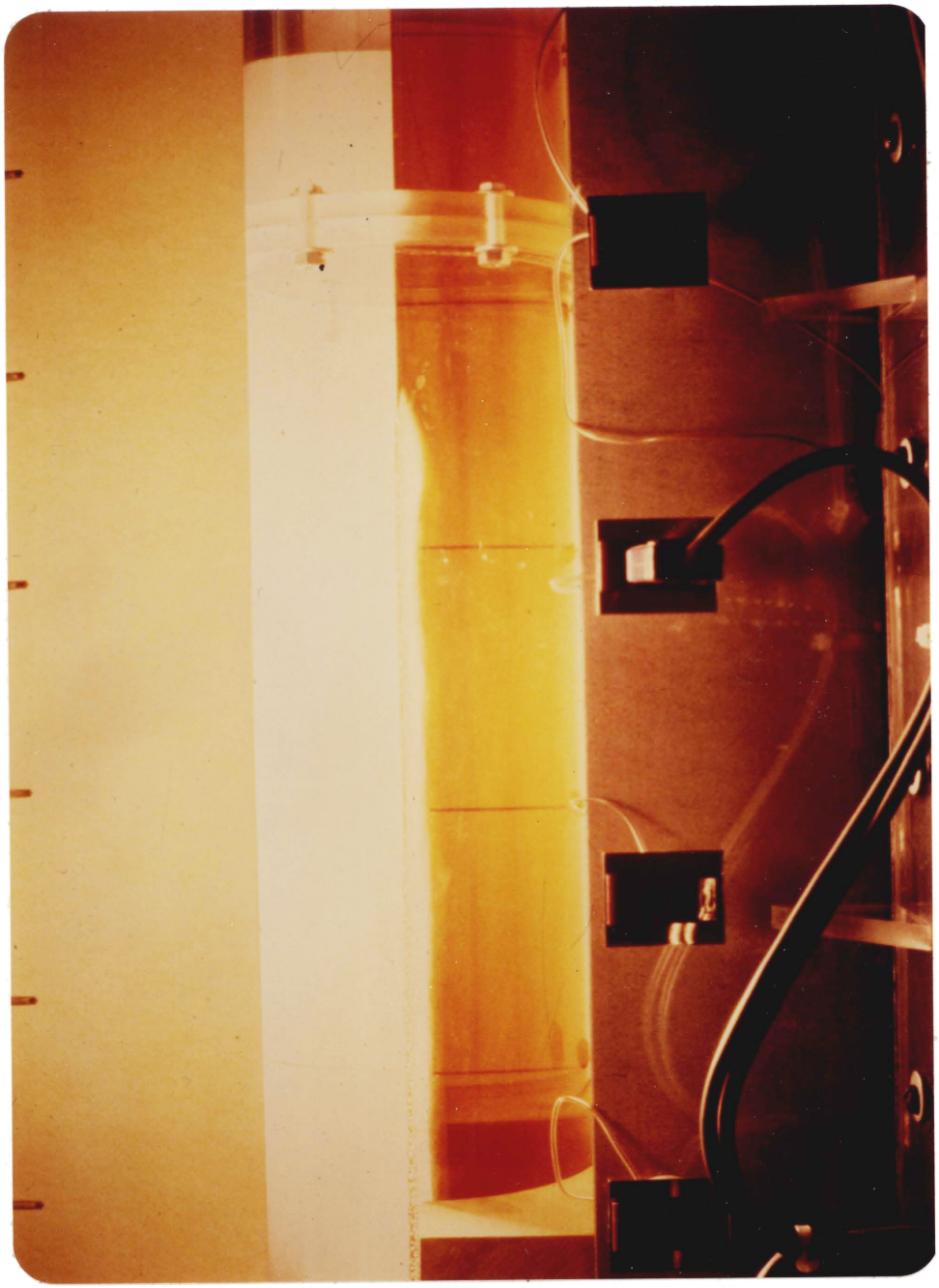

FIGURE VI-1: A PHOTOGRAPH OF PENTANE SPREADING ON WATER

spreading. The pentane is spreading from left to right and the water was dyed with a red color. As observed in Figure VI-1, pentane is thicker near the spreading front and becomes thinner in the tail. The general shape is consistent with Hoult's (1972a) theoretical prediction of the thickness profile in the gravity-inertia regime (see Figure II-12).

As the pentane spreads further downstream, it becomes thinner and thinner. The viscous drag then dominates as the retarding force and the spreading front is no longer thicker than the tail.

The experiments show that the early spreading of pentane on water agrees well with the prediction from the theoretical model of one-dimensional spreading developed by Hoult (1972a). Figure VI-2 presents the experimental results for pentane spills of various volumes. The data show the dimensionless spreading distance is proportional to the dimensionless time raised to the two-third power. The intercept value is equal to 1.72 and this is the value taken as the coefficient η in equation (II-9). Substituting into equation (II-10), the value of λ is obtained and equal to 1.64. These values of λ and η are slightly different from those obtained by Suchon (1970), 1.6 and 1.40 respectively. This may be due to the different geometry of the spill apparatus used. λ and η are therefore considered to be functions of the geometry of the spill apparatus and the values obtained here will be applied to the modeling analysis of all cryogen spills in this study. In Figure VI-3, experimental values and the theoretical predictions are compared for pentane spills. Except the end points where pentane spreading has a transition into the gravity-viscous regime, the agreement between theory and experiment is very good.

Hoult's correlation was developed for the ideal assumption of an instantaneous spill. Because the data for pentane spills agrees very well with the correlation, it is assumed that the experimental distributor's performance closely approaches an instantaneous spill for the largest side port opening

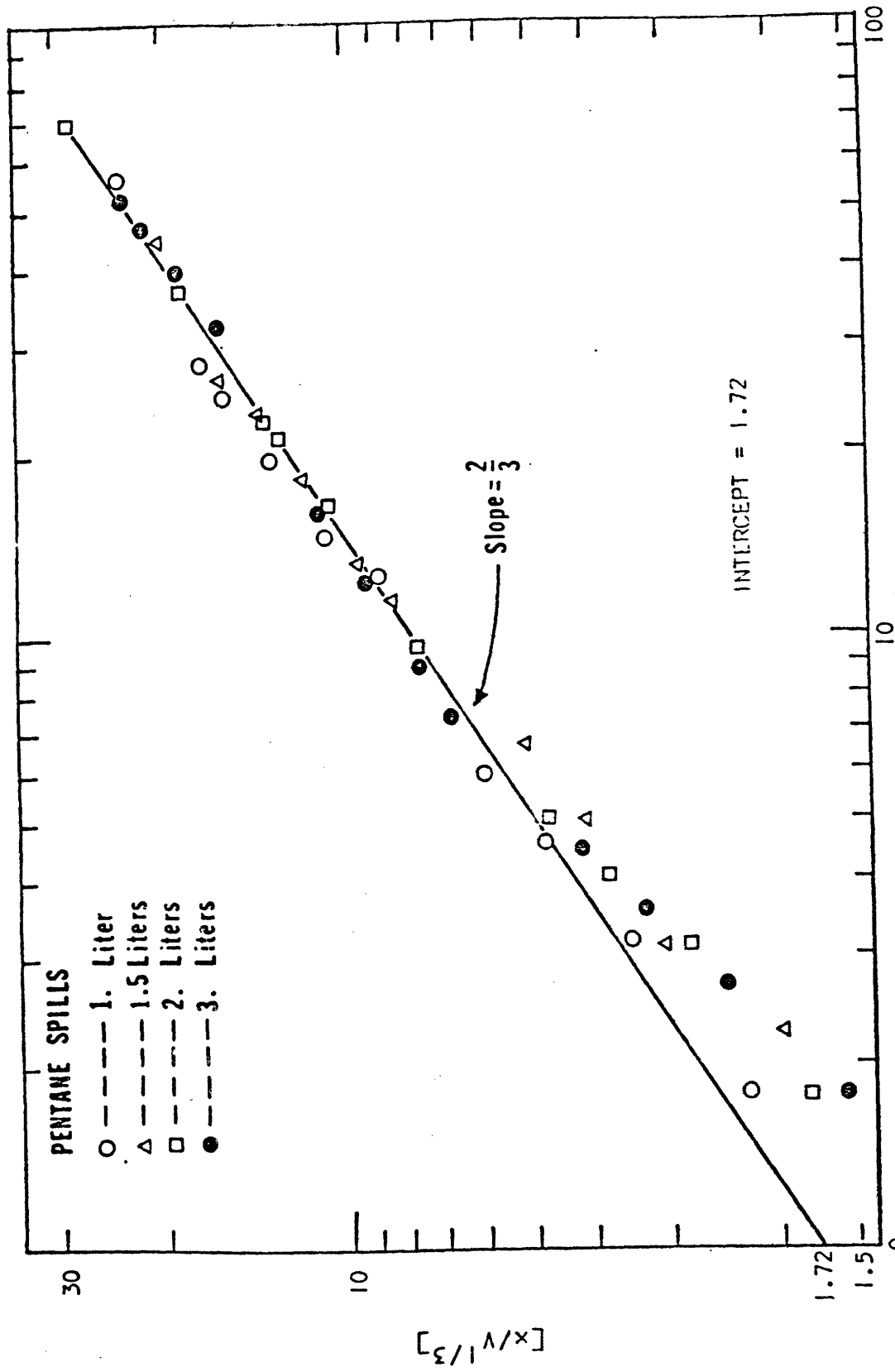

FIGURE VI-2: DIMENSIONLESS CORRELATION OF SPREADING DISTANCE WITH TIME FOR PENTANE SPILLS.

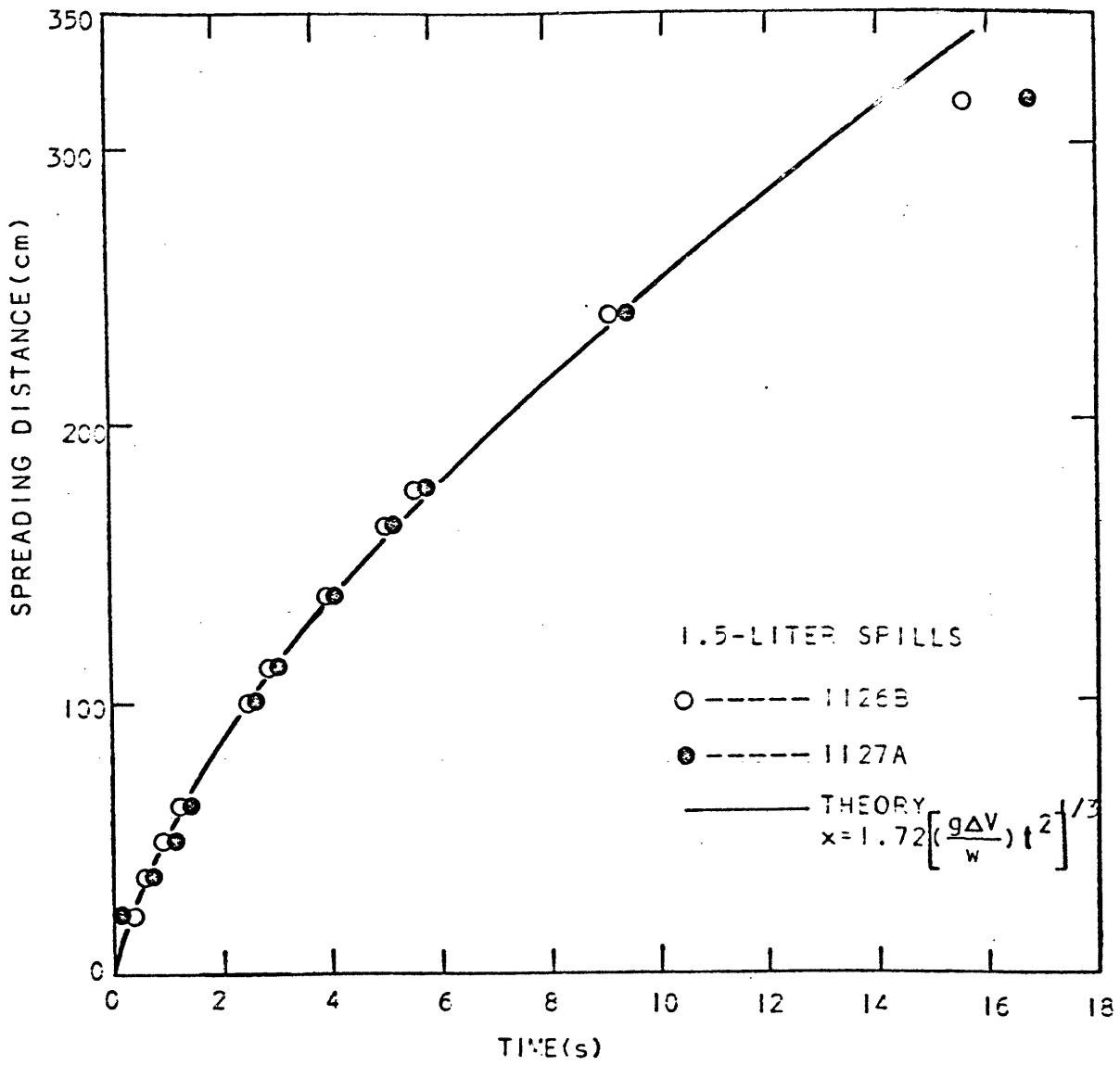

FIGURE VI-3: SPREADING DISTANCE AS A FUNCTION OF TIME FOR FOR PENTANE SPILLS. EXPERIMENTAL DATA AND THEORETICAL PREDICTIONS COMPARED.

(48.4 cm^2). This opening is used for all cryogen spills (descriptions follow) except in the case of propane where its size is varied.

B. BOILING AND SPREADING OF CRYOGENS ON WATER

For cryogens spilled on water in an unconfined area, boiling and spreading occur simultaneously. The movement of the spreading front was recorded with thermocouples by the Real Time Computer. With all the necessary measurements from experiments, the local boil-off rate as a function of time were estimated by the data analysis scheme described in Chapter IV.

Liquid Nitrogen

Safety considerations dictated that initial equipment tests be made with liquid nitrogen because of its non-flammability. Six spills of nitrogen were performed. The experimental conditions for these tests are given in Table VI-2.

The spreading distance as a function of time for nitrogen spills are given in Figures VI-4 and VI-5. Figure VI-4 also demonstrates good reproducibility in the experiments. The length of the spill apparatus allows the measurement of maximum spreading distance only for 0.5 - and 1.0 - liter nitrogen spills. The values of the maximum spreading distance are given in Table VI-3.

Figure VI-6 is a photograph of the simultaneous boiling and spreading of liquid nitrogen on water. Liquid nitrogen is spreading from left to right. Again the general shape is the same as that observed in the pentane spills: a thicker spreading front followed by a thinner tail. Viewed from above the spreading front is perpendicular to the direction of the flow. This general shape persists until almost the end of the spreading phenomena when liquid nitrogen no longer uniformly covers the water surface.

During the spreading, many bubbles form at the liquid nitrogen - water

TABLE VI-2

Experimental Conditions for Nitrogen Spills

Test	Volume Spilled (liter)	Cross-Sectional Area of Distributor Opening (cm^2)
1211B	0.5	48.4
1211F	1.0	48.4
61201	1.0	48.4
1211G	1.5	48.4
1210B	2.0	48.4
1207A	2.0	48.4

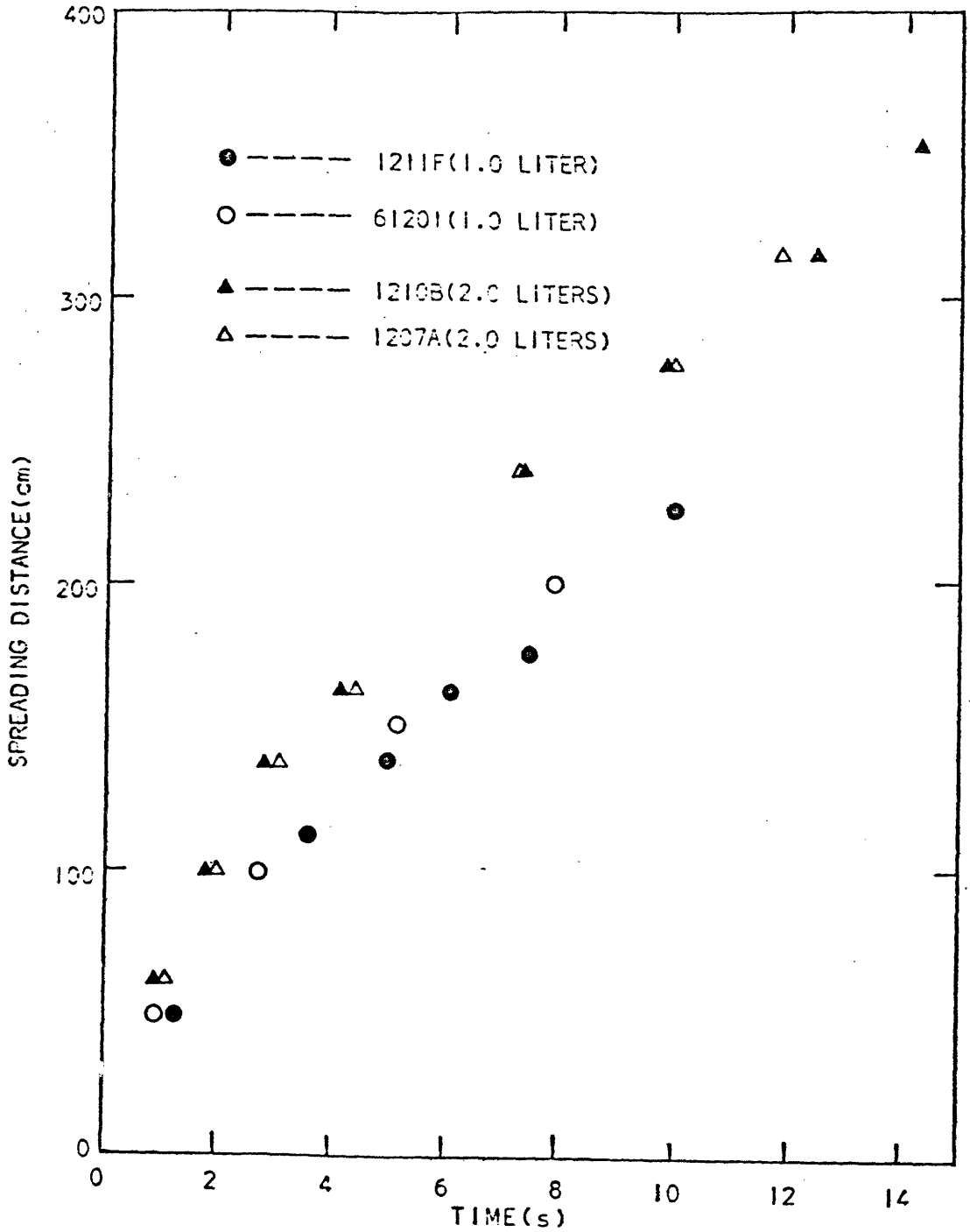

FIGURE VI-4: SPREADING DISTANCE AS A FUNCTION OF TIME FOR LIQUID NITROGEN SPILLS.

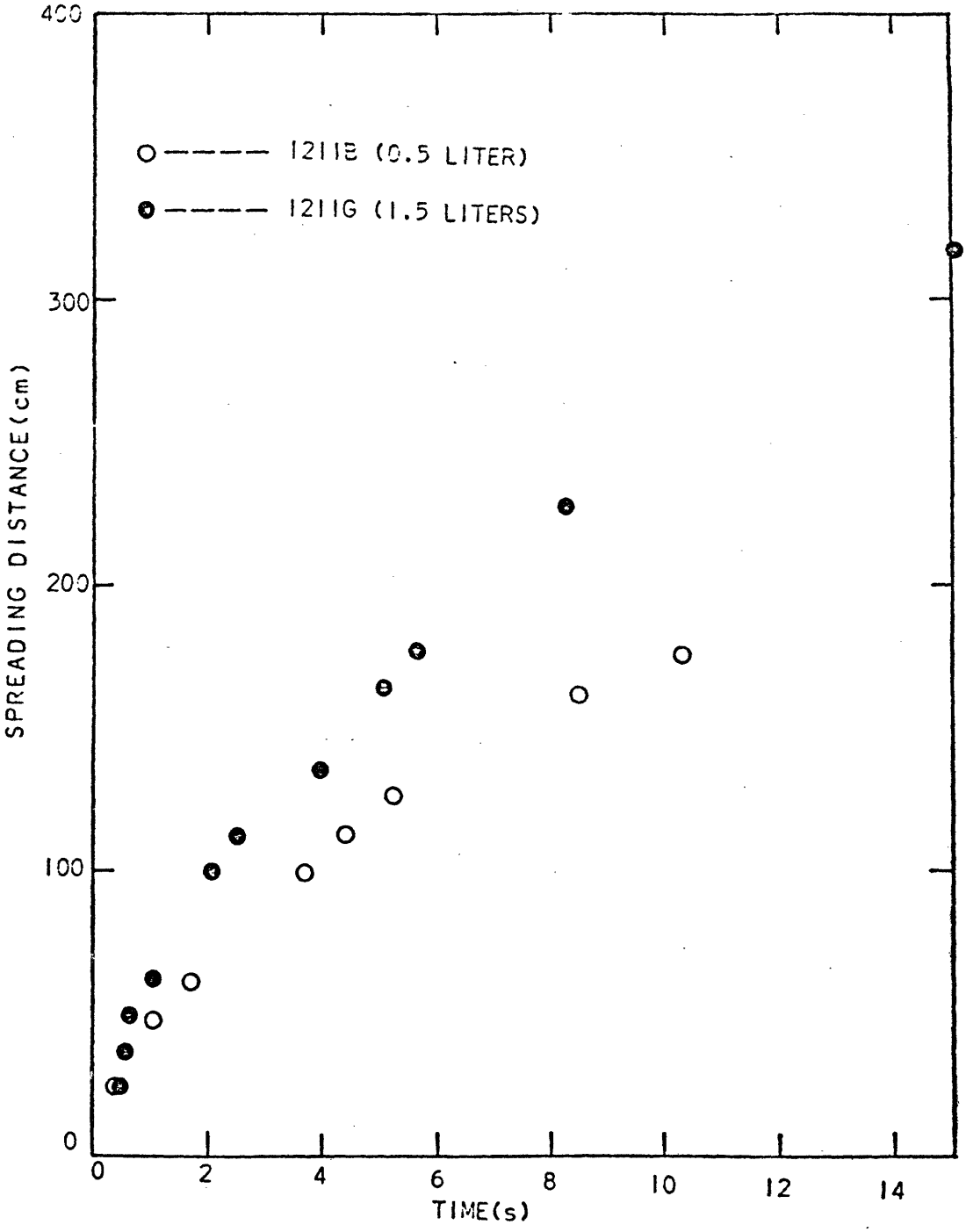

FIGURE VI-5: SPREADING DISTANCE AS A FUNCTION OF TIME FOR LIQUID NITROGEN SPILLS.

TABLE VI-3

Maximum Spreading Distance for Nitrogen Spills

Test	Volume Spilled (liter)	Maximum Spreading Distance (cm)
1211B	0.5	226
1211F	1.0	315
61201	1.0	305

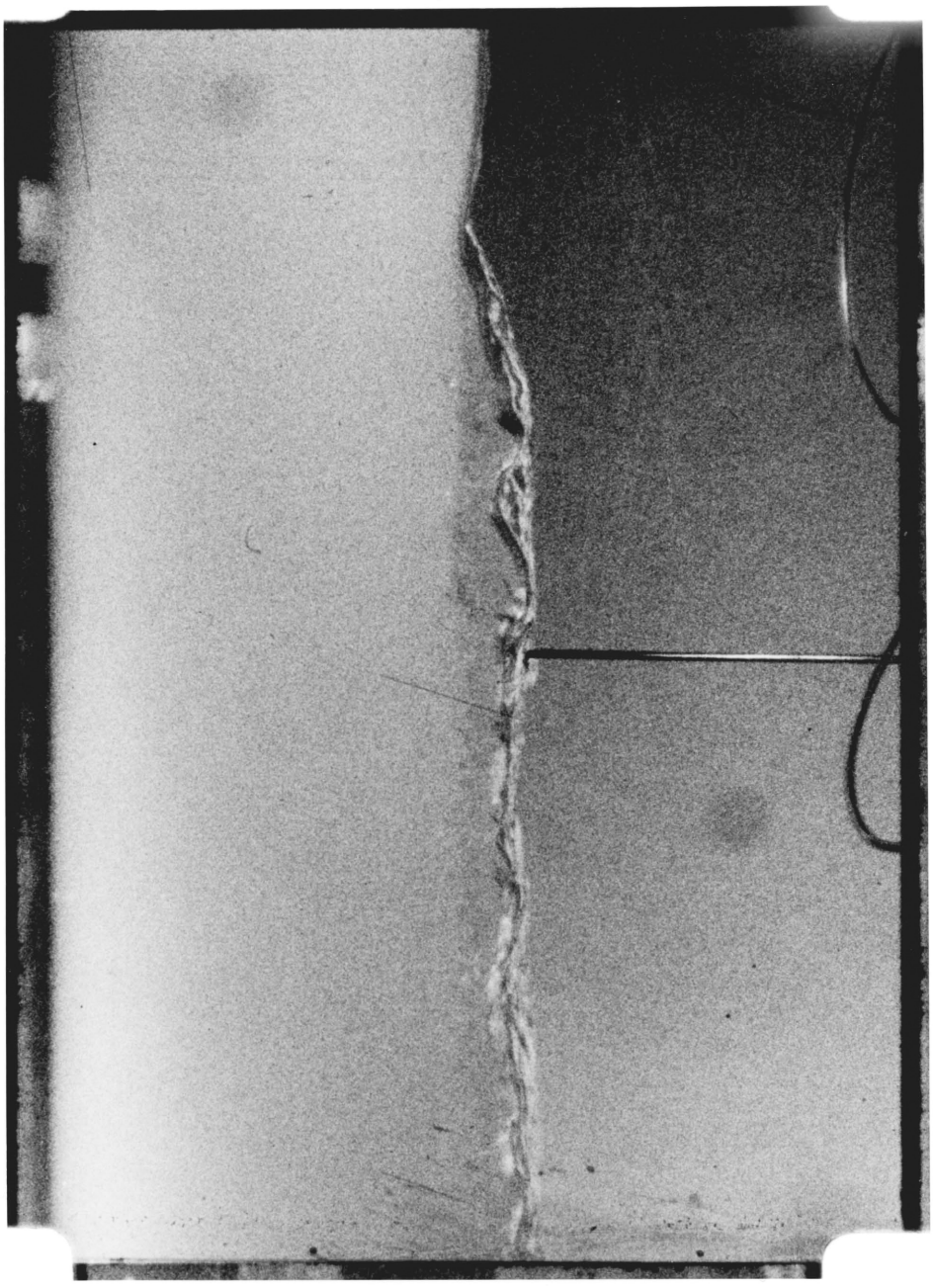

FIGURE VI-6: A PHOTOGRAPH OF LIQUID NITROGEN SPREADING ON WATER

interface and cause sever agitation. A layer of ice uniformly forms on the water surface downstream of the cryogen distributor. In the vicinity of the distributor, no ice formation has been observed. It was noted that, in the experiment with liquid nitrogen, the water immediately adjacent to the distributor becomes liquid nitrogen free very soon after the spreading front has passed.

Liquid Methane

Five spills of methane on water were conducted with George Dainis as a part of his M.S. Thesis. The experimental conditions are given in Table VI-4. Figures VI-7 and VI-8 present the spreading data versus time for methane spills. Table VI-5 gives the values of maximum spreading distance for small quantity spills.

Liquid methane spreads similar to liquid nitrogen, but faster than nitrogen for the same initial spilled volume. A photograph of the spreading front of methane is shown in Figure VI-9. Again the spreading front is thicker and the methane layer thins out in the tail. Ice forms sooner on the water surface for methane spills than for spills of liquid nitrogen. The upper surface of the ice layer is uniform but the under side is irregularly shaped and suggestive of closely packed ping-pong balls. The ice also has a milky color, different from the transparent form found in nitrogen spills. The bubbles formed were somewhat larger than that noted for nitrogen spills and no foam was observed.

A test (number 72401) was conducted with certified purity grade methane (minimum purity, 99. mole%). The results essentially overlap with those from a test (number 71101) made with ultra high purity grade methane (minimum purity 99.97 mole %), shown in Figure VI-7. This comparison indicates the effect of impurities present in the certified purity grade methane on the spreading of methane on water is not significant.

TABLE VI-4

Experimental Conditions for Methane Spills

Test	Volume Spilled (liter)	Methane Purity (mole %)	Cross-Sectional Area of Distributor Opening (cm^2)
70201	0.5	99.97	48.4
70901	0.75	99.97	48.4
71101	1.0	99.97	48.4
72401	1.0	99.0	48.4
72201	2.0	99.0	48.4

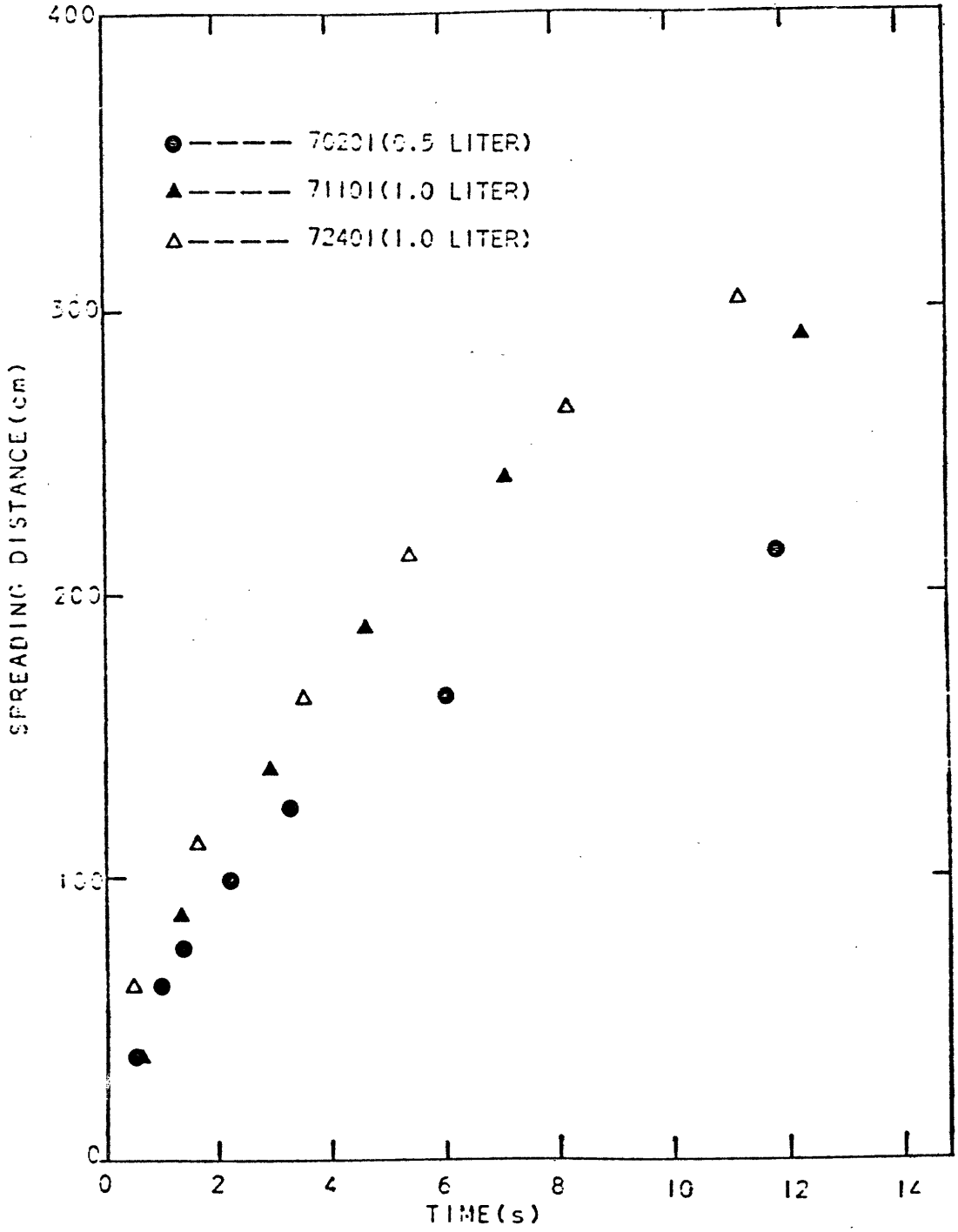

FIGURE VI-7: SPREADING DISTANCE AS A FUNCTION OF TIME FOR LIQUID METHANE SPILLS.

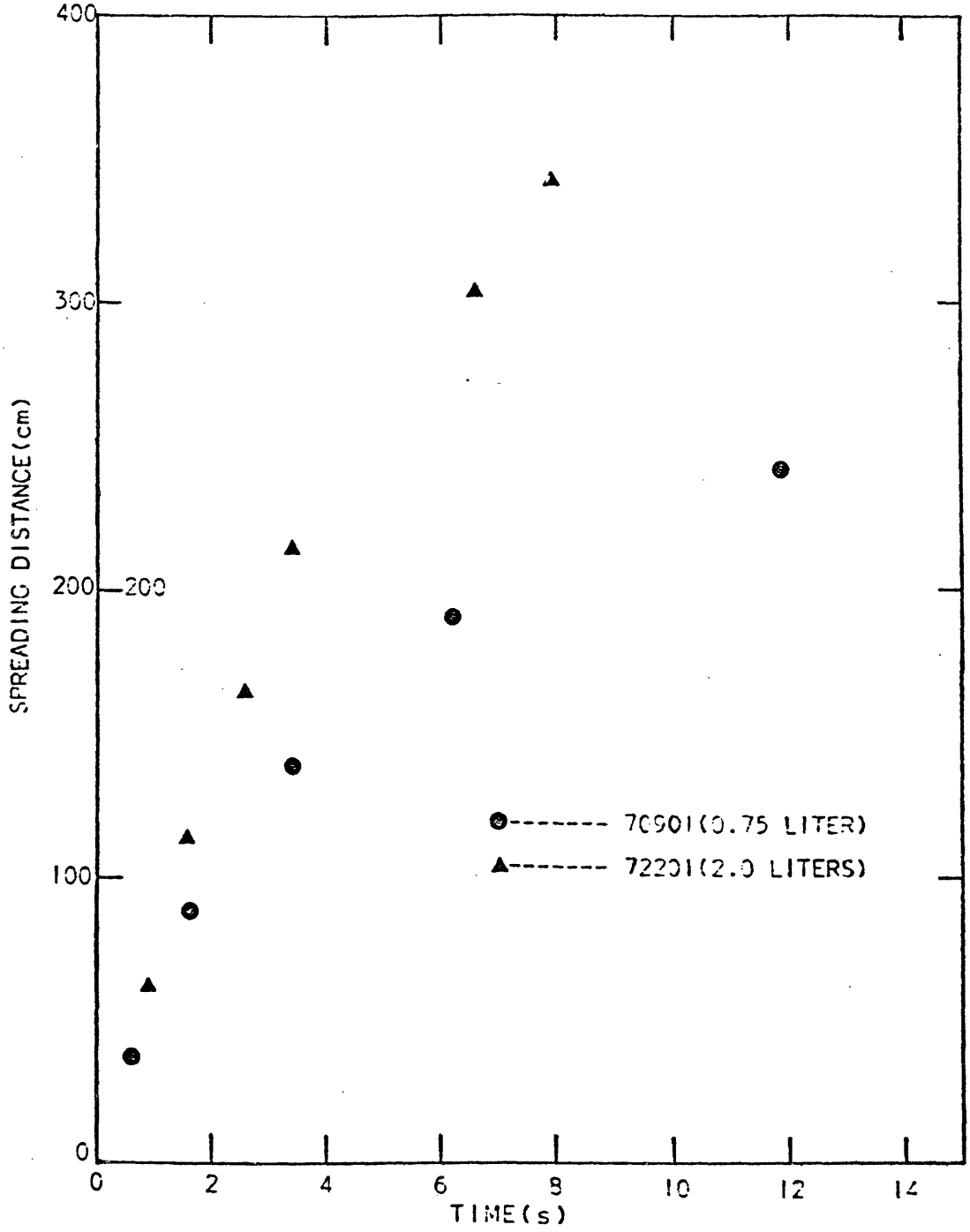

FIGURE VI-8: SPREADING DISTANCE AS A FUNCTION OF TIME FOR LIQUID METHANE SPILLS.

TABLE VI-5

Maximum Spreading Distance for Methane Spills

Test	Volume Spilled (liter)	Maximum Spreading Distance (cm)
70201	0.5	229
70901	0.75	279
71101	1.0	317
72401	1.0	317

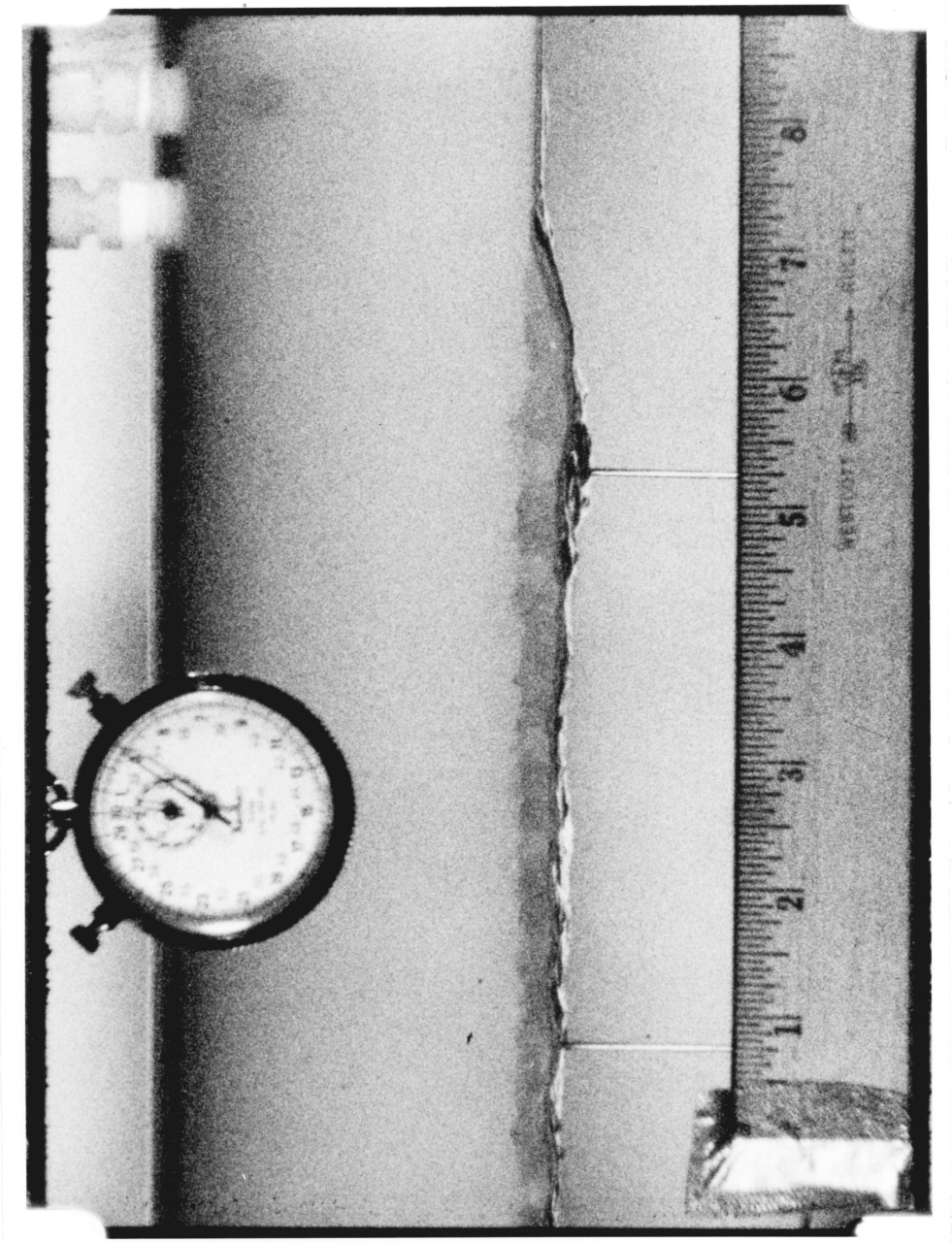

FIGURE VI-9: A PHOTOGRAPH OF LIQUID METHANE SPREADING ON WATER

Liquid Propane

Twenty spills of propane on water were made. Experimental conditions for these tests are given in Table VI-6. The spreading distance as a function of time is shown in Figures VI-10 through VI-15. Upon contacting the water, propane boils very rapidly and violently. Ice forms almost immediately on the water surface. Within a few seconds, the boiling rates drop to considerably lower values as seen in Figures VI-16 through VI-31.

The initial violent boiling of propane causes considerable churning of the water. As water contacts the bulk of liquid propane it freezes in a very irregular fashion. This is shown in Figure VI-32. Once irregular ice covers the water surface, the interaction becomes less vigorous and propane continues to boil on the surface of the ice.

The ice formed is opaque and somewhat yellowish in color. The rough ice sheet traps liquid propane and forms a dam which hinders the propane spreading. As the propane continues to vaporize, the bubbling cryogen eventually rises over the "ice dam" and continues to spread. The discontinuities observed in Figures VI-11, VI-12 and VI-15 are where the "ice dams" form. However, the exact location of the "ice dam" is not predictable.

The maximum spreading distance for a propane spill is much smaller than that for a nitrogen or methane spill of the same volume. Table VI-7 presents the values of maximum spreading distance for thirteen propane spills.

As the propane reaches its maximum spreading distance during the experiment, there is some portion of liquid propane trapped in the "puddles" on the ice layer which continues to boil on the ice surface. Considerable amount of propane remains near the cryogen distributor. The ice layer first melts downstream and, as the local propane continues to boil away, the ice melts and the ice front recedes toward the distributor.

Furthermore, late in the spreading experiments, liquid propane occasion-

TABLE VI-6

Experimental Conditions for Propane Spills

Test	Volume Spilled (liter)	Cross-Sectional Area of Distributor Opening (cm^2)
62301	0.5	48.4
70801	0.5	48.4
1014G	0.5	48.4
1015G	0.5	48.4
62401	0.75	48.4
1016G	0.75	48.4
1019G	0.75	48.4
62801	1.0	48.4
80501	1.0	48.4
80601	1.0	48.4
71401	1.5	48.4
71601	1.5	48.4
1017G	1.5	48.4
1018G	1.5	48.4
1021G	1.5	48.4
82102	2.0	48.4
1020G	2.0	48.4
70301	3.0	48.4
1023G	1.0	19.4
1027G	2.0	19.4
1028G	3.0	19.4

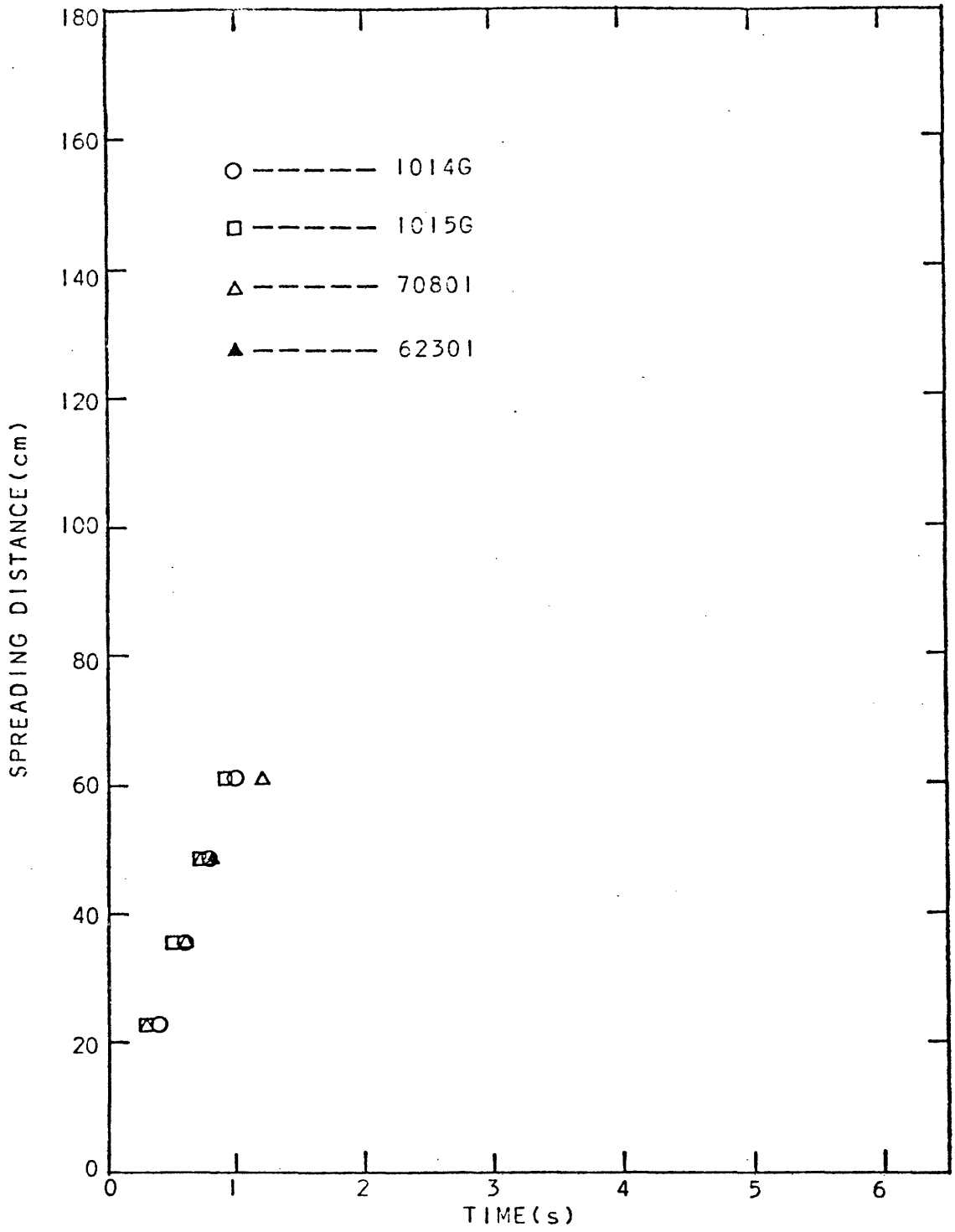

FIGURE VI-10: SPREADING DISTANCE AS A FUNCTION OF TIME FOR 0.5-LITER PROPANE SPILLS.

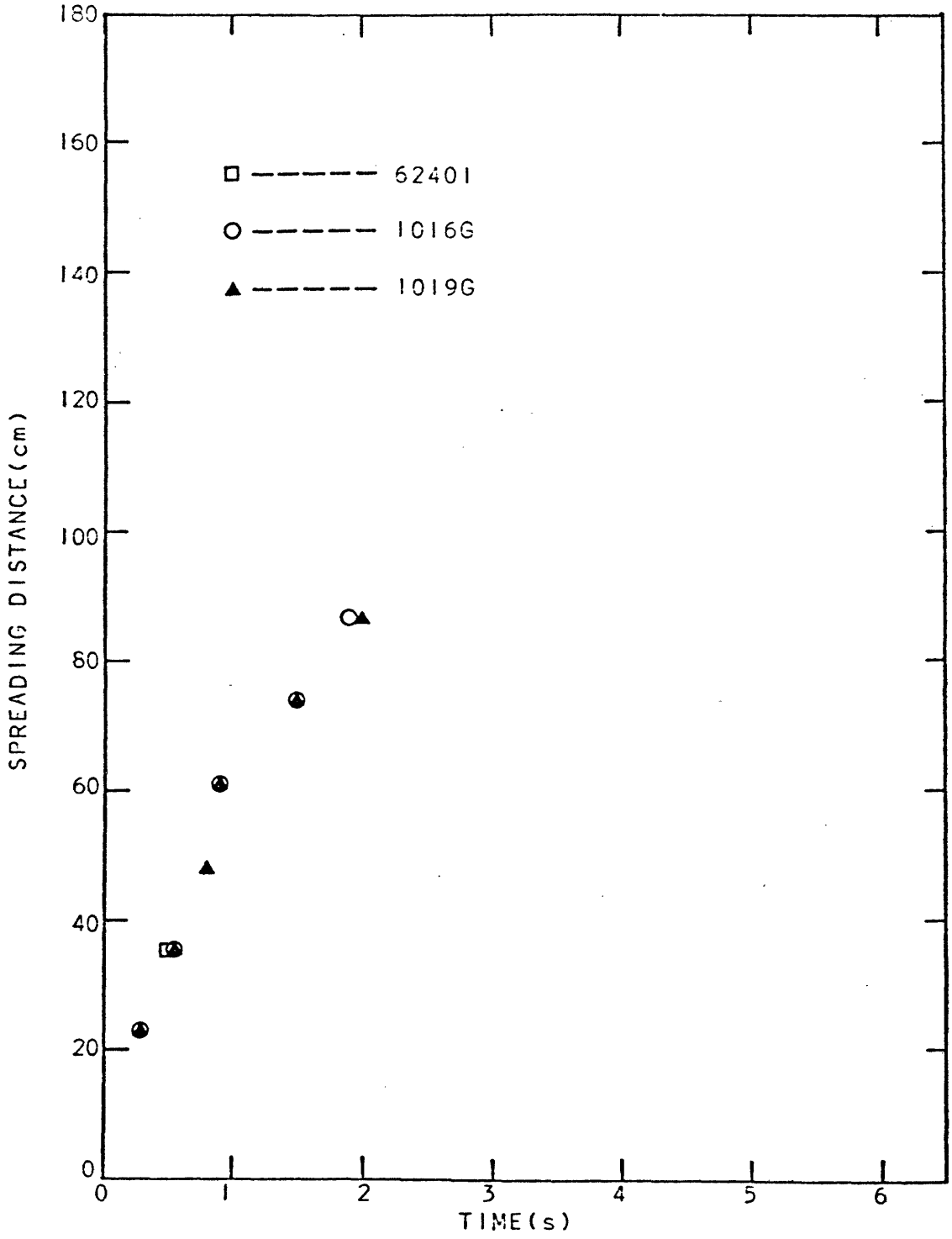

FIGURE VI-11: SPREADING DISTANCE AS A FUNCTION OF TIME FOR 0.75-LITER PROPANE SPILLS.

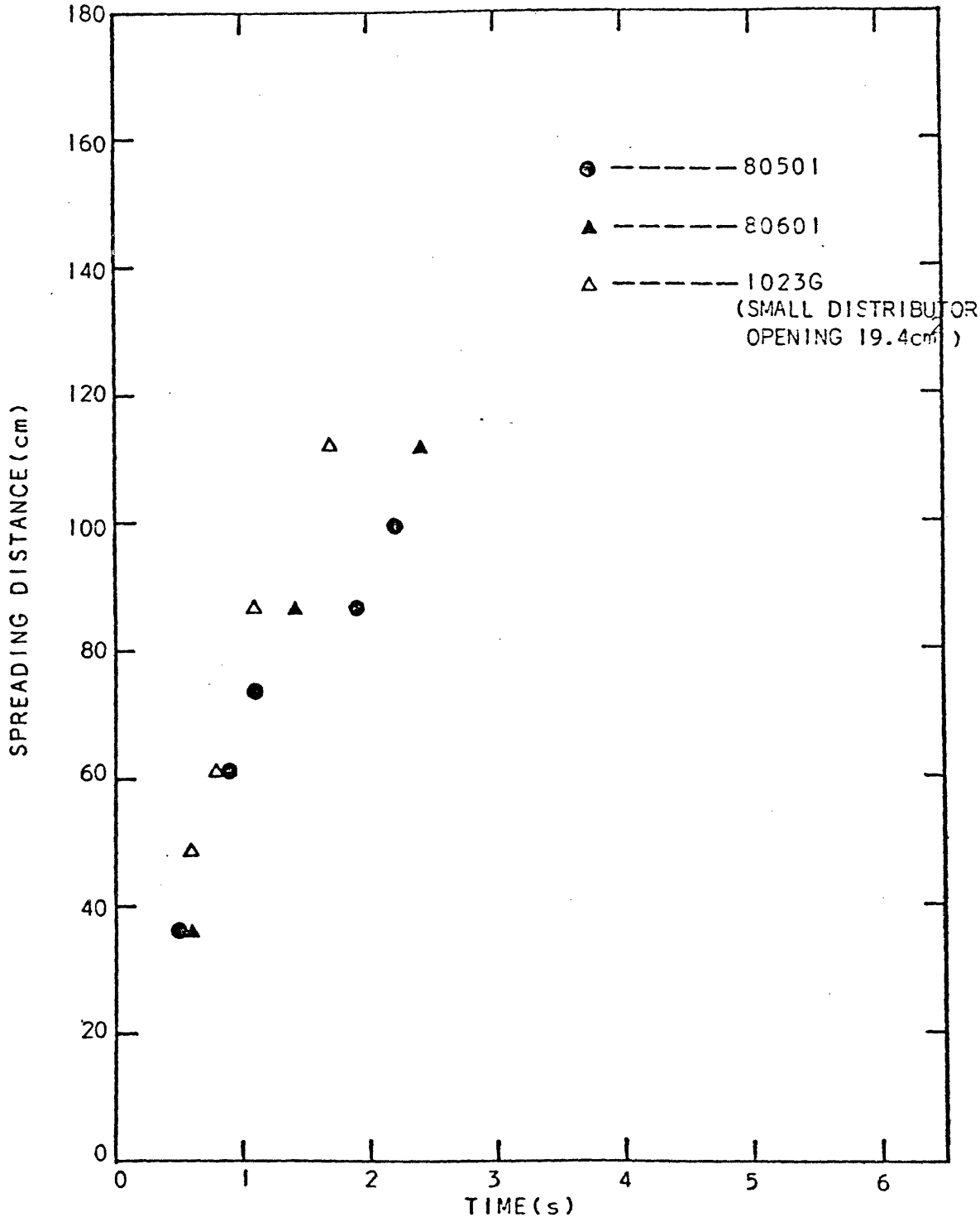

FIGURE VI-12: SPREADING DISTANCE AS A FUNCTION OF TIME FOR 1.0-LITER PROPANE SPILL.

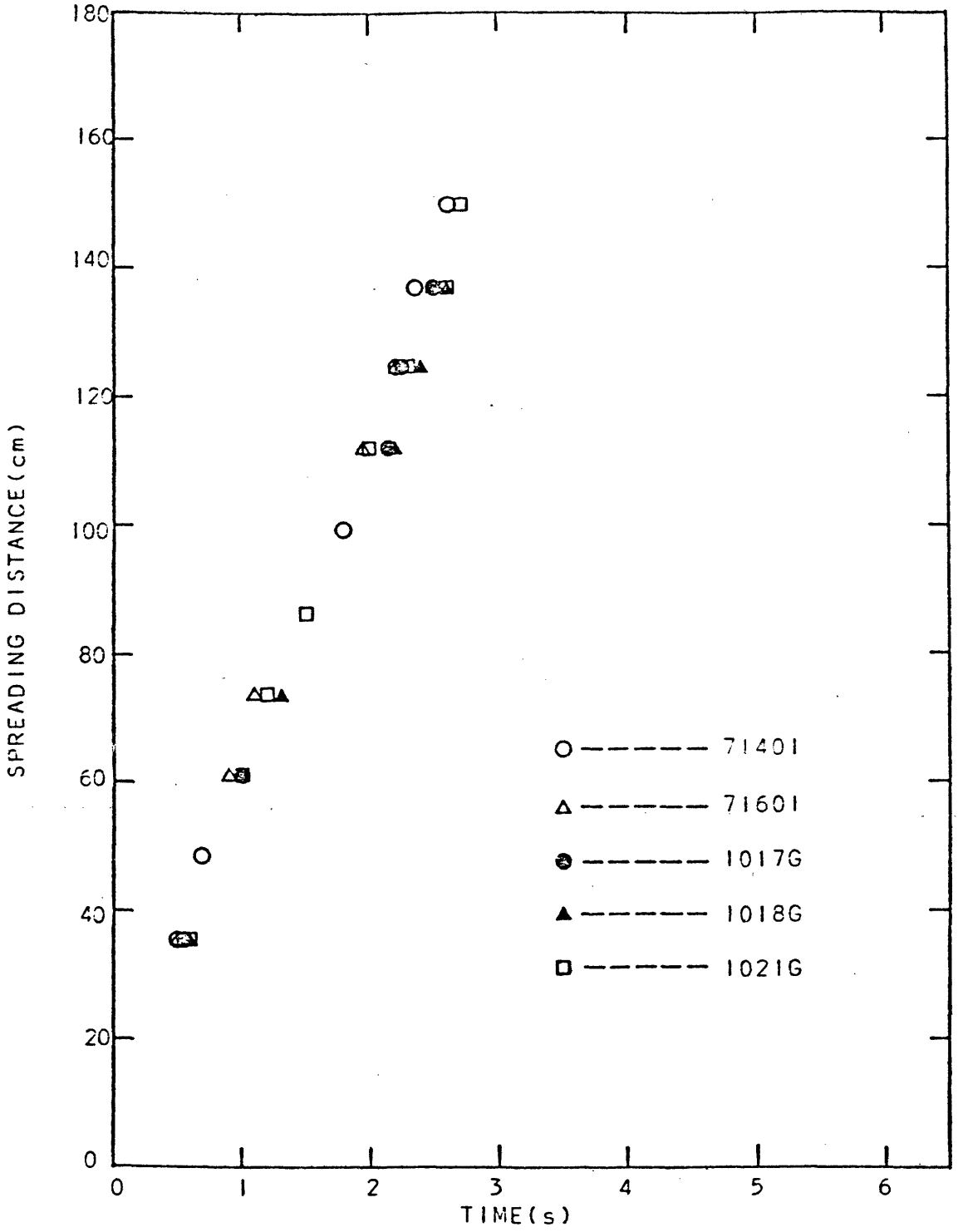

FIGURE VI-13: SPREADING DISTANCE AS A FUNCTION OF TIME FOR 1.5-LITER PROPANE SPILLS.

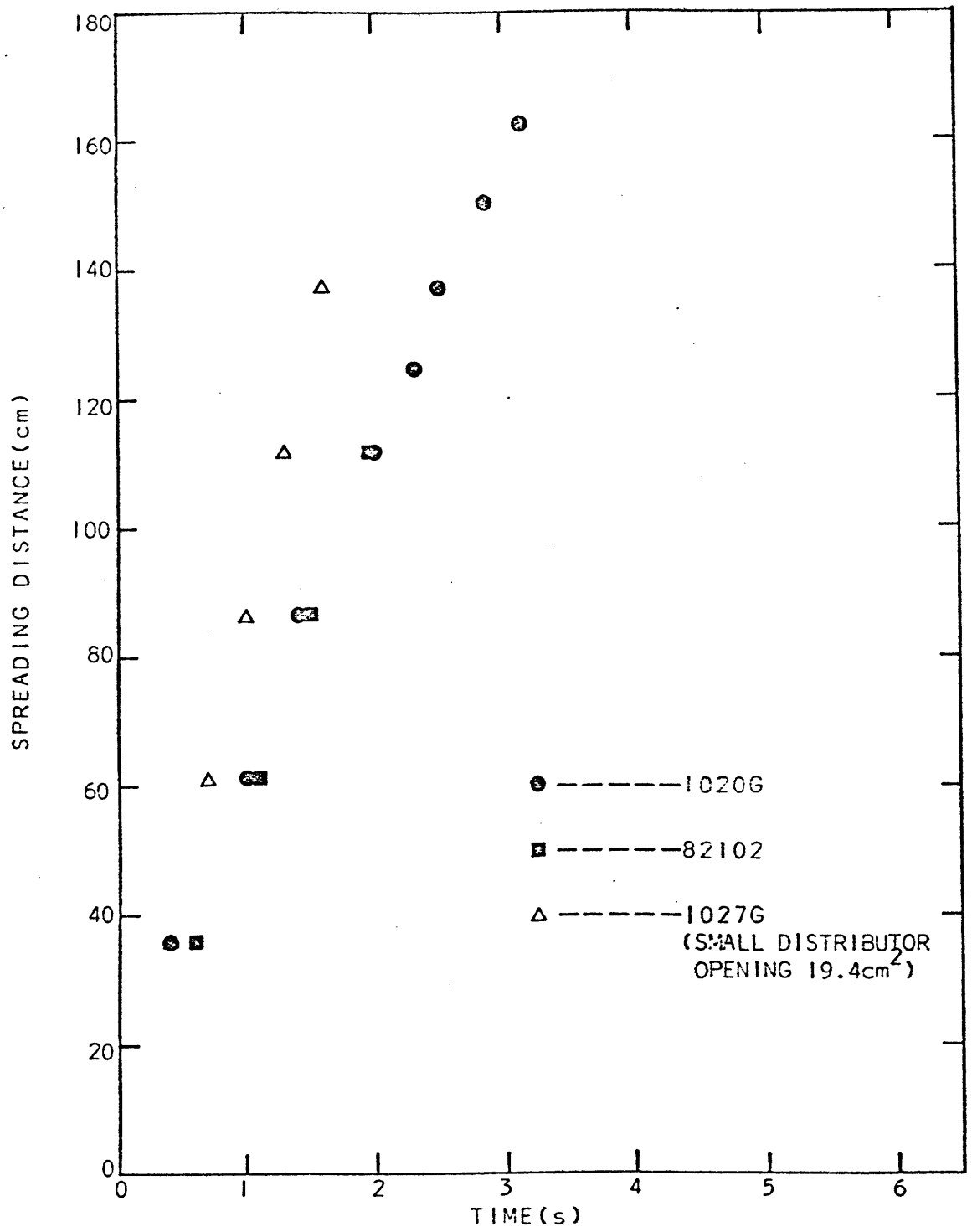

FIGURE VI-14: SPREADING DISTANCE AS A FUNCTION OF TIME FOR 2.0-LITER PROPANE SPILLS.

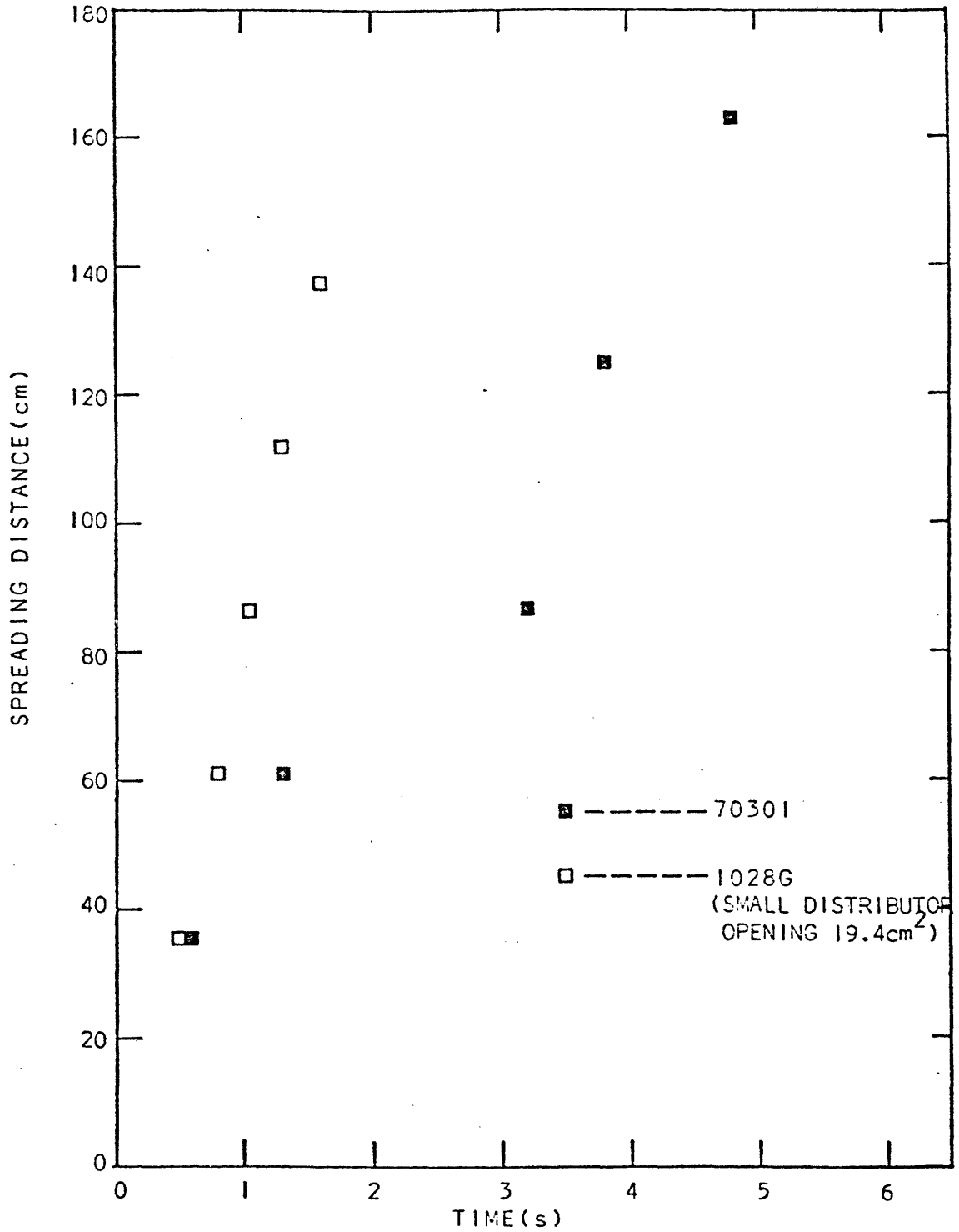

FIGURE VI-15: SPREADING DISTANCE AS A FUNCTION OF TIME FOR 3.0-LITER PROPANE SPILLS.

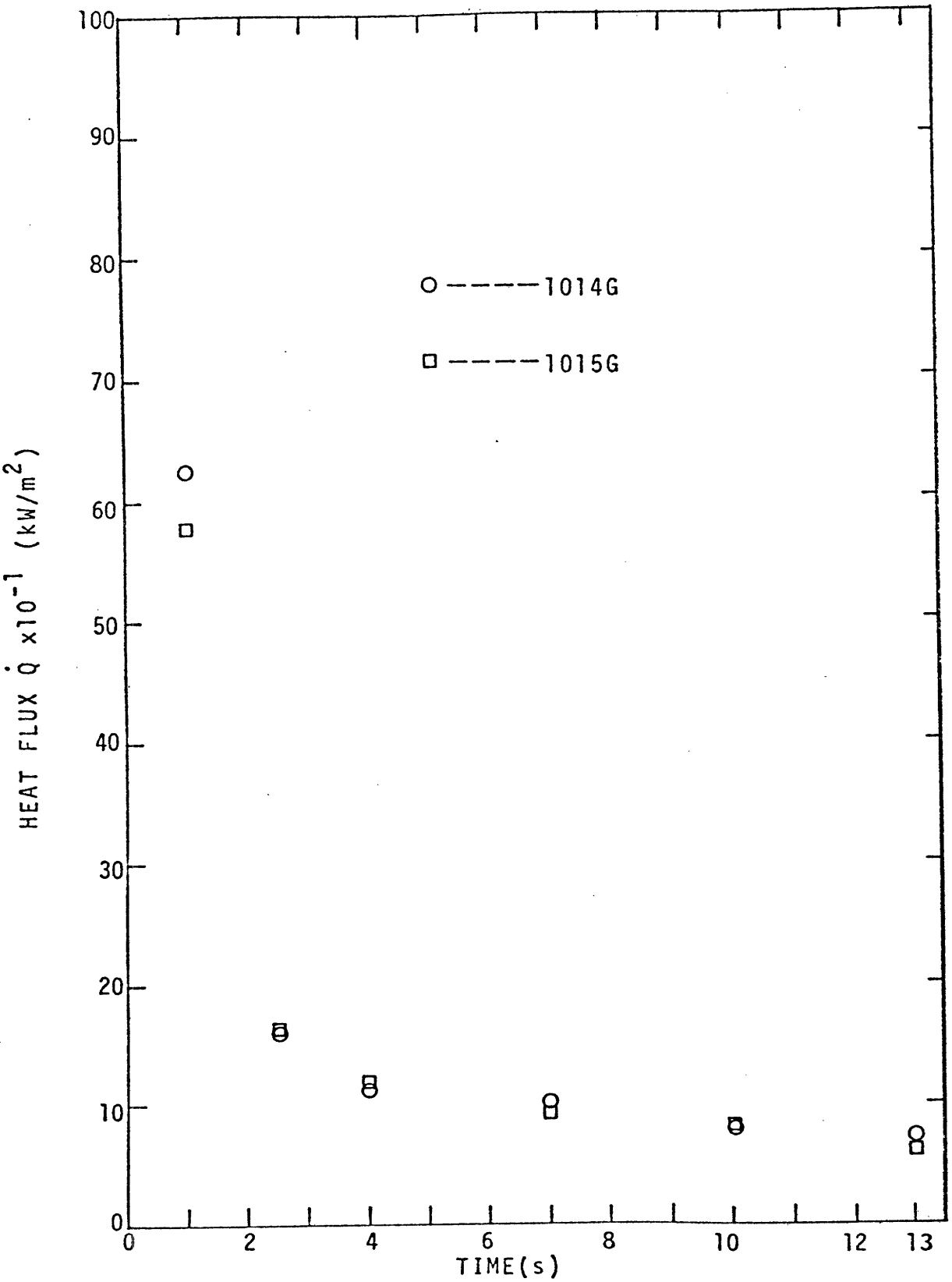

FIGURE VI-16: LOCAL BOIL-OFF RATE AS A FUNCTION OF TIME FOR 0.5-LITER PROPANE SPILLS AT THE FIRST SAMPLING STATION.

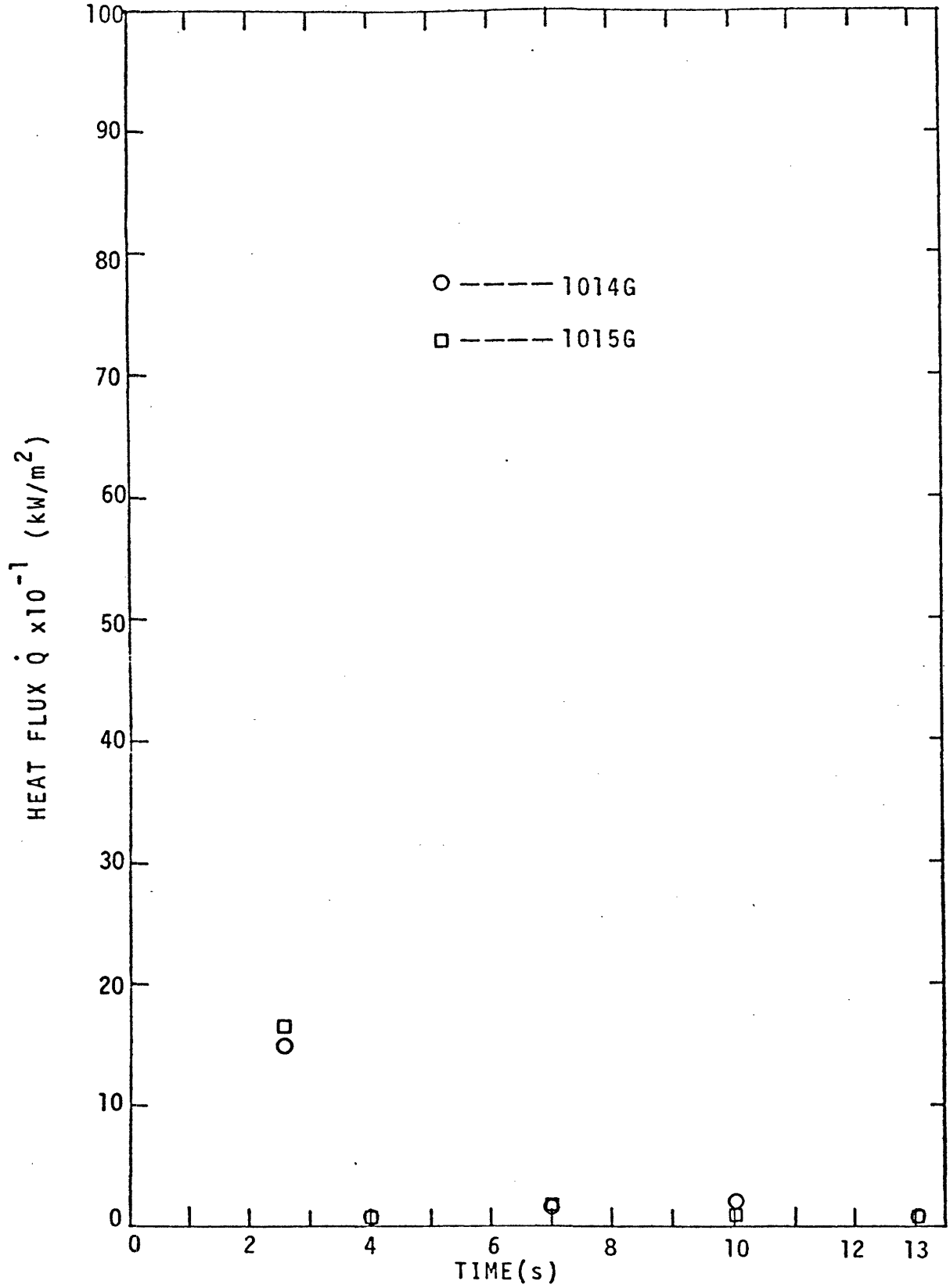

FIGURE VI-17: LOCAL BOIL-OFF RATE AS A FUNCTION OF TIME FOR 0.5-LITER PROPANE SPILLS AT THE SECOND SAMPLING STATION.

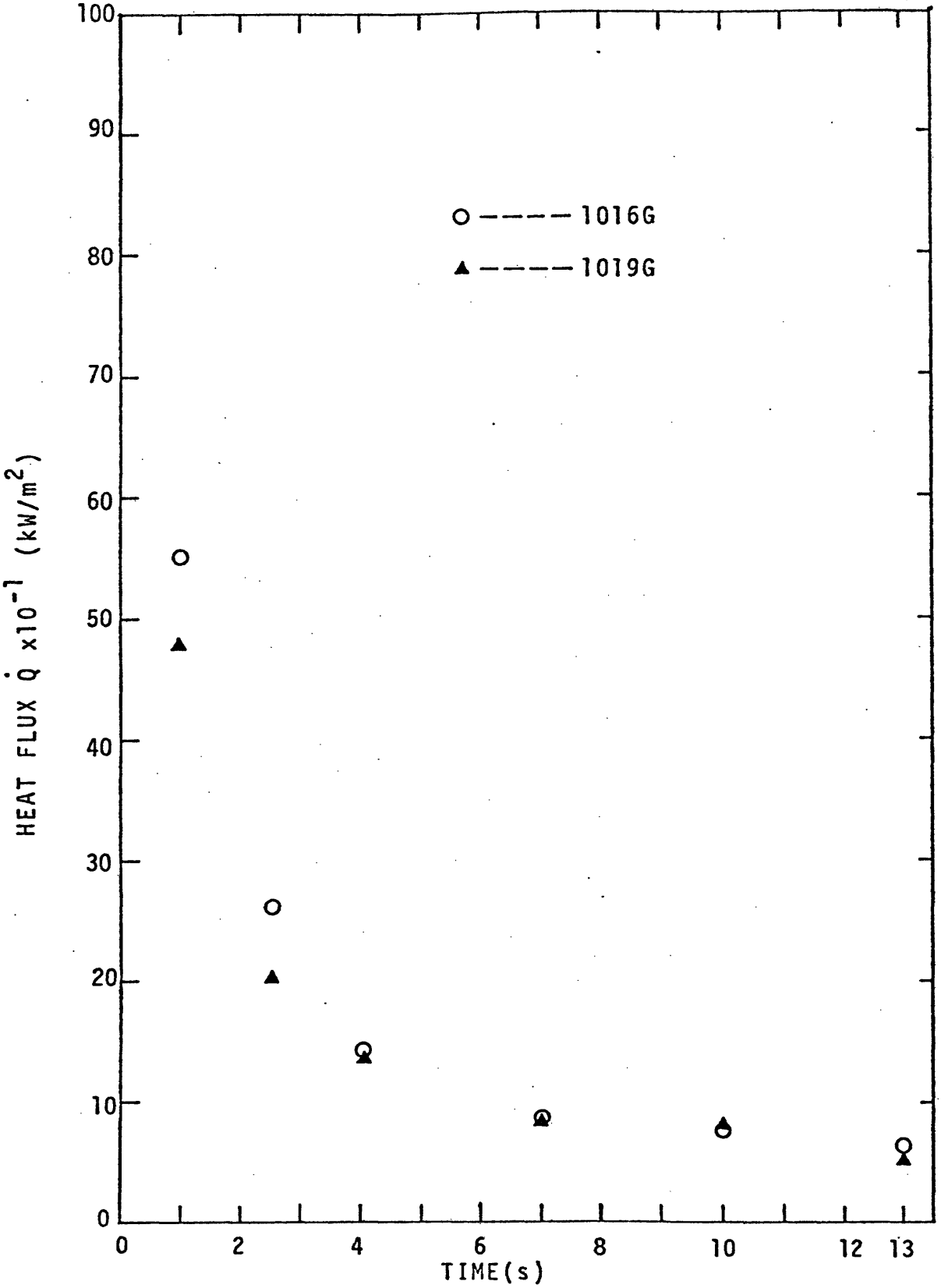

FIGURE VI-18: LOCAL BOIL-OFF RATE AS A FUNCTION OF TIME FOR 0.75-LITER PROPANE SPILLS AT THE FIRST SAMPLING STATION.

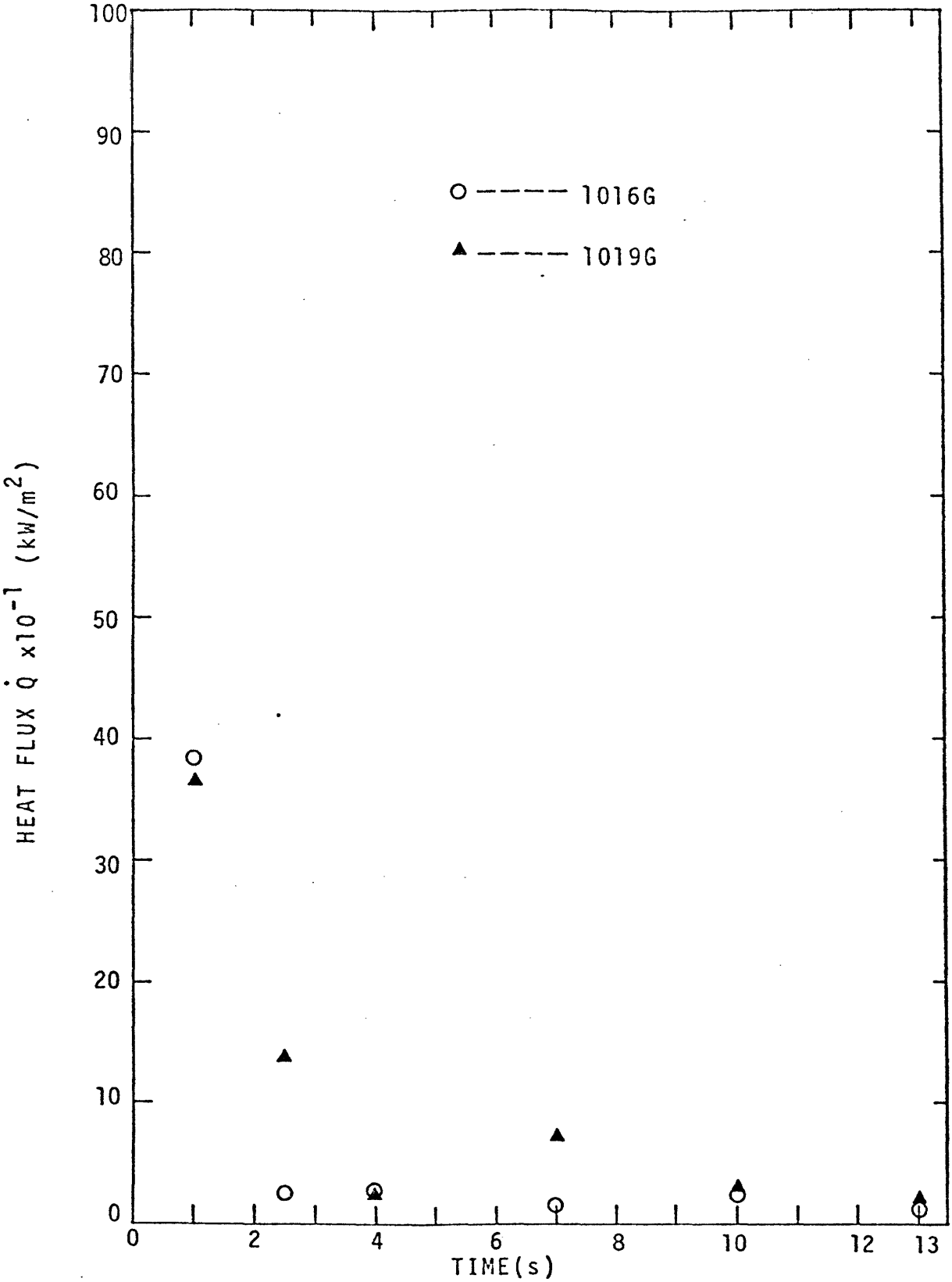

FIGURE VI-19: LOCAL BOIL-OFF RATE AS A FUNCTION OF TIME FOR 0.75-LITER PROPANE SPILLS AT THE SECOND SAMPLING STATION.

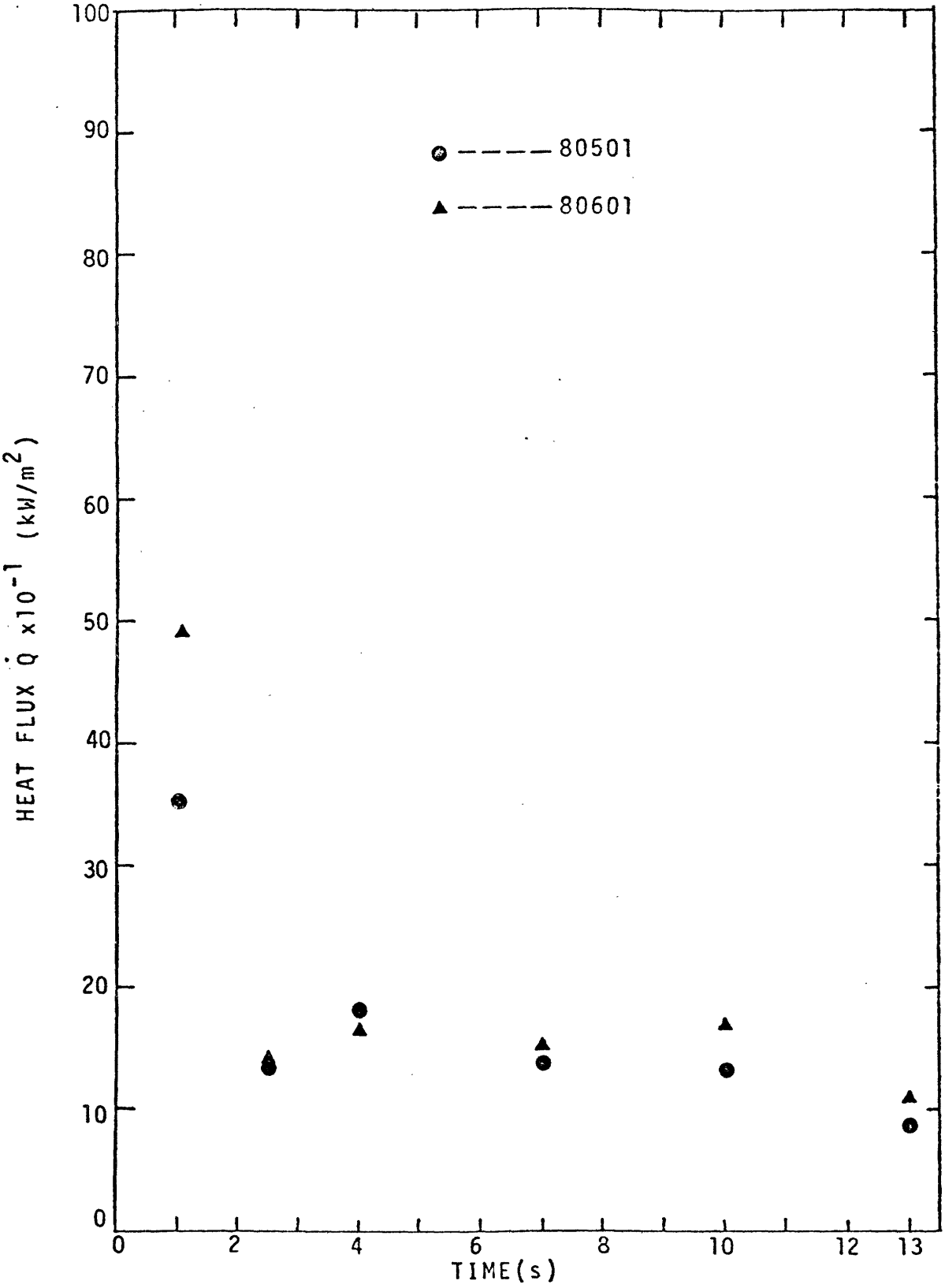

FIGURE VI-20: LOCAL BOIL-OFF RATE AS A FUNCTION OF TIME FOR 1.0-LITER PROPANE SPILLS AT THE FIRST SAMPLING STATION.

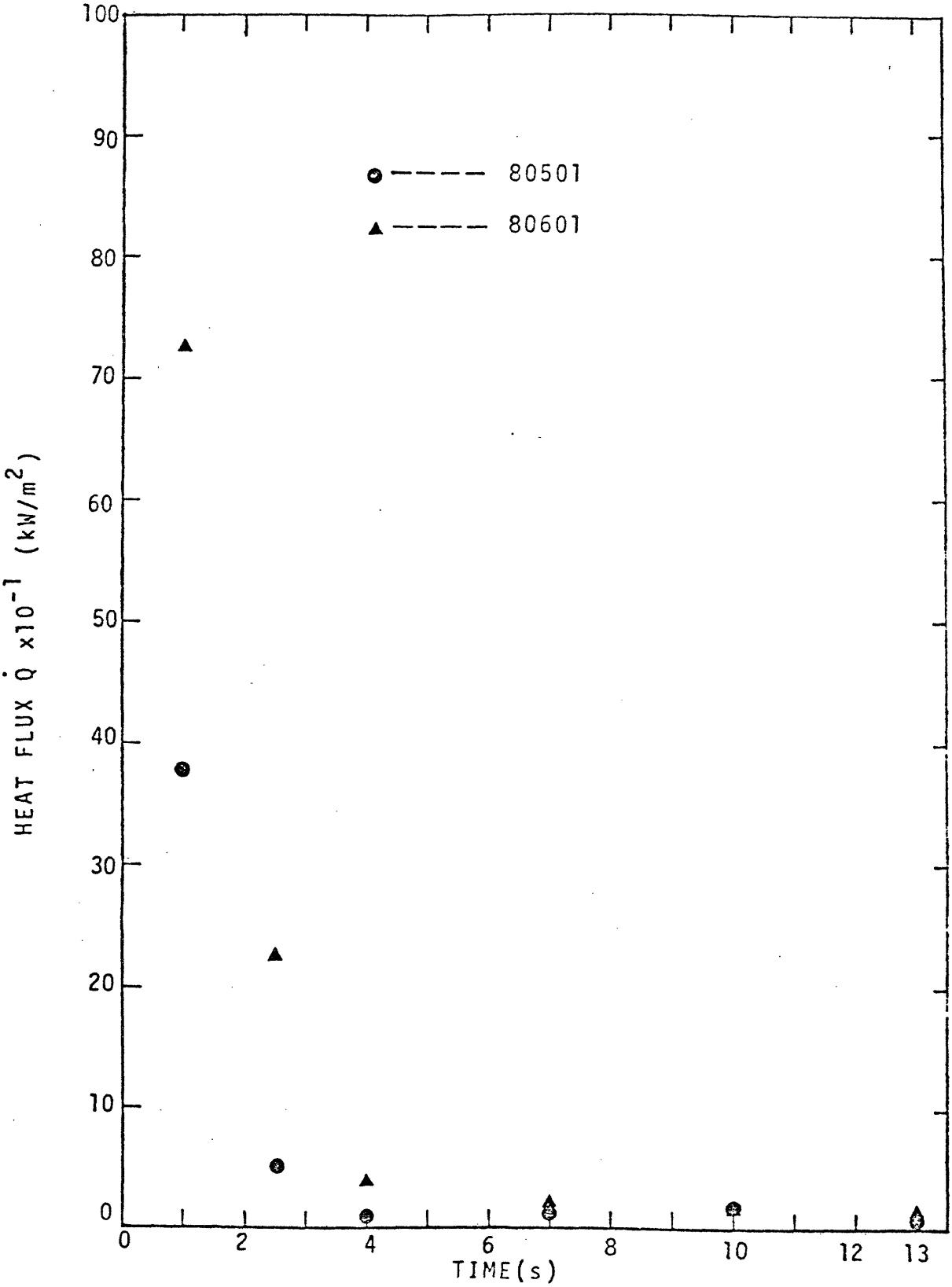

FIGURE VI-21: LOCAL BOIL-OFF RATE AS A FUNCTION OF TIME FOR 1.0-LITER PROPANE SPILLS AT THE SECOND SAMPLING STATION.

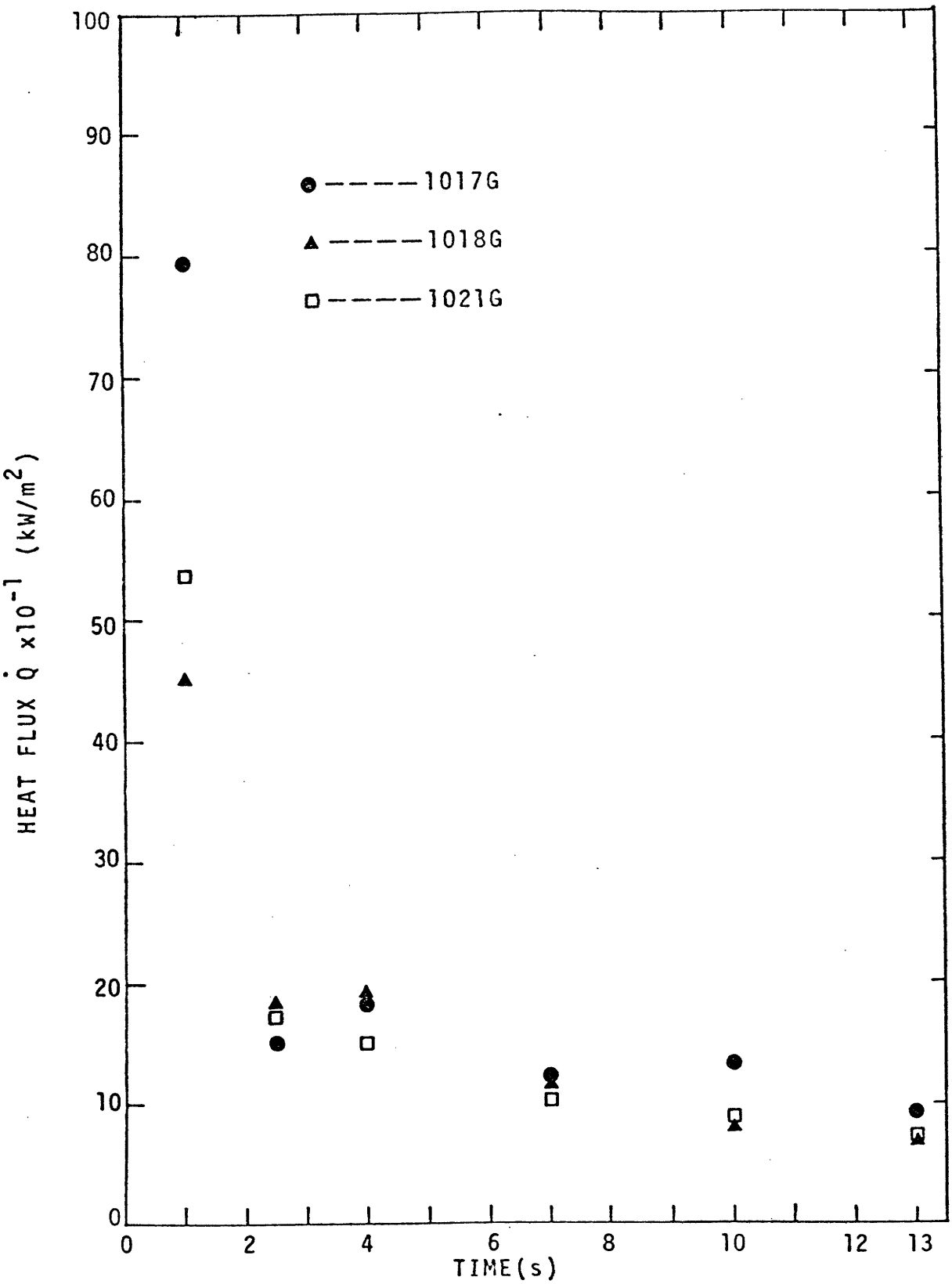

FIGURE VI-22: LOCAL BOIL-OFF RATE AS A FUNCTION OF TIME FOR 1.5-LITER PROPANE SPILLS AT THE FIRST SAMPLING STATION.

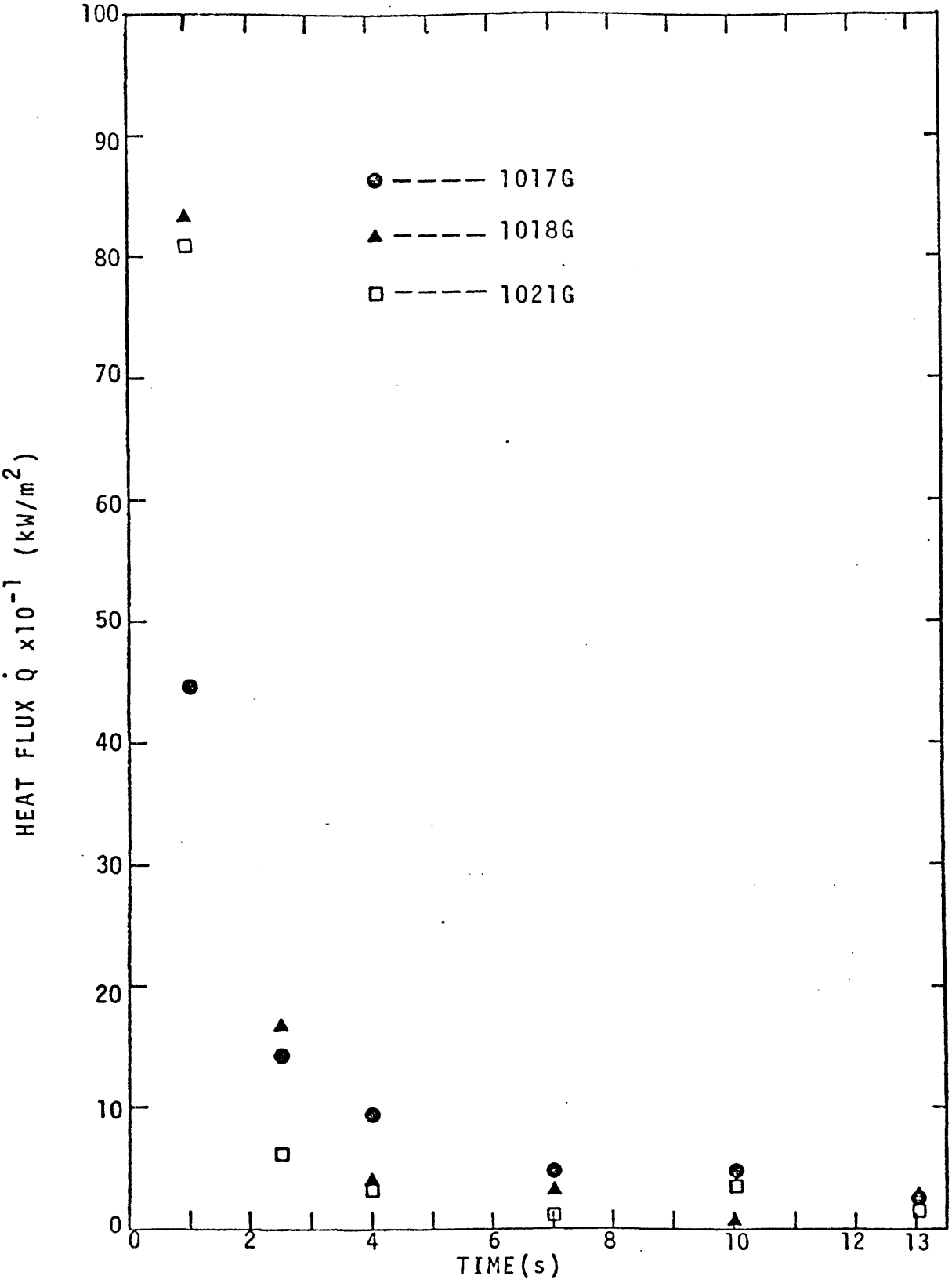

FIGURE VI-23: LOCAL BOIL-OFF RATE AS A FUNCTION OF TIME FOR 1.5-LITER PROPANE SPILLS AT THE SECOND SAMPLING STATION.

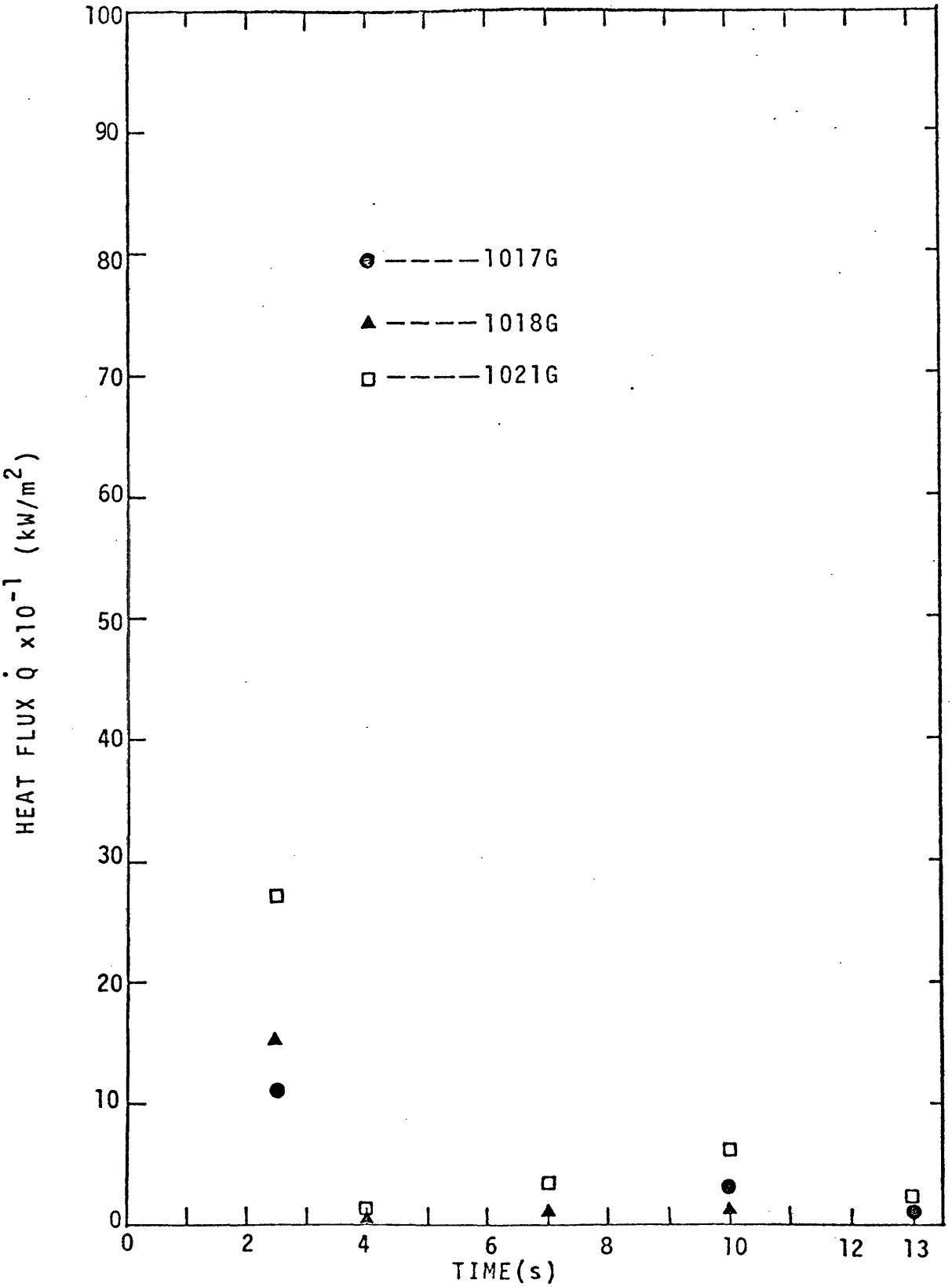

FIGURE VI-24: LOCAL BOIL-OFF RATE AS A FUNCTION OF TIME FOR 1.5-LITER PROPANE SPILLS AT THE THIRD SAMPLING STATION.

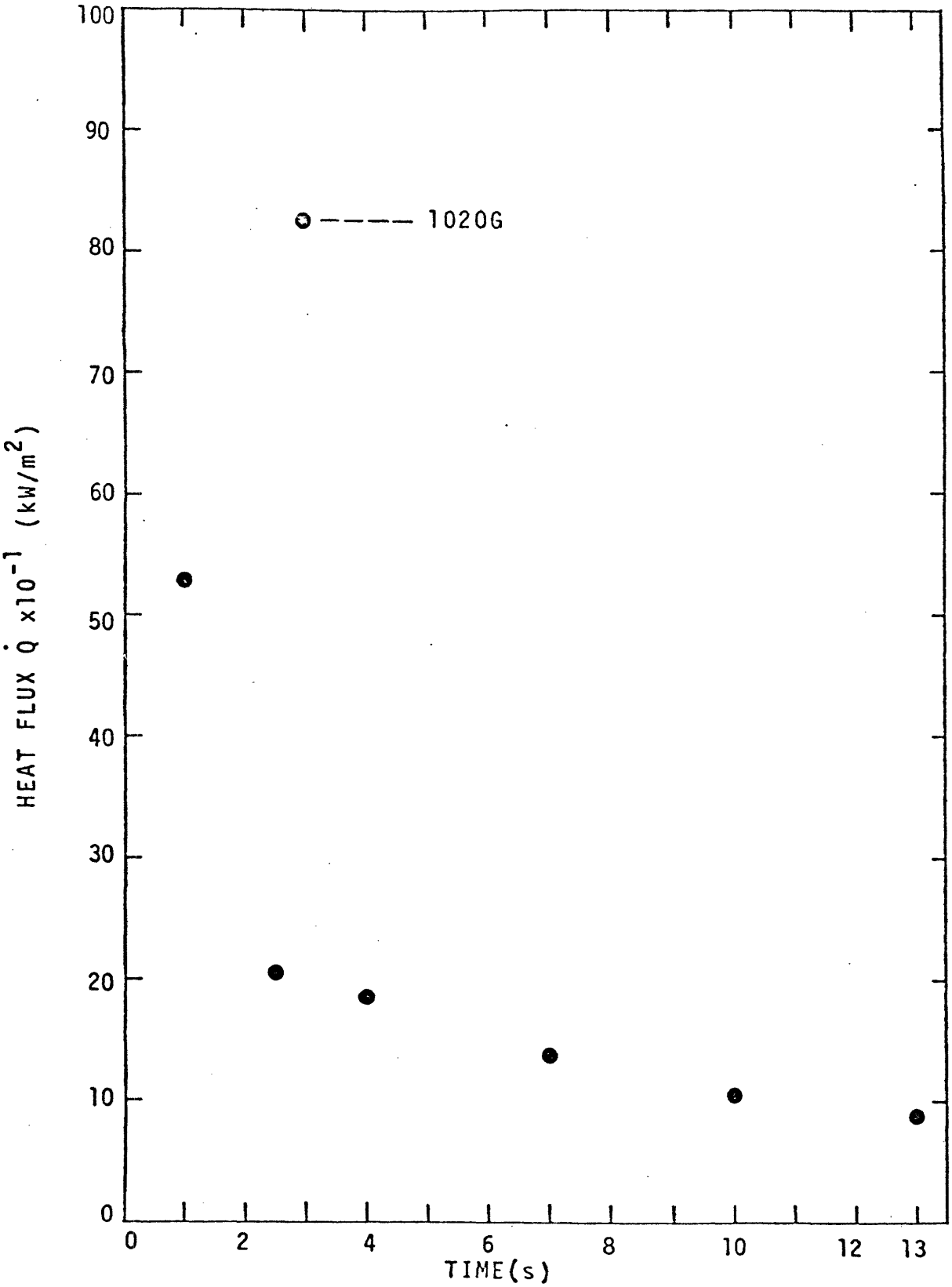

FIGURE VI-25: LOCAL BOIL-OFF RATE AS A FUNCTION OF TIME FOR 2.0-LITER PROPANE SPILLS AT THE FIRST SAMPLING STATION.

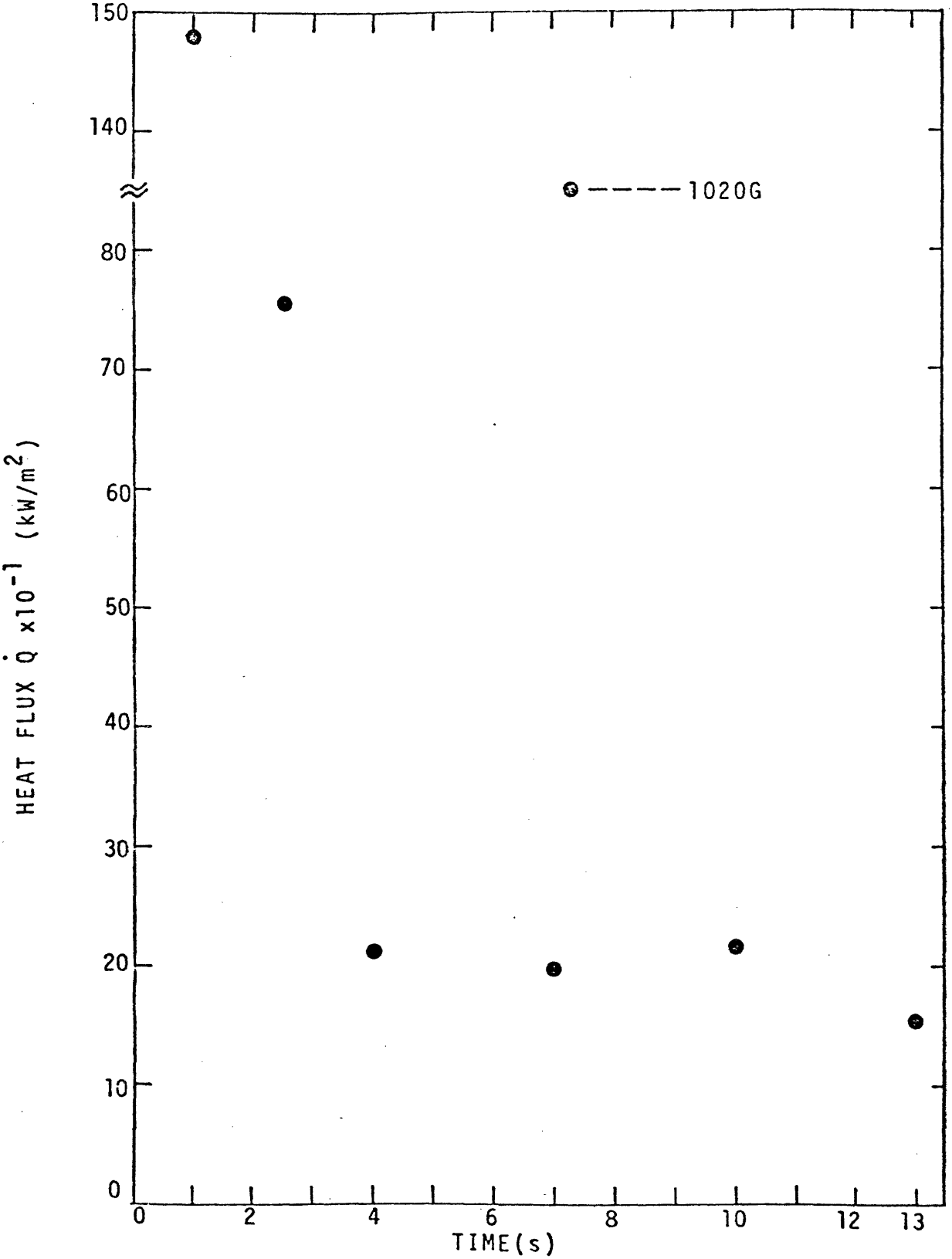

FIGURE VI-26: LOCAL BOIL-OFF RATE AS A FUNCTION OF TIME FOR 2.0-LITER PROPANE SPILL AT THE SECOND SAMPLING STATION.

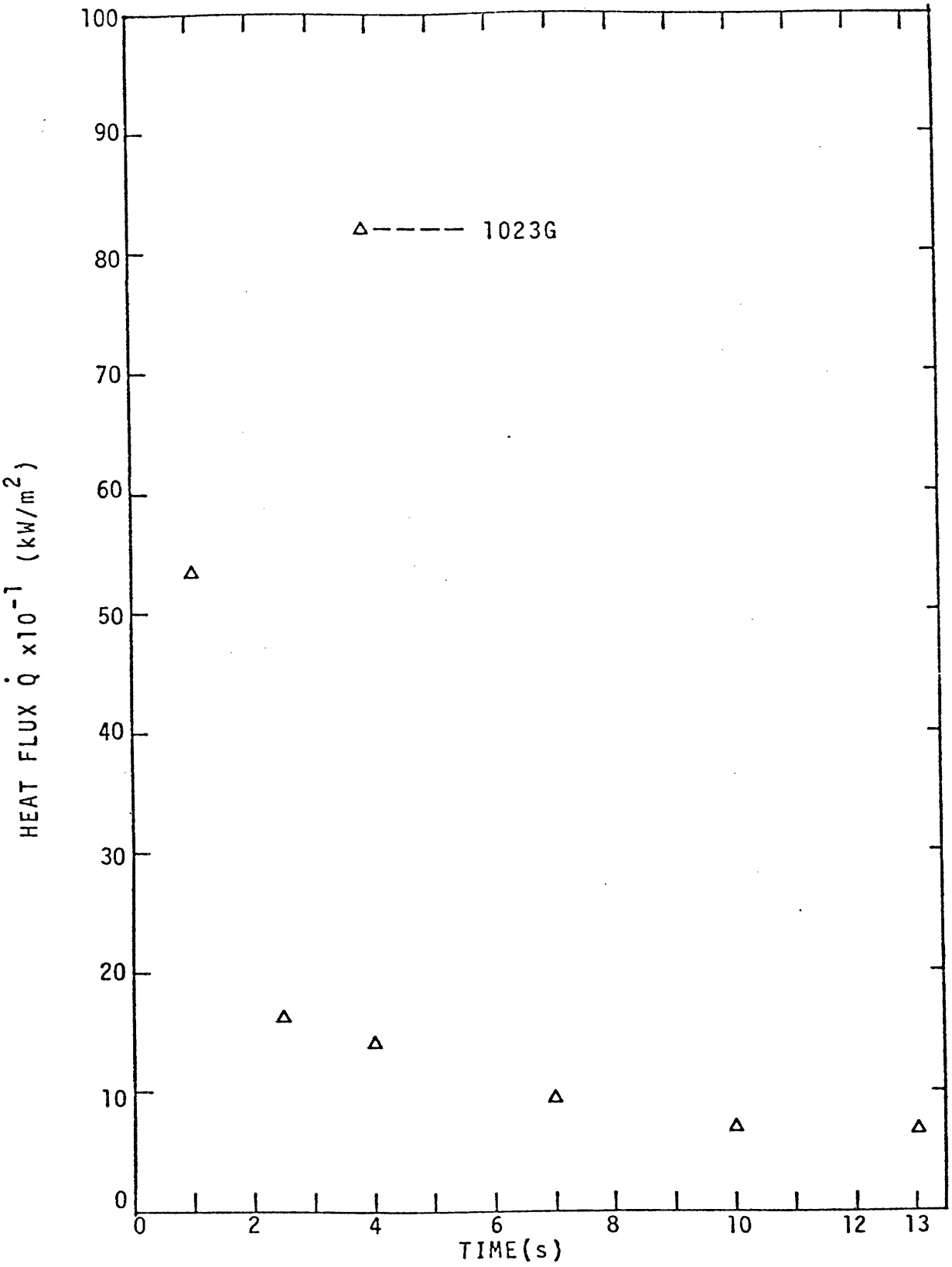

FIGURE VI-27: LOCAL BOIL-OFF RATE AS A FUNCTION OF TIME FOR 1.0-LITER PROPANE SPILL AT THE FIRST SAMPLING STATION WITH SMALL DISTRIBUTOR OPENING(19.4cm^2).

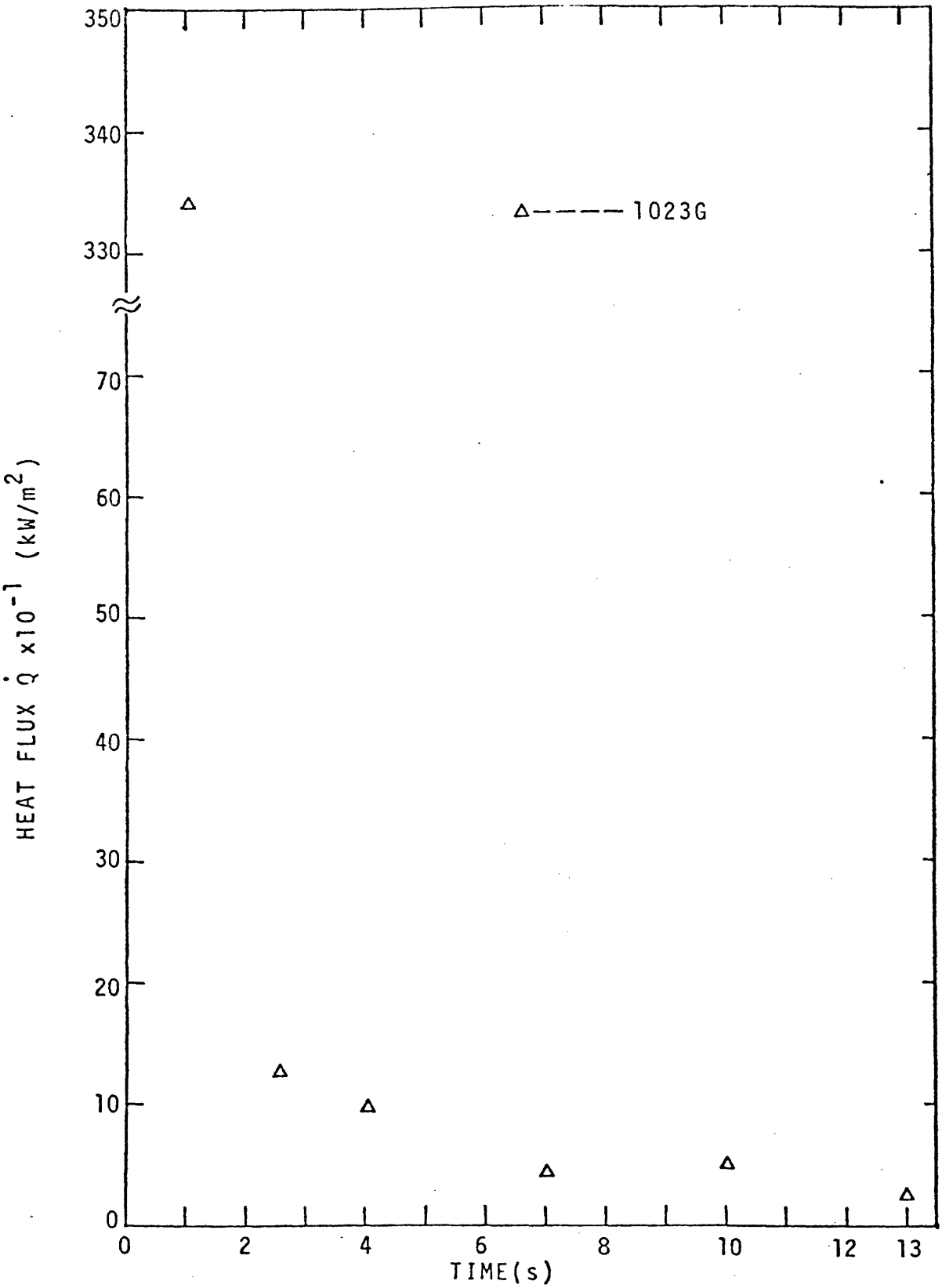

FIGURE VI-28: LOCAL BOIL-OFF RATE AS A FUNCTION OF TIME FOR 1.0-LITER PROPANE SPILL AT THE SECOND SAMPLING STATION WITH SMALL DISTRIBUTOR OPENING($19.4 cm^2$).

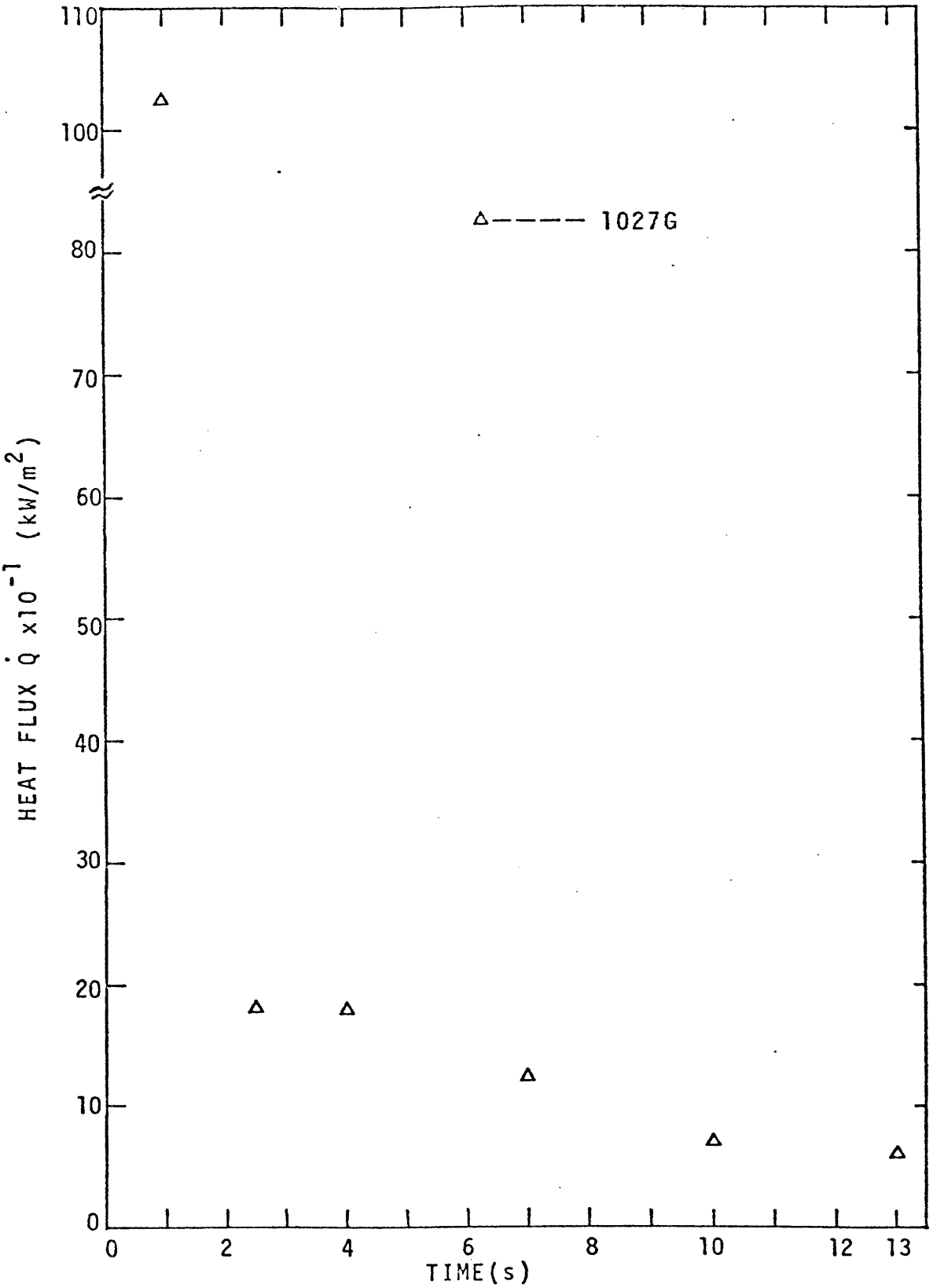

FIGURE VI-29: LOCAL BOIL-OFF RATE AS A FUNCTION OF TIME FOR 2.0-LITER PROPANE SPILL AT THE FIRST SAMPLING STATION WITH SMALL DISTRIBUTOR OPENING(19.4cm^2).

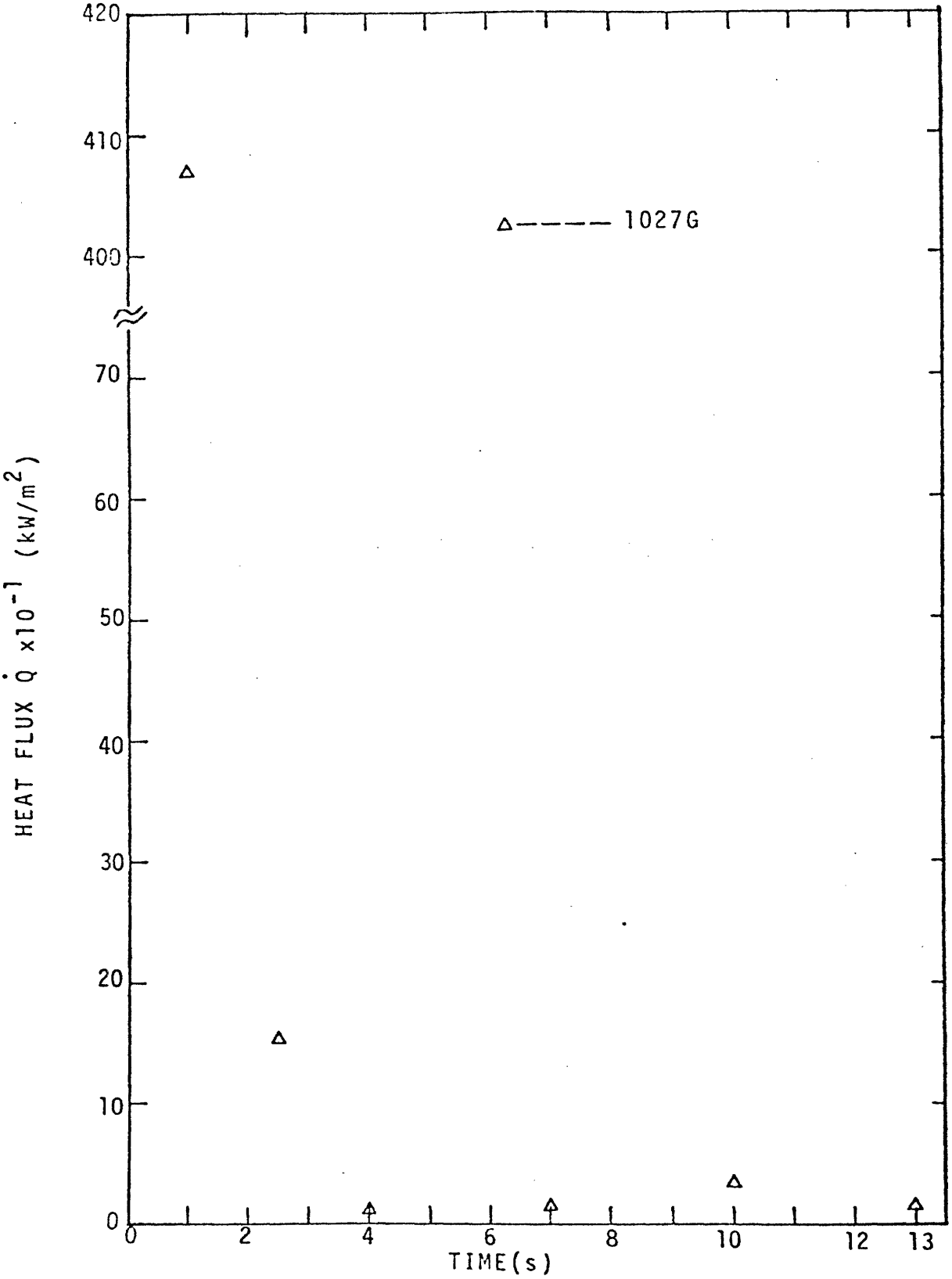

FIGURE VI-30: LOCAL BOIL-OFF RATE AS A FUNCTION OF TIME FOR 2.0-LITER PROPANE SPILL AT THE SECOND SAMPLING STATION WITH SMALL DISTRIBUTOR OPENING(19.4cm^2).

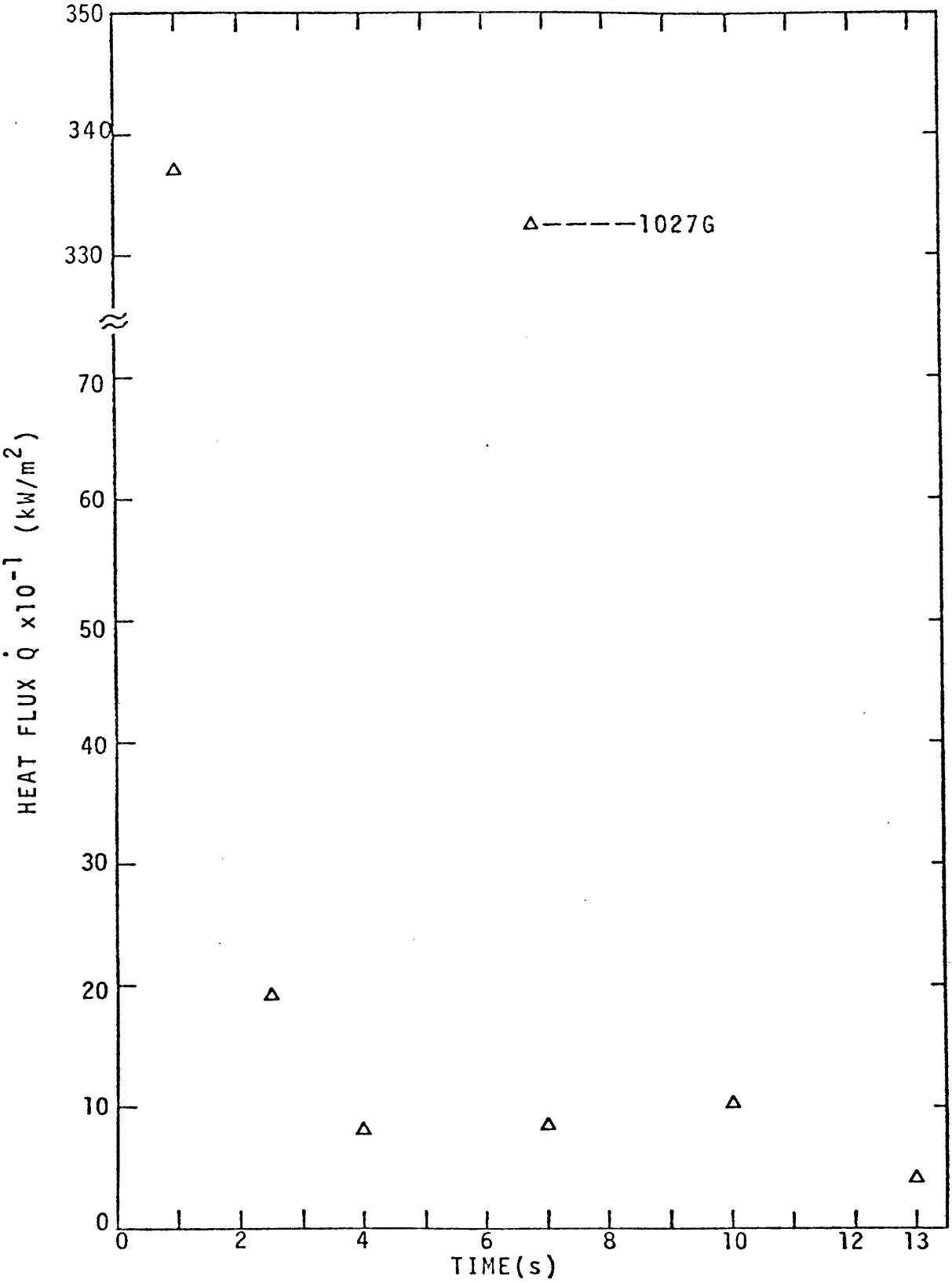

FIGURE VI-31: LOCAL BOIL-OFF RATE AS A FUNCTION OF TIME FOR 2.0-LITER PROPANE SPILL AT THE THIRD SAMPLING STATION WITH SMALL DISTRIBUTOR OPENING(19.4cm^2).

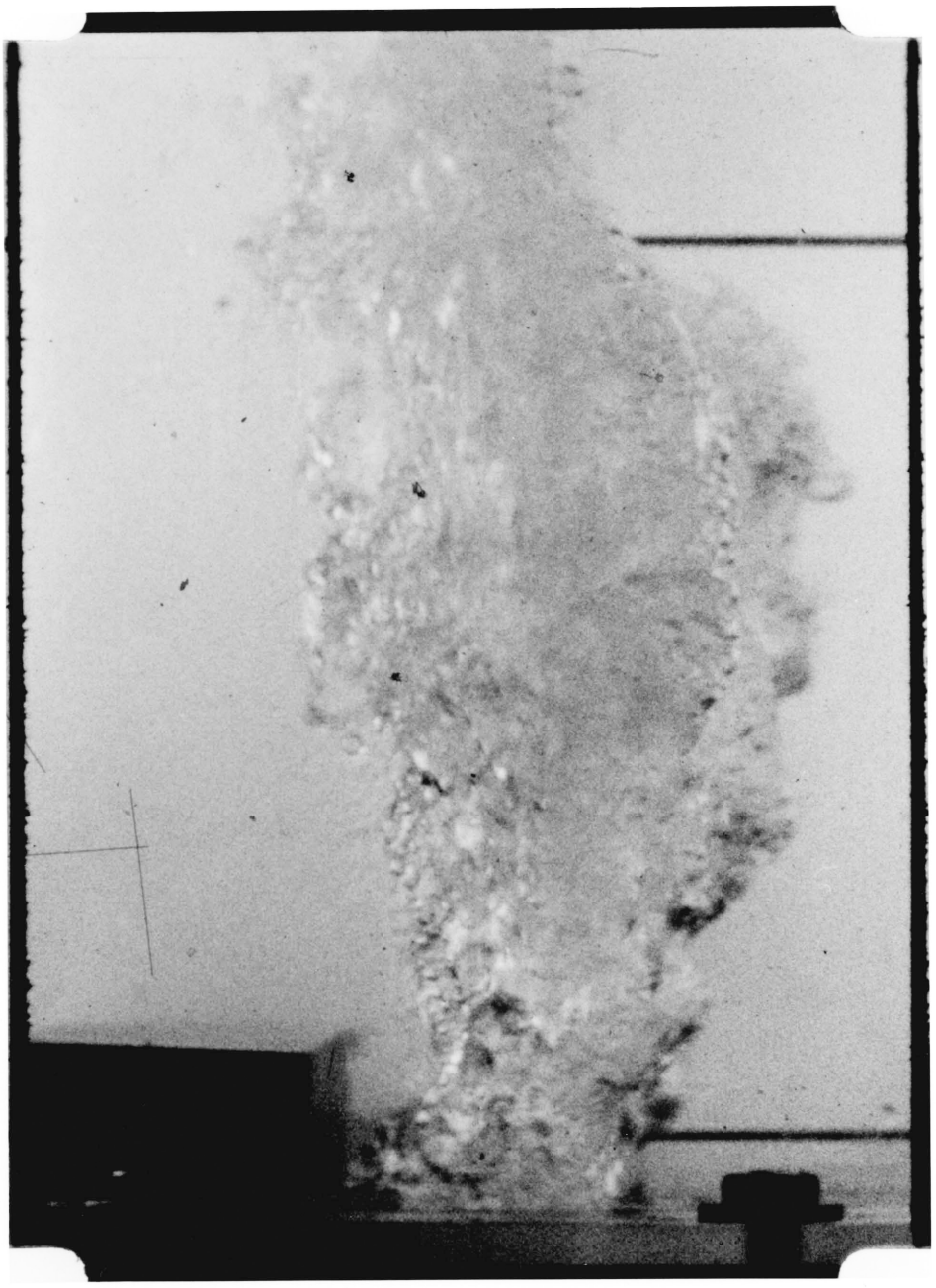

FIGURE VI-32: A PHOTOGRAPH OF LIQUID PROPANE SPREADING ON WATER

TABLE VI-7

Maximum Spreading Distance for Propane Spills

Test	Volume Spilled (liter)	Maximum Spreading Distance (cm)
62301	0.5	63
70801	0.5	68
62401	0.75	
1019G	0.75	91
80501	1.0	104
80601	1.0	112
*1023G	10.	112
71401	1.5	150
1017G	1.5	142
1020G	2.0	163
*1027G	2.0	155
70301	3.0	163
*1028G	3.0	163

*Propane spilled through small distributor opening

ally spreads under the ice crust. This propane vaporizes and forms cracks in the weak portions of the ice layer and literally elevates sections of the ice. This phenomenon produced an increase in the boiling rate as indicated in Figures VI-20 and VI-22.

Figures VI-12, VI-14 and VI-15 show that spills with a smaller distributor opening produce faster spreading rates than spills with the standard sized opening. However, the maximum spreading distances of the spills with the smaller opening are the same as those obtained from spills with the standard sized opening, as seen in Table VI-7. No discontinuity is observed in the spreading curves from spills with the smaller opening.

Ethane-Propane Mixtures

Two spills of ethane-propane mixtures on water were performed. The experimental conditons are given in Table VI-8. The spreading data are presented in Figure VI-33. Again the discontinuity due to "ice dam" formation is observed. The boiling rate as a function of time is shown in Figures VI-34 and VI-35. The initial boil-off rate is very high and then decreases very rapidly. Figures VI-36 and VI-37 show the vapor composition as a function of time at the first sampling station.

The ice forms very quickly and is non-uniform in shape, similar to the case of a pure propane spill.

Propane-n-Butane Mixtures

One spill of a propane-n-butane mixture on water was made. The experimental condition is given in Table VI-8. The spreading curve as a function of time is shown in Figure VI-38. Again the discontinuity is observed. Vigorous boiling immediately results from the cryogen contacting the water. Rough ice forms quickly on the water surface, after which the boiling proceeds in a calmer manner. Figures VI-39 and VI-40 show the boiling rate curves for

TABLE VI-8

Experimental Conditions for LPG Mixtures

Test	Composition (mole %)	Volume Spilled (liter)	Cross-Sectional Area of Distributor Opening (cm^2)
72901	Ethane 13.0 Propane 87.0	1.0	48.4
73101	Ethane 4.5 Propane 95.5	1.0	48.4
80101	Propane 95.0 n-Butane 5.0	1.0	48.4
80401	Ethane 1.05 Propane 84.0 n-Butane 5.5	1.0	48.4

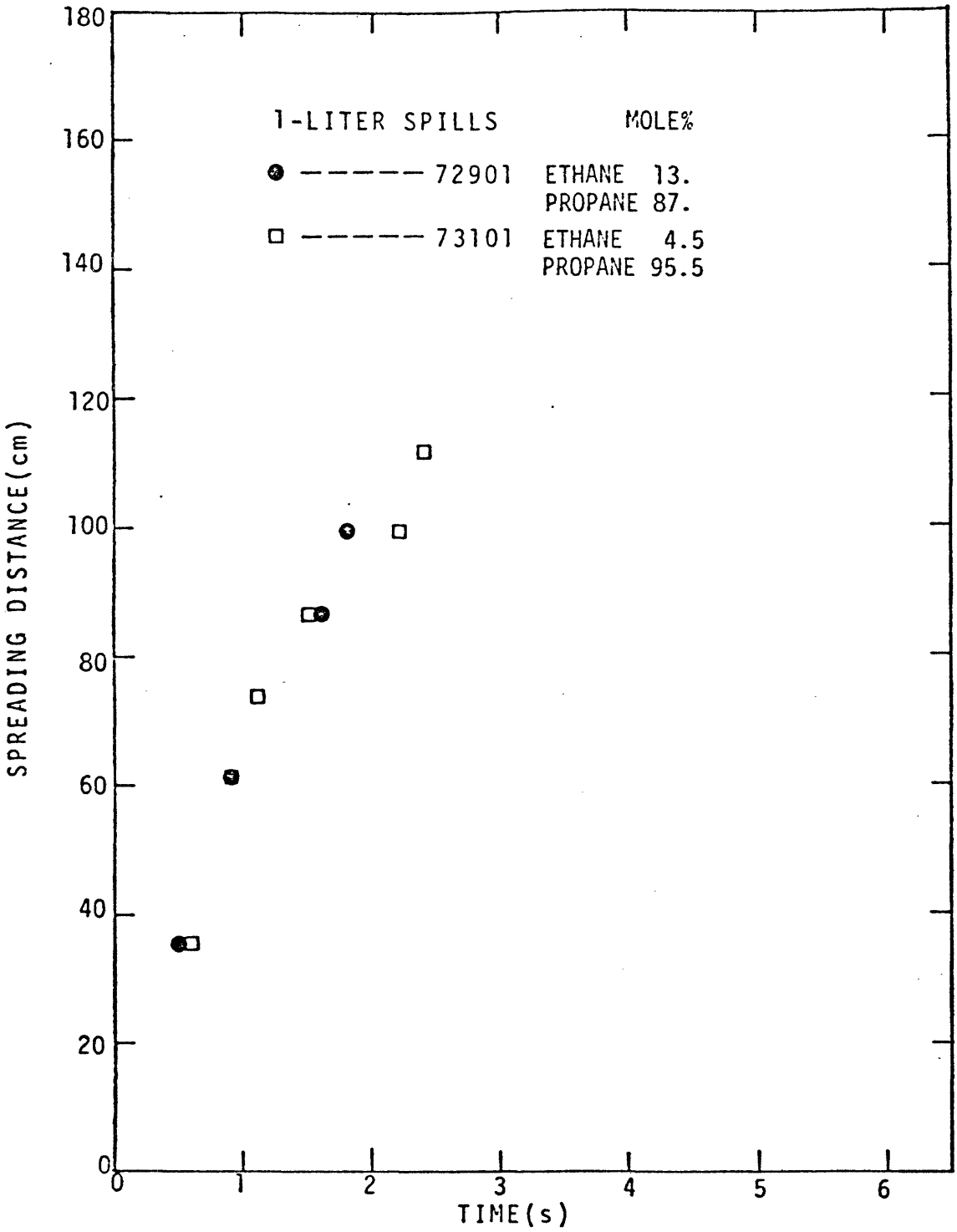

FIGURE VI-33: SPREADING DISTANCE AS A FUNCTION OF TIME FOR ETHANE-PROPANE MIXTURES.

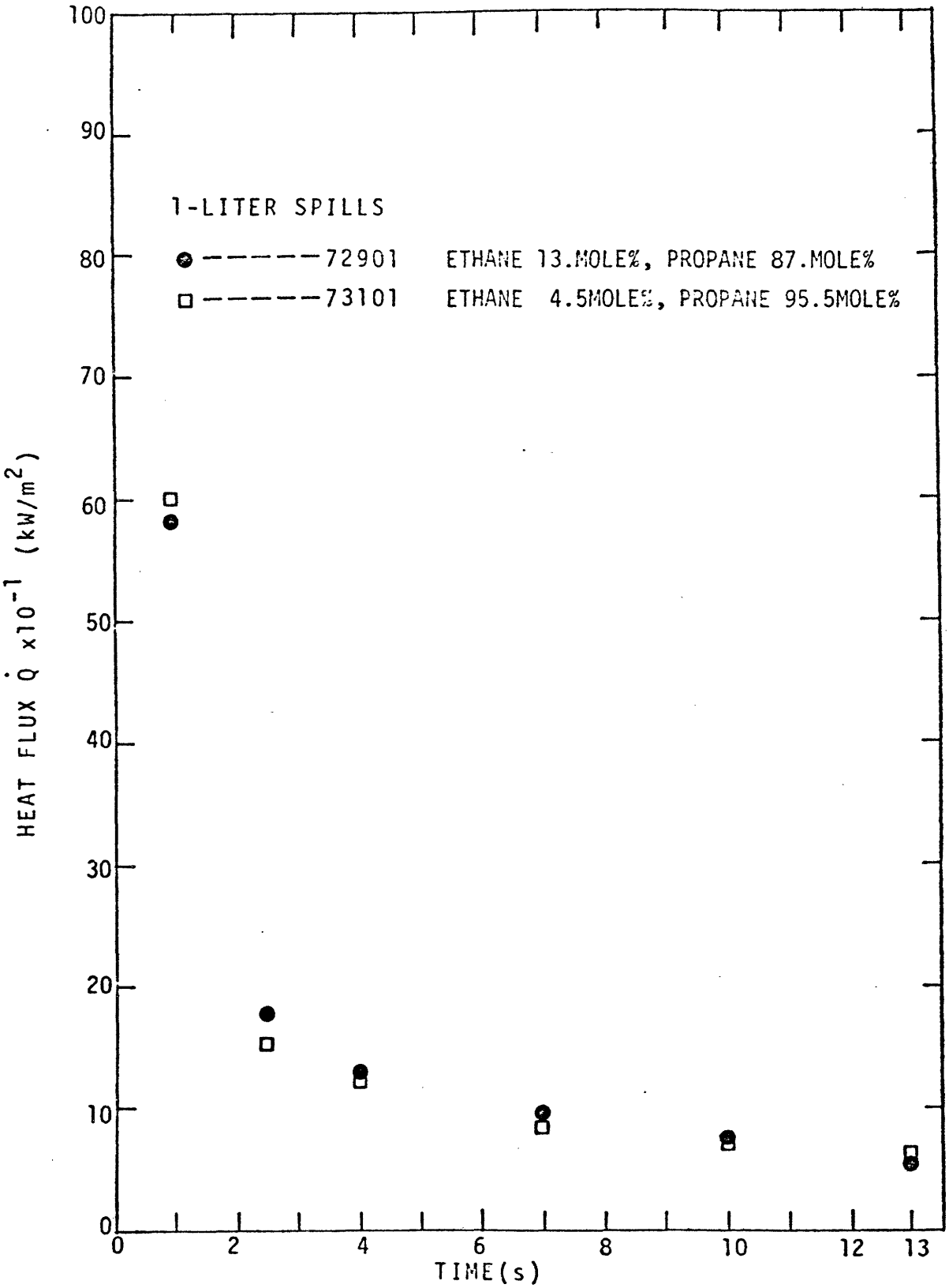

FIGURE VI-34: LOCAL BOIL-OFF RATE AS A FUNCTION OF TIME FOR ETHANE-PROPANE MIXTURES AT THE FIRST SAMPLING STATION.

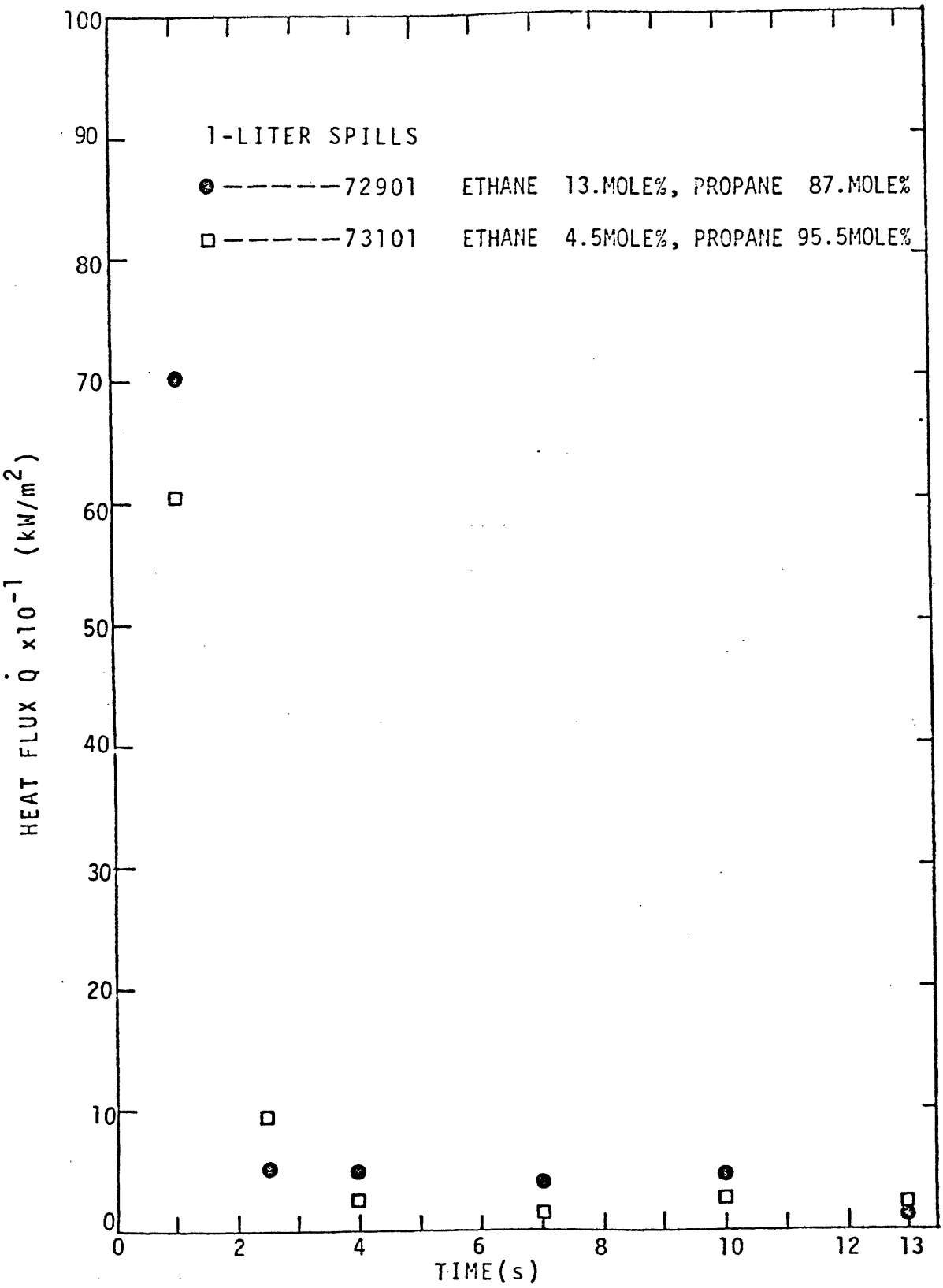

FIGURE VI-35: LOCAL BOIL-OFF RATE AS A FUNCTION OF TIME FOR ETHANE-PROPANE MIXTURES AT THE SECOND SAMPLING STATION.

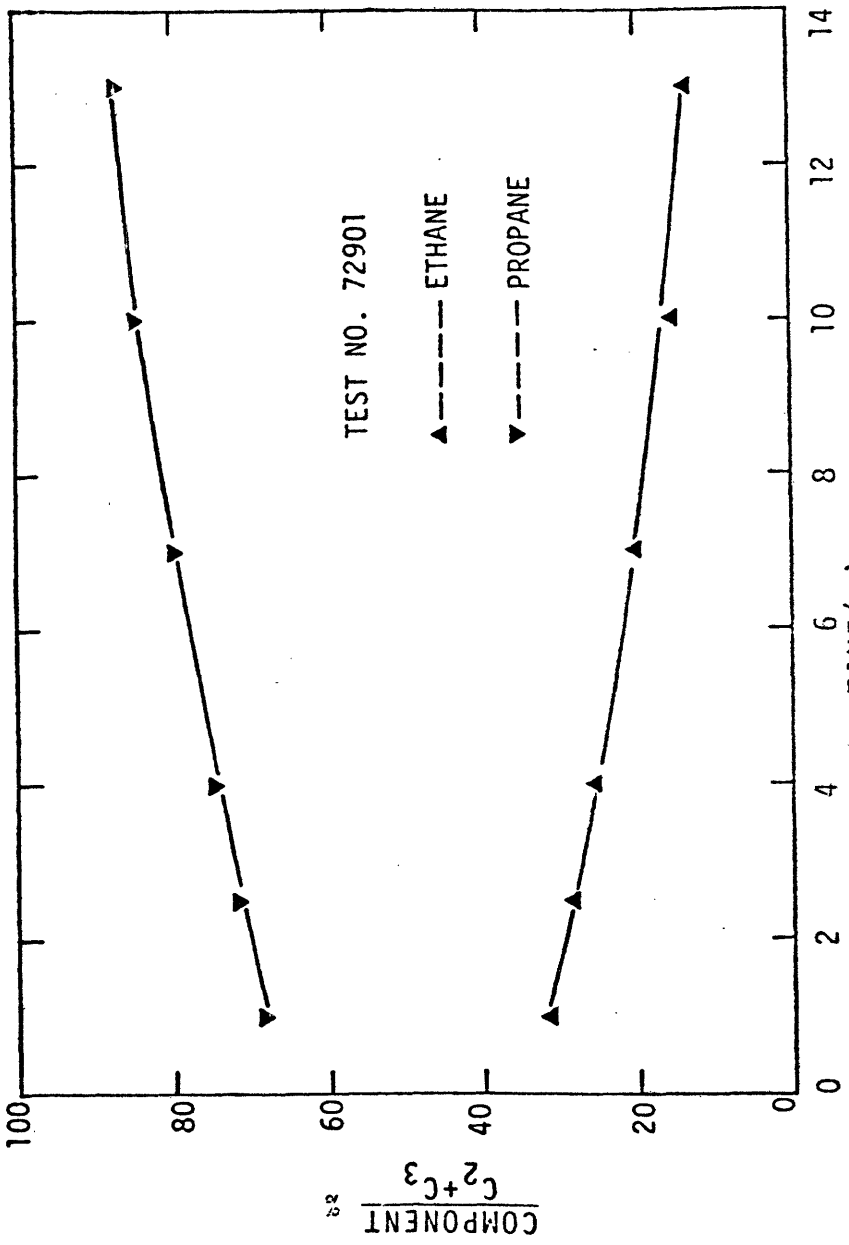

FIGURE VI-36: VAPOR COMPOSITION AS A FUNCTION OF TIME AT THE FIRST SAMPLING STATION FOR A SPILL OF AN ETHANE-PROPANE MIXTURE(TEST NO. 72901).

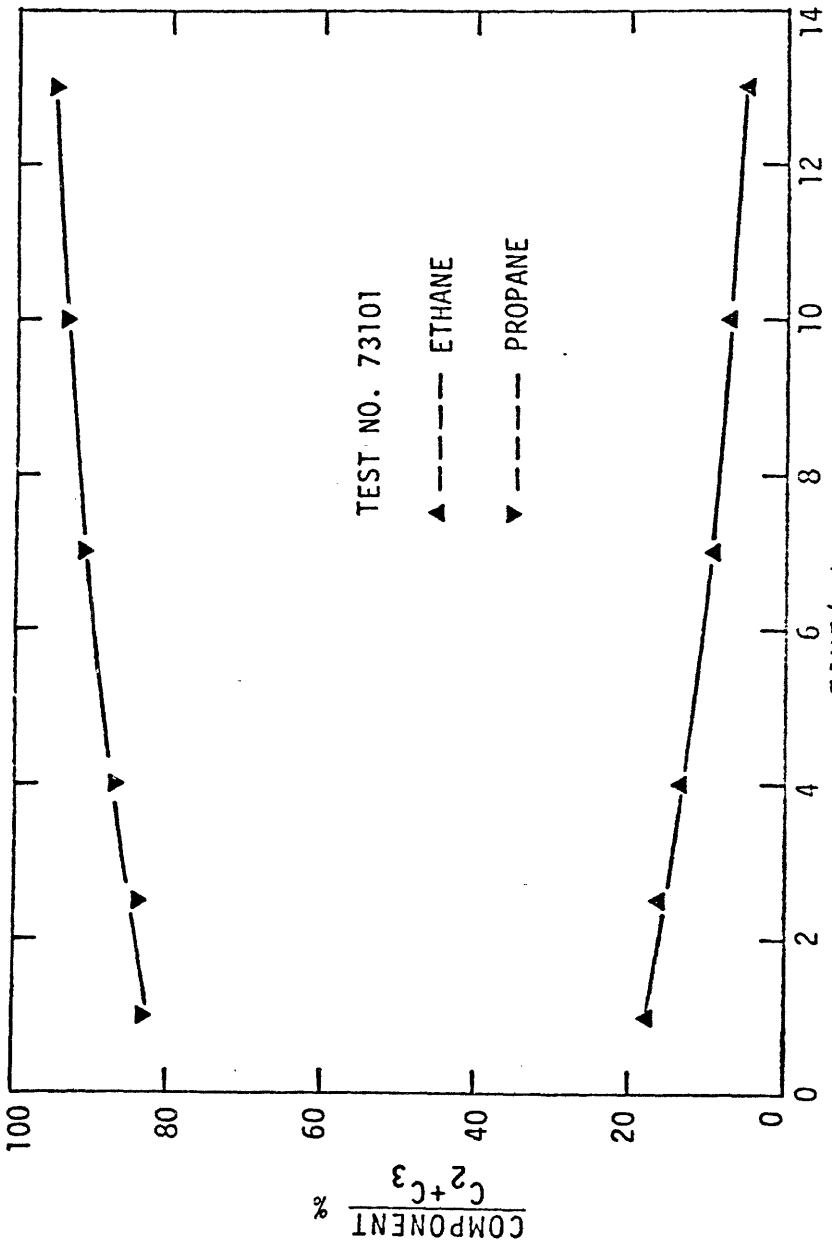

FIGURE VI-37: VAPOR COMPOSITION AS A FUNCTION OF TIME AT THE FIRST SAMPLING STATION FOR A SPILL OF AN ETHANE-PROPANE MIXTURE(TEST NO. 73101).

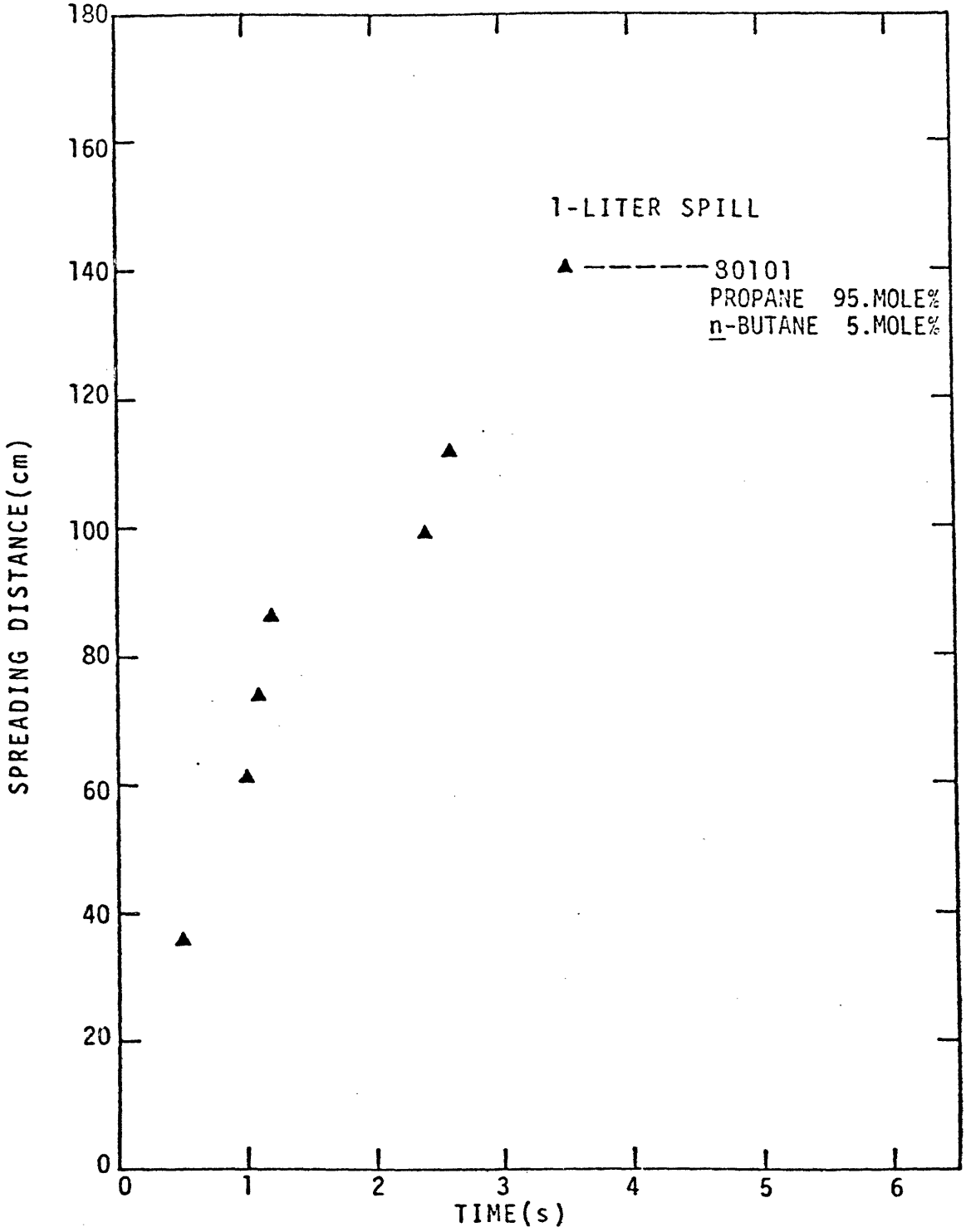

FIGURE VI-38: SPREADING DISTANCE AS A FUNCTION OF TIME FOR A PROPANE-n-BUTANE MIXTURE.

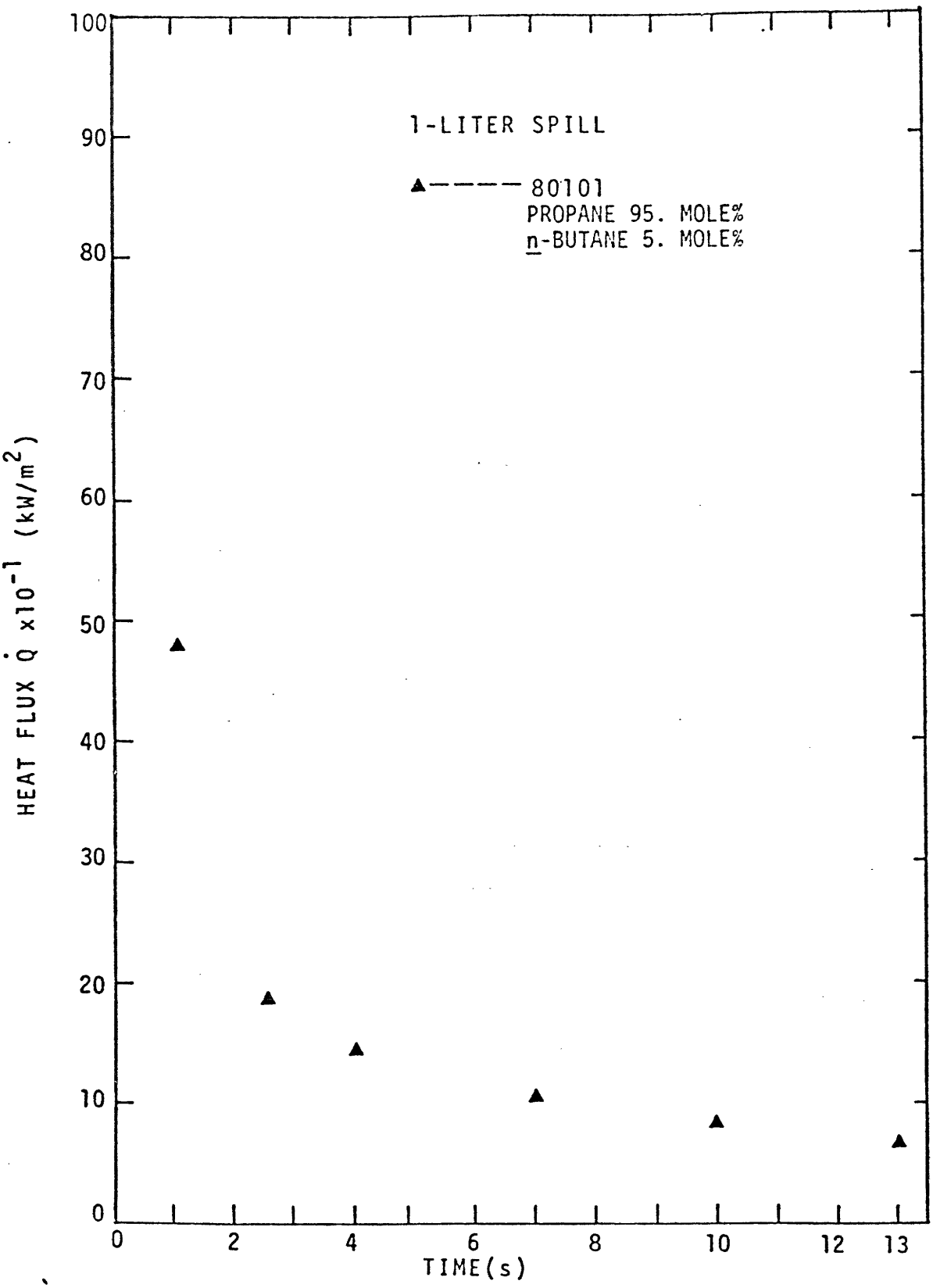

FIGURE VI-39: LOCAL BOIL-OFF RATE AS A FUNCTION OF TIME FOR PROPANE-n-BUTANE MIXTURE AT THE FIRST SAMPLING STATION.

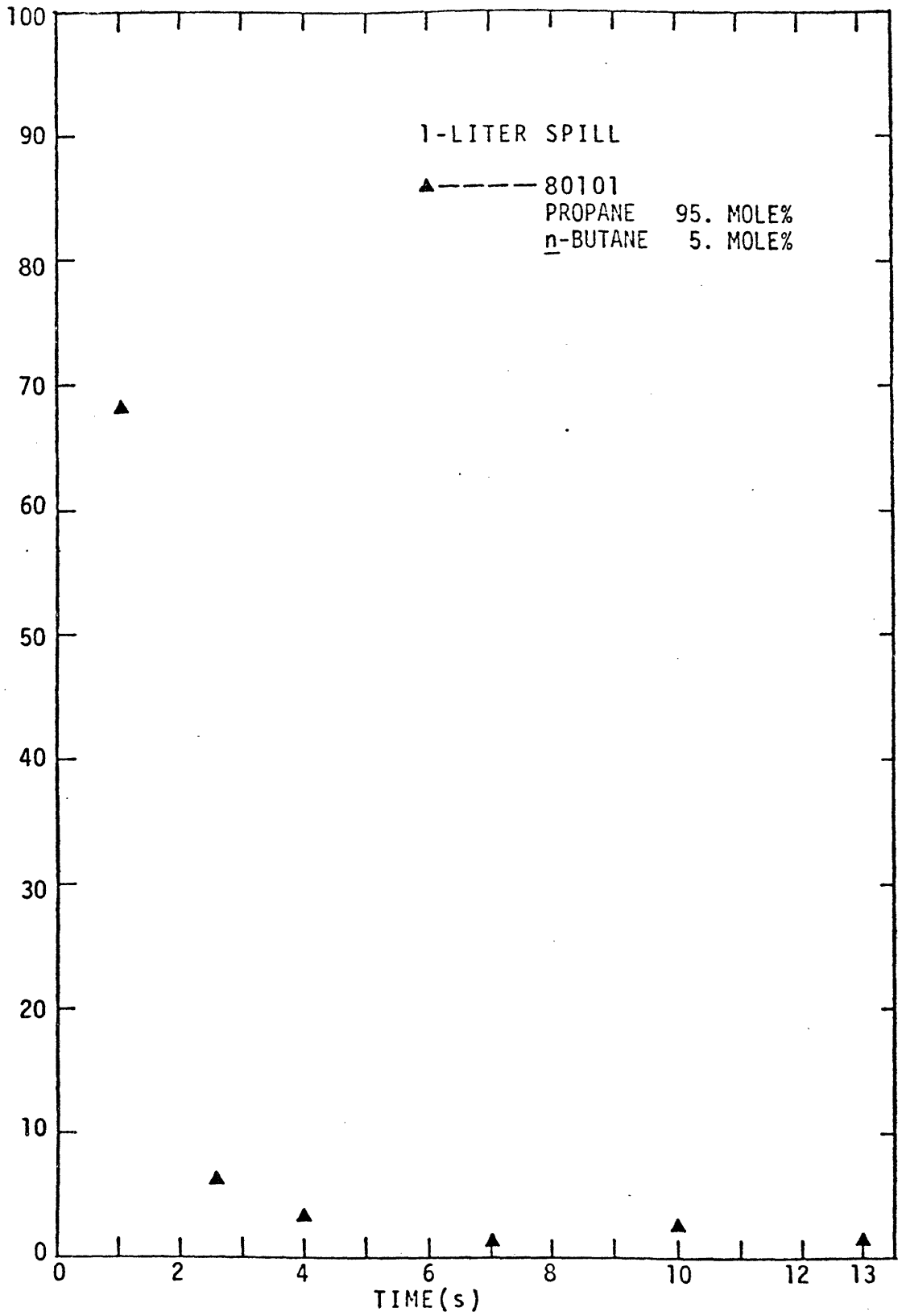

FIGURE VI-40: LOCAL BOIL-OFF RATE AS A FUNCTION OF TIME FOR PROPANE-n-BUTANE MIXTURE AT THE SECOND SAMPLING STATION.

the propane-n-butane spill. The vapor mole fraction of n- butane is seen to be very small (see Figure VI-41).

Ethane-Propane-n-Butane Mixtures

One spill of a ternary mixture on water was made. The experimental condition is given in Table VI-8. The spreading and boiling rate curves for this test are given in Figures VI-42 through VI-44. As in the case of pure propane, the cryogen mixture boils rapidly and violently when the water is initially contacted. Irregular ice forms quickly on the water surface. Once this rough ice covers the water surface, boiling becomes smooth in an uneventful fashion. Occasionally, cryogen spreads beneath the ice, evaporates and erupts through weak areas in the ice. A photograph of the LPG mixture spreading on water is given in Figure VI-45. A thick and rough ice layer is noted. The composition of the mixture in the vapor phase as a function of time is shown in Figure VI-46. The mole fraction of ethane decreases with time and n-butane remains at a very low concentration. Table VI-9 gives the maximum spreading distances from the spills of four mixtures which model LPG.

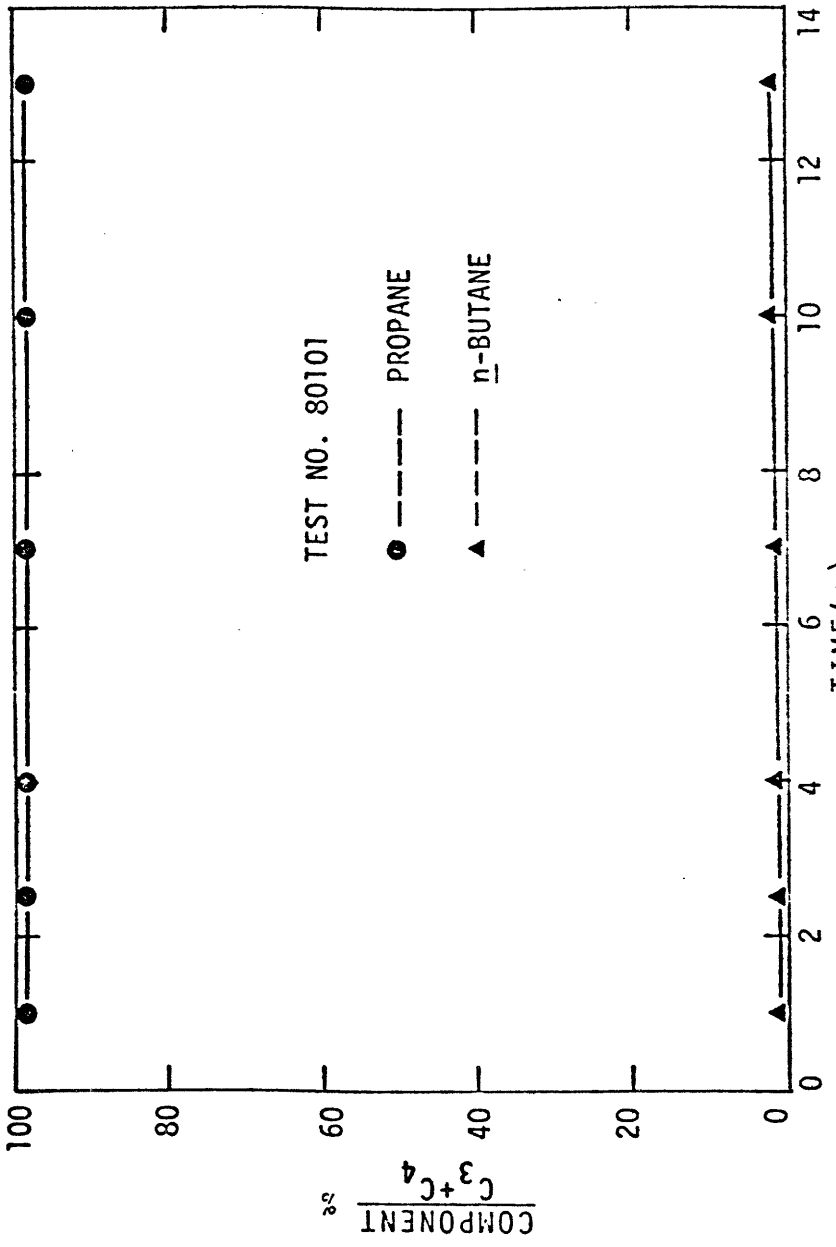

FIGURE VI-41: VAPOR COMPOSITION AS A FUNCTION OF TIME AT THE FIRST SAMPLING STATION FOR A SPILL OF PROPANE-n-BUTANE MIXTURE.

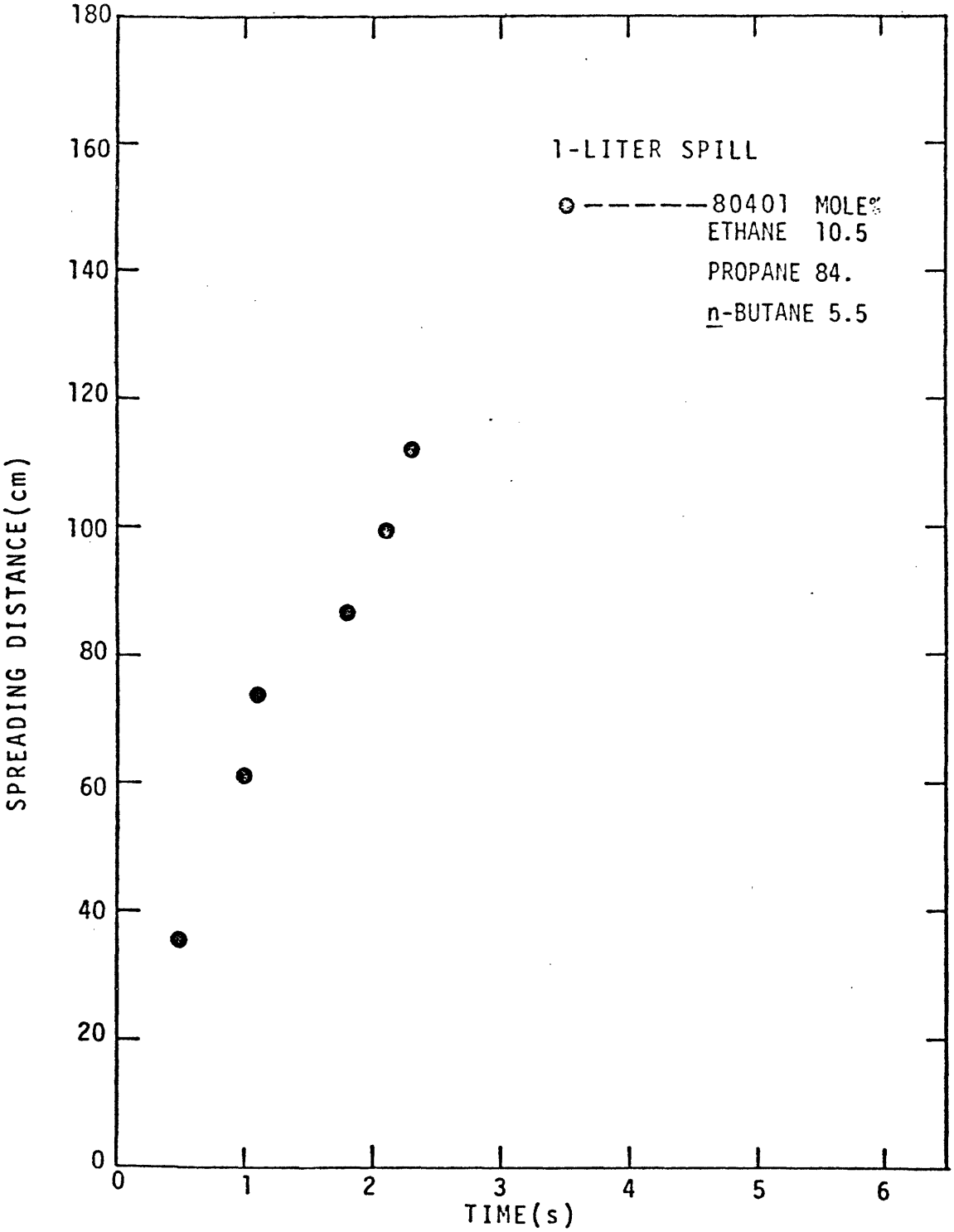

FIGURE VI-42: SPREADING DISTANCE AS A FUNCTION OF TIME FOR AN ETHANE-PROPANE-n-BUTANE MIXTURE.

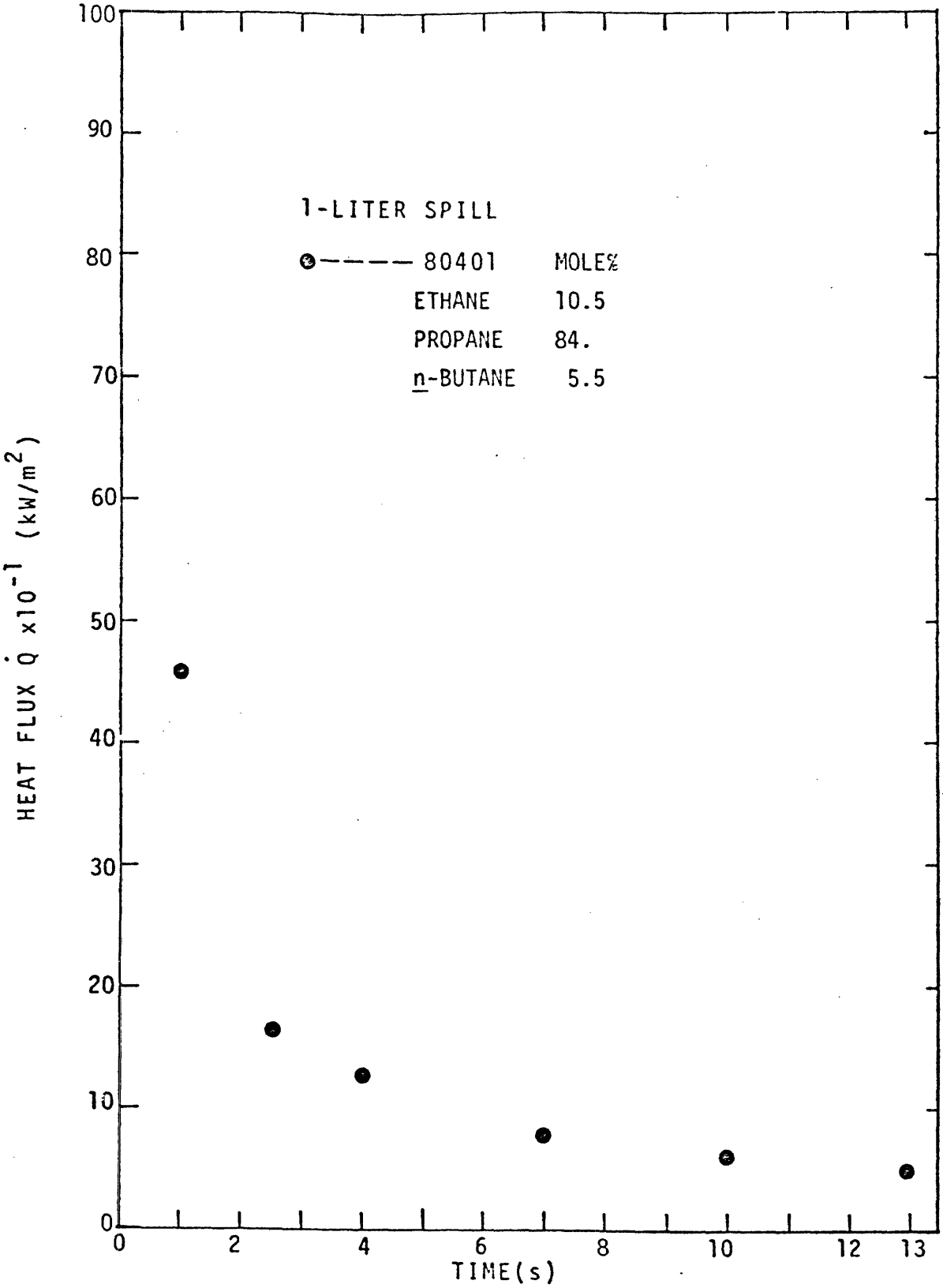

FIGURE VI-43: LOCAL BOIL-OFF RATE AS A FUNCTION OF TIME FOR ETHANE-PROPANE-n-BUTANE MIXTURE AT THE FIRST SAMPLING STATION.

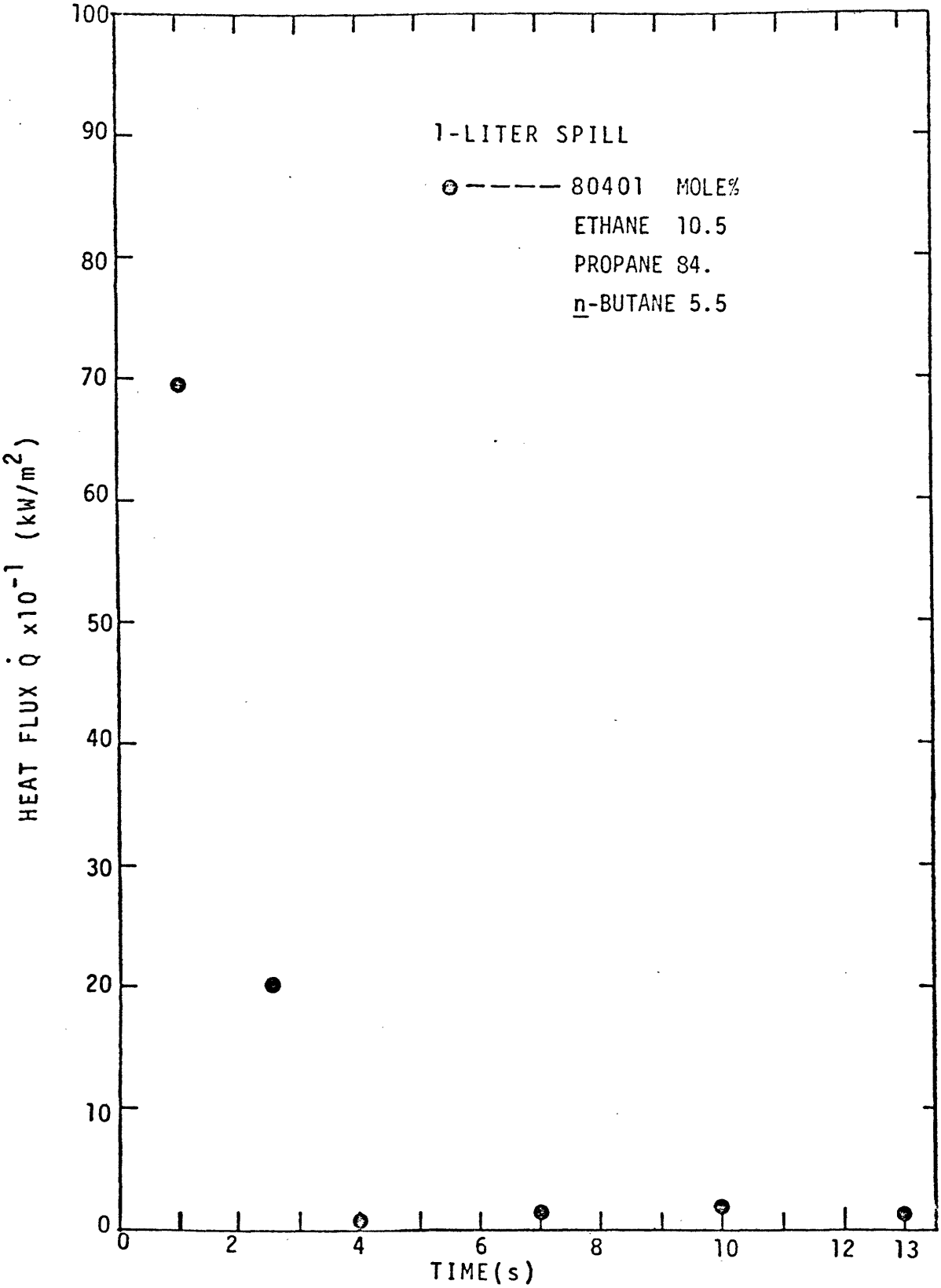

FIGURE VI-44: LOCAL BOIL-OFF RATE AS A FUNCTION OF TIME FOR ETHANE-PROPANE-n-BUTANE MIXTURE AT THE SECOND SAMPLING STATION.

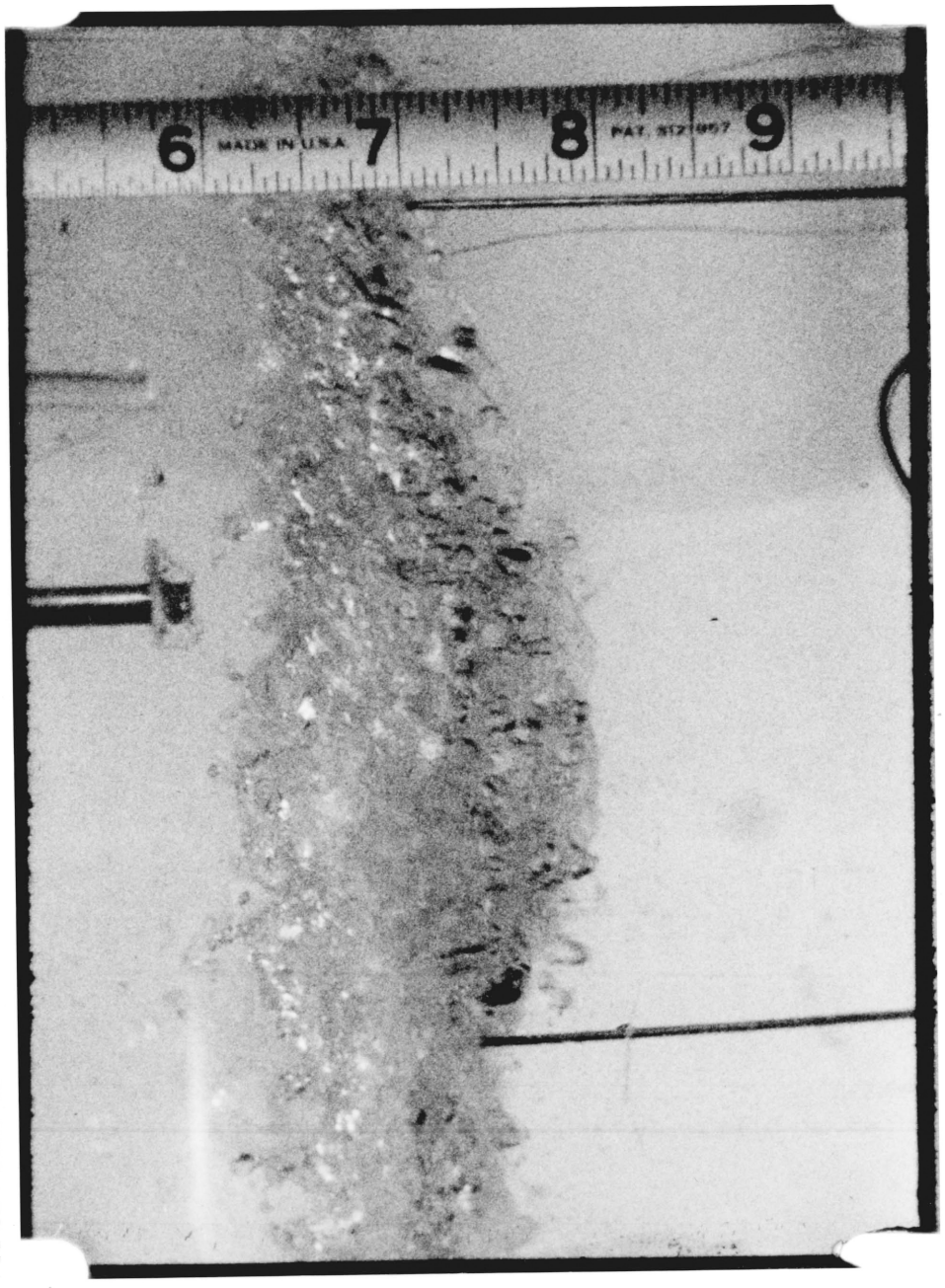

FIGURE VI-45: A PHOTOGRAPH OF LPG SPREADING ON WATER

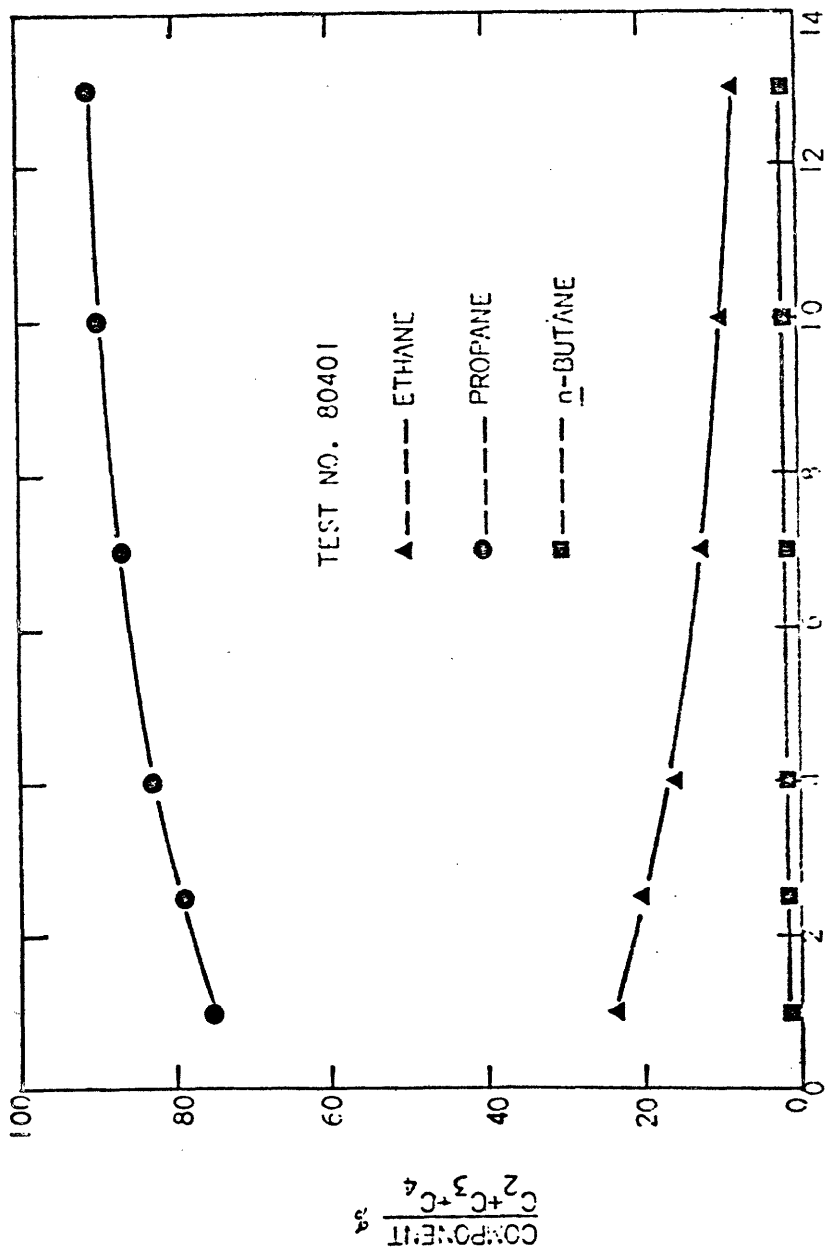

FIGURE VI-46: VAPOR COMPOSITION AS A FUNCTION OF TIME AT THE FIRST SAMPLING STATION FOR A SPILL OF ETHANE-PROPANE-n-BUTANE MIXTURE.

TABLE VI-9

Maximum Spreading Distance for LPG Mixtures

Test	Composition (mole %)	Volume Spilled (liter)	Maximum Spreading Distance (cm)
72901	Ethane 13.0 Propane 87.0	1.0	104
73101	Ethane 4.5 Propane 95.5	1.0	112
80101	Propane 95.0 n-Butane 5.0	1.0	112
80401	Ethane 10.5 Propane 84.0 n-Butane 5.5	1.0	112

VII. DISCUSSION

In this chapter, the results of cryogen spills for various compositions and experimental conditions are discussed. Predictions from the model developed in Chapter V are compared with the experimental results. Previous models from the literature, related to the present work, are also discussed.

Liquid Nitrogen

For nitrogen spills, it was noted that a thin layer of ice formed on the water surface downstream of the cryogen distributor. Initially film boiling occurs because of the large temperature difference between liquid nitrogen and water. As the surface temperature of water decreases and patches of ice form and become subcooled, the ice surface initiates nucleate boiling. No ice formation has been observed in the vincinity of the distributor. This may be due to the severe agitation of the water near the distributor opening. Another possible explanation is that the thin tail of the spreading cryogen evaporates quickly and the cooling effect is not sufficient for ice formation.

Spreading nitrogen exhibits a characteristic profile: the cryogen has a thicker spreading front followed by a tail thinning toward the distributor. This observation agrees with the assumption that liquid nitrogen spreads in the gravity-inertia regime.

In Figure VII-1, the spreading distance is shown as a function of time for liquid nitrogen and pentane spills of the same initial volume. The results essentially overlap. Liquid nitrogen has a higher density than pentane. If no evaporation occurs when nitrogen spreads on water, Hoult's (1972a) theory (equation (II-9)) for oil spills could be applied and would predict that liquid nitrogen should spread slower than pentane. Actually liquid nitrogen does vaporize when it spreads and therefore its volume decreases with time. The same

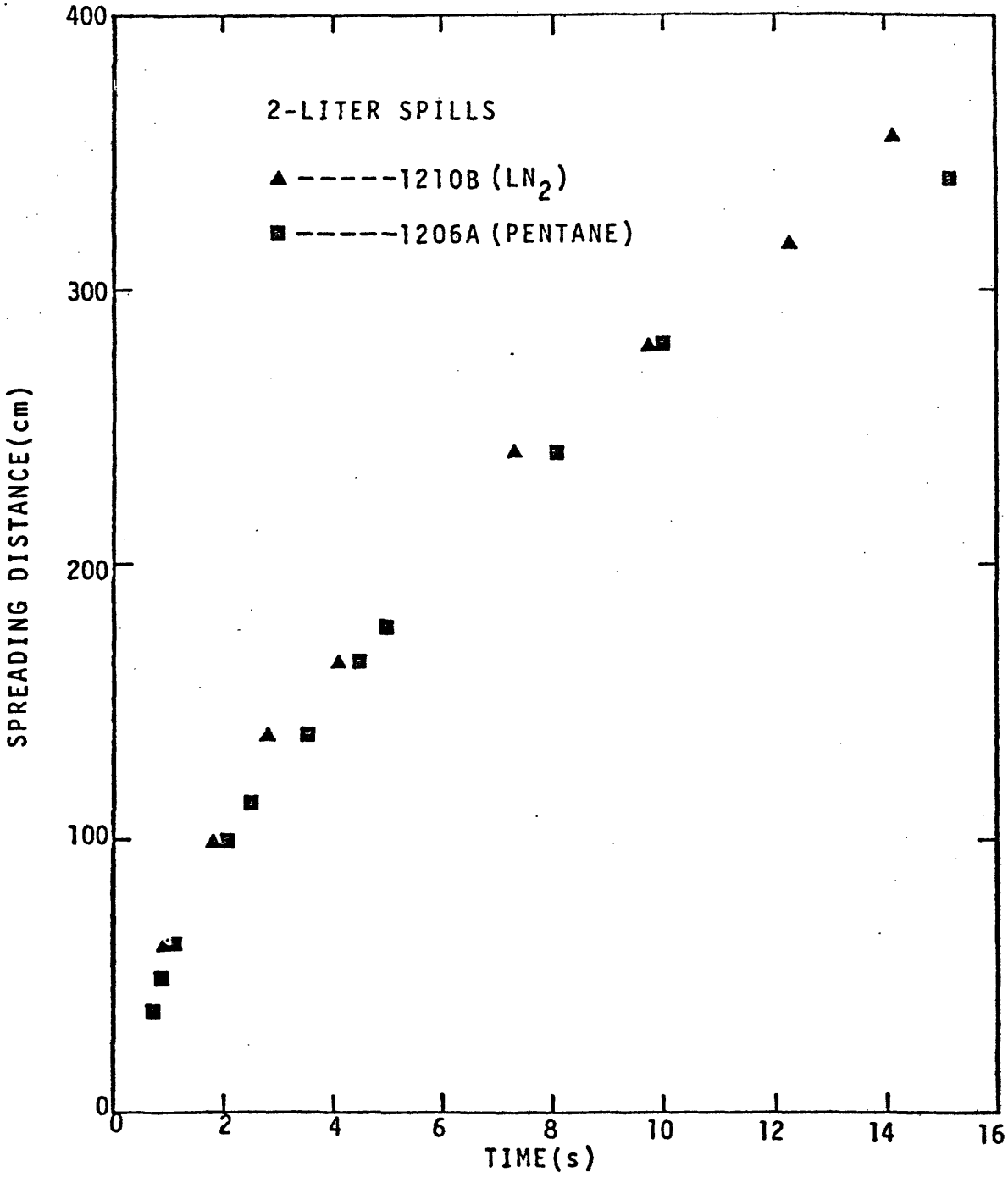

FIGURE VII-1: A COMPARISON OF THE SPREADING DISTANCE AS A FUNCTION OF TIME FOR PENTANE AND LIQUID NITROGEN SPILLS.

correlation would therefore predict that liquid nitrogen should spread even more slowly than pentane. This was not observed. A possible reason is that bubbles of evaporated nitrogen alter the effective density of the liquid nitrogen layer. The effective density is less than the original density and the bubbles further increase the volume of the nitrogen layer. This may explain the larger-than-expected liquid nitrogen spreading rates.

A procedure that estimates the bubble effect on the cryogen density is given in Chapter V. The numerical model developed in Chapter V for a one-dimensional boiling/spreading process has accounted for the bubble effect.

In Figures VII-2 and VII-3, the experimental spreading data for liquid nitrogen spills and the corresponding predictions of the numerical model are compared; the boil-off rate of nitrogen is assumed constant and equal to 40 kW/m^2. This is an average value of the 26 to 60 kW/m^2 range reported in the literature. The effective density of nitrogen is calculated using equation (V-23) and the estimated value of the bubble rising velocity was chosen as 24 cm/sec. The effective density of the nitrogen layer is then determined to be 0.66 g/cm^3 which is used in the numerical model for spreading distance predictions. The true density of liquid nitrogen at its boiling point (77K) is 0.8 g/cm^3. Good agreement is observed between the experimental data and the predicted values, as seen in Figures VII-2 and VII-3.

The numerical model also gives predictions of the thickness profile of cryogen during the boiling-spreading process. No thickness measurements of the profile were made during any cryogen spills. However, the thickness within the spreading front predicted by the numerical model, shown in Figure V-5, agrees qualitatively with the experimental observations of the thickness profile, that is, the leading edge is thicker than the tail.

As nitrogen evaporates during the spreading process, a trailing edge

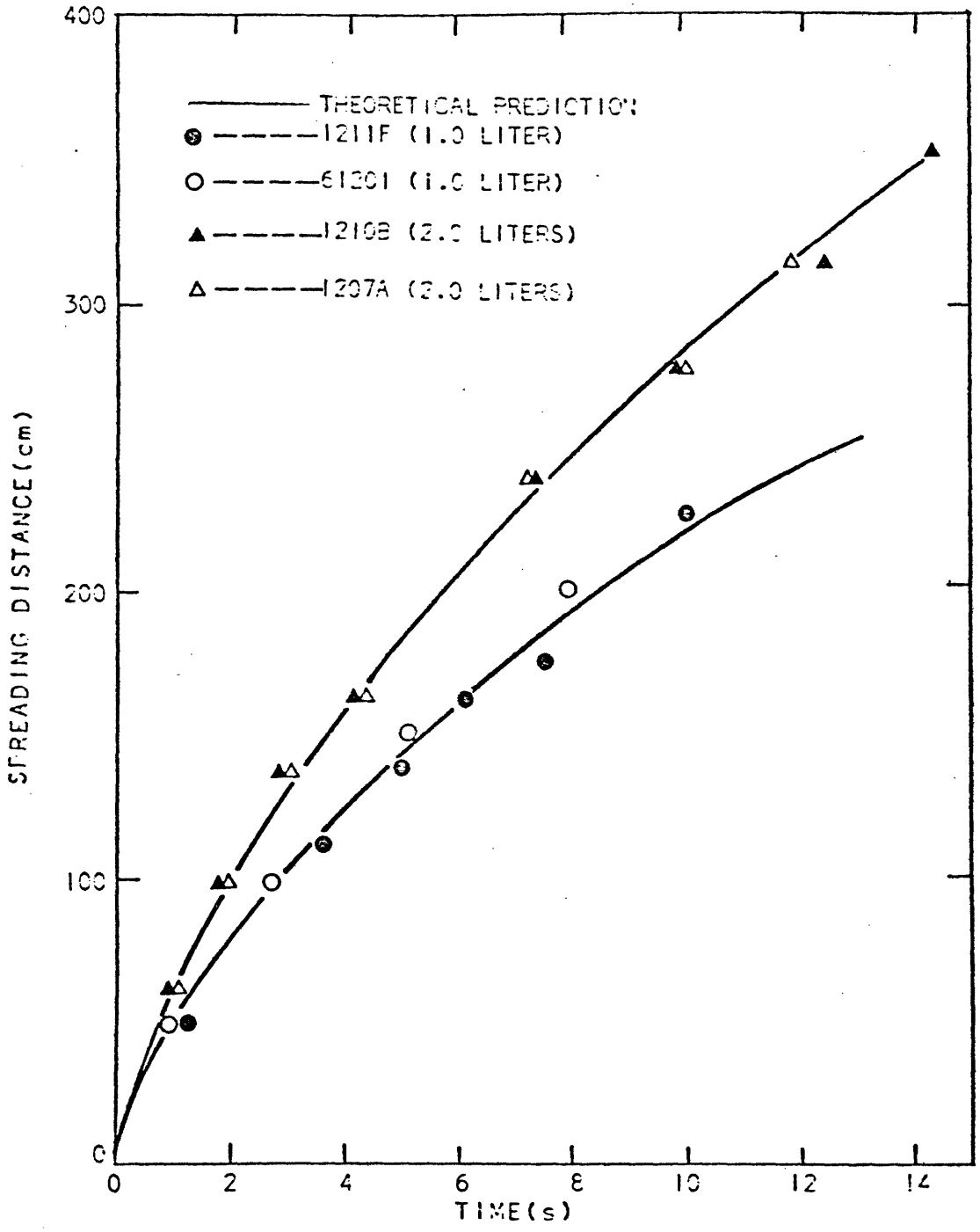

FIGURE VII-2: SPREADING CURVES FOR LIQUID NITROGEN SPILLS. EXPERIMENTAL DATA AND NUMERICAL PREDICTIONS COMPARED.

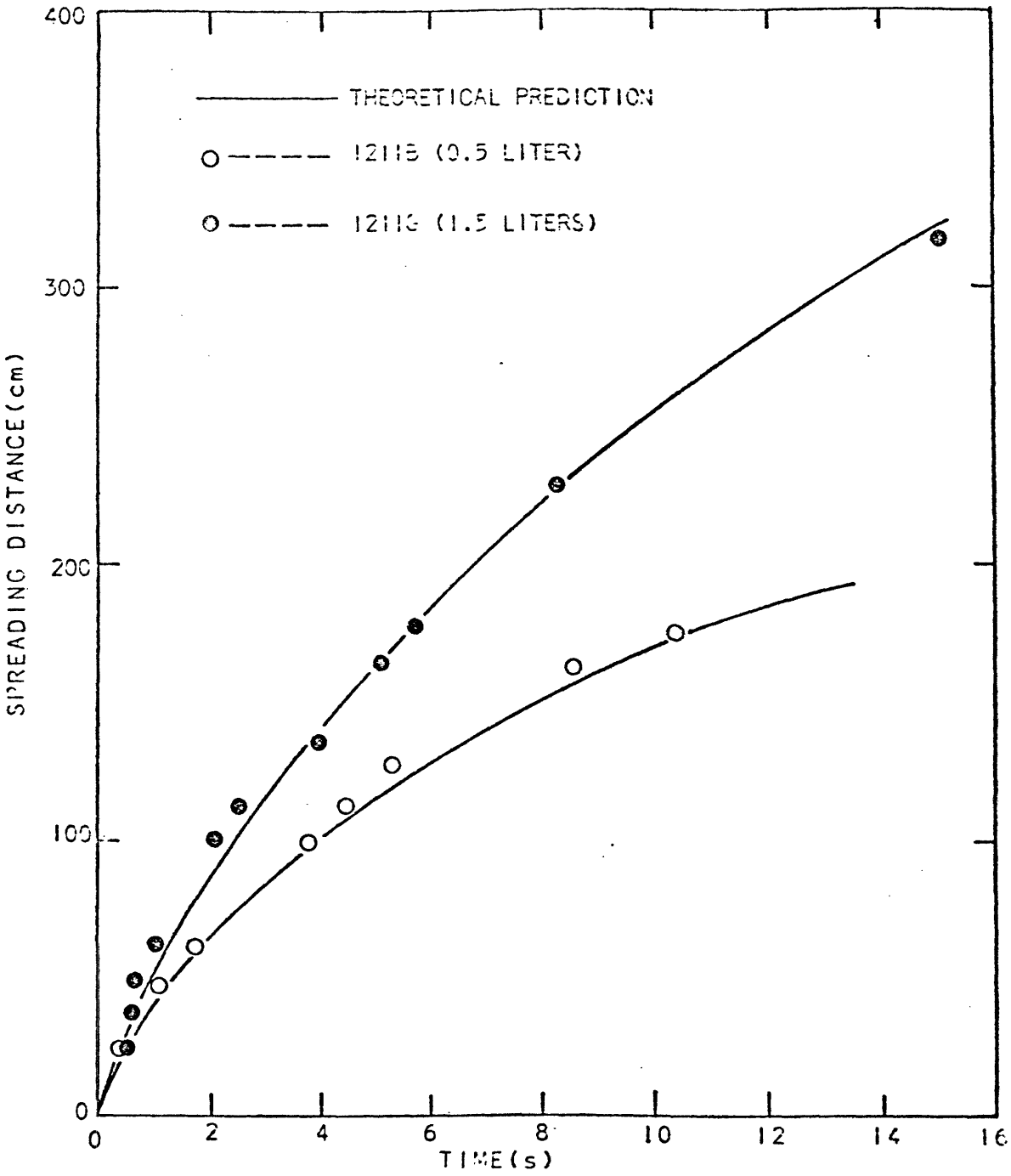

FIGURE VII-3: SPREADING CURVES FOR LIQUID NITROGEN SPILLS. EXPERIMENTAL DATA AND NUMERICAL PREDICTIONS COMPARED.

appears where the cryogen has completely evaporated. This edge starts at the distributor and moves downstream. The numerical model can also predict the trailing-edge path, as seen in Figure VII-4. The intersection of the leading edge and trailing edge determines the maximum spreading distance and the time for complete vaporization of nitrogen spilled on water.

Table VII-1 shows that the numerical model gives reasonable predictions of the maximum spreading distance for nitrogen spills. No experimental measurement of the trailing edge position profile has been made. Theoretical predictions of the time for complete vaporization with various initial volumes of nitrogen spills are also given in Table VII-1.

One previous model which describes the simultaneous boiling and spreading process for a one-dimensional configuration was developed by Raj (1977). A detailed description of Raj's model was given in Chapter II (equation (II-41)). According to Raj's model, using the assumption that the boiling rate per unit area is constant, the spreading distance is predicted to be the following function of time:

$$x = 1.39\left(\frac{g\Delta\, V_o\, t^2}{w}\right)^{1/3} + 0.097\,\left(\frac{\dot{q}}{\rho\Delta H_v}\right)\left[\frac{(g\Delta)^2\, wt^7}{V_o}\right]^{1/3} \qquad \text{(II-41)}$$

Predictions from this equation are compared to experimental data for nitrogen spills in Figure VII-5. Raj's model underestimates the spreading distance. When the effective density is used instead of the original density of liquid nitrogen in equation (II-41), Raj's model predicts spreading distances which are closer to those measured experimentally, as shown in Figure VII-6. However, in Raj's analysis, he used the leading-edge boundary condition (equation (V-3)) with λ equal to 1. If the same value of λ obtained from this work, 1.64, is used in Raj's model, one obtains

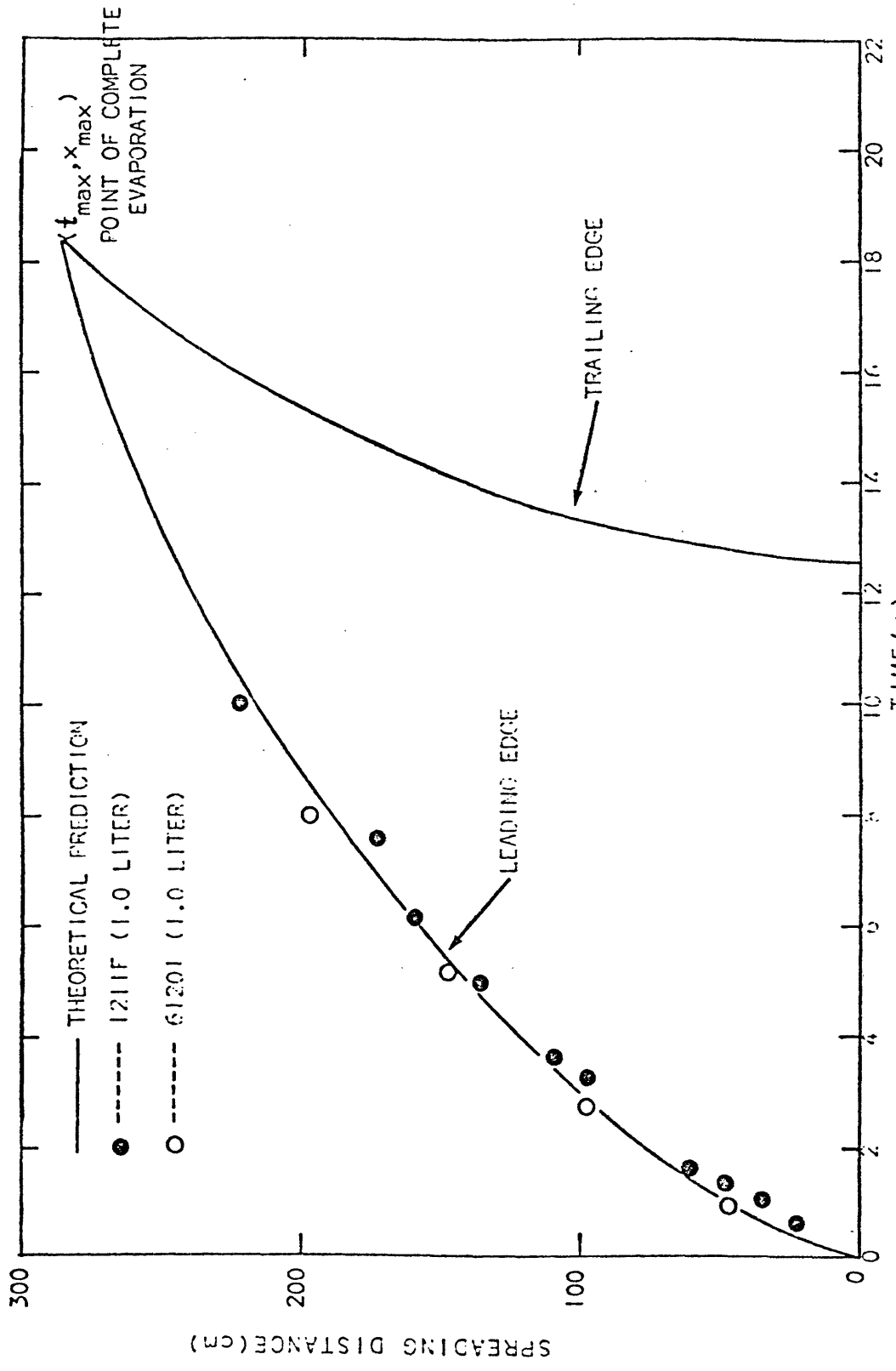

FIGURE VII-4: PATHS OF THE LEADING AND TRAILING EDGES FOR LIQUID NITROGEN SPILLS. NUMERICAL PREDICTIONS AND EXPERIMENTAL DATA ARE COMPARED.

TABLE VII-1

Maximum Spreading Distance and the Time for Complete Vaporization for Liquid Nitrogen Spills

Volume Spilled	Maximum Spreading Distance (cm) Experiment	Maximum Spreading Distance (cm) Numerical Prediction	Time for Complete Vaporization (sec) Numerical Prediction
0.5 liter	226	193	13.9
0.75 liter	---	246	16.3
1.0 liter	---	293	18.3
1.5 liters	-*-	374	21.6
2.0 liters	-*-	444	24.2

* The spread-tube was only 360 cm long.

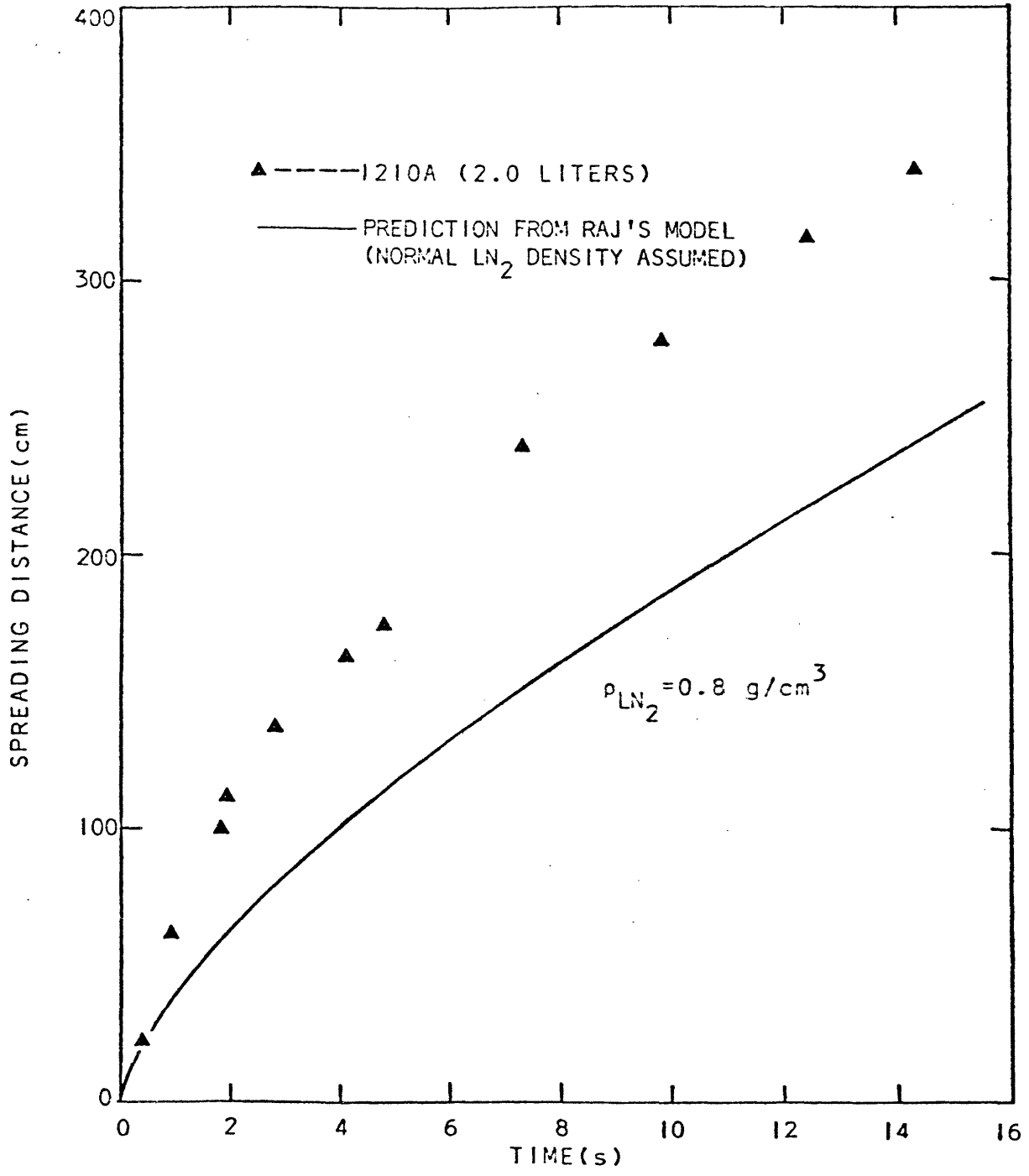

FIGURE VII-5: SPREADING DISTANCE AS A FUNCTION OF TIME FOR A LIQUID NITROGEN SPILL. EXPERIMENTAL DATA AND PREDICTION FROM RAJ'S MODEL COMPARED.

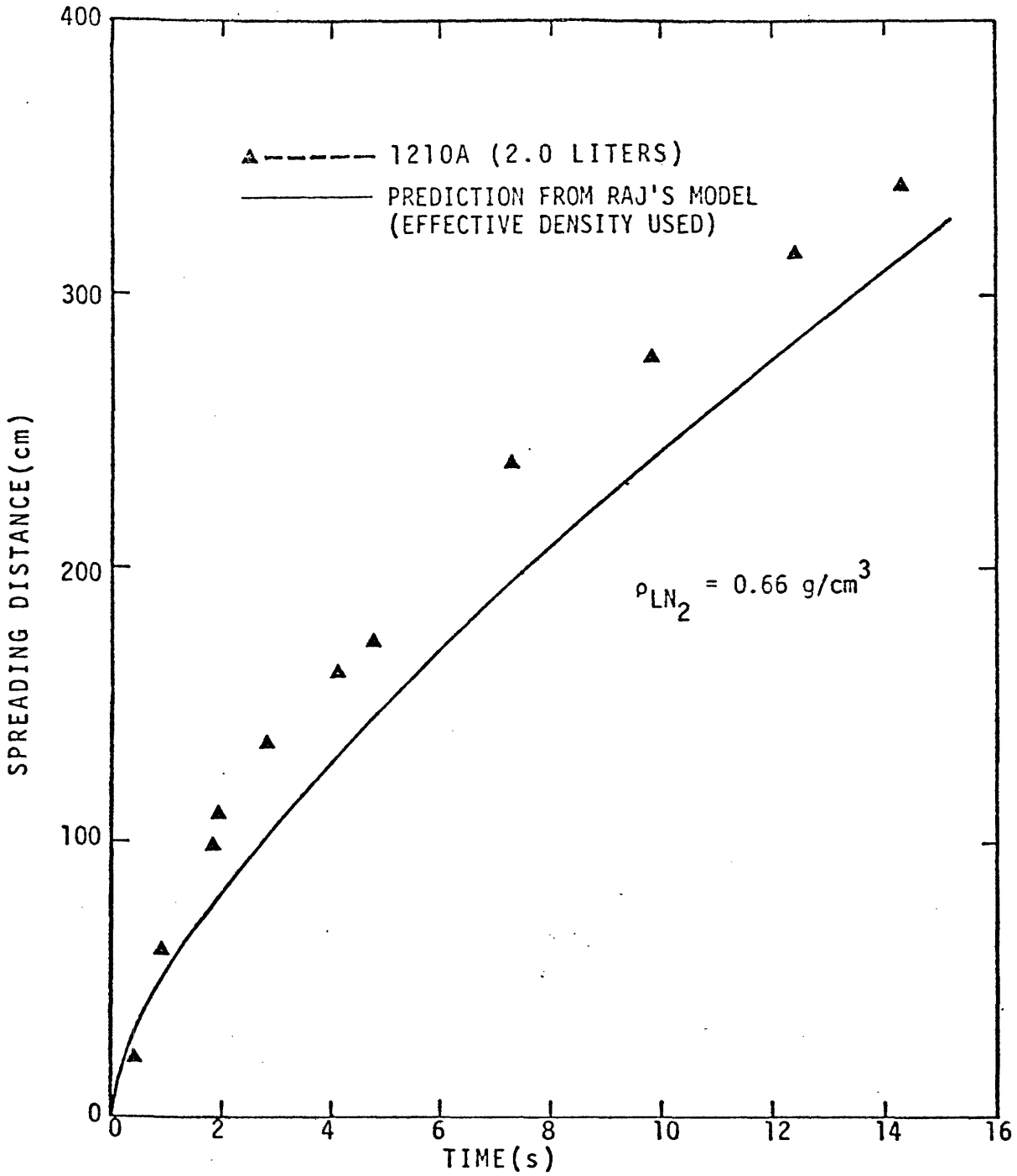

FIGURE VII-6: SPREADING DISTANCE AS A FUNCTION OF TIME FOR A LIQUID NITROGEN SPILL. EXPERIMENTAL DATA AND PREDICTION FROM RAJ'S MODEL COMPARED.

$$x = 1.72 \left(\frac{g\Delta\, V_o\, t^2}{w}\right)^{1/3} + 0.078 \left(\frac{\dot{q}}{\rho \Delta H_v}\right) \left[\frac{(g\Delta)^2\, wt^7}{V_o}\right]^{1/3} \qquad \text{(VII-1)}$$

Predictions from equation (VII-1), using both the normal density and the effective density of liquid nitrogen, are compared to experimental values in Figure VII-7. Neither version of equation (VII-1) predicts the spreading front position accurately. Furthermore, Raj's model assumes that the thickness of cryogen is uniform during the spreading; i.e., the cryogen thickness is only a function of time but independent of position. Experimental observations do not support this mean thickness approximation.

The close agreement between the experimental data and the theoretical predictions, using an assumed constant heat flux for nitrogen, proves the validity of the assumption. It is concluded that the numerical model successfully describes the boiling-spreading phenomena for nitrogen spills on water.

Liquid Methane

The boiling-spreading process for liquid methane on water is very similar to that of liquid nitrogen except that methane evaporates more rapidly than nitrogen. No boiling rate data have been obtained from these experiments. In the simulations, as in the case of nitrogen, the boil-off rate per unit area is assumed constant but equal to 92 kW/m^2; this value is obtained from previous work (Burgess et al. (1970)) and is consistent with values used in most of the other theoretical modelling work. The effective density of liquid methane is estimated through a procedure similar to nitrogen. The value of methane's effective density is estimated to be 0.254 g/cm^3 (the normal density of liquid methane at 111K is 0.425 g/cm^3).

Numerical predictions for the spreading front path of methane on a water surface are compared to experimental data in Figures VII-8 and VII-9. The agreement between the model and experiment is very good.

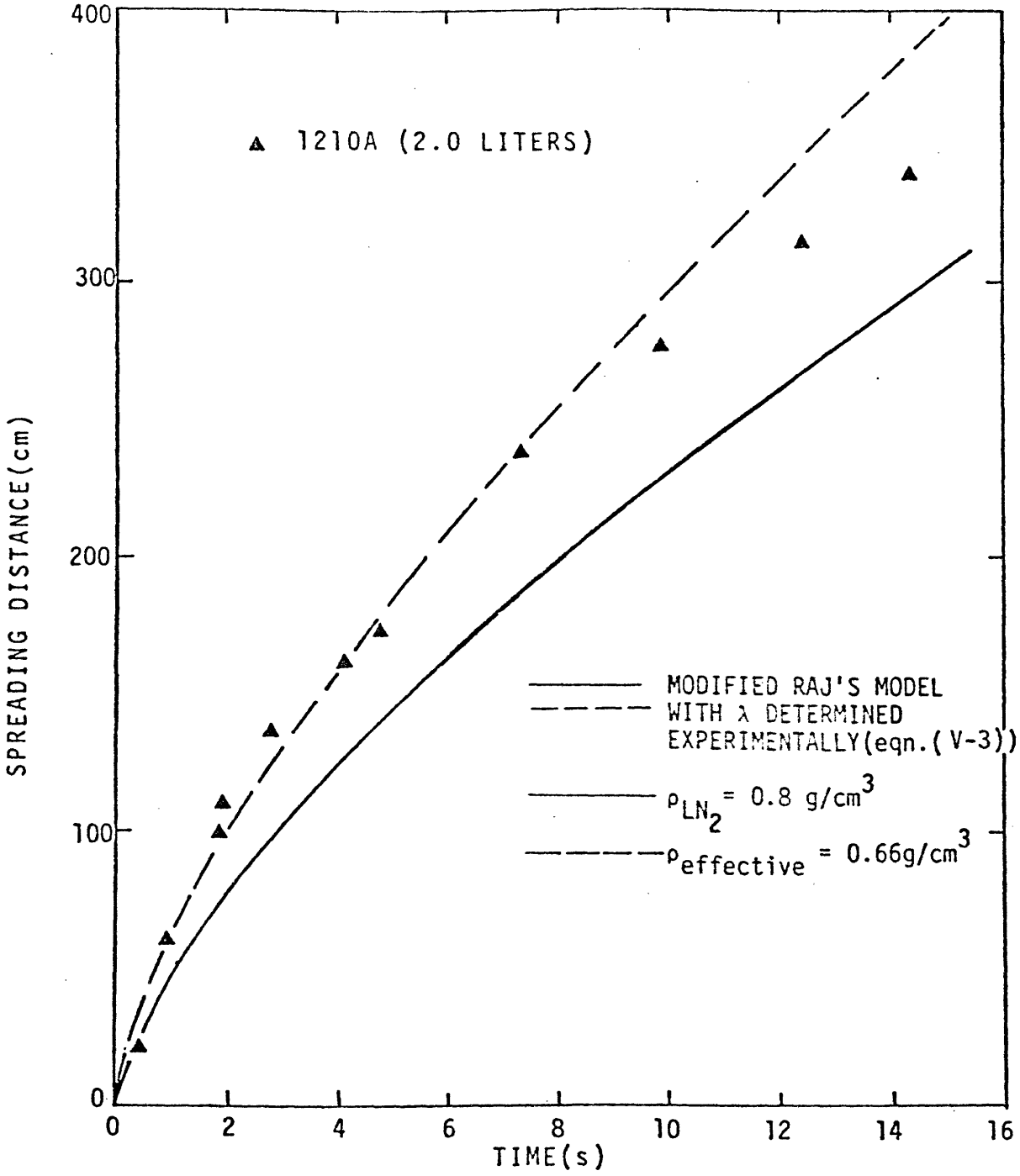

FIGURE VII-7: SPREADING DISTANCE AS A FUNCTION OF TIME FOR A LIQUID NITROGEN SPILL. EXPERIMENTAL DATA AND PREDICTIONS FROM MODIFIED RAJ'S MODEL COMPARED.

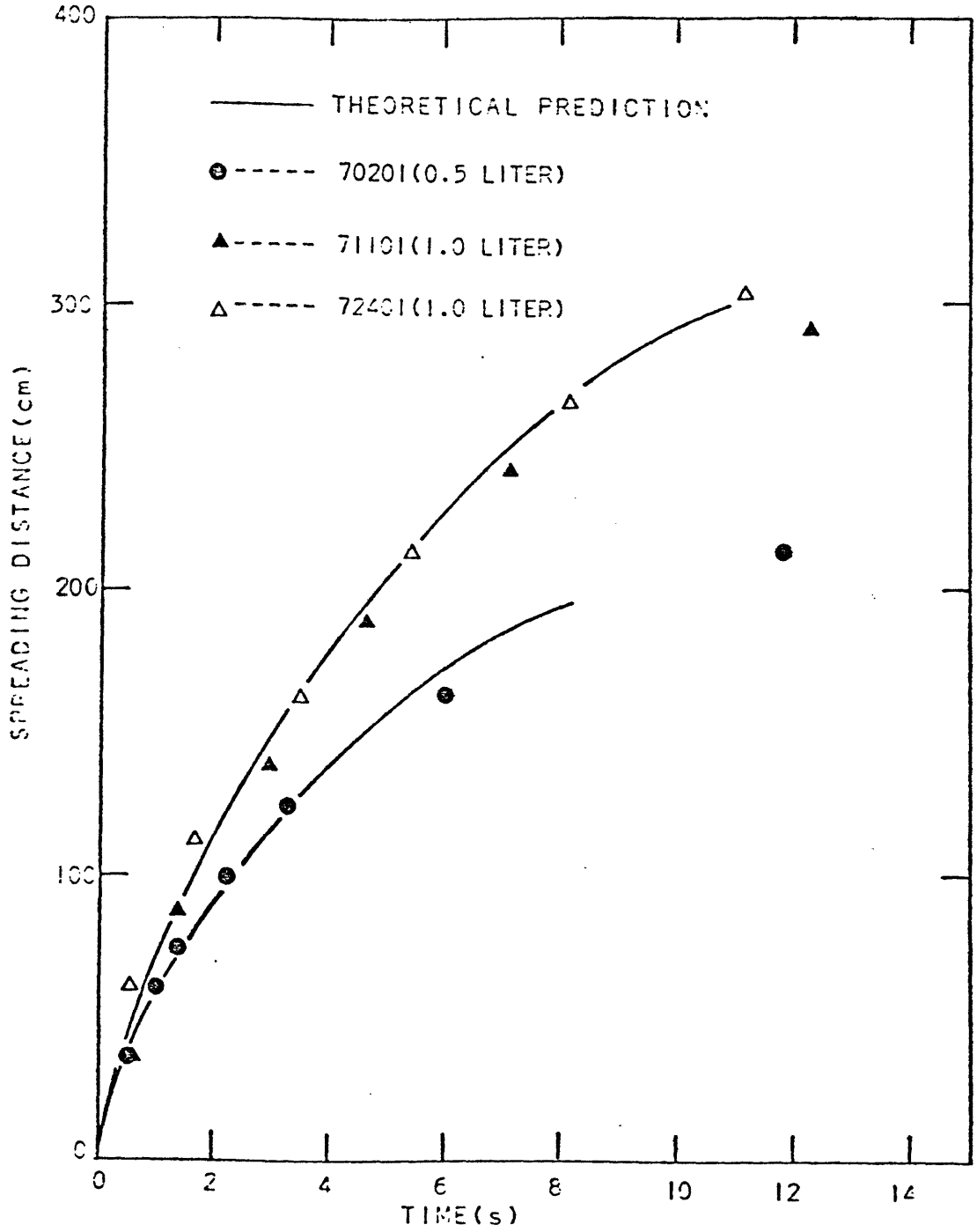

FIGURE VII-8: SPREADING CURVES FOR LIQUID METHANE SPILLS. EXPERIMENTAL DATA AND NUMERICAL PREDICTIONS COMPARED.

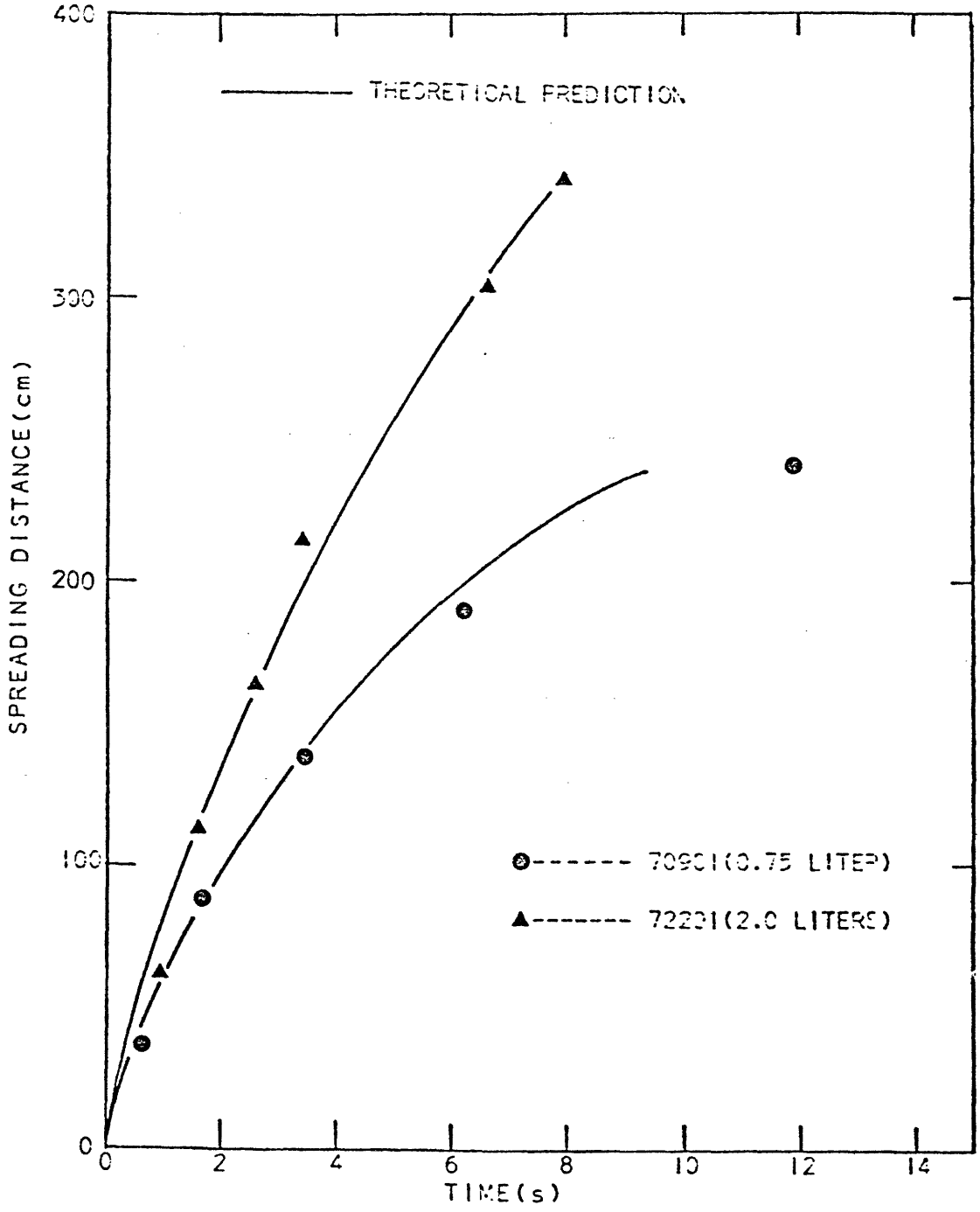

FIGURE VII-9: SPREADING CURVES FOR LIQUID METHANE SPILLS. EXPERIMENTAL DATA AND NUMERICAL PREDICTIONS COMPARED.

Liquid methane exhibits a thickness profile similar to that for liquid nitrogen during spreading. The theoretical prediction of the thickness profile (a thick spreading front followed by a thinner tail) is shown in Figure V-5. This is consistent with observations from experiments.

The values of the maximum spreading distance and the time for complete vaporization predicted by the numerical model for methane spills are presented in Table VII-2 for various initial spilled volumes. A satisfactory agreement between theory and experiment is observed.

In Figures VII-10 and VII-11, predictions of the spreading-front path from Raj's model (equation (II-41)) and equation (VII-1), using both the normal liquid density and the effective density of methane, are compared to experimental data. Raj's model does not adequately describe the boiling-spreading phenomena for methane spills.

The numerical model using a constant heat flux assumption accurately describes the boiling-spreading process for methane spills. One can conclude that the assumption of constant boil-off rate per unit area is valid and the numerical model is adequate for simulating methane spills (at least for the volumes spilled in this study).

Propane and LPG Mixtures

When propane or LPG is spilled on water, violent boiling occurs immediately upon contact. In the first second or two very high boiling heat fluxes are observed. Since the water surface near the distributor opening is severely agitated during this period, it is very difficult to define the true area of contact between cryogen and water. Qualitatively, agitation of the interface increases with the quantity of cryogen spilled. Therefore, it is not possible to obtain reliable quantitative values of heat fluxes in this violent initial boiling period. It is thought that the values of the heat flux should be similar to those expected in a peak nucleate flux region (see Chapter II).

TABLE VII-2

Maximum Spreading Distance and the Time for Complete Varporization for Liquid Methane Spills

Volume Spilled	Maximum Spreading Distance (cm) Experiment	Maximum Spreading Distance (cm) Numerical Prediction	Time for Complete Vaporization (sec) Numerical Prediction
0.5 liter	229	197	8.2
0.75 liter	279	251	9.7
1.0 liter	317	298	10.8
1.5 liters	-*-	380	12.7
2.0 liters	-*-	452	14.3

* The spread-tube was only 360 cm long.

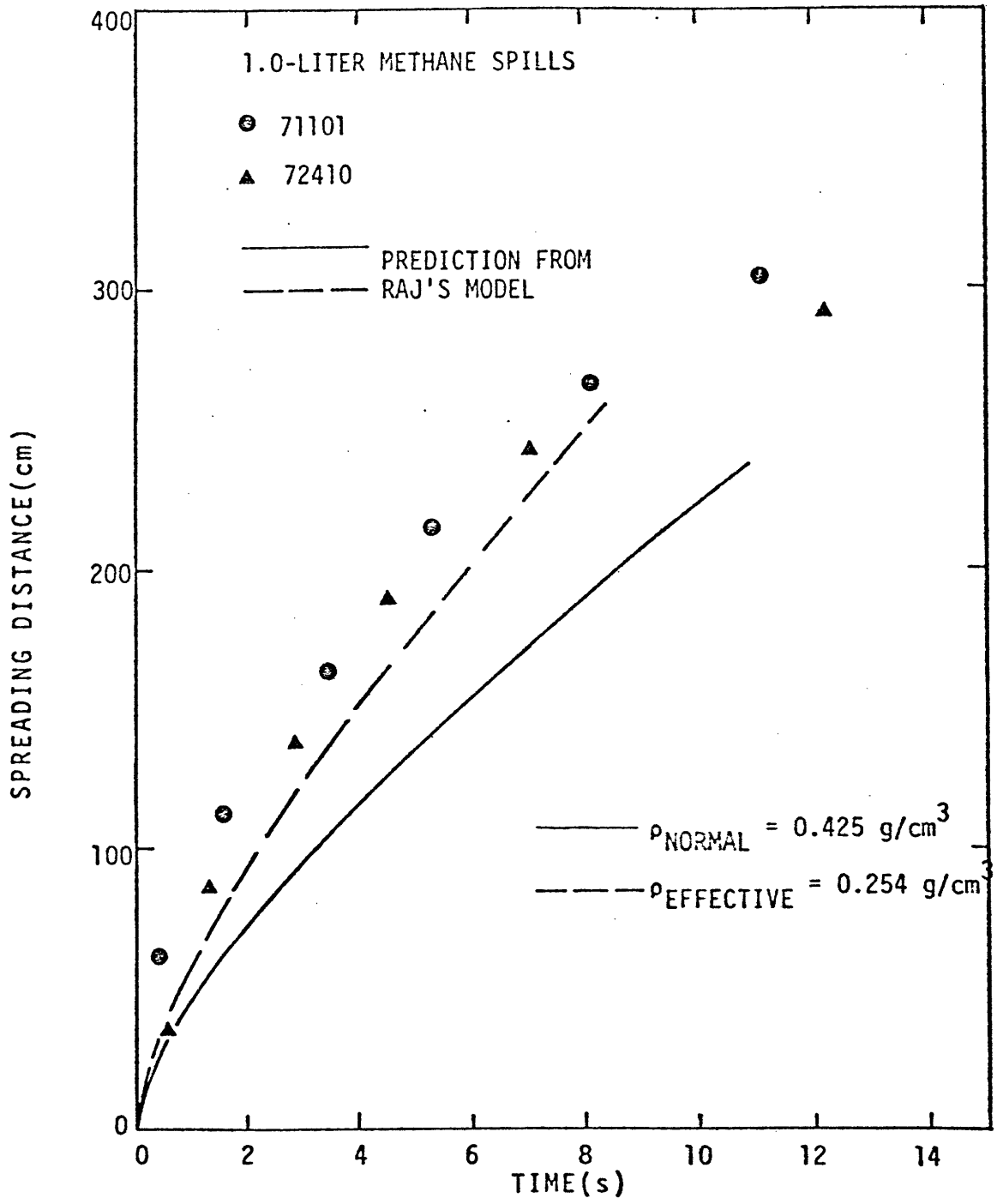

FIGURE VII-10: SPREADING DISTANCE AS A FUNCTION OF TIME FOR LIQUID METHANE SPILLS. EXPERIMENTAL DATA AND PREDICTIONS FROM RAJ'S MODEL COMPARED.

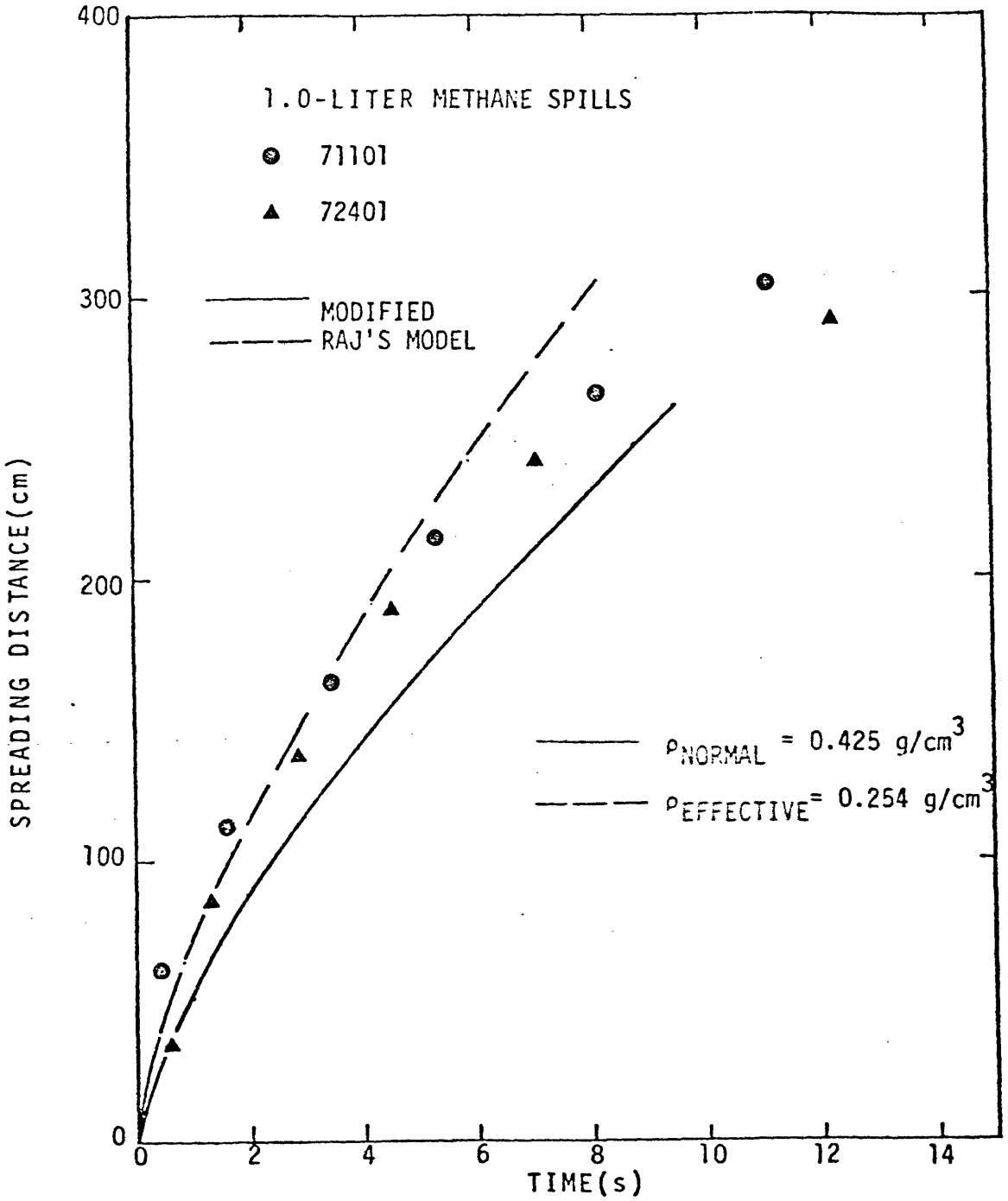

FIGURE VII-11: SPREADING DISTANCE AS A FUNCTION OF TIME FOR LIQUID METHANE SPILLS. EXPERIMENTAL DATA AND PREDICTIONS FROM MODIFIED RAJ'S MODEL COMPARED.

About one second after the propane or LPG contacts the water, a very rough ice layer forms. After this point, the heat transfer is controlled by the conduction through the ice and water; the boiling rate decreases further with time as the ice shield grows thicker. During this stage the local vaporization can be reasonably well described by a moving-boundary heat-transfer model developed for confined LPG spills. A detailed description of this model is given in Appendix-I. The model leads to the conclusion that the local heat flux is inversely proportional to the square root of corrected time t_{c_i}:

$$\dot{Q}_i = \varepsilon\, t_{c_i}^{-1/2} \quad (kW/m^2) \qquad \text{(VII-2)}$$

where t_{c_i} is defined as :

$$t_{c_i} = t_i - t_\delta \quad (s)$$

ε is a function of the physical properties of ice and is evaluated at an average temperature between the freezing point and the LPG boiling point. t_δ is a time associated with the initial ill-defined boiling phase. t_i is the time elasped after the initial contact of water with cryogen at a position x_i where the heat flux is $\dot{Q}_i$.

The value of t_δ is set equal to one second. This time was determined from an analysis of high speed motion picture photographs taken during many propane and LPG spills

Predictions from equation (VII-2) are compared with experimental data in Figures VII-12 through VII-27 for propane and LPG spills. The moving boundary model and experiments agree reasonably well for the first sampling station. Note that most of the values of the heat fluxes obtained from the second and third stations are below those predicted by the moving boundary model. The

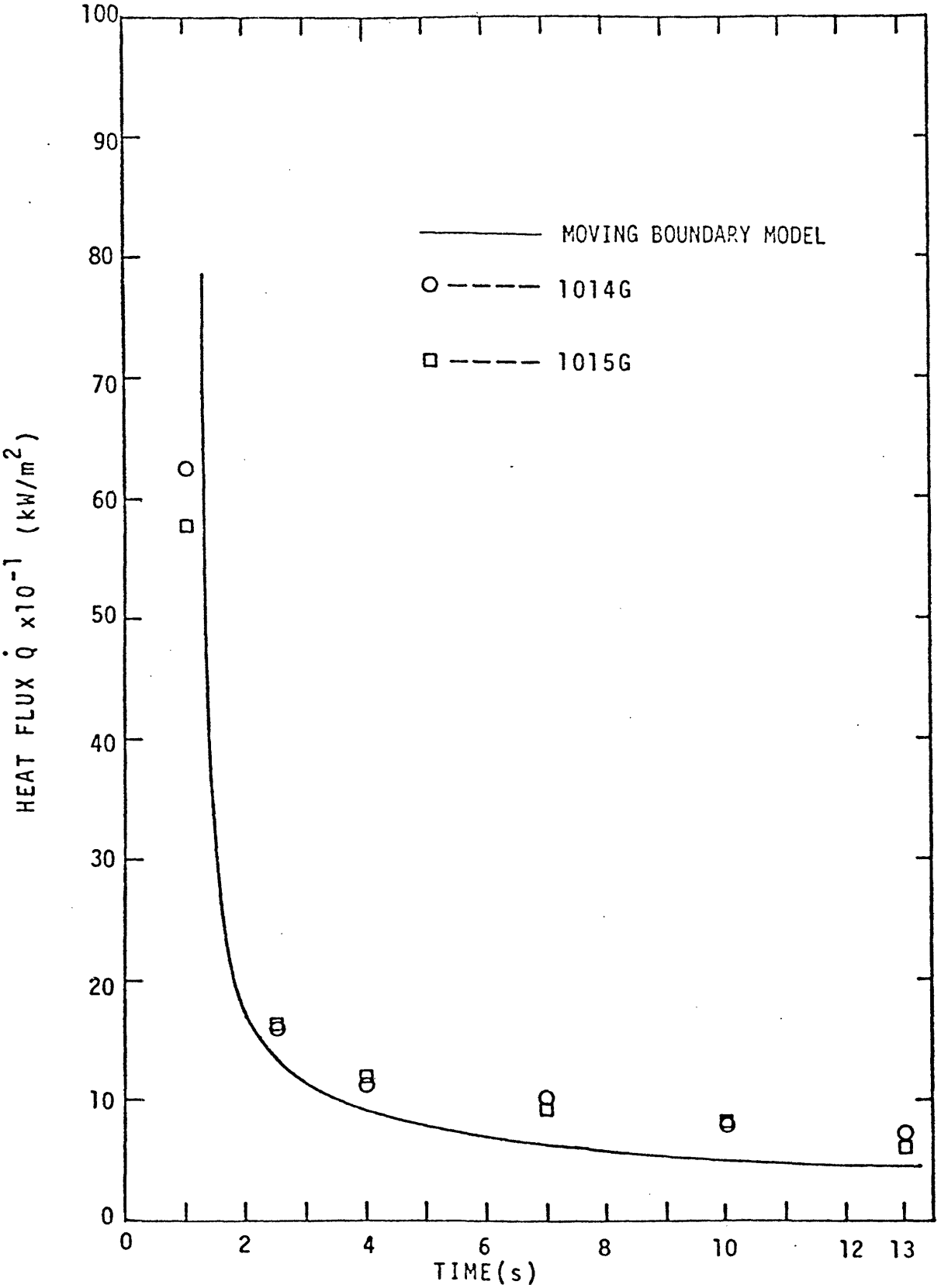

FIGURE VII-12: LOCAL BOIL-OFF RATE CURVES FOR 0.5-LITER PROPANE SPILLS AT THE FIRST SAMPLING STATION. EXPERIMENTAL DATA COMPARED WITH PREDICTIONS FROM MOVING BOUNDARY MODEL.

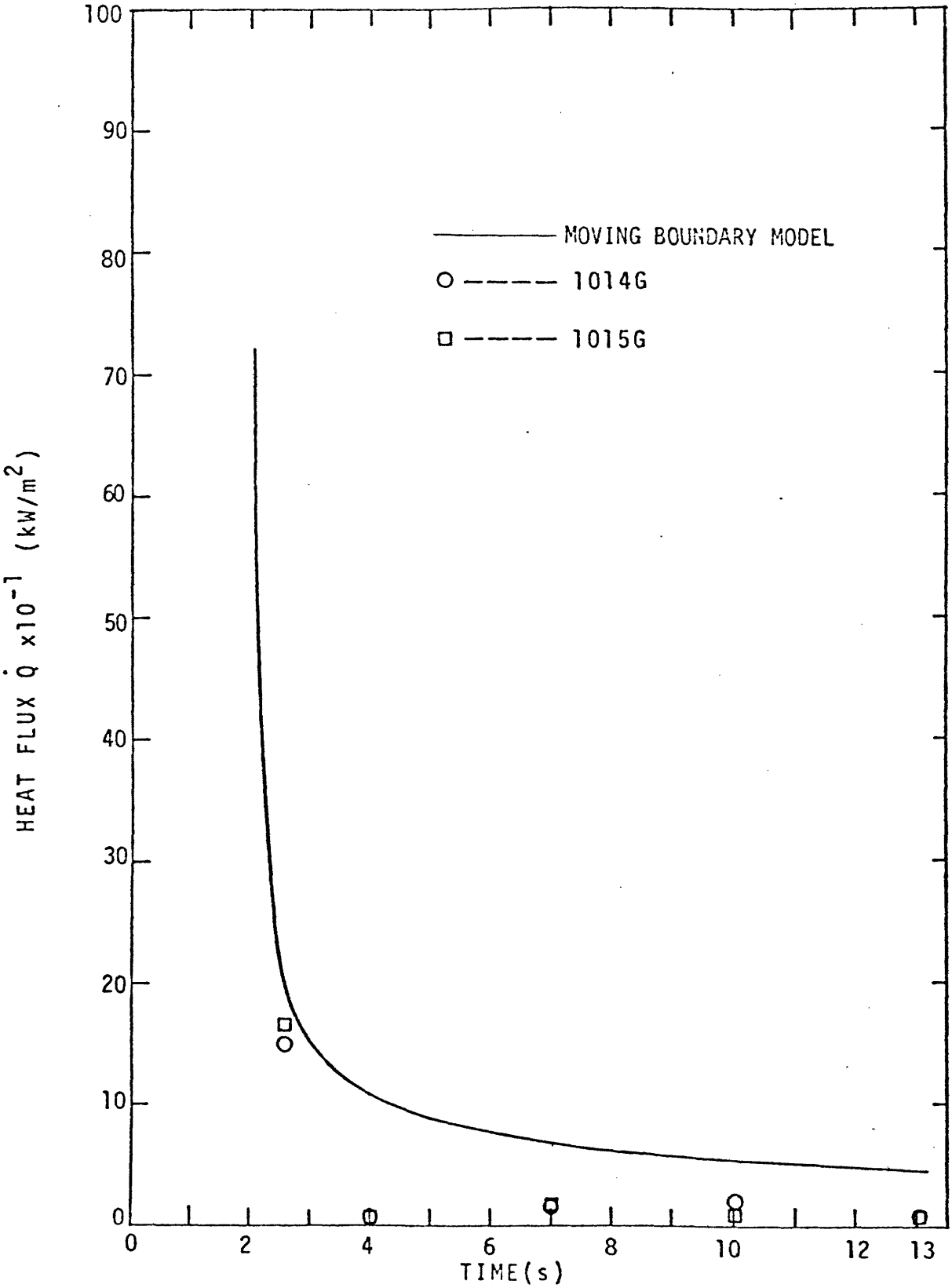

FIGURE VII-13: LOCAL BOIL-OFF RATE CURVES FOR 0.5-LITER PROPANE SPILLS AT THE SECOND SAMPLING STATION. EXPERIMENTAL DATA COMPARED WITH PREDICTIONS FROM MOVING BOUNDARY MODEL.

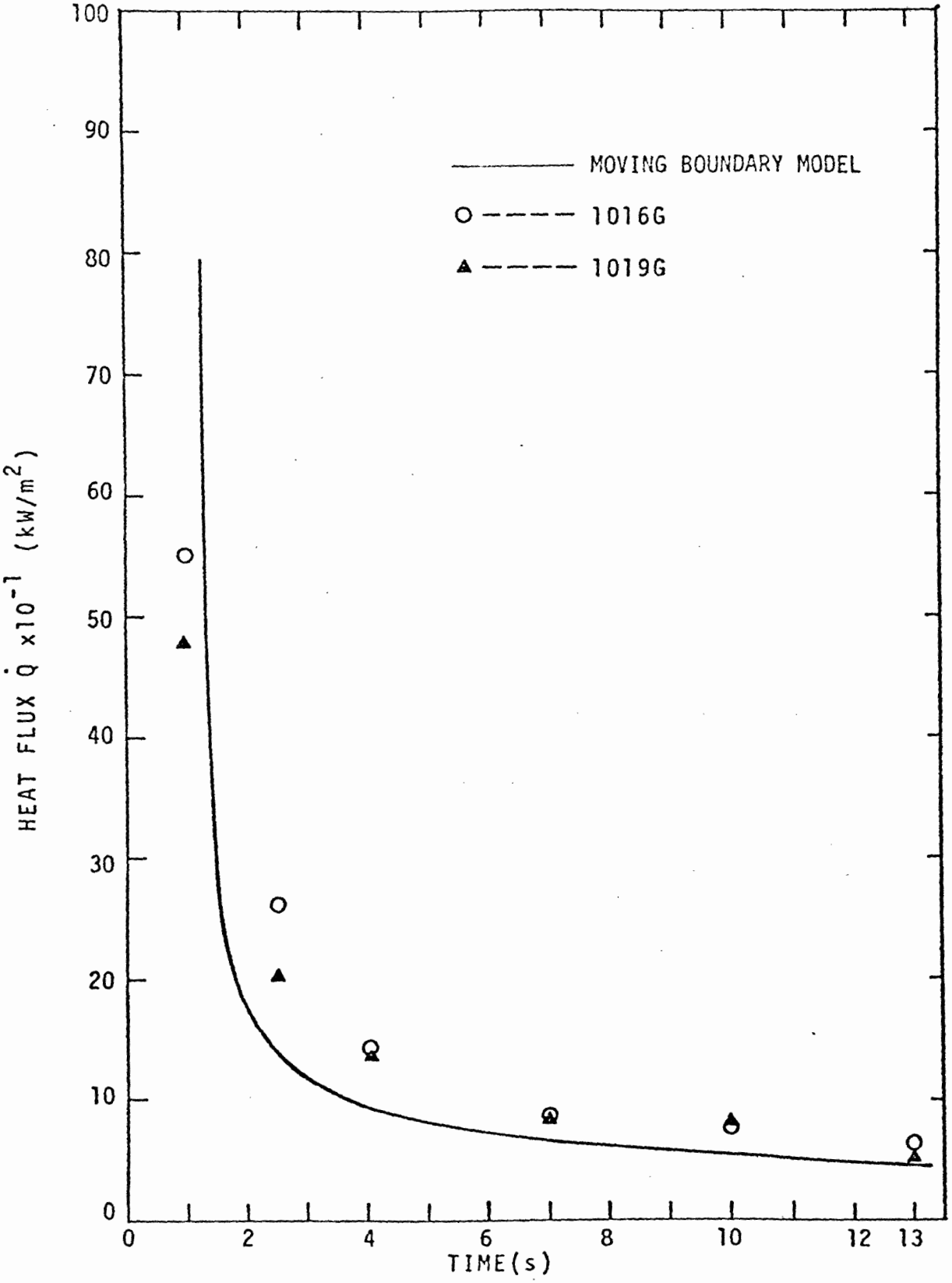

FIGURE VII-14: LOCAL BOIL-OFF RATE CURVES FOR 0.75-LITER PROPANE SPILLS AT THE FIRST SAMPLING STATION. EXPERIMENTAL DATA COMPARED WITH PREDICTIONS FROM MOVING BOUNDARY MODEL.

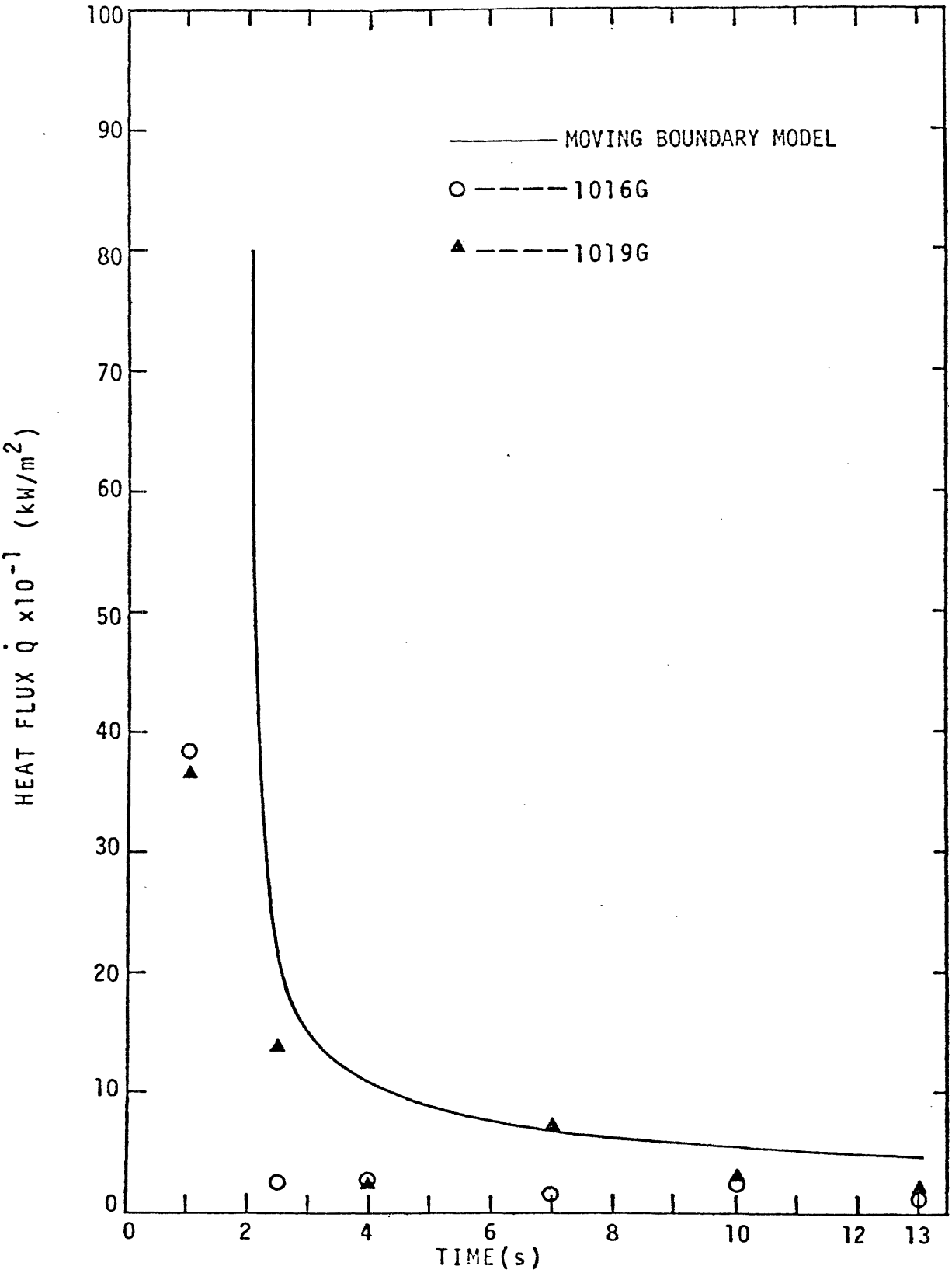

FIGURE VII-15: LOCAL BOIL-OFF RATE CURVES FOR 0.75-LITER PROPANE SPILLS AT THE SECOND SAMPLING STATION. EXPERIMENTAL DATA COMPARED WITH PREDICTIONS FROM MOVING BOUNDARY MODEL.

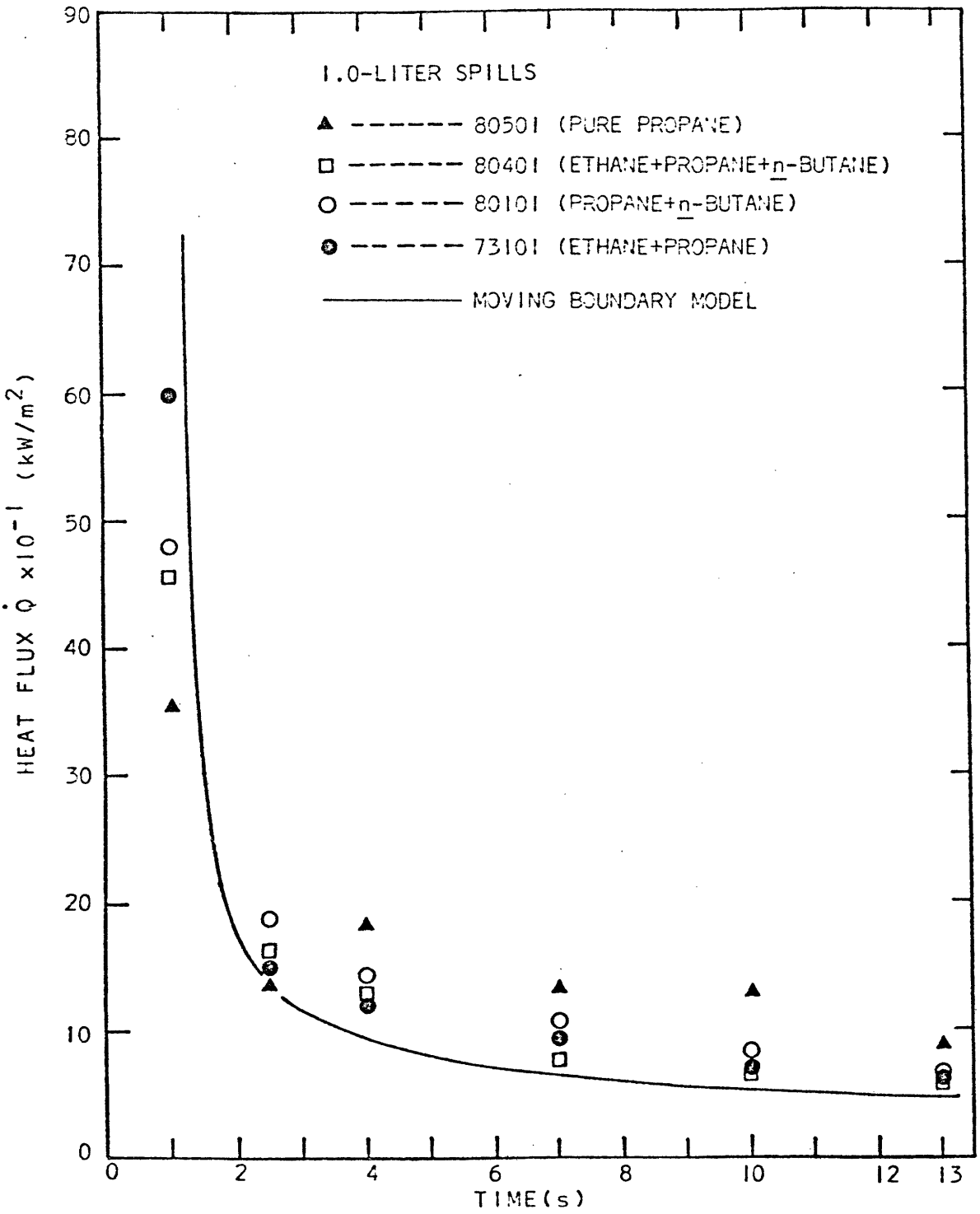

FIGURE VII-16: LOCAL BOIL-OFF RATE CURVES FOR PROPANE AND LPG SPILLS AT THE FIRST SAMPLING STATION. EXPERIMENTAL DATA COMPARED WITH PREDICTIONS FROM MOVING BOUNDARY MODEL.

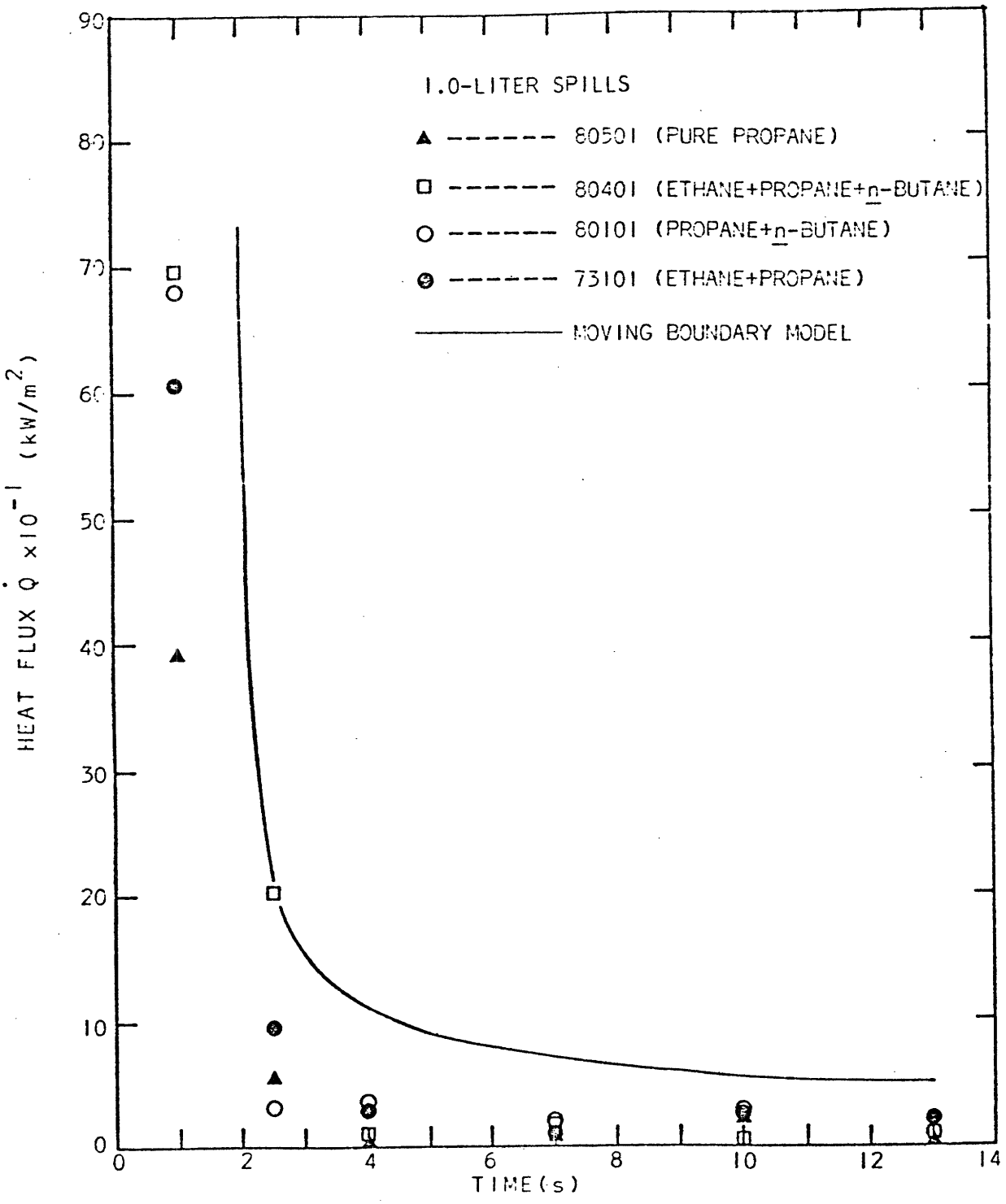

FIGURE VII-17: LOCAL BOIL-OFF RATE CURVES FOR PROPANE AND LPG SPILLS AT THE SECOND SAMPLING STATION. EXPERIMENTAL DATA COMPARED WITH PREDICTIONS FROM MOVING BOUNDARY MODEL.

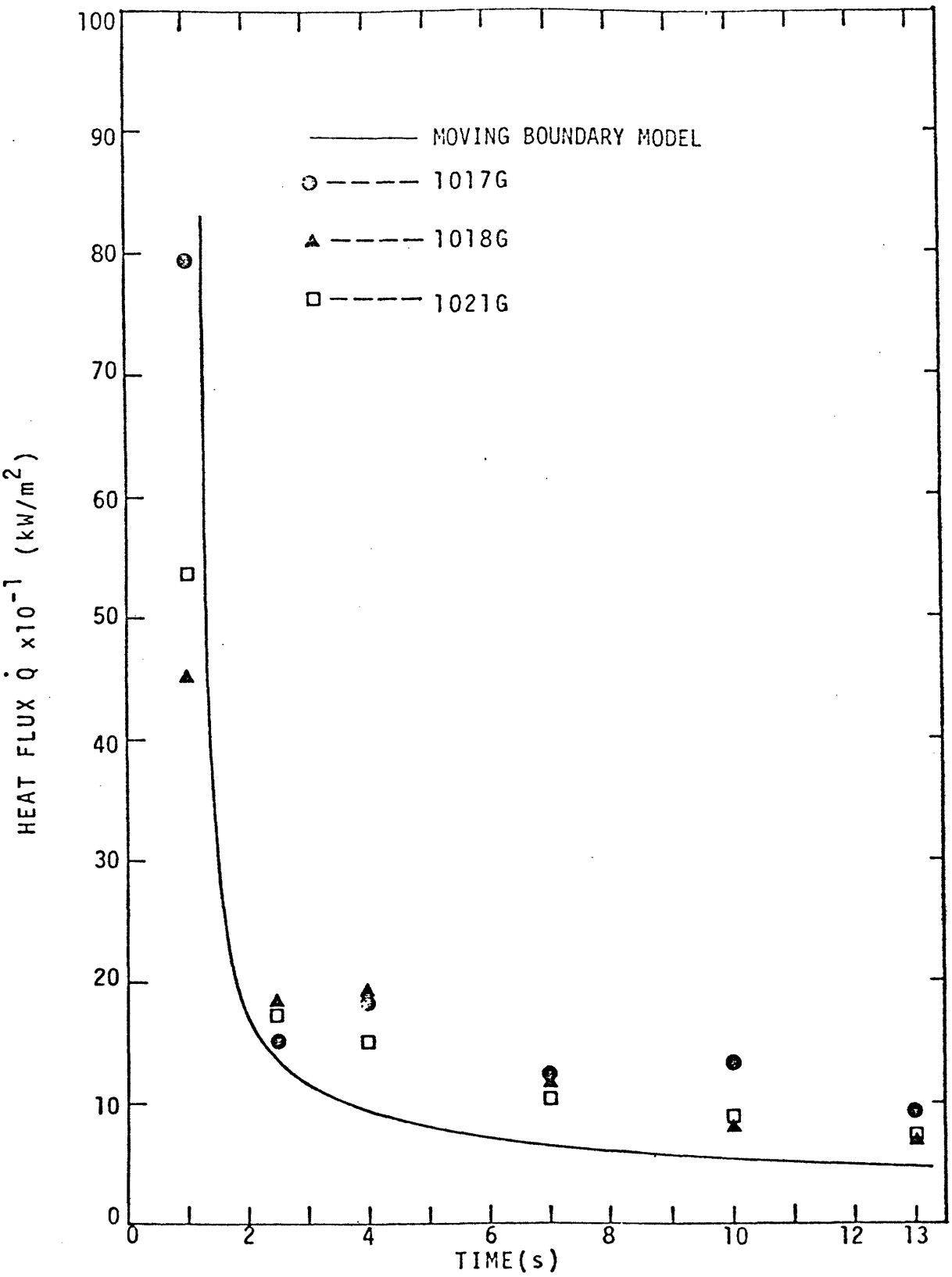

FIGURE VII-18: LOCAL BOIL-OFF RATE CURVES FOR 1.5-LITER PROPANE SPILLS AT THE FIRST SAMPLING STATION. EXPERIMENTAL DATA COMPARED WITH PREDICTIONS FROM MOVING BOUNDARY MODEL.

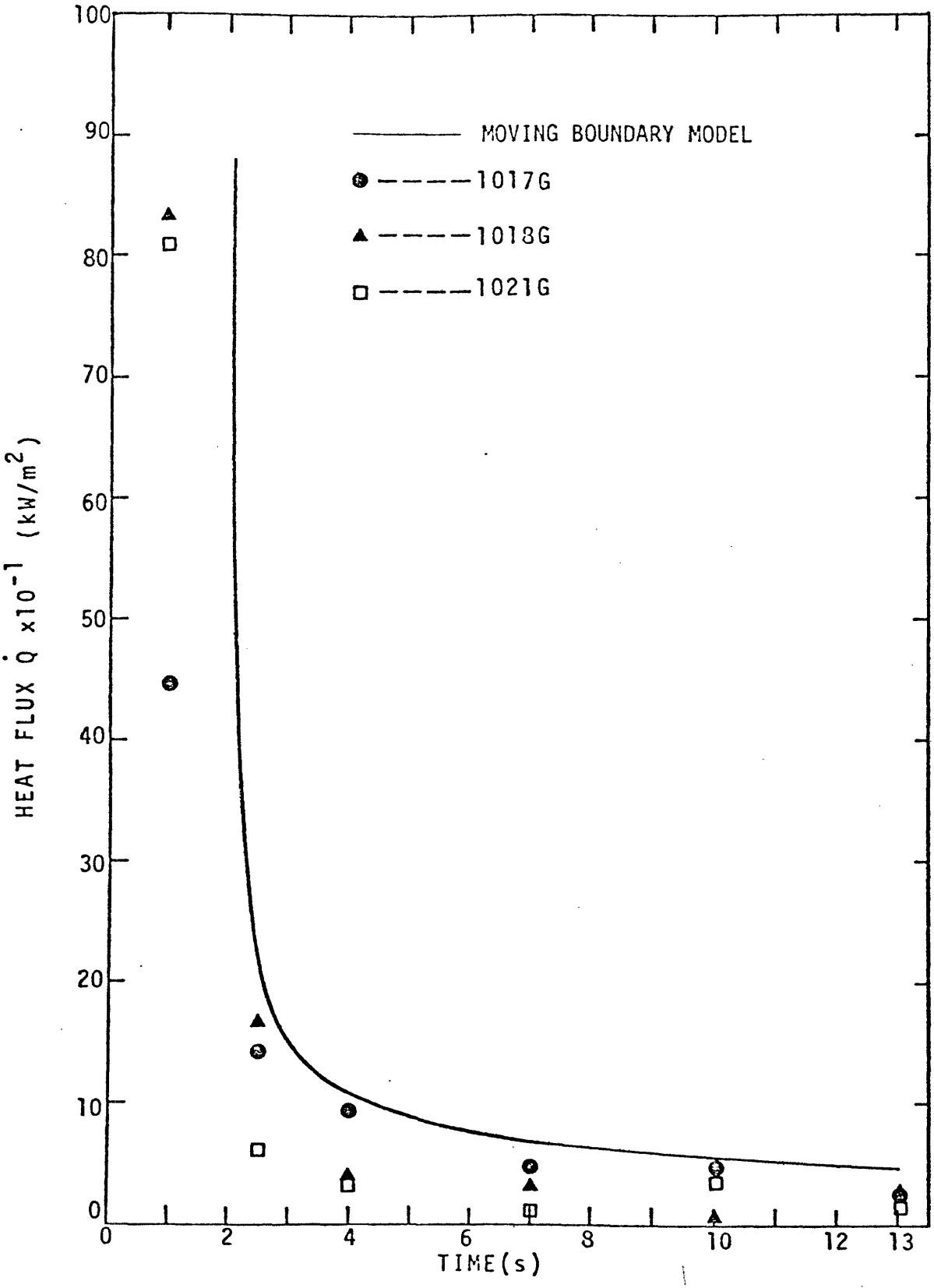

FIGURE VII-19: LOCAL BOIL-OFF RATE CURVES FOR 1.5-LITER PROPANE SPILLS AT THE SECOND SAMPLING STATION. EXPERIMENTAL DATA COMPARED WITH PREDICTIONS FROM MOVING BOUNDARY MODEL.

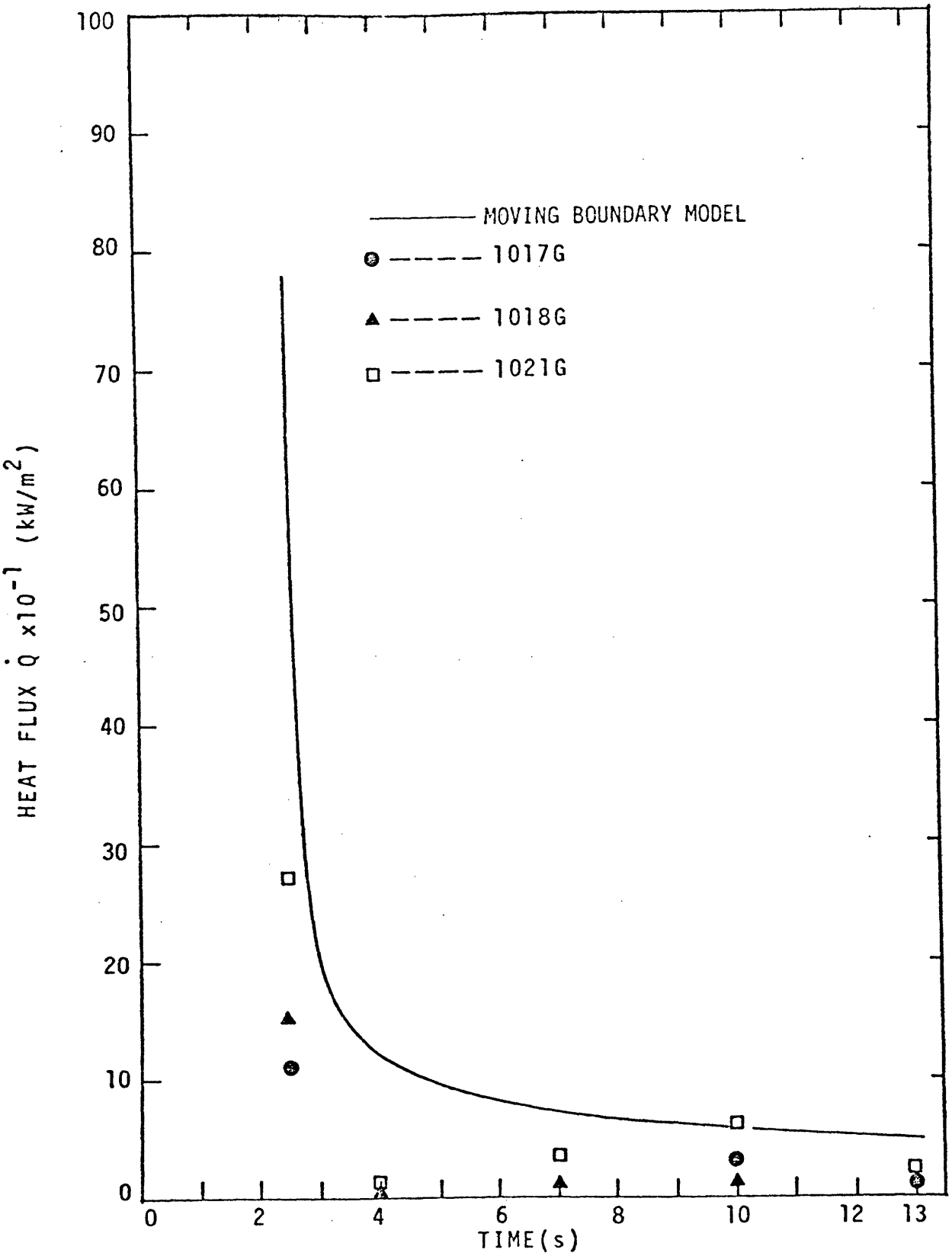

FIGURE VII-20: LOCAL BOIL-OFF RATE CURVES FOR 1.5-LITER PROPANE SPILLS AT THE THIRD SAMPLING STATION. EXPERIMENTAL DATA COMPARED WITH PREDICTIONS FROM MOVING BOUNDARY MODEL.

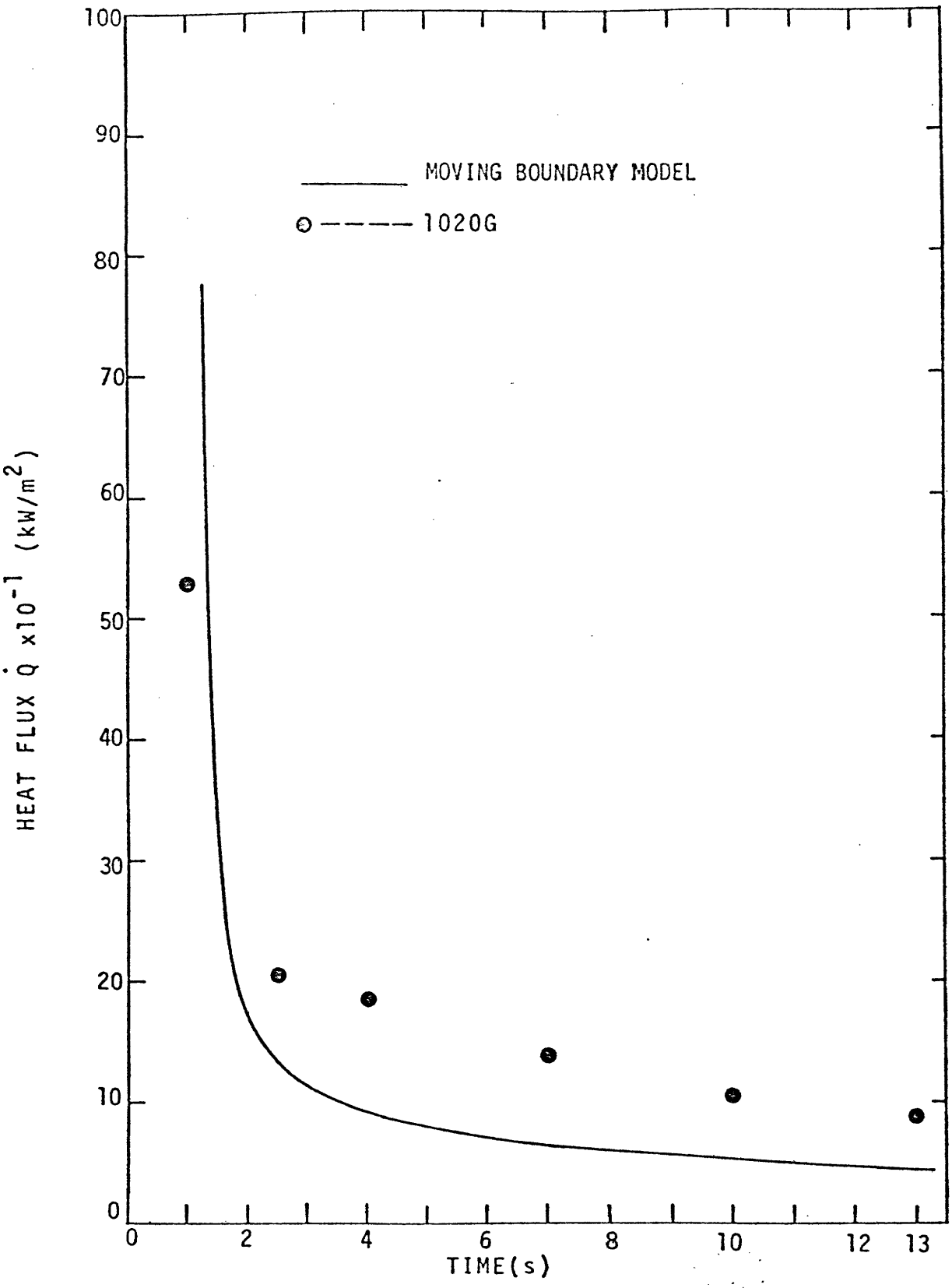

FIGURE VII-21: LOCAL BOIL-OFF RATE CURVES FOR 2.0-LITER PROPANE SPILLS AT THE FIRST SAMPLING STATION. EXPERIMENTAL DATA COMPARED WITH PREDICTIONS FROM MOVING BOUNDARY MODEL.

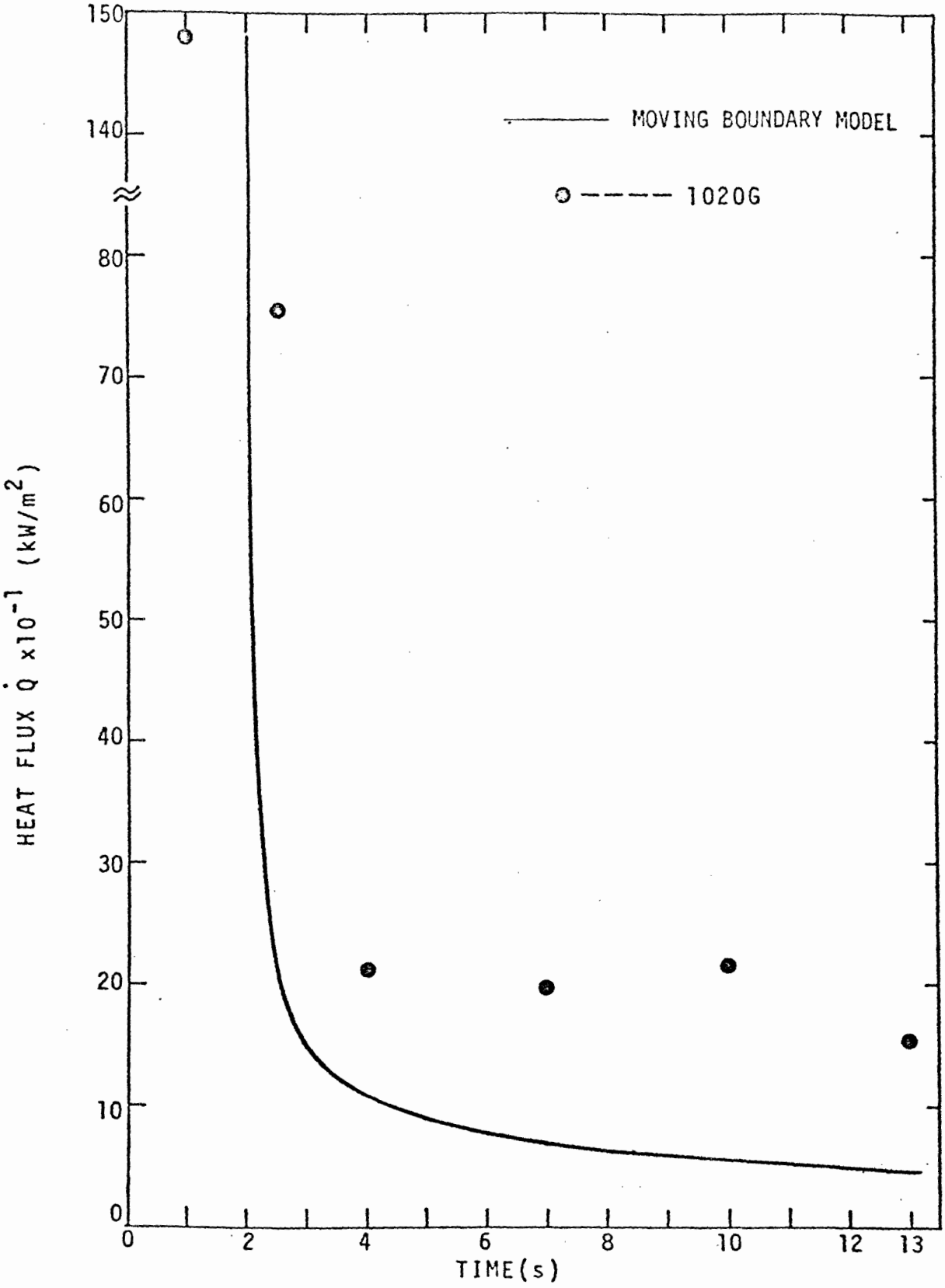

FIGURE VII-22: LOCAL BOIL-OFF RATE CURVES FOR 2.0-LITER PROPANE SPILL AT THE SECOND SAMPLING STATION. EXPERIMENTAL DATA COMPARED WITH PREDICTIONS FROM MOVING BOUNDARY MODEL.

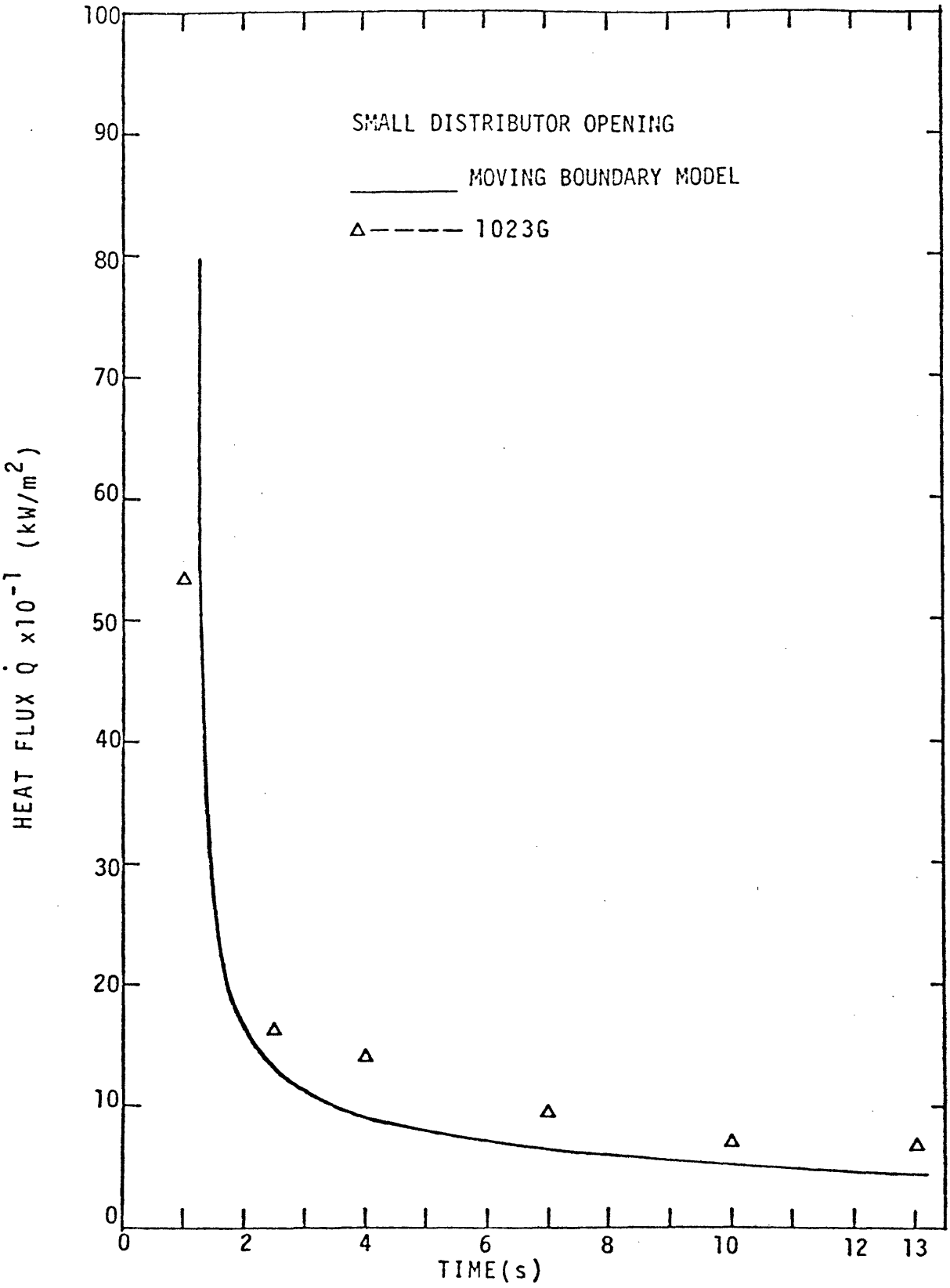

FIGURE VII-23: LOCAL BOIL-OFF RATE CURVES FOR A 1.0-LITER PROPANE SPILL(SMALL DISTRIBUTOR OPENING) AT THE FIRST SAMPLING STATION. EXPERIMENTAL DATA COMPARED WITH PREDICTIONS FROM MOVING BOUNDARY MODEL.

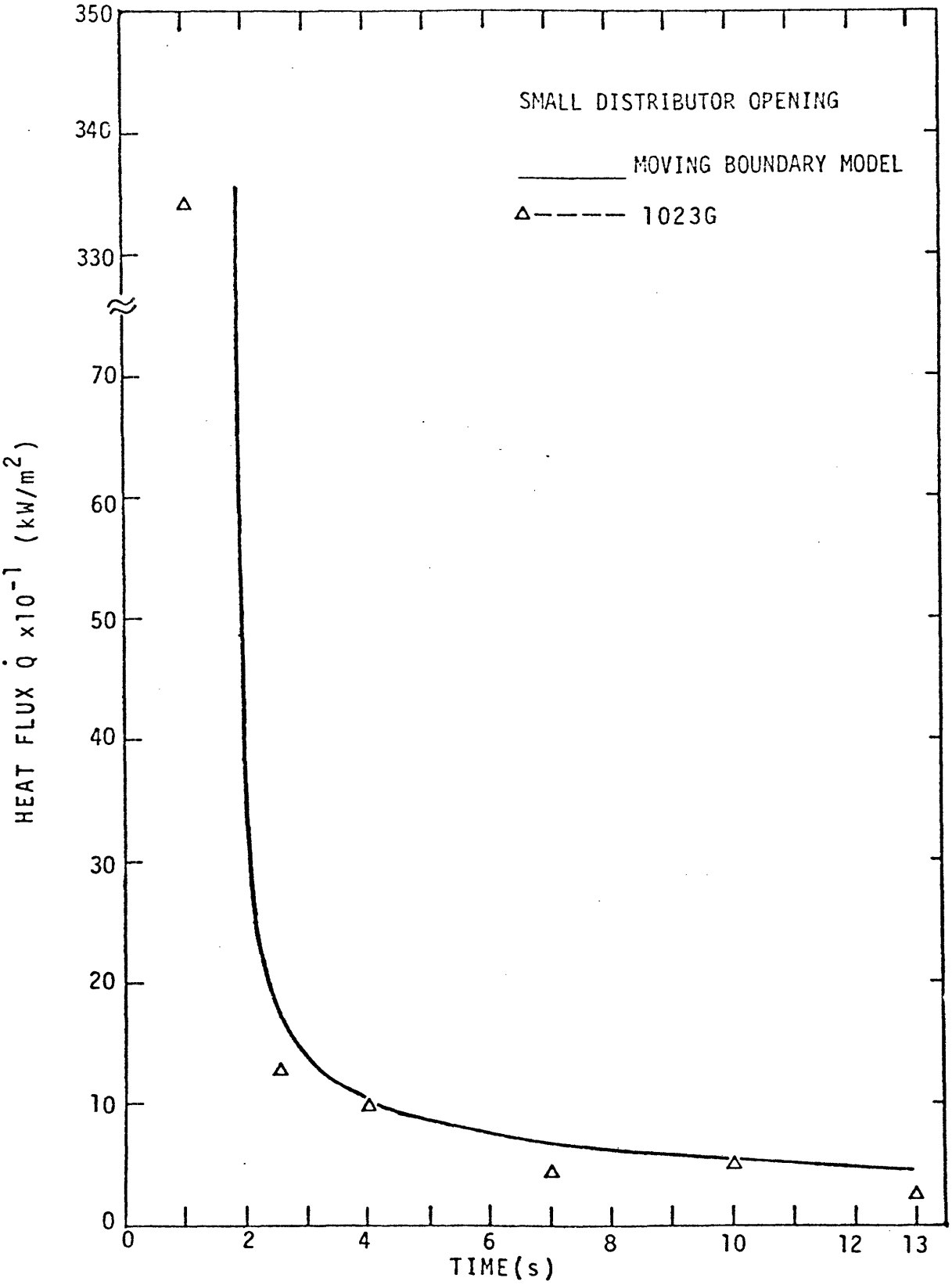

FIGURE VII-24: LOCAL BOIL-OFF RATE CURVES FOR A 1.0-LITER PROPANE SPILL(SMALL DISTRIBUTOR OPENING) AT THE SECOND SAMPLING STATION. EXPERIMENTAL DATA COMPARED WITH PREDICTIONS FROM MOVING BOUNDARY MODEL.

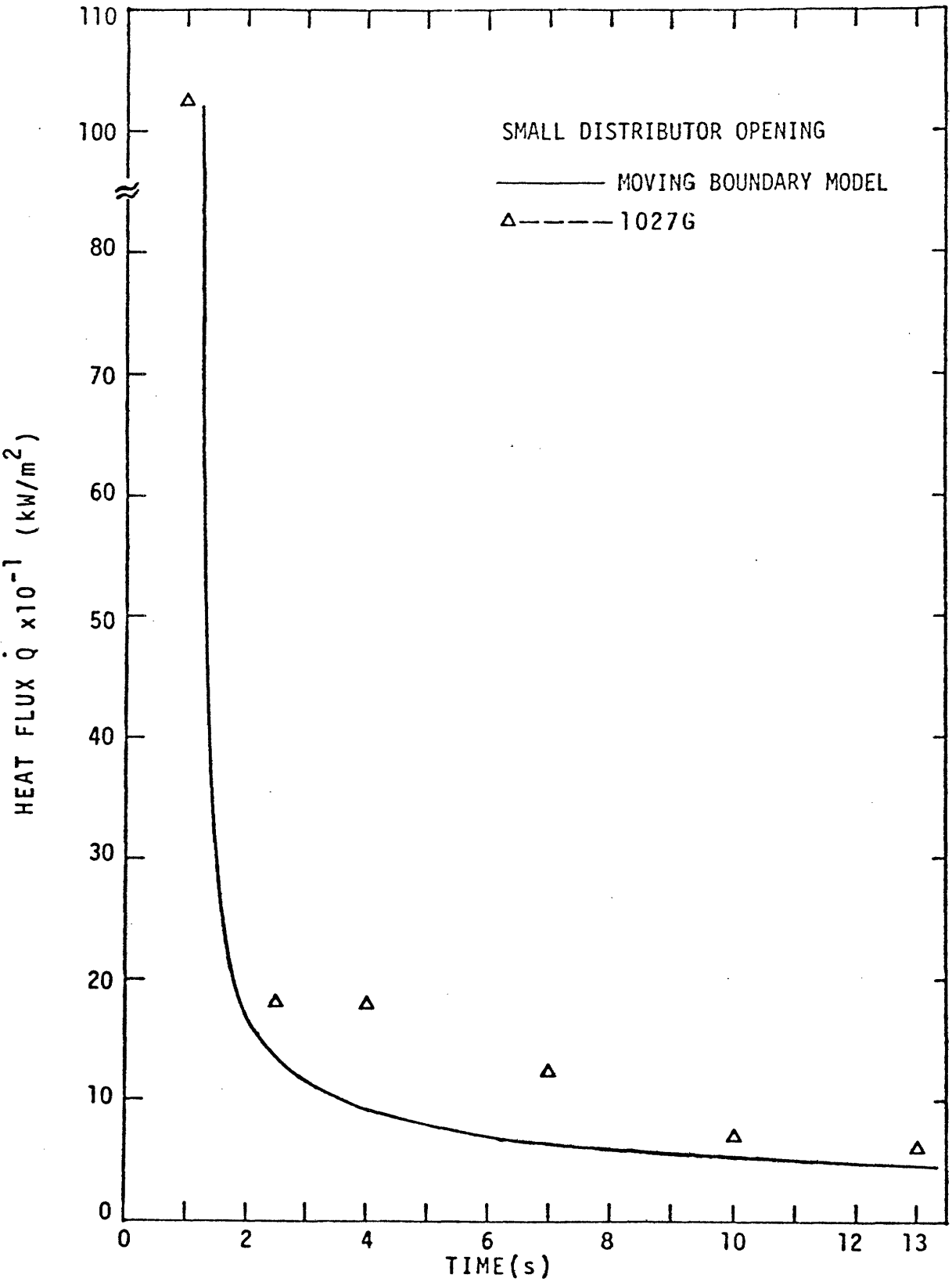

FIGURE VII-25: LOCAL BOIL-OFF RATE CURVES FOR A 2.0-LITER PROPANE SPILL(SMALL DISTRIBUTOR OPENING) AT THE FIRST SAMPLING STATION. EXPERIMENTAL DATA COMPARED WITH PREDICTIONS FROM MOVING BOUNDARY MODEL.

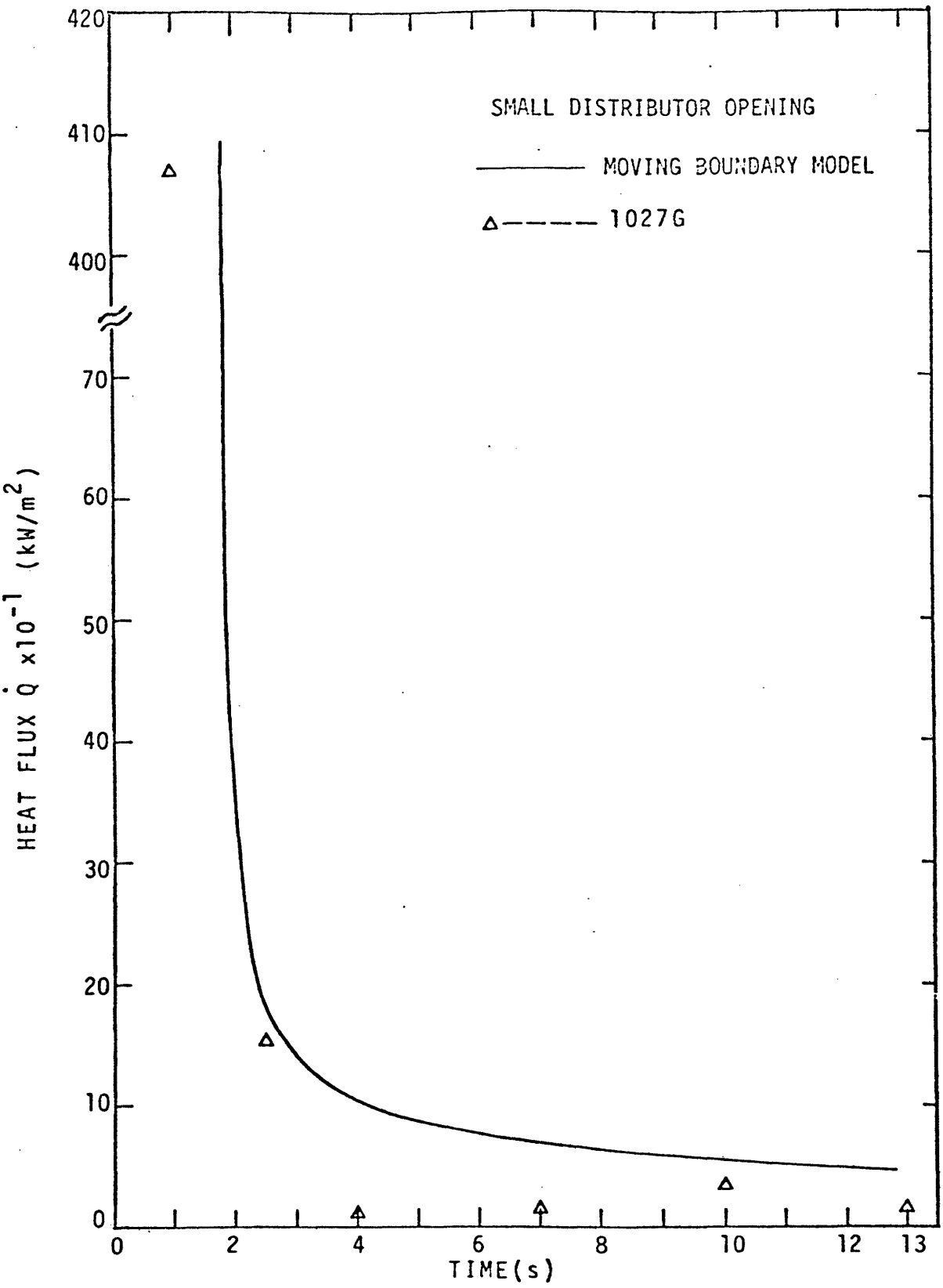

FIGURE VII-26: LOCAL BOIL-OFF RATE CURVES FOR A 2.0-LITER PROPANE SPILL(SMALL DISTRIBUTOR OPENING) AT THE SECOND SAMPLING STATION. EXPERIMENTAL DATA COMPARED WITH PREDICTIONS FROM MOVING BOUNDARY MODEL.

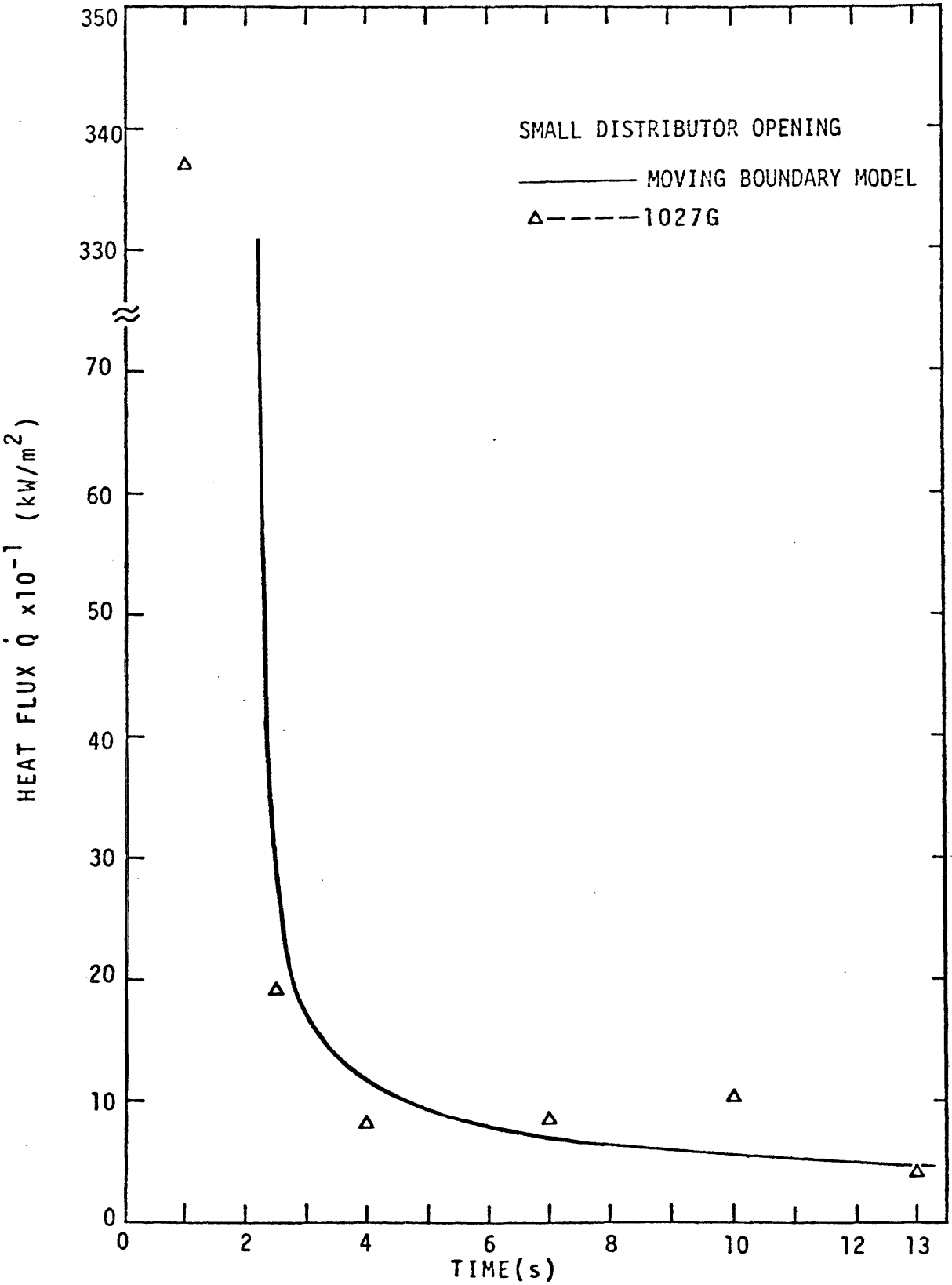

FIGURE VII-27: LOCAL BOIL-OFF RATE CURVES FOR A 2.0-LITER PROPANE SPILL(SMALL DISTRIBUTOR OPENING) AT THE THIRD SAMPLING STATION. EXPERIMENTAL DATA COMPARED WITH PREDICTIONS FROM MOVING BOUNDARY MODEL.

explanation for this is that propane or LPG initially evaporates very fast and there is not enough cryogen to cover evenly the entire surface area between sampling stations during the period when vapor samples are collected. The value of $\dot{Q}$ estimated by the data analysis scheme described in Chapter IV is the average heat flux between two neighboring samples stations.

In Figures VII-16 and VII-17, heat fluxes for LPG of various compositions are compared. There is essentially no effect from the addition of small quantities of ethane or n-butane to propane on the heat flux curves. This is consistent with the conclusion obtained from LPG spills on confined water surfaces, that impurities do not affect the boiling rate of LPG on water.

The numerical model developed in Chapter V can be used to simulate the boiling-spreading process for LPG, except the assumption of constant boiling rate per unit area can no longer be made. Instead, the boiling rate is allowed to change with the time according to the following equation:

$$\dot{Q}_i = \varepsilon_o \qquad 0 \leq t_i \leq 1.0 \text{ sec} \qquad \text{(VII-3)}$$

$$\dot{Q}_i = \varepsilon \, (t_i - t_o)^{-1/2} \qquad t_i > 1.0 \text{ sec}$$

where $\dot{Q}_i$ is in kW/m^2 and

$$t_o = t_\delta - \left(\frac{\varepsilon}{\varepsilon_o}\right)^2 \qquad \text{(s)}$$

Equation (VII-3) attempts to account for the high evaporation rate, ε_o, observed in the first second of contact between water and cryogen where the initial contact area is ill-defined. The value of ε_o is selected to be 10^3 kW/m^2, which is about the same as the average value of the heat fluxes experimentally obtained from various propane and LPG spills during the first second after LPG

contacts the water surface.

The effective density of propane (LPG) is estimated using an average evaporation rate (per unit area) for the first 13 seconds after LPG contacts the water. This value is found to be 0.3 g/cm^3 (the normal density of propane at its boiling point (231 K) is 0.582 g/cm^3).

The predicted spreading distance as a function of time is compared with experimental data in Figures VII-28 through VII-32. Note that in these figures propane and LPG seem to spread at a constant rate. The numerical model does not accurately predict the spreading front position. The highly irregular ice formed in propane and LPG spills is very difficult to characterize, and its effect on hindering the spreading of cryogen cannot be accurately accounted for in the theory.

In Figure VII-33, where the spreading data for various initial spill volumes are plotted on one graph, the curves are found to overlap and appear to be almost linear with respect to time, ignoring the discontinuities introduced by the "ice dam". The linear relationship between spreading distance and time is also true for the case where spills are made with the smaller distributor opening (19.4 cm^2), as seen in Figure VII-34. The slope, however, appears to be larger for the case with the smaller distributor opening.

As cryogen spills onto the water through the opening, the water near the distributor is agitated. A large opening leads to a larger introduction rate of cryogen into the system and causes a more severe agitation of water. Correspondingly, the proportion of momentum transferred from cryogen to water is larger. A smaller opening minimized the initial momentum transfer between cryogen and water. This may explain the higher spreading rate of cryogen through the small distributor opening.

Figure VII-30 also shows that the composition of LPG has no effect on the

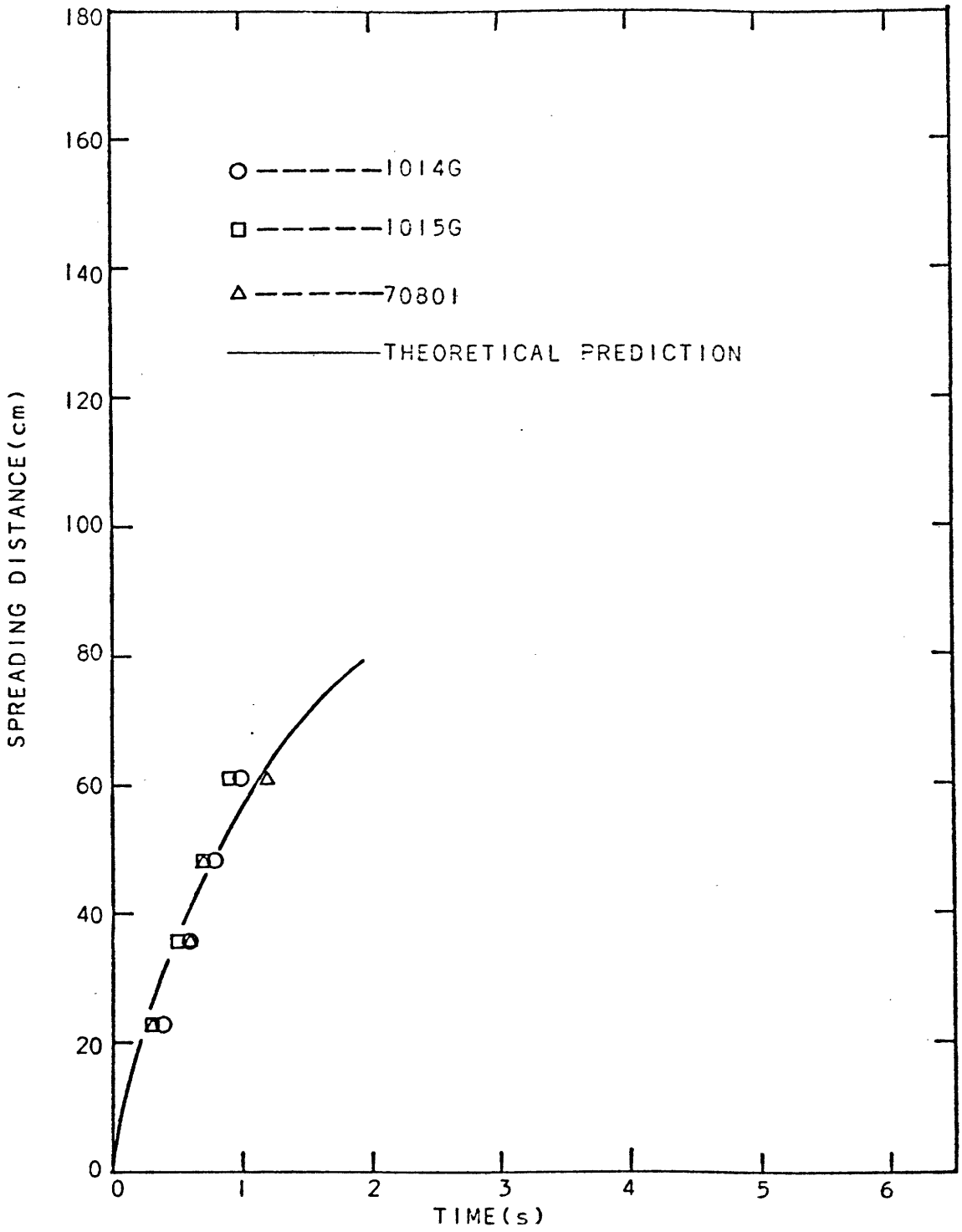

FIGURE VII-28: SPREADING CURVES FOR 0.5-LITER PROPANE SPILL. EXPERIMENTAL DATA AND NUMERICAL PREDICTIONS COMPARED.

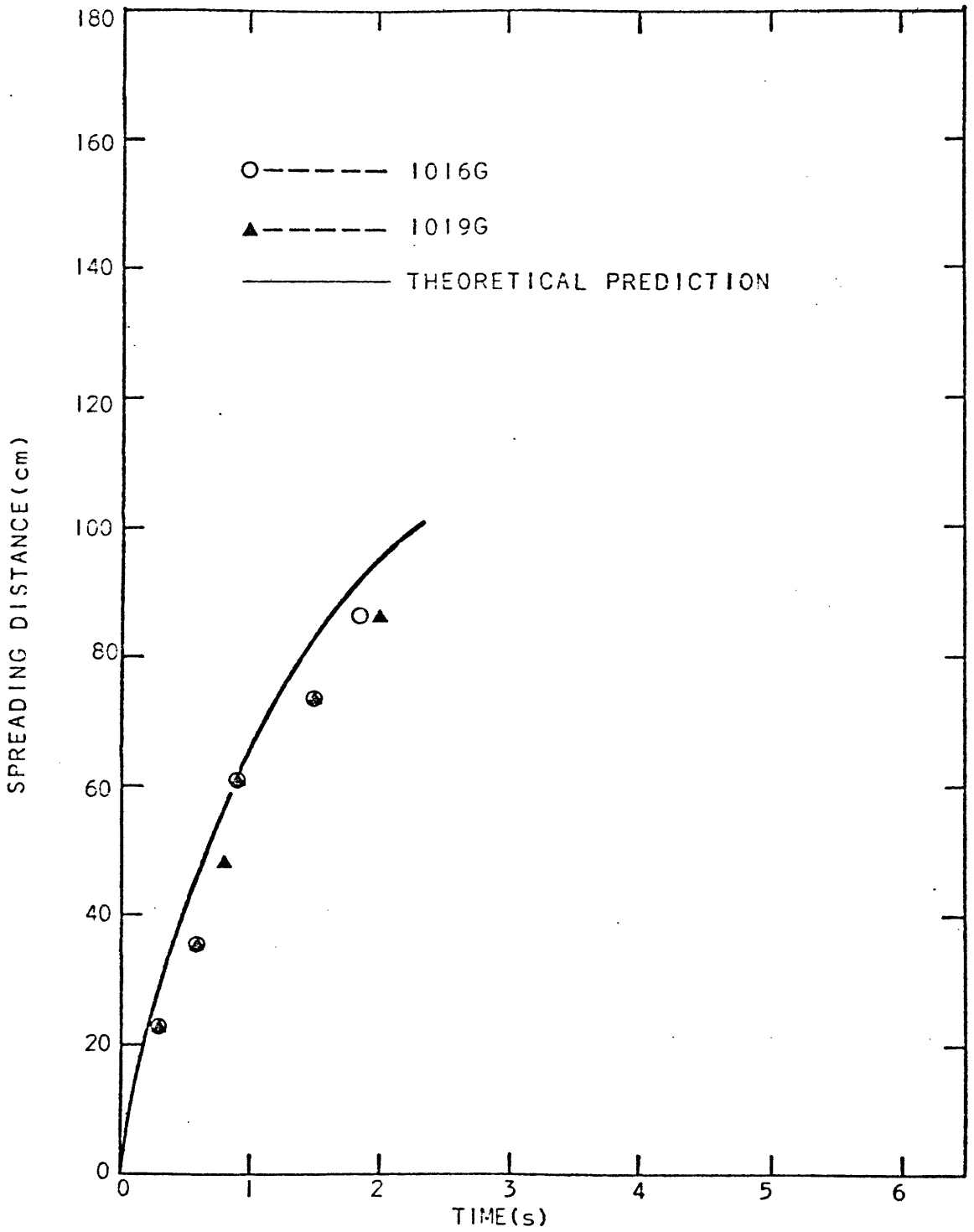

FIGURE VII-29: SPREADING CURVES FOR 0.75-LITER PROPANE SPILL. EXPERIMENTAL DATA AND NUMERICAL PREDICTIONS COMPARED.

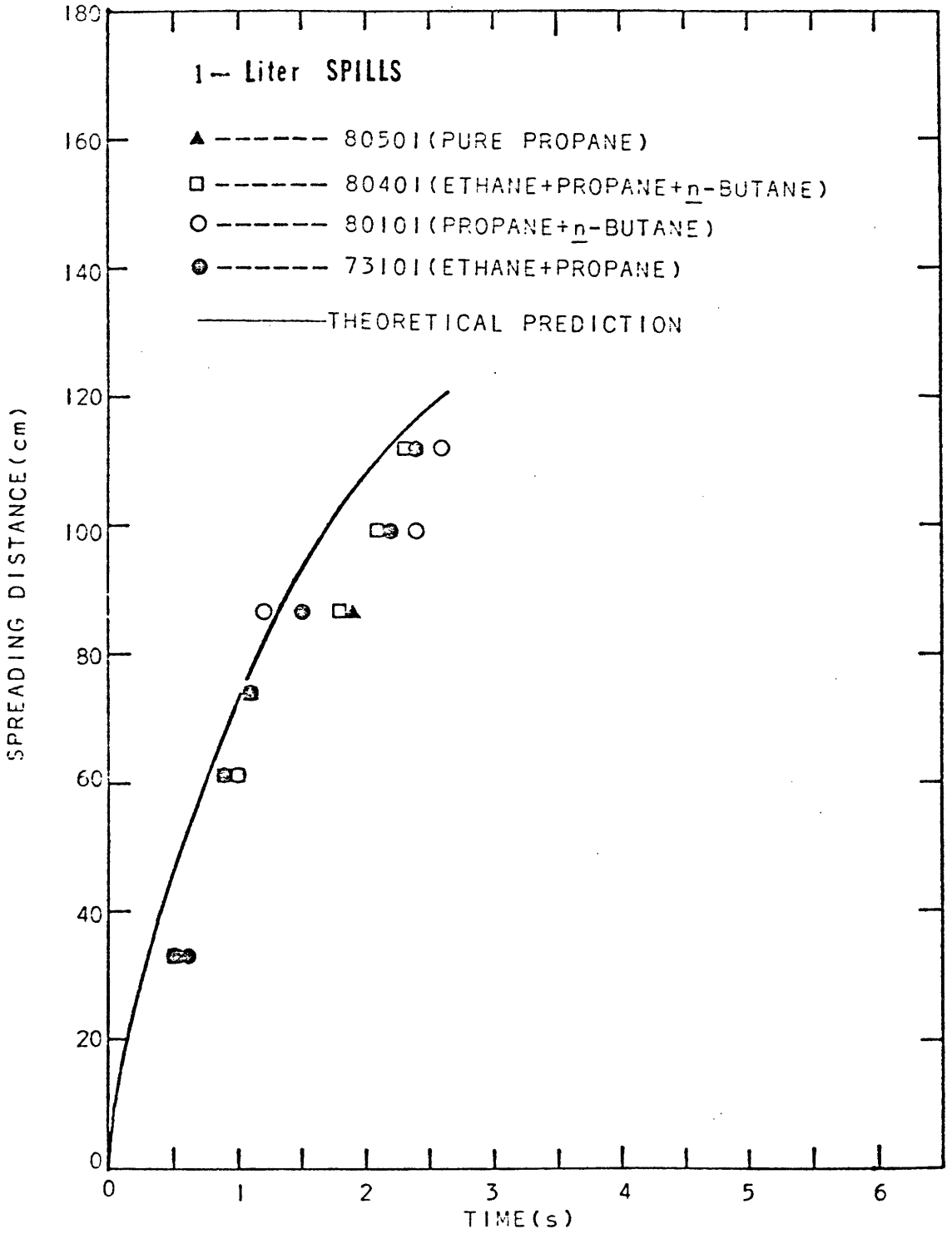

FIGURE VII-30: SPREADING CURVES FOR 1.0-LITER PROPANE AND LPG SPILLS. EXPERIMENTAL DATA AND NUMERICAL PREDICTIONS COMPARED.

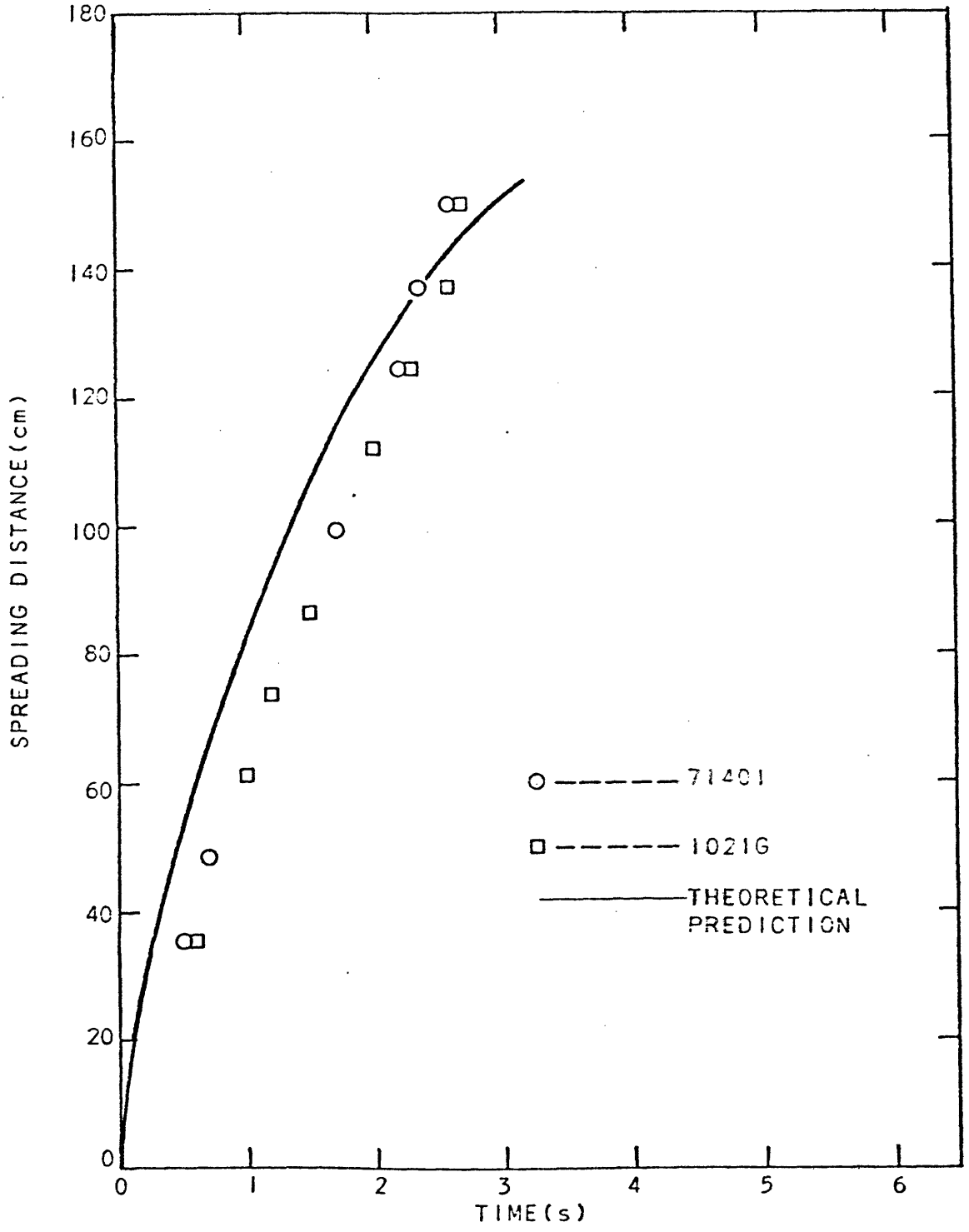

FIGURE VII-31: SPREADING CURVES FOR 1.5-LITER PROPANE SPILLS. EXPERIMENTAL DATA AND NUMERICAL PREDICTIONS COMPARED.

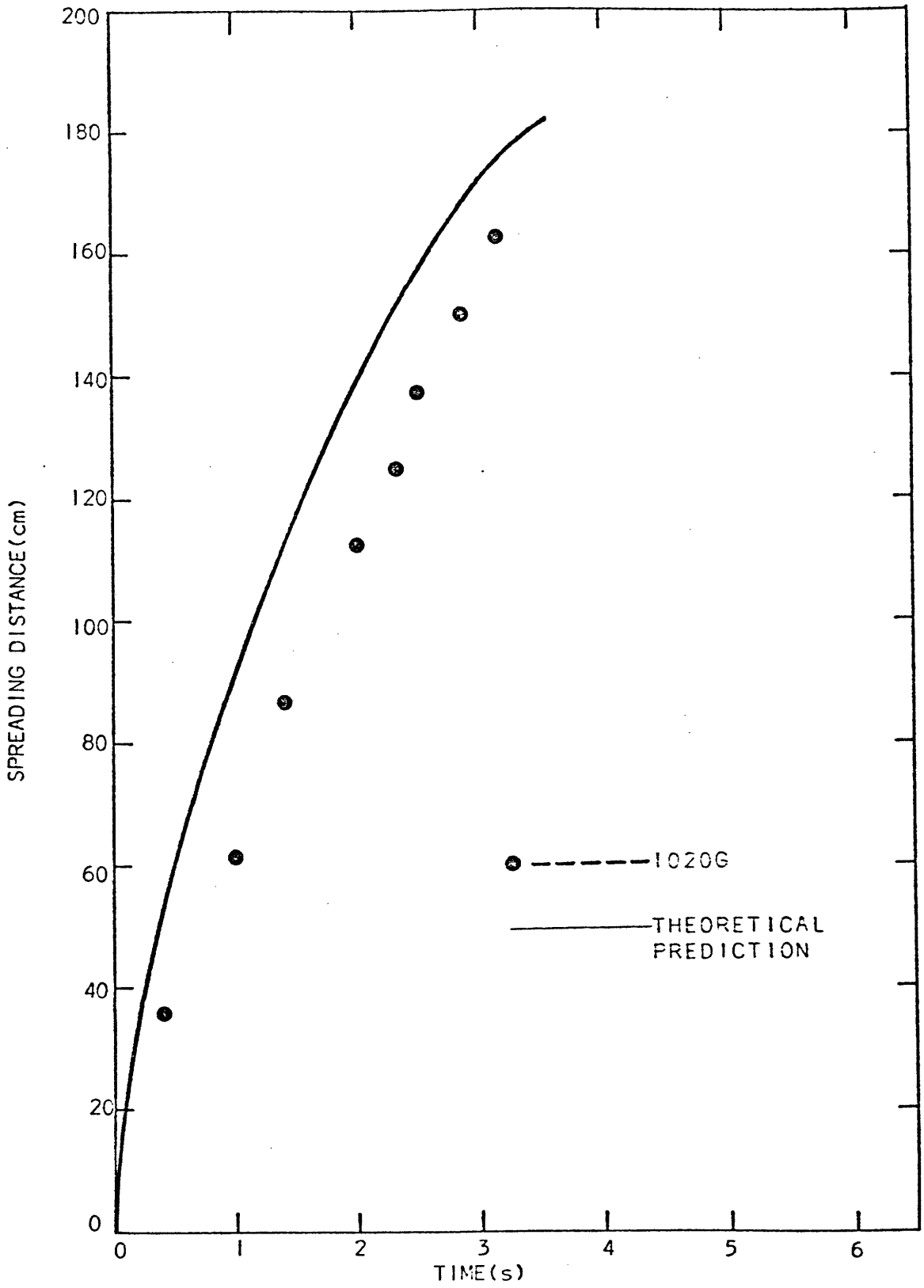

FIGURE VII-32: SPREADING CURVES FOR 2.0-LITER PROPANE SPILLS. EXPERIMENTAL DATA AND NUMERICAL PREDICTIONS COMPARED.

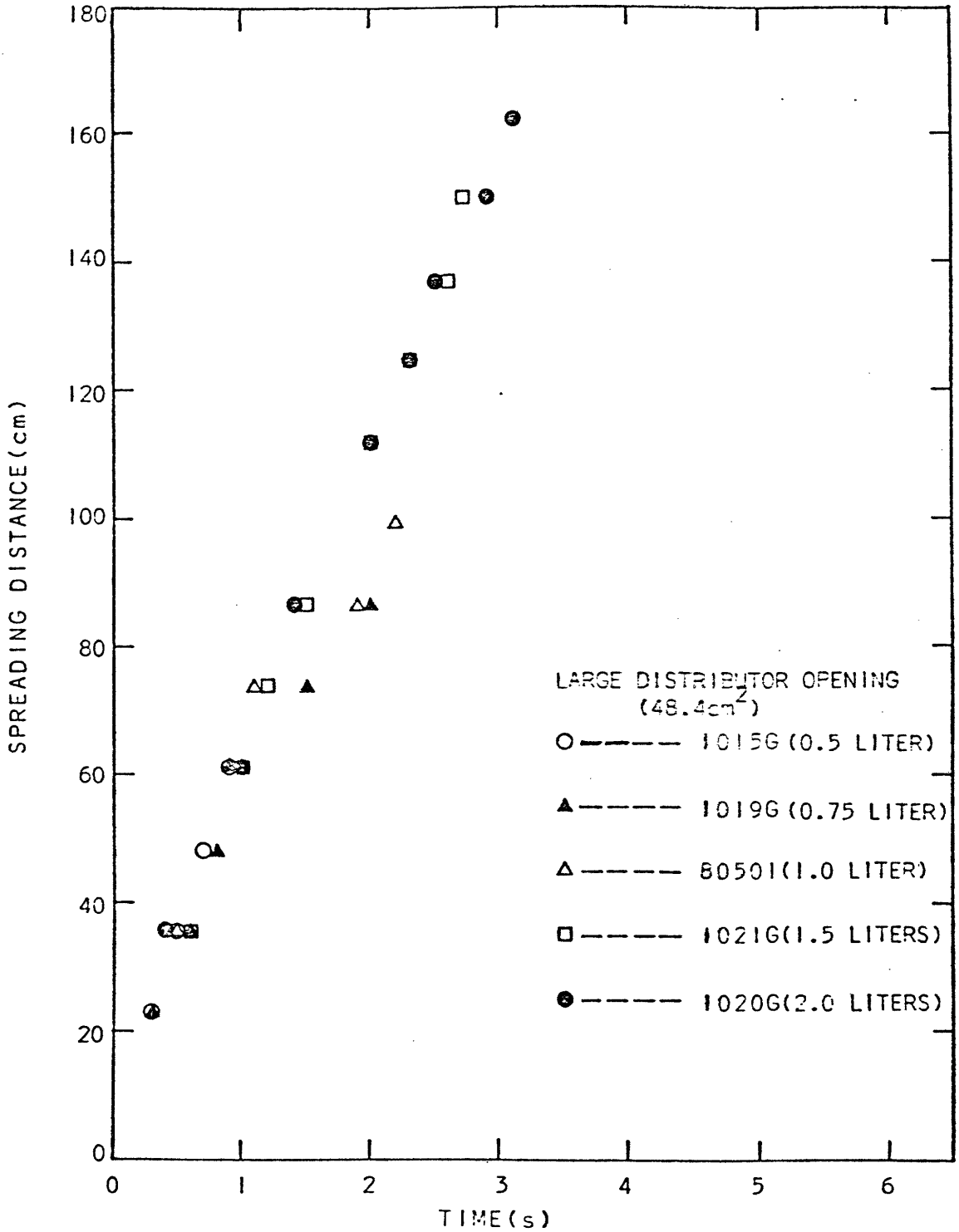

FIGURE VII-33: SPREADING DISTANCE AS A FUNCTION OF TIME FOR PROPANE SPILLS OF VARIOUS VOLUMES(LARGE DISTRIBUTOR OPENING).

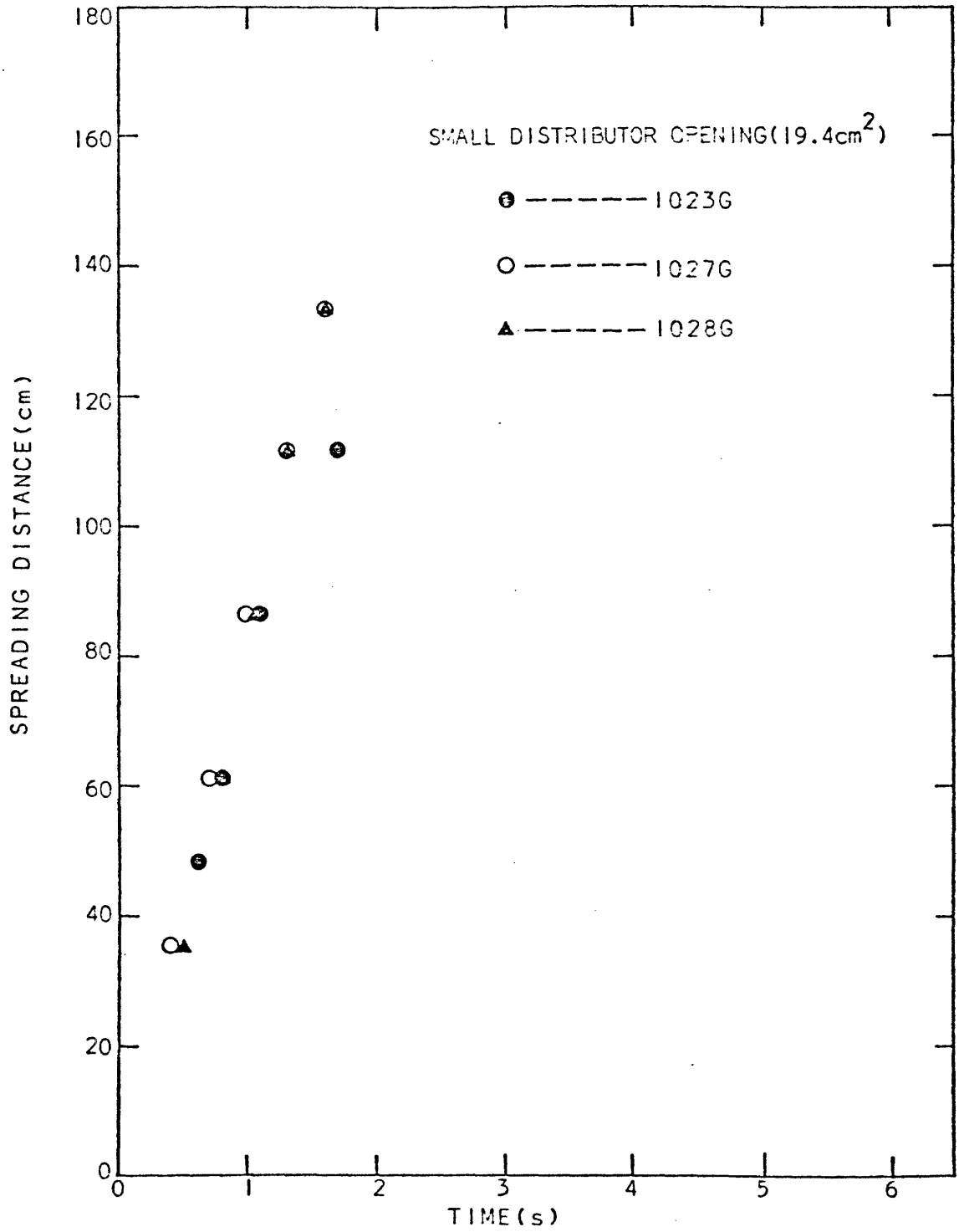

FIGURE VII-34: SPREADING DISTANCE AS A FUNCTION OF TIME FOR PROPANE SPILLS OF VARIOUS VOLUMES(SMALL DISTRIBUTOR OPENJNG).

spreading process. Therefore, it is concluded that the boiling-spreading process for LPG spills is independent of its composition; i.e., LPG can be well represented by pure propane.

The values of the maximum spreading distance predicted by the numerical model for propane spills are given in Table VII-3. The model and experiment agree reasonably well.

Furthermore, Figure VII-35 gives the theoretical prediction of the thickness profile for a propane spill. Note that propane does not completely vaporize when it reaches the maximum spreading distance; propane is thicker near the distributor and thins out downstream. This is consistent with the experimental observation on propane spills.

Table VI-7 shows that the maximum spreading distances for propane spills are not affected by the size of the distributor opening. This suggests that the spreading of propane on water is controlled by the irregular ice formed during the boiling-spreading process for the system used in this study.

In Table VII-4, the maximum spreading distances for methane and propane spills are compared; methane spreads over a much larger area than propane for the same volume spilled. The explanation for this is that propane has a very high initial boiling rate and forms a rough ice sheet which hinders its spreading.

TABLE VII-3

Experimental Data and Theoretical Prediction of Maximum Spreading Distance for Propane Spills

Volume Spilled	Maximum Spreading Distance (cm) Experiment	Numerical Prediction
0.5 liter	68	79
0.75 liter	90	101
1.0 liter	110	120
1.5 liters	150	153
2.0 liters	163	182

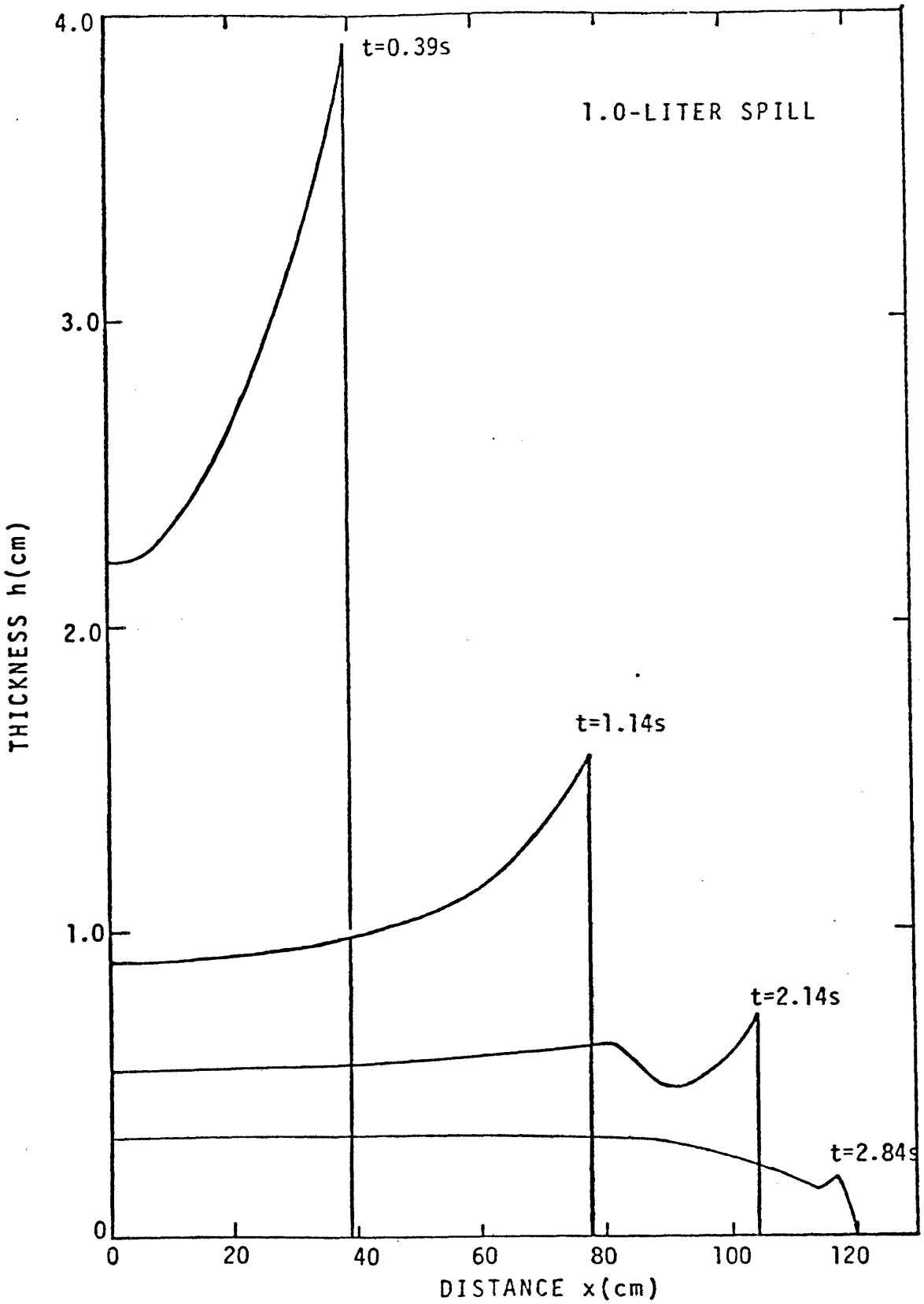

FIGURE VII-35: THICKNESS PROFILE PREDICTED BY THE NUMERICAL MODEL FOR LIQUID PROPANE SPREADING ON WATER.

TABLE VII-4

*Maximum Spreading Distance for Methane and Propane Spills

Volume Spilled	Maximum Spreading Distance (cm) Methane	Propane
0.5 liter	229	68
0.75 liter	279	90
1.0 liter	317	110
1.5 liter	380**	150
2.0 liter	452**	163

* Experimental Data

**Theoretical Prediction

VIII. CONCLUSIONS

1. An apparatus was designed and constructed to monitor the spreading of a boiling liquid on water. The apparatus allows measurement of vapor temperatures and compositions. These data can be used to infer liquid vaporization rates.
2. For liquid nitrogen and methane spills, film boiling occurs initially upon contact with water. Ice forms on the water surface during the spreading. Before an ice layer appears, most of the cryogen has evaporated. Because there is little ice growth before most of the liquid nitrogen or methane has evaporated, their boiling rates were found to be nearly constant. This conclusion would not be valid for a large spill.
3. Liquid nitrogen and methane exhibit similar thickness profiles during spreading, that is, the spreading front is thickest, and the profile thins out toward the spill origin.
4. The bubbles of evaporated cryogen entrained in the liquid affect the spreading of cryogen on water. The bubbles alter the effective density of the cryogen layer and this effect has been accounted for in the model development.
5. A numerical technique using the method of characteristics has been developed that successfully describes the boiling-spreading phenomena for liquid nitrogen and methane spills on water. The model provides information of the maximum spreading distance and the time for complete vaporiztion for various quantity spills.
6. For liquid propane or LPG spills, nucleate boiling occurs upon initial contact with water. Highly irregular ice forms very quickly and the local

boil-off rates monotonically decrease with time. A moving boundary heat transfer model can adequately describe the boiling phenomena. This is consistent with earlier observations made for propane or LPG spills on confined water surfaces.

7. For LPG mixture spills, fractionation occurs with the more volatile components vaporizing preferentially.
8. Addition of small quantities of ethane or n-butane to pure propane has little effect on the boiling process. This was also the case in confined propane and LPG spills.
9. Propane or LPG does not spread in a manner similar to liquid nitrogen or methane. The formation of a rough ice layer hinders the spreading of propane and LPG and the spreading was found to be linear with respect to time.
10. The composition of LPG has essentially no effect on the spreading phenomena. Pure propane will simulate actual LPG behavior. The same conclusion was obtained in confined LPG spill experiments.
11. Irregular ice formations in LPG spills are difficult to characterize and their effect on hindering the spreading of LPG cannot be adequately accounted for in the theory. The numerical model does not adequately describe the boiling-spreading phenomena for LPG spills.
12. The size of the distributor opening affects the spreading rate of propane on water but has no effect on its maximum spreading distance. This suggests that the irregular ice controls the propane spreading process for the system in this study.
13. In an industrial accident, it is expected that LNG will spread over a much larger area than LPG for the same volume spilled. In this case, the formation of an ice layer beneath the cryogen may lead to much lower vapor-

ization rates.

14. The high-speed motion picture photographic study improved the understanding of cryogen movements, ice formation and bubble growth in the boiling/spreading process.

IX. RECOMMENDATIONS

1. All experiments have been conducted on a calm water surface. In order to simulate the real case where cryogen spills on an ocean-air interface, agitation of the spreading surface should be introduced to evaluate the wave effect on the boiling/spreading process.
2. Distilled water has been used in the present work. Experiments with salt water should be carried out to simulate cryogen spills on various environments (such as river, coastal, open ocean).
3. Determination of the characteristics of ice formation is very important in developing a model to predict successfully the boiling/spreading phenomena for LPG spills.
4. Evaluation of the extent of the preferential evaporation of more volatile components is needed in certain hazard models where properties of the vapor cloud are used.
5. Experiments with various spill rates should be conducted to provide a better understanding of the mechanism of LPG boiling and spreading on water.
6. The one-dimensional boiling/spreading model should be scaled to large radial spills so as to provide a higher degree of reliability in hazard analysis calculations that are now being made for hypothetical LPG and LNG tanker accidents.

APPENDIX - I

MOVING BOUNDARY HEAT TRANSFER MODEL

Consider the liquid which fills the region $x > 0$ at an initial temperature T_2 in Figure A.I-1. At time $\tau = 0$ the surface is exposed to temperature T_1 which is lower than the phase change temperature T_p. Solidification will start and the interface separating the solid and liquid phases will propagate to larger values of x. At a time τ, the surface separating the liquid and solid phases is at $X(\tau)$. The bulk temperature of the liquid at large x is T_2 and is constant. Heat is conducted, therefore, from the liquid through the solid phase to the free surface.

At time τ, the region $x < X(\tau)$ is a solid phase with constant properties k_1, α_1, ρ_1, C_1; t_1 is the temperature in this phase and it must satisfy the equation,

$$\frac{\partial^2 t_1}{\partial x_1^2} - \frac{1}{\alpha_1}\frac{\partial t_1}{\partial \tau} = 0 \qquad \text{(A.I-1)}$$

with $t_1 = T_1$ at $x_1 = 0$.

At any time τ, the region $x > X(\tau)$ is a liquid phase with properties k_2, α_2, ρ_2, C_2; t_2 is the temperature in this phase and it must follow the equation

$$\frac{\partial^2 t_2}{\partial x_2^2} - \frac{1}{\alpha_2}\frac{\partial t_2}{\partial \tau} = 0 \qquad \text{(A.I-2)}$$

with $t_2 = T_2$ at $x \to \infty$

In the solidification of water to ice, the temperatures of ice and water are not constant in each phase. The physical properties are functions of temperature. For simplification the physical properties are assumed to be constant. The values estimated at the average temperature of $(T_1 + T_p)/2$ are used for the ice phase. For the water phase the properties are taken at the bulk temperature

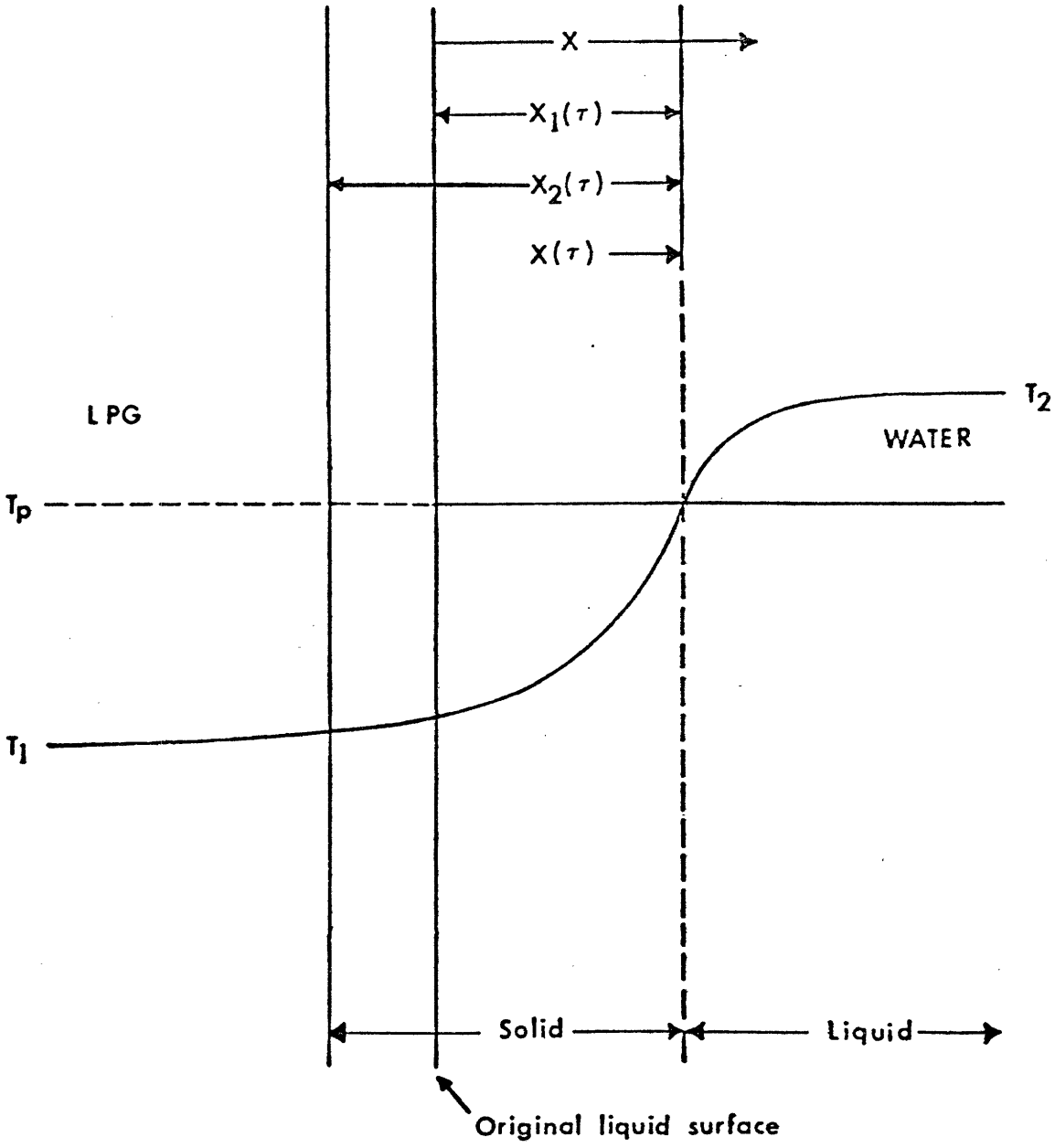

FIGURE A.1-1: HEAT CONDUCTION DURING SOLIDIFICATION OF A LIQUID.

of T_2 since the water temperature a few mm below the surface does not change significantly during the boiling process.

During the solidification process there is an increase in volume and the ice surface will move away from the original surface according to the density of each phase. This can be accounted for by

$$\frac{X_1}{X_2} = \frac{\rho_2}{\rho_1} = \beta \qquad \text{(A.I-3)}$$

At the ice-water interface,

$$t_1 = t_2 = T_p \qquad \text{at } x_1 = X_1(\tau) \text{ or } x_2 = X_2(\tau) \qquad \text{(A.I-4)}$$

when the ice-water interface advances a distance $dX_1(\tau)$, a quantity of heat $\rho_1 \Delta H^f \, dX_1(\tau)$ is liberated per unit area and must be removed by conduction

$$k_1 \left(\frac{\partial t_1}{\partial x_1}\right)_{x_1 = X_1(\tau)} - k_2 \left(\frac{\partial t_2}{\partial x_2}\right)_{x_2 = X_2(\tau)} = \rho_1 \Delta H^f \, dX_1(\tau) \qquad \text{(A.I-5)}$$

Given the above conditions, Eckert and Drake (1975) and Carslaw and Jaeger (1959) describe a solution which leads to the following temperature profiles in the solid and the liquid phases, respectively,

$$\frac{t_1 - T_p}{T_1 - T_p} = 1 - \frac{\operatorname{erf}(x_1/2\sqrt{\alpha_1 \tau})}{\operatorname{erf}(K\beta/2\sqrt{\alpha_1})} \qquad \text{(A.I-6)}$$

and

$$\frac{t_2 - T_p}{T_2 - T_p} = 1 - \frac{\operatorname{erfc}(x_2/2\sqrt{\alpha_2 \tau})}{\operatorname{erfc}(K/2\sqrt{\alpha_2})} \qquad \text{(A.I-7)}$$

in which K is calculated from

$$\frac{(T_p - T_1)\, k_1 \exp(-K^2\beta^2/4\alpha_1)}{\sqrt{\pi\alpha_1}\ \mathrm{erf}(K\beta/2\sqrt{\alpha_1})} - \frac{(T_2 - T_p)\, k_2 \exp(-K^2/4\alpha_2)}{\sqrt{\pi\alpha_2}\ \mathrm{erfc}(K/2\sqrt{\alpha_2})}$$

$$= \frac{\Delta H^f \rho_1 K\beta}{2} \qquad \text{(A.I-8)}$$

The heat transfer across the cryogen-ice interface is given by

$$q/A = - k_1 \left.\frac{\partial t_1}{\partial x_1}\right|_{x_1 = 0} \qquad \text{(A.I-9)}$$

where q/A is the heat flux. Differentiating equation (A.I-6) with respect to x_1 and substituting into equation (A.I-9), one obtains

$$q/A = - \frac{(T_p - T_1)\, k_1\, \tau^{-1/2}}{\sqrt{\pi\alpha_1}\ \mathrm{erf}(K\ /2\sqrt{\alpha_1})} = \varepsilon\tau^{-1/2} \qquad \text{(A.I-10)}$$

The values of ice and water properties are shown in Table A.I-1.

The value of K is found numerically to be 6.2675×10^{-4} m/s$^{1/2}$. Equation (A.I-10) then yields

$$q/A = 154\ \tau^{-1/2} \quad (\mathrm{kW/m^2}) \qquad \text{(A.I-11)}$$

TABLE A.I-1

Physical Properties of Ice and Water

Ice (at -21°C)	Water (at 20°C)
$k_1 = 2.43 W/mK$	$k_2 = 0.580\ W/mK$
$\rho_1 = 913\ kg/m^3$	$\rho_2 = 1 \times 10^3\ kg/m^3$
$c_1 = 1.93 \times 10^3\ W\ s/kg\ K$	$c_2 = 4.181 \times 10^3\ W\ s/kg\ K$
$\alpha_1 = 1.354 \times 10^{-6}\ m^2/s$	$\alpha_2 = 1.388 \times 10^{-7}\ m^2/s$
$\Delta H^f = 3.335 \times 10^5\ W\ s/kg$	
$\beta = 1.087$	

APPENDIX-II

COMPUTER PROGRAMS TO MONITOR DATA ACQUISITION

```
C     THIS PROGRAM CONTROLS THE ACQUISITION OF DATA FOR LNG AND
C     LPG SPREADING ON WATER
C     DATA ARE STORED IN INTEGER BINARY FORMAT
      CHANTASK  12,4
      EXTERNAL TICTAC,SCAN
      COMMON/BLK3/NC,LAPS
      DIMENSION NAME1(5)
      TYPE'RAW DATA FILE NAME'
      READ(11,100) (NAME1(I),I=1,5)
100   FORMAT(5A2)
      NF=1
      INW=2
      ACCEPT'NUMBER OF CHANNELS', NC
      CALL OPEN(1,NAME1,2,IER)
      WRITE(12,150) (NAME1(I),I=1,5)
150   FORMAT(1H1////////////1H,5X,'RAW DATA FILE:',5A2)
      CALL ITASK(TICTAC,1,1,IER)
      CALL ITASK(SCAN,2,2,IER)
      CALL KILL
      END


      TASK   TICTAC
      COMMON/BLK3/NC,LAPS
      DIMENSION  IDATE(3)
      CALL HOLD(2,IER)
      LAPS=1
      CALL DATE(IDATE,IER)
      CALL FGTIM(IH,IM,IS)
      WRITE(12,100) IH,IM,IS,IDATE
100   FORMAT(1HO,5X,'STARTING TIME',2(I2,':'),I2,10X,'DATE',2(I2,'/'),I2)
300   CALL RELSE(2,IER)
      CALL FDELY(10)
      LAPS=LAPS+1
      GO TO 300
      END
```

```
      TASK SCAN
     COMMON/BLK3/NC,LAPS
      COMMON/BLK10/IGAIN(16),ICHAN(16)
      COMMON/BLK5/ INVOLT(16),IVOLT(16,580)
      DATA IGAIN/11,11,11,11,11,11,11,11,11,11,11,11,11,11,11,11/
      DATA ICHAN/0,1,2,3,4,5,6,7,8,9,10,11,12,13,14,15/
10    CALL MGAIR(NC,ICHAN,IGAIN,INVOLT,IER)
      DO 20 I=1,16
      IVOLT(I,LAPS)=INVOLT(I)
20    CONTINUE
      CALL DASW(IFLIP)
      IF(IFLIP.EQ.1) GO TO 99
      CALL SUSP
      GO TO 10
99    CONTINUE
      LAST=LAPS
      CALL FGTIM(IH,IM,IS)
      WRITE(12,401) IH,IM,IS
401   FORMAT(1HO,'TEST ENDED AT',2(I2,':'),I2)
      DO 30 J=1,LAST
      WRITE BINARY(1) J,(IVOLT(I,J),I=1,16)
30    CONTINUE
      CALL CLOSE(1,IER)
      CALL KILL
      CALL EXIT
      END
```

```
C       THIS PROGRAM READS A RAW DATA FILE (VOLTS),
C       GENERATES A REDUCED DATA FILE (TEMPERATURE)
C       AND PRINTS THESE VALUES.
        COMMON/BLK3/NC,NF,INW
        COMMON/BLK4/NSTOP,LAPS,IFLIP,ITRAP
        DIMENSION NAME(5)
        TYPE'RAW DATA FILE NAME'
        READ(11,100)  (NAME(I),I=1,5)
100     FORMAT(5A2)
        ACCEPT'TOTAL NUMBER OF CHANNELS',NC
        ACCEPT'NUMBER OF POINTS',NPT
        CALL OPEN(1,NAME,2,IER)
        ITRAP=0
        ACCEPT'SCAN FREQUENCY',NF
        NSTOP=0
        WRITE(12,150) (NAME(I),I=1,5)
150     FORMAT(1H1//////////////////1H,5X,'RAW DATA FILE:',5A2)
        CALL TICTAC(NPT)
        CALL EXIT
        END



        SUBROUTINE TICTAC(NPT)
        COMMON/BLK3/NC,NF,IARRAY
        COMMON/BLK4/NSTOP,LAPS,IFLIP,ITRAP
        COMMON/BLK5/IH,IM,IS
        DIMENSION IDATE(3)
        CALL DATE(IDATE,IER)
        CALL FGTIM(IH,IM,IS)
        WRITE(12,100)IH,IM,IS,IDATE
100     FORMAT(1H0,5X,'BEGIN READING',2(I2,':'),I2
       1,10X,'DATE',2(I2,'/'),I2)
        IFLIP=0
300     CALL SCAN
        IF (LAPS.GE.NPT) GO TO 400
        CALL REDUCE(IARRAY)
```

```
      GO TO 300
400   CALL FGTIM(IH,IM,IS)
      NSTOP=LAPS
      CALL REDUCE(IARRAY)
      RETURN
      END



      SUBROUTINE SCAN
      COMMON/BLK1/IVOLT(16,450)
      COMMON/BLK2/ITRACK(450)
      COMMON/BLK3/NC,NF,IARRAY
      COMMON/BLK4/NSTOP,LAPS,IFLIP,ITRAP
      DIMENSION INVOLT(16)
      COMMON/BLK10/IGAIN(16),ICHAN(16)
      DATA IGAIN/11,11,11,11,11,11,11,11,11,11,11,11,11,11,11,11/
      DATA ICHAN/0,1,2,3,4,5,6,7,8,9,10,11,12,13,14,15/
      IF(NSTOP.NE.0) GO TO 99
      IARRAY=IARRAY+1
      IF(IARRAY.EQ.451)   IARRAY=1
      READ BINARY(1) LAPS,(IVOLT(L,IARRAY),L=1,NC)
99    RETURN
      END



      SUBROUTINE REDUCE(JJ)
      DIMENSION TEMP(16)
      COMMON/BLK1/IVOLT(16,450)
      COMMON/BLK2/ITRACK(450)
      COMMON/BLK3/NC,NF,INW
      COMMON/BLK4/NSTOP,LAPS,IFLIP,ITRAP
      COMMON/BLK5/IH,IM,IS
      COMMON/BLK8/IX
      IF(ITRAP.GT.1) GO TO 5
      WRITE(12,150)
```

```
150   FORMAT(1H1,/////1H0,'TIME',16X,'T1',5X,'T2',5X,'T3',5X,'T4'
     1,5X,'T5',5X,'T6',5X,'T7',5X,'T8',5X,'T9',4X,'T10',4X,'T11',4X,
     2'T12',4X,'T13',4X,'T14',4X,'T15',4X,'T16'/1H,1X,'SEC',
     311X,16(6X,'C')/1H,4('-'),11X,16(2X,5('=')))
      ITRAP=2
      IX=0
5     IF(JJ.EQ.451)  JJ=1
      DO 10 KK=1,NC
      VOLT=IVOLT(KK,JJ)
      V=VOLT*10./FLOAT(NF)/4096.
      IF(V.LT.-5.237)  GO TO 330
      IF(V.GT.0.000) GO TO 340
      A=-0.00045358
      B1=17.046794
      B2=-0.26734292
      B3=0.016190789
      B4=-0.00069602
      B5=0.0001379275
      GO TO 350
330   A=-80.92576715
      B1=-20.576476
      B2=-4.0017909
      B3=0.67598041
      B4=0.14711677
      B5=0.0077871064
      GO TO 350
340   A=0.00137701
      B1=17.037897
      B2=-0.22068369
      B3=0.0055912366
      B4=-0.000337065
      B5=0.0000302242
350   TEMP(KK)=A+B1*V+B2*V**2+B3*V**3+B4*V**4+B5*V**5
10    CONTINUE
      IX=IX+1
      WRITE(12,200) IX,LAPS,(TEMP(IJK),IJK=1,NC)
200   FORMAT(1H0,I4,I6,5X,16F7.1)
```

```
      IF(NSTOP.NE.0) GO TO 90
      RETURN
90    WRITE(12,100) IH,IM,IS
100   FORMAT(1HO,'TEST ENDED AT',2(I2,':'),I2)
      CALL CLOSE(1,IER)
      RETURN
      END
```

APPENDIX - III

EVALUATION OF THE PLUG FLOW ASSUMPTION USED IN THE DATA ANALYSIS SCHEME

The vapor flow of tracer gas, CO_2, and propane (or LPG) mixtures above the water surface can be shown to be turbulent from the size of the Reynolds number, estimated in the following way.

For turbulent flow through a tube, the Reynolds number is defined by (Bird, Stewart, and Lightfoot, 1960)

$$N_{R_e} = \frac{4R_h < v > \rho}{\mu} \qquad \text{(A-III-1)}$$

where R_h is a "mean hydraulic radius" which is defined as

$$R_h = \frac{\text{cross-section of the stream, S}}{\text{wetted perimeter, Z}}$$

$< v >$ is the average gas velocity over the cross-sectional area S. ρ is the density and μ is the viscosity of the gas mixture.

For the spill apparatus used in this study, the water trough is half filled with water and its diameter d is 16.5 cm. The "mean hydraulic radius", R_h, is equal to

$$R_h = \frac{\frac{1}{2}\left(\frac{\pi d^2}{4}\right)}{\left(\frac{\pi d}{2} + d\right)} = 2.52 \text{ cm} \qquad \text{(A-III-2)}$$

The gas velocity is estimated by the data analysis scheme described in chapter IV. The heat transfer rate of LPG decreases with time and consequently the horizontal vapor velocity decreases. To ensure that the vapor flow in the system is turbulent during the sampling period, the Reynolds number is estimated on the basis of the horizontal gas velocity at the end of the sampling period, which is found experimentally to be about 45 cm/sec. This value is used as $< v >$ and applied in equation (A-III-1). In addition, the concentration of the tracer gas (CO_2) at this time is about 33 mole% of the vapor mixture.

The vapor temperatures recorded from propane (LPG) spills during the

period are between 230K and 250K. For gases, the viscosity increases and the density decreases with increasing temperature. For a conservative estimate for the Reynolds number, the values of density and viscosity evaluated at 250K are used in equation (A-III-1).

At 250 K, the viscosities of CO_2 and propane are

$$\mu_{CO_2} = 1.24 \times 10^{-4} \text{ g/cm-s}$$

$$\mu_{C_3} = 7.0 \times 10^{-5} \text{ g/cm-s}$$

The viscosity of a binary gas mixture can be estimated by the following equation (Reid, Prausnitz and Sherwood, 1977)

$$\mu_{mix} = \frac{y_1 \mu_1}{y_1 + y_2 \phi_{12}} + \frac{y_2 \mu_2}{y_2 + y_1 \phi_{21}} \qquad \text{(A-III-3)}$$

where μ_{mix} = viscosity of mixture

μ_1, μ_2 = pure-component viscosities

y_1, y_2 = mole fractions

ϕ_{21}, ϕ_{21} = binary interaction parameters

and

$$\phi_{12} = \frac{\left[1 + \left(\frac{\mu_1}{\mu_2}\right)^{1/2} \left(\frac{M_2}{M_1}\right)^{1/4}\right]^2}{\left\{8\left[1 + \left(\frac{M_1}{M_2}\right)\right]\right\}^{1/2}} \qquad \text{(Wilke, 1950) (A-III-4)}$$

$$\phi_{21} = \phi_{12} \frac{\mu_2 M_1}{\mu_1 M_2} \qquad \text{(A-III-5)}$$

where M_1, M_2 = molecular weights

The values of ϕ_{12} and ϕ_{21} for carbon dioxide - propane mixtures are found

to be 1.358 and 0.765 respectively. μ_{mix}, obtained from equation (A-III-3), is 8.40×10^{-5} g/cm-s.

The density of the gas mixture is related to its molar volume, obtained from the equation of state:

$$V_{mix} = \frac{Z_{mix}\, RT}{P} \qquad \text{(A-III-6)}$$

where the compressibility factor (Z_{mix}) depends on the reduced temperature T_r and pressure P_r of the mixture.

The critical temperature T_{cm} and pressure P_{cm} of the CO_2 - propane mixture are evaluated by a mole-fraction average method:

$$T_{cm} = \sum_i (y_i\, T_{c_i}) = 347.9\text{K} \qquad \text{(A-III-7)}$$

$$P_{cm} = \sum_i (y_i\, P_{c_i}) = 52.2 \text{ atm} \qquad \text{(A-III-8)}$$

where T_{c_i} and P_{c_i} are the critical temperature and pressure of ith component respectively. The reduced properties of the vapor mixture T_r and P_r are defined as

$$T_r = \frac{T}{T_{cm}} = 0.72 \qquad \text{(A-III-9)}$$

$$P_r = \frac{P}{P_{cm}} = 0.019 \qquad \text{(A-III-10)}$$

Using the generalized compressibility charts (Perry and Chilton, 5th edition), Z_{mix} is found to be 0.978. The molar volume of the gas mixture at 250K and 1 atmosphere pressure is then evaluated as 2.00×10^4 cm^3/mole. The density of the mixture (ρ_{mix}) under these conditions is equal to 2.2×10^{-3} g/cm^3.

After substituting the values of R_h, $\langle v \rangle$, ρ_{mix} and μ_{mix} into equation

(A-III-1), one obtains N_{R_e} = 11890 which falls in the turbulent flow regime.

Turbulent flow is characterized by the highly irregular motion of poorly defined "eddies" of many sizes rolling and mixing with each other. The mixing and blending of the eddies results in a rapid dispersion of fluid particles in a turbulent stream. This is referred to as eddy diffusion.

For a mixture flowing through a pipe, the dimensionless group, $[\frac{D_a}{uL}]$, represents the ratio of material transferred by eddy diffusion to material transport by bulk flow in the axial direction. The axial velocity is u, the length of the pipe is L and D_a is the eddy diffusion coefficient. This dimensionless number indicates the extent of axial dispersion due to the turbulence diffusion. When the value of $[\frac{D_a}{uL}]$ is very small, transfer by eddy is negligible compared to the bulk flow and therefore the system approaches the plug flow.

For a system with a known Reynolds number, the value of $[\frac{D_a}{uL}]$ can be estimated, using the correlations reviewed by Levenspiel (1972). For the present system which has a Reynolds number of 11890, $[\frac{D_a}{uL}]$ is very small and equal to 0.018. The axial dispersion due to turbulent diffusion can therefore be neglected in our analysis.

During a propane (or LPG) spill experiment, the fast evaporation of liquid propane produces large vapor velocities in the vertical direction (perpendicular to the cryogen spreading direction) and therefore enhances the dispersion of propane vapor in the vertical direction. The range in observed evaporation rates of LPG can be converted into hypothetical vertical velocities varying between 5 and 50 cm/sec. The height of the vapor space above the water surface in the spill tube is about 8 cm. Because the time duration of the sample-taking is 0.5 second, the vertical distances traveled by the fluid particles are between 2.5 and 25 cm, sizable distances when compared with the vertical dimension of the spill tube. Furthermore, the vapor samples have been col-

lected from locations midway between the water surface and the top of the spill tube. Considering both the location of the sampler and the magnitude of the vertical motion during the sampling period, the vapor samples collected during the experiments can represent the average composition of the carbon dioxide-propane mixtures in the cross-sectional area. Moreover, the visual observations of the rapid vertical mist motion relative to the horizontal velocity in the vapor phase offer additional evidence. The assumption of plug flow in the data analysis scheme of Chapter IV is therefore valid.

APPENDIX - IV

A. THE BOILING/SPREADING OF CRYOGENS OCCURS IN THE GRAVITY-INERTIA REGIME: A JUSTIFICATION

B. DETAILED DERIVATIONS OF THE MASS AND MOMENTUM CONSERVATION EQUATIONS

C. APPLICATION OF HOULT'S SOLUTION FOR INITIAL CONDITION AT SMALL TIME

D. DETAILED COMPUTATION ALGORITHM FOR THE ONE-DIMENSIONAL BOILING/SPREADING MODEL

E. DERIVATION OF CHARACTERISTIC LENGTH AND TIME FOR ONE-DIMENSIONAL BOILING/SPREADING PROCESS WITH A CONSTANT BOILING RATE PER UNIT AREA

F. COMPUTER PROGRAM FOR ONE-DIMENSIONAL BOILING/SPREADING MODEL

A. THE BOILING/SPREADING OF CRYOGENS OCCURS IN THE GRAVITY-INERTIA REGIME: A JUSTIFICATION

For an instantaneous spill of LNG or LPG on water, by an order of magnitude analysis, the four basic forces which tend to accelerate or retard the spread can be estimated as (Fay, 1969)

$$\text{Gravity:} \quad (\Delta\rho g h)h\ell \tag{A.IV-1}$$

$$\text{Surface tension:} \quad \sigma\ell \tag{A.IV-2}$$

$$\text{Inertia:} \quad \rho(\ell t^{-2})h\ell^2 \tag{A.IV-3}$$

$$\text{Viscous:} \quad [\mu_w(\ell t^{-1})\delta^{-1}]\ell^2 \tag{A.IV-4}$$

where ρ is the cryogen density, σ is the surface tension coefficient, $\delta = (\mu_w t/\rho_w)^{1/2}$ is the water boundary-layer thickness, μ_w is the viscosity and ρ_w the density of water. g is the gravitational acceleration. ℓ is the pool diameter, h is the thickness of cryogen and t is time.

In the gravity-inertia regime in which the gravity force and the inertia force dominate as the spreading and retarding forces respectively, the following inequalities have to be met:

$$h > \left[\frac{\sigma}{\rho g \Delta}\right]^{1/2} \tag{A.IV-5}$$

$$h > \frac{(\rho_w \mu_w t)^{1/2}}{\rho} \tag{A.IV-6}$$

For LNG, with σ = 18.7 dynes/cm, ρ = 0.425 g/cm^3 and g = 980 cm/sec^2,

$$\left[\frac{\sigma}{\rho g \Delta}\right]^{1/2} = 0.28 \text{ cm}$$

For LPG, with σ = 15.4 dynes/cm and ρ = 0.582 g/cm^3,

$$\left[\frac{\sigma}{\rho g \Delta}\right]^{1/2} = 0.25 \text{ cm}$$

In the spreading process, gravity dominates surface tension when the thickness of the cryogen is greater than $[\frac{\sigma}{\rho g \Delta}]^{1/2}$.

In the order of magnitude analysis, accounting for the volume change due to the evaporation of the cryogen during spreading, the conservation of mass is

$$\ell^2 h = \frac{V_o}{2} \tag{A.IV-7}$$

Equating equation (A.IV-1) to (A.IV-3) and using equation (A.IV-7) yields the radial spreading law for cryogen in the gravity-inertia regime:

$$\ell = \left(\frac{\Delta g V_o t^2}{2}\right)^{1/4} \tag{A.IV-8}$$

Rearranging equation (A.IV-8) and combining with equation (A.IV-7), the following expression is obtained:

$$t = \left[\frac{V_o}{2\Delta g}\right]^{1/2} \frac{1}{h} \tag{A.IV-9}$$

Substituting into equation (A.IV-6), one obtains

$$h > \frac{1}{\rho}\left[\frac{\rho_w^2 \mu_w^2}{2\Delta g}\right]^{1/6} V_o^{1/6} \tag{A.IV-10}$$

with $\rho_w = 1$ g/cm^3 and $\mu_w = 1.0037 \times 10^{-2}$ g/cm-sec, for LNG;

$$h > 0.18\ V_o^{1/6} \text{ (cm)} \tag{A.IV-11}$$

and for LPG:

$$h > 0.12\ V_o^{1/6} \text{ (cm)} \tag{A.IV-12}$$

For a large scale instantaneous spill of LNG or LPG, 10^5 liters ($100m^3$) for example, the critical thickness h_{cr} below which the retarding of the cryogen is

is dominated by the viscous forces is very small.

$$\text{LNG:} \quad h_{cr} = 0.39 \text{ cm}$$

$$\text{LPG:} \quad h_{cr} = 0.26 \text{ cm}$$

For LNG and LPG spills on water, the cryogen spreads in the gravity-inertia regime until the thickness of the cryogen has thinned to h_{cr}, after which the cryogen's spreading moves into the gravity-viscous regime. Before this transition occurs, most of the cryogen has already evaported. Therefore, for LNG or LPG spills on water, only the gravity-inertia regime is important.

B. DETAILED DERIVATIONS OF THE MASS AND MOMENTUM CONSERVATION EQUATIONS

For a one-dimensional spreading of a cryogenic liquid on water, the general continuity equation is expressed as (see Bird, Stewart and Lightfoot, 1960)

$$\frac{\partial \rho}{\partial t} + \frac{\partial}{\partial x}(\rho v_x) + \frac{\partial}{\partial z}(\rho v_z) = 0 \qquad \text{(A.IV-13)}$$

In the gravity-inertia regime, the gravitational force balances the acceleration of the cryogen, the equations of motion take the following forms (see Figure A.IV-1):

$$\text{x - component} \qquad \rho\left\{\frac{\partial v_x}{\partial x} + v_x \frac{\partial v_x}{\partial x} + v_z \frac{\partial v_x}{\partial z}\right\} = -\frac{\partial P}{\partial x} \qquad \text{(A.IV-14)}$$

$$\text{z - component} \qquad \rho\left\{\frac{\partial v_z}{\partial t} + v_x \frac{\partial v_z}{\partial x} + v \frac{\partial v_z}{\partial z}\right\} = -\frac{\partial P}{\partial z} - \rho g \qquad \text{(A.IV-15)}$$

Because the thickness of the spreading cryogen is much smaller than the horizontal length of the spill and the slope of $\partial h/\partial x$ is small, it is valid to assume that the cryogen is in hydrostatic equilibrium in the vertical direction and $\frac{\partial v_z}{\partial t}$, $v_x \frac{\partial v_z}{\partial x}$, and $v_z \frac{\partial v_z}{\partial z}$ are negligible compared to gravitational acceleration

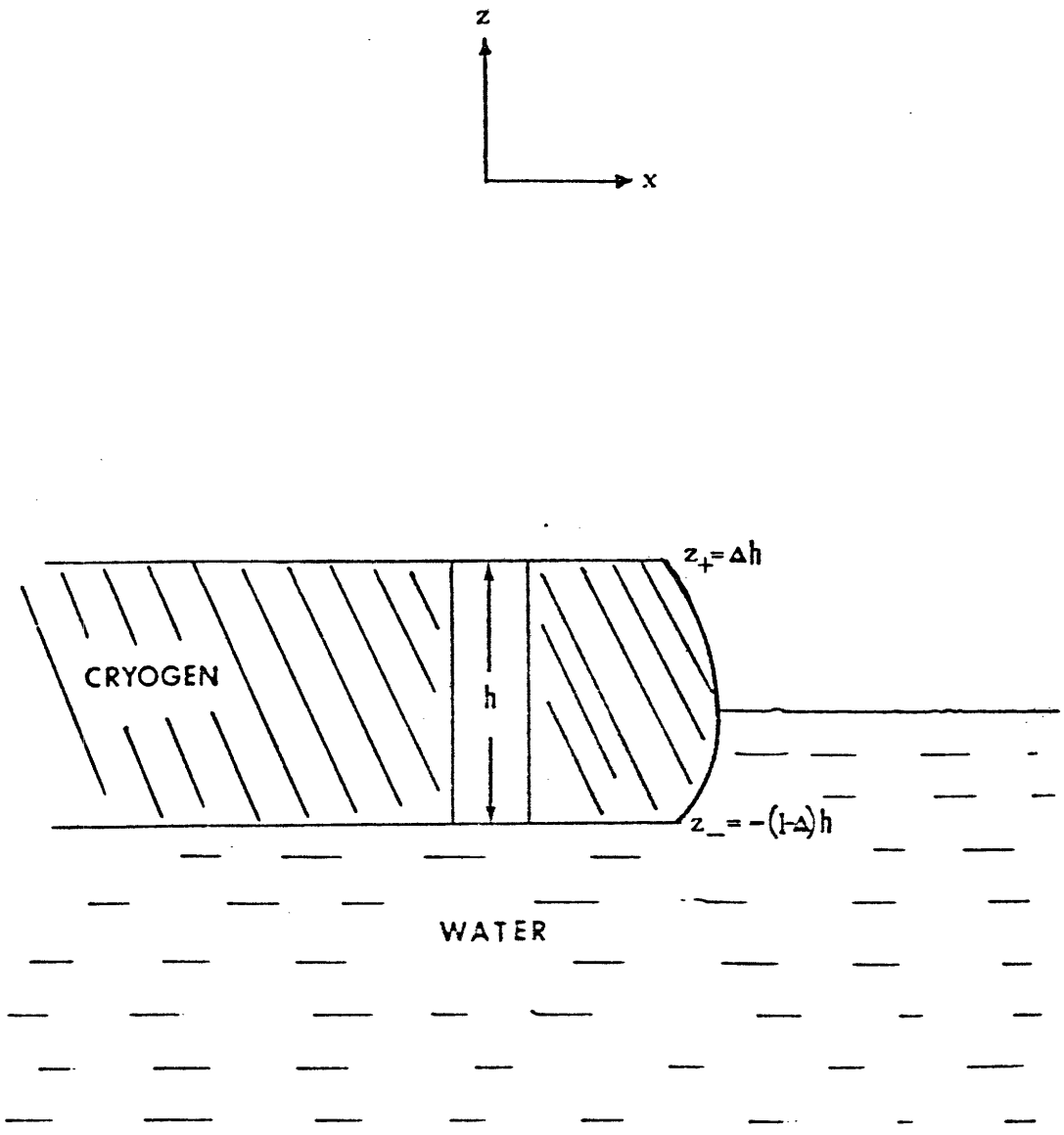

FIGURE A.IV-1: DIFFERENTIAL VOLUME OF LIQUID CRYOGEN SPREADING ON WATER.

g. Thus, equation (A.IV-15) becomes

$$\frac{\partial \rho}{\partial z} = - \rho g \qquad \text{(A.IV-16)}$$

Based on the hydrostatic equilibrium assumption, the height of the cryogen above the water level is equal to Δh and the depth below the water level is $(1-\Delta)h$, where Δ is defined as the ratio of density difference between water and cryogen to water density $(\rho_w - \rho)/\rho_w$.

Integrating equation (A.IV-13) in the vertical direction from $z_- = -(1-\Delta)h$ to $z_+ = \Delta h$, i.e., over the thickness of the spreading liquid at any x and t, using the "Leibnitz formula":

$$\frac{\partial}{\partial t} \int_{z_-}^{z_+} \rho dz - \left[\rho_{z_+} \frac{\partial z_+}{\partial t} - \rho_{z_-} \frac{\partial z_-}{\partial t}\right] + \frac{\partial}{\partial x} \int_{z_-}^{z_+} \rho v_x dz$$

$$- \left[\left(\rho v_x\right)_{z_+} \frac{\partial z_+}{\partial x} - \left(\rho v_x\right)_{z_-} \frac{\partial z_-}{\partial x}\right] + \left(\rho v_z\right)_{z_+} - \left(\rho v_z\right)_{z_-} = 0 \qquad \text{(A.IV-17)}$$

Assuming ρ and v_x are independent of z and substituting z_+ and z_- with Δh and $-(1-\Delta)h$ respectively, into equation (A.IV-17), one obtains

$$h \frac{\partial \rho}{\partial t} + h \frac{\partial}{\partial x} (\rho v_x) + \rho\left[\left(v_z\right)_{z_+} - \left(v_z\right)_{z_-}\right] = 0 \qquad \text{(A.IV-18)}$$

where the third term, for the case without evaporation, is

$$\left(v_z\right)_{z_+} - \left(v_z\right)_{z_-} = \frac{Dh}{Dt} \equiv \frac{\partial h}{\partial t} + v_x \frac{\partial h}{\partial x} \qquad \text{(A.IV-19)}$$

For cryogens, with the local mass boil-off rate $\dot{m}$ (x, t),

$$\left(v_z\right)_{z_+} - \left(v_z\right)_{z_-} - \frac{\dot{m}}{\rho} = \frac{\partial h}{\partial t} + v_x \frac{\partial h}{\partial x} \qquad \text{(A.IV-20)}$$

Combining equations (A.IV-17) and (A.IV-20), one obtains the following form for mass conservation:

$$\frac{\partial}{\partial t}(\rho h) + \frac{\partial}{\partial x}(\rho h\, v_x) = -\dot{m} \qquad \text{(A.IV-21)}$$

Integrating equation (A.IV-16) in the z-direction, the following equation is obtained:

$$P = -\rho g z + f(x, t) \qquad \text{(A.IV-22)}$$

Using the boundary conditon:

$$P = P_o + \rho g h \quad \text{at } z = -(1-\Delta)h \qquad \text{(A.IV-23)}$$

where P_o is atmospheric pressure, $f(x, t)$ is given by

$$f(x, t) = P_o + \rho g h \Delta \qquad \text{(A.IV-24)}$$

Substituting into equation (A.IV-22) and differentiating with respect to x, one obtains

$$\frac{\partial P}{\partial x} = \rho g \frac{\partial}{\partial x}(h\Delta) \qquad \text{(A.IV-25)}$$

Combining equation (A.IV-14) with equation (A.IV-13) multiplied by v_x, the following equation is formed:

$$\frac{\partial}{\partial t}(\rho v_x) + \frac{\partial}{\partial x}(\rho v_x^2) + \frac{\partial}{\partial z}(\rho v_x\, v_z) = -\frac{\partial P}{\partial x} \qquad \text{(A.IV-26)}$$

Substitution of equation (A.IV-25) into equation (A.IV-26) and integrating in the vertical direction from z_- to z_+, one obtains

$$\frac{\partial}{\partial t}(\rho h\, v_x) - \rho v_x \frac{\partial h}{\partial t} + \frac{\partial}{\partial x}(\rho h\, v_x^2) - \rho v_x^2 \frac{\partial h}{\partial x} +$$

$$\rho v_x \left[\left(v_z \right)_{z_+} - \left(v_z \right)_{z_-} \right] = - h \frac{\partial}{\partial x} (\rho g h \Delta) \qquad \text{(A.IV-27)}$$

Multiplying equation (A.IV-20) with v_x and combining with equation (A.IV-27), the following equation of momentum is obtained:

$$\frac{\partial v_x}{\partial t} + v_x \frac{\partial v_x}{\partial x} = - \frac{g}{\rho} \frac{\partial}{\partial x} (\rho h \Delta) \qquad \text{(A.IV-28)}$$

Assuming the density of the cryogen is a constant and using the notation U instead of v_x, the final forms of the equations of continuity and motion are

$$\frac{\partial h}{\partial t} + \frac{\partial}{\partial x} (hU) + \frac{\dot{m}}{\rho} = 0 \qquad \text{(A.IV-29)}$$

$$\frac{\partial U}{\partial t} + U \frac{\partial U}{\partial x} + g\Delta \frac{\partial h}{\partial x} = 0 \qquad \text{(A.IV-30)}$$

C. APPLICATION OF HOULT'S SOLUTION FOR INITIAL CONDITION AT SMALL TIME

The initial conditions, given in the form of thickness and velocity profiles, were provided by Hoult's (1972a) analytic solution in the gravity-inertia flow regime in one-dimensional configuration. As mentioned previously, the entire solution was then determined using the method of characteristics.

The initial time, t_o, (starting point of the analysis) was chosen to be equal to 0.01 sec. It has been found that the numerical solution is insensitive to the value of t_o. Figure A.IV-2 shows that for t_o = 0.01, 0.03, 0.05 and 0.07 sec, the numerical solutions are essentially identical.

The proportion of spilled volume that has evaporated at t_o is, under most circumstances, insignificant. In the 1-liter LNG spill with $\dot{q}$ = 92 kW/m^2 and t_o = 0.01 sec, for example, only ~0.01% of the total spill volume was lost via evaporation. In the case of an LPG spill with V_o = 1 liter, using $\dot{q} = 10^3$ kW/m^2 for t_o = 0.01 sec, only ~0.05% of the total spill volume evaporated away. These cal-

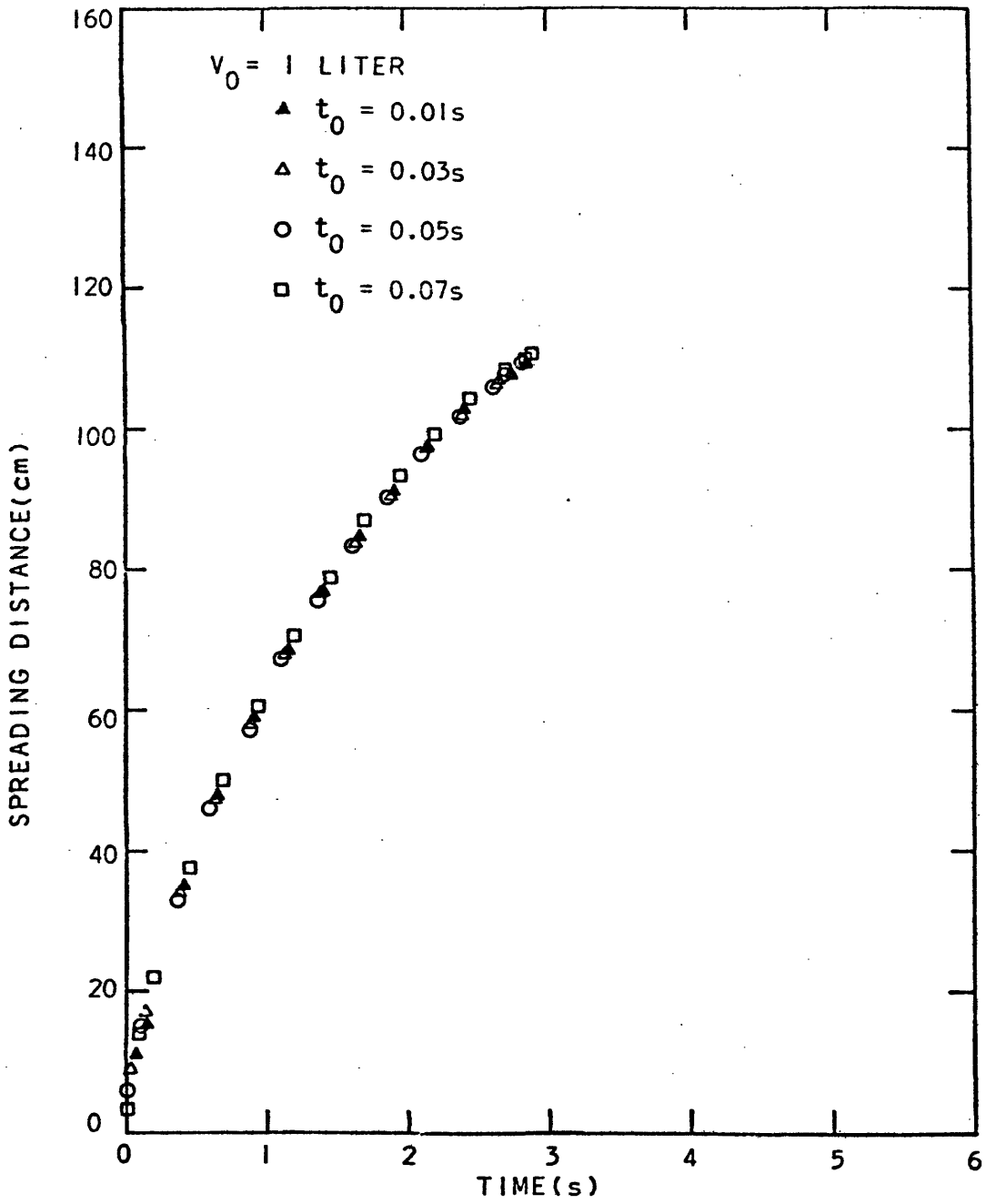

FIGURE A.IV-2: SENSITIVITY OF PREDICTED SPREADING POSITION PROFILE FOR A PROPANE SPILL TO CHANGES IN t_o, THE TIME FOR INITIATING THE METHOD OF CHARACTERISTICS.

calculations show that using the analytic solution for an oil spill adequately describe LNG and LPG spills at very small times (t_o).

D. DETAILED COMPUTATION ALGORITHM FOR THE ONE-DIMENSIONAL BOILING/SPREADING MODEL

Equations (V-12) and (V-13) are rearranged in the following manner:

$$[U + (\Delta\, g\, h)^{1/2}]\, dt - dx = 0 \qquad \text{(A.IV-31)}$$

$$[U - (\Delta\, g\, h)^{1/2}]\, dt - dt = 0 \qquad \text{(A.IV-32)}$$

$$h dU + h^{1/2}\, dh + \frac{\dot{m}}{\rho}\left[\frac{(\Delta\, g\, h)^{1/2}}{U + (\Delta\, g\, h)^{1/2}}\right] dx = 0 \qquad \text{(A.IV-33)}$$

$$h dU - h^{1/2}\, dh - \frac{\dot{m}}{\rho}\left[\frac{(\Delta g\, h)^{1/2}}{U - (\Delta\, g\, h)^{1/2}}\right] dx = 0 \qquad \text{(A.IV-34)}$$

As mentioned previously, every solution of the system of equations (V-12) and (V-13) satisfies the original system of the partial differential equations (V-1) and (V-2). Finite difference approximations are used to solve the equations (A.IV-31) through (A.IV-34) for the values of U and h as functions of x and t.

Two methods of approximating equations (A.IV-31) through (A.IV-34) are described here. One finite difference approximation is expressed by the formula:

$$\int_{x_o}^{x_1} f(x)\, dx \approx f(x_o)\,(x_1 - x_o) \qquad \text{(A.IV-35)}$$

and is called a first-order approximation.

The second finite difference approximation is expressed by the trapezoidal rule formula:

$$\int_{x_o}^{x_1} f(x)\, dx \approx \frac{1}{2}\left[f(x_o) + f(x_1)\right](x_1 - x_o) \qquad \text{(A.IV-36)}$$

and is called a second-order approximation.

It is assumed that U and h are considered as known functions of x at time t, either as given initial conditions or as the results of a previous step in the calculations. In the computation scheme, the time interval (Δt) and space interval (Δx) are specified. For illustrative purposes, the values of U and h are assumed to be known on the line $t = T$, seen in Figure A.IV-3, and are to be found on the line $t = T + \Delta t$. Let P be a typical point on the line $t = T + \Delta t$ (P is not a boundary point or the point next to the boundary) and A, B, C are three adjacent points on the line $t = T$. The characteristic curve I at P intersect ACB at R and the characteristic curve II at P intersect ACB at S.

Since x_P and t_P are known, U_P and h_P are to be found. The computation proceeds as follows:

1. The equations

$$\left[U + (g\,\Delta\, h)^{1/2}\right]_C (t_P - t_R) = x_P - x_R \qquad \text{(A.IV-37)}$$

$$\left[U - (g\,\Delta\, h)^{1/2}\right]_C (t_P - t_S) = x_P - x_S \qquad \text{(A.IV-38)}$$

give the x-coordinates of R and S respectively.

2. Using linear interpolation, U_R, U_S, h_R, h_S can be found from:

$$U_R = U_C \left\{1 - \left[U + (g\,\Delta\, h)^{1/2}\right]_C \theta\right\} + U_A \left[U + (g\,\Delta\, h)^{1/2}\right]_C \theta \qquad \text{(A.IV-39)}$$

$$h_R = h_C \left\{1 - \left[U + (g\,\Delta\, h)^{1/2}\right]_C \theta\right\} + h_A \left[U + (g\,\Delta\, h)^{1/2}\right]_C \theta \qquad \text{(A.IV-40)}$$

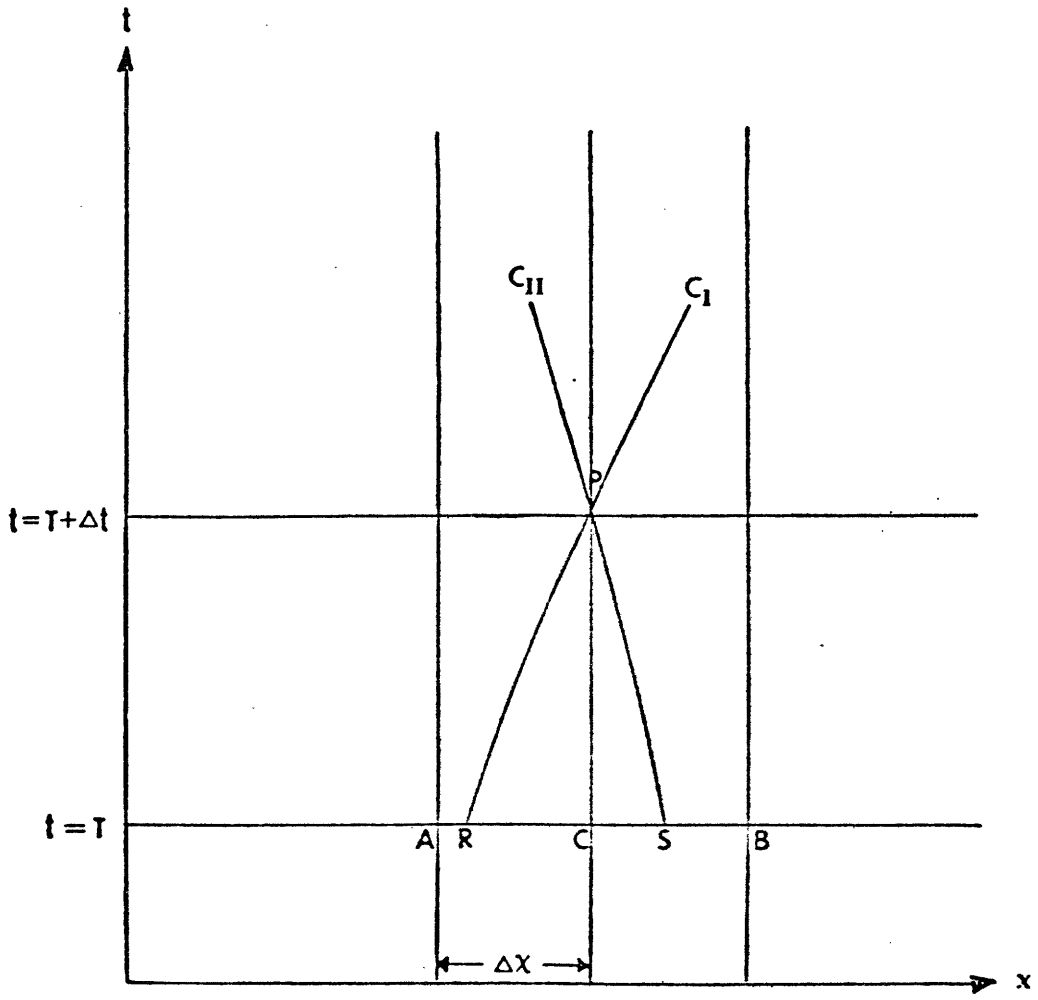

FIGURE A.IV-3: SCHEMATIC OF THE METHOD OF CHARACTERISTICS FOR A NORMAL POINT.

$$U_S = U_C \left\{1 - [U - (g \Delta h)^{1/2}]_C \theta\right\} + U_B [U - (g \Delta h)^{1/2}]_C \theta \quad \text{(A.IV-41)}$$

$$h_S = h_C \left\{1 - [U - (g \Delta h)^{1/2}]_C \theta\right\} + h_B [U - (g \Delta h)^{1/2}]_C \theta \quad \text{(A.IV-42)}$$

where $\theta = \Delta t/\Delta x$.

It has been assumed that because Δt is sufficiently small, the parts of the characteristics between P and R and between P and S are straight lines and that the slope of PR at P is $[U + (g \Delta h)^{1/2}]_C^{-1}$ and the slope of PS at P is $[U - (g \Delta h)^{1/2}]_C^{-1}$.

3. U_P and h_P can now be obtained by solving simultaneously the following two equations:

$$h_C (U_P - U_R) + (h_C)^{1/2} (h_P - h_R) + \left\{\frac{\dot{m} (g \Delta h)^{1/2}}{\rho [U + (g \Delta h)^{1/2}}\right\}_C (x_P - x_R) = 0 \quad \text{(A.IV-43)}$$

$$h_C (U_P - U_S) - (h_C)^{1/2} (h_P - h_S) - \left\{\frac{\dot{m} (g \Delta h)^{1/2}}{\rho[U - (g \Delta h)^{1/2}]}\right\}_C (x_P - x_S) = 0 \quad \text{(A.IV-44)}$$

Equations (A.IV-37) - (A.IV-44) form a process with first-order accuracy. In order to obtain a higher degree of accuracy, the values of U_P and h_P estimated from steps 1, 2, and 3 are used as initial estimates for the second-order process, which is shown below:

4. The equations

$$\frac{1}{2} \left\{[U + (g \Delta h)^{1/2}]_P^{(k)} + [U + (g \Delta h)^{1/2}]_R^{(k)}\right\}(t_p - t_R) = x_p - x_R^{(k+1)} \quad \text{(A.IV-45)}$$

$$\frac{1}{2} \left\{[U - (g \Delta h)^{1/2}]_P^{(k)} + [U - (g \Delta h)^{1/2}]_S^{(k)}\right\}(t_p - t_S) = x_p - x_S^{(k+1)} \quad \text{(A.IV-46)}$$

give the x-coordinates of R and S at the (k+1)th iteration.

5. Using a formula for quadratic interpolation, $U_R^{(k+1)}$, $U_S^{(k+1)}$, $h_R^{(k+1)}$, and $h_S^{(k+1)}$ can be calculated.

$$U_R^{(k+1)} = U_C - \frac{1}{2\Delta x}(U_A - U_B)(x_R^{(k+1)} - x_C) + \frac{1}{2(\Delta x)^2}(U_A + U_B - 2U_C)(x_R^{(k+1)} - x_C)^2 \qquad \text{(A.IV-47)}$$

$$h_R^{(k+1)} = h_C - \frac{1}{2\Delta x}(h_A - h_B)(x_R^{(k+1)} - x_C) + \frac{1}{2(\Delta x)^2}(h_A + h_B - 2h_C)(x_R^{(k+1)} - x_C)^2 \qquad \text{(A.IV-48)}$$

$$U_S^{(k+1)} = U_C - \frac{1}{2\Delta x}(U_A - U_B)(x_S^{(k+1)} - x_C) + \frac{1}{2(\Delta x)^2}(U_A + U_B - 2U_C)(x_S^{(k+1)} - x_C)^2 \qquad \text{(A.IV-49)}$$

$$h_S^{(k+1)} = h_C - \frac{1}{2\Delta x}(h_A - h_B)(x_S^{(k+1)} - x_C) + \frac{1}{2(\Delta x)^2}(h_A + h_B - 2h_C)(x_S^{(k+1)} - x_C)^2 \qquad \text{(A.IV-50)}$$

6. $U_P^{(k+1)}$ and $h_P^{(k+1)}$ can then be obtained by solving simultaneously the equations:

$$\frac{1}{2}\left(h_R^{(k+1)} + h_P^{(k)}\right)\left(U_P^{(k+1)} - U_R^{(k+1)}\right) + \frac{1}{2}\left\{\left[h_R^{(k+1)}\right]^{1/2} + \left[h_P^{(k)}\right]^{1/2}\right\}\left(h_P^{(k+1)} - h_R^{(k+1)}\right) + \frac{1}{2\rho}\left\{\left[\frac{\dot{m}(g\Delta h)^{1/2}}{U + (g\Delta h)^{1/2}}\right]_R^{(k+1)} + \left[\frac{\dot{m}(g\Delta h)^{1/2}}{U + (g\Delta h)^{1/2}}\right]_P^{(k)}\right\}(x_p - x_R^{(k+1)}) = 0 \qquad \text{(A.IV-51)}$$

$$\left(\frac{1}{2}\ h_S^{(k+1)} + h_P^{(k)}\right) - \left(U_P^{(k+1)} - U_S^{(k+1)}\right) - \frac{1}{2}\left\{\left[h_S^{(k+1)}\right]^{1/2} + \left[h_P^{(k+1)}\right]^{1/2}\right\}$$

$$\left(h_P^{(k+1)} - h_S^{(k+1)}\right) - \frac{1}{2\rho}\left\{\left[\frac{\dot{m}\,(g\Delta h)^{1/2}}{U - (g\Delta h)^{1/2}}\right]_S^{(k+1)} + \left[\frac{\dot{m}\,(g\Delta h)^{1/2}}{U - (g\Delta h)^{1/2}}\right]_P^{(k)}\right\}$$

$$\left(x_P - x_S^{(k+1)}\right) = 0 \qquad \text{(A.IV-52)}$$

The iterative procedure is repeated until the values of U_P and h_P converge to the third decimal place.

The appropriate end point which represents the spreading front demands special attention. The spreading front must move in accordance with the boundary condition, equation (V-3). The computation procedure for this endpoint is described in the next section.

Boundary Points

Consider the case in which the point B lies in the boundary. As indicated earlier, the values of U and h at time t = T are assumed to be known. Points A and C are adjacent to point B. The following are the steps in the computation for U_M and h_M at the leading-edge point at $t = T + \Delta t$.

1. X_M can be approximated from the relation

$$x_M - x_B = U_B\,(t_M - t_B) \qquad \text{(A.IV-53)}$$

2. The leading-edge point, M, with advancing t is always located at the intersection of the characteristic curve I of the point, R, adjacent to the leading-edge point B, with the leading-edge path. The equation

$$x_M - x_R = \left[U + (g\,\Delta\,h)^{1/2}\right]_B (t_M - t_R) \qquad \text{(A.IV-54)}$$

gives the x-coordinate of R.

3. U_R and h_R are obtained using linear interpolation:

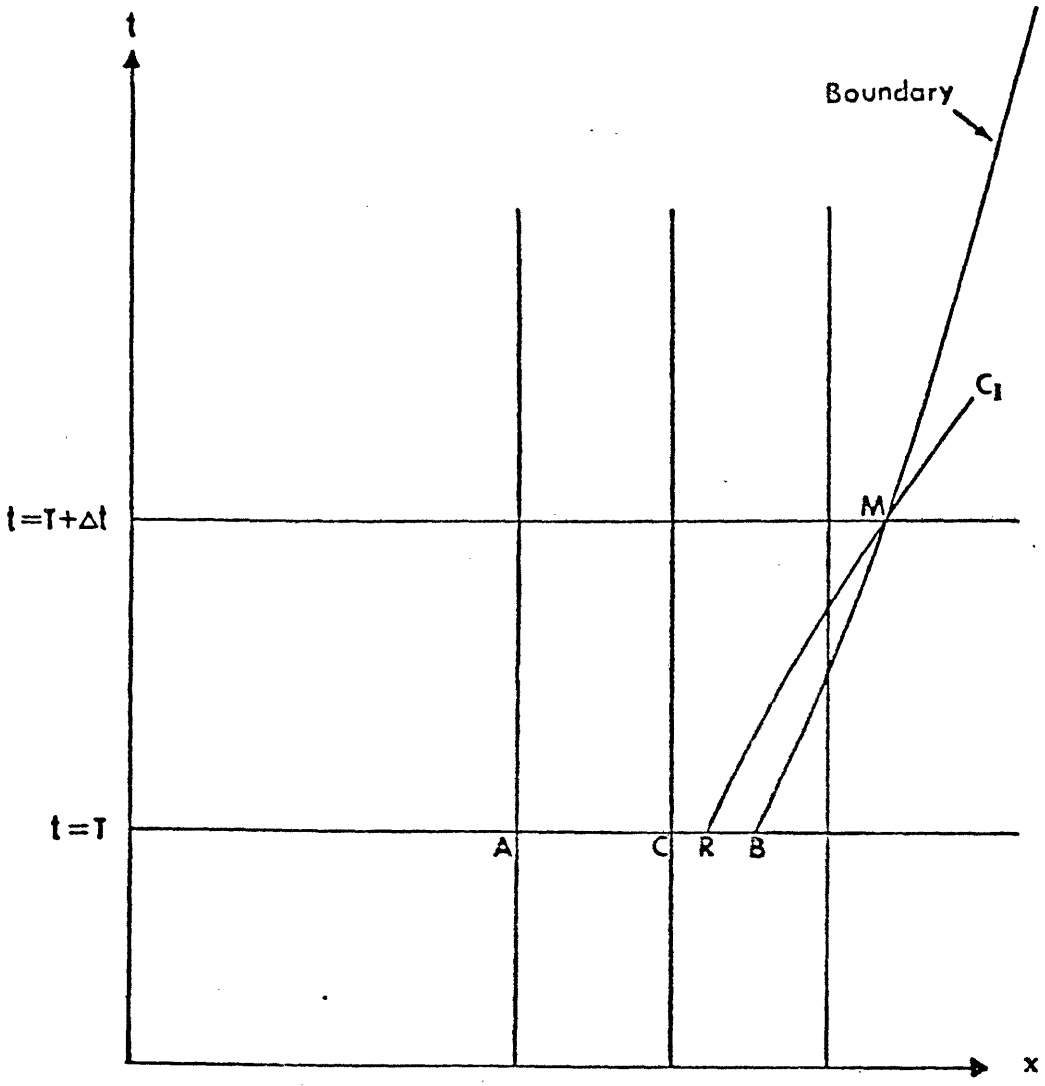

FIGURE A.IV-4: SCHEMATIC OF THE METHOD OF CHARACTERISTICS FOR A BOUNDARY POINT.

$$U_R = U_C + (U_B - U_C) \frac{(x_R - x_C)}{\zeta \Delta x} \qquad \text{(A.IV-55)}$$

$$h_R = h_C + (h_B - h_C) \frac{(x_R - x_C)}{\zeta \Delta x} \qquad \text{(A.IV-56)}$$

where ζ is defined as the ratio of $(x_B - x_C)/\Delta x$.

4. The values of U_M and h_M must satisfy the following equations simultaneously:

$$h_B (U_M - U_R) + (h_B)^{1/2} (h_M - h_R) + \frac{1}{\rho} \left[\frac{\dot{m} (g\Delta h)^{1/2}}{U + (g\Delta h)^{1/2}} \right]_B (x_M - X_R) = 0 \qquad \text{(A.IV-57)}$$

$$h_M = \frac{U_M^2}{\lambda g \Delta} \qquad \text{where } \lambda = 1.64 \qquad \text{(A.IV-58)}$$

Equations (A.IV-53) - (A.IV-58) are the first-order approximations to the original partial differential equations. Again to determine accurately the values of x_M, U_M, and h_M, the second-order approximation with interation procedure is required.

The formulas for the second-order process are as follows:

5. $x_M^{(k+1)}$ can be calculated from the equation

$$x_M^{(k+1)} - x_B = \frac{1}{2} (U_B + U_M^{(k)}) (t_M - t_B) \qquad \text{(A.IV-59)}$$

6. The equation

$$\frac{1}{2} \left\{ [U + (g\Delta h)^{1/2}]_M^{(k)} + [U + (g\Delta h)^{1/2}]_R^{(k)} \right\} (t_M - t_R) = x_M^{(k+1)} - x_R^{(k+1)} \qquad \text{(A.IV-60)}$$

gives the value of x_R at the (k+1)st iteration.

7. Using the following quadratic interpolation formulas, $U_R^{(k+1)}$ and $h_R^{(k+1)}$ can be found:

$$U_R^{(k+1)} = U_C - \frac{\zeta^2 U_A + (1-\zeta^2) U_C - U_B}{\zeta(1+\zeta)\Delta x} (x_R^{(k+1)} - x_C) +$$

$$\frac{\zeta U_A - (1+\zeta) U_C + U_B}{\zeta (1+\zeta) (\Delta x)^2} (x_R^{(k+1)} - x_C)^2 \qquad \text{(A.IV-61)}$$

$$h_R^{(k+1)} = h_C - \frac{\zeta^2 h_A + (1-\zeta^2) h_C - h_B}{\zeta (1+\zeta)\Delta x} (x_R^{(k+1)} - x_C) +$$

$$\frac{\zeta h_A - (1+\zeta) h_C + h_B}{\zeta (1+\zeta) (\Delta x)^2} (x_R^{(k+1)} - x_C)^2 \qquad \text{(A.IV-62)}$$

7. The relationships between $U_M^{(k+1)}$ and $h_M^{(k+1)}$ are:

$$\frac{1}{2} \left(h_M^{(k)} + h_R^{(k+1)}\right) \left(U_M^{(k+1)} - U_R^{(k+1)}\right) + \frac{1}{2} \left[\left(h_M^{(k)}\right)^{1/2} + \left(h_R^{(k+1)}\right)^{1/2}\right]$$

$$\left(h_M^{(k+1)} - h_R^{(k+1)}\right) + \frac{1}{2\rho} \left\{\left[\frac{\dot{m} (g\Delta h)^{1/2}}{U + (g\Delta h)^{1/2}}\right]_M^{(k)} + \left[\frac{\dot{m} (g\Delta h)^{1/2}}{U + (g\Delta h)^{1/2}}\right]_R^{(k+1)}\right\}$$

$$\left(x_M^{(k+1)} - x_R^{(k+1)}\right) = 0 \qquad \text{(A.IV-63)}$$

$$h_M^{(k+1)} = \frac{[U_M^{(k+1)}]^2}{\lambda g \Delta} \qquad \text{(A.IV-64)}$$

and can be used to find $U_M^{(k+1)}$ and $h_M^{(k+1)}$.

For point P, near the boundary of the spreading front (see Figure A.IV-5), the computational scheme used to find U_p and h_p at $t = T + \Delta t$ is described in the following section.

Points Near the Boundary

The formulas for the first-order approximation process follow.

1. To find the x- and t- coordinates of N, the point of intersection of the characteristic curve II at P and the boundary, the following equations have to be solved simultaneously:

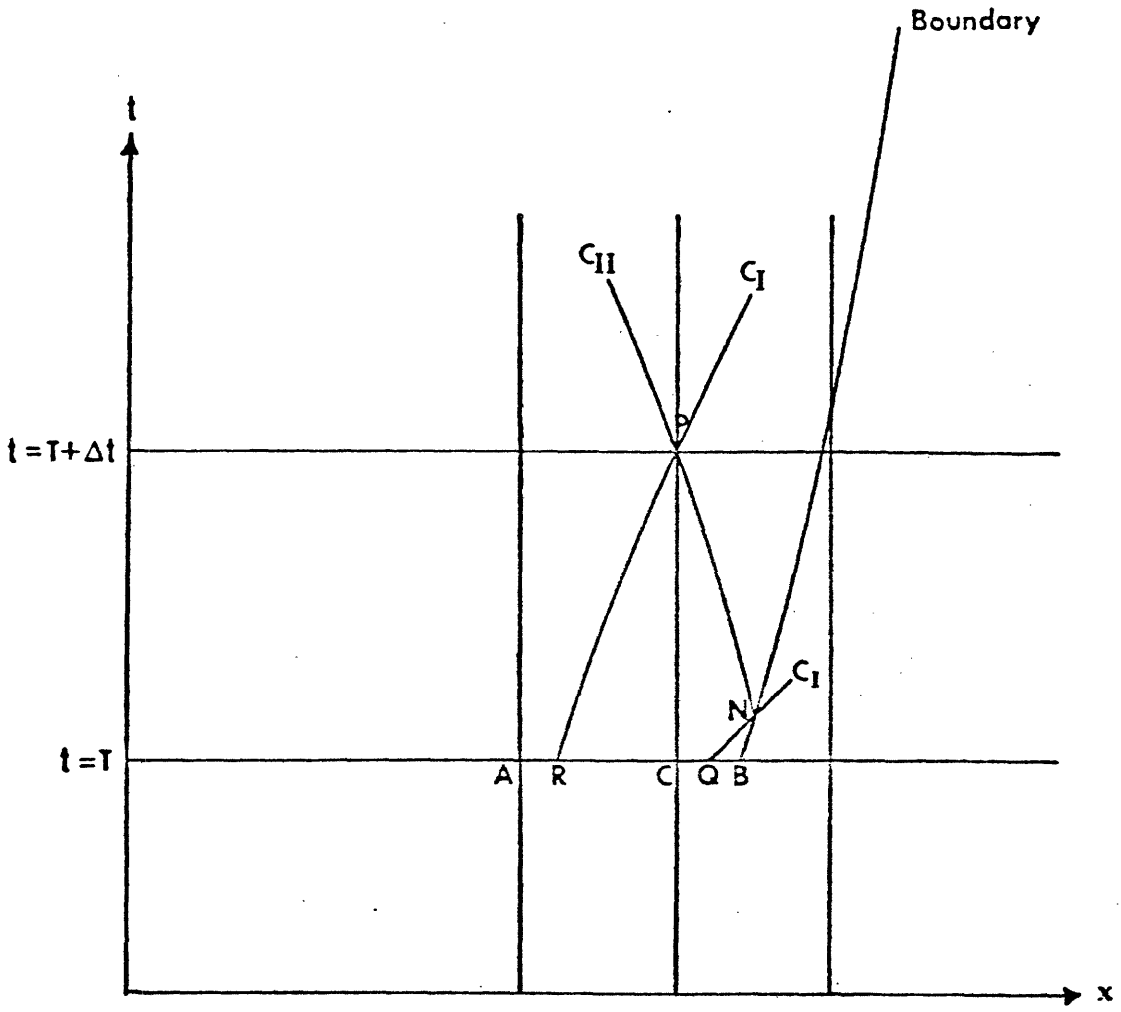

FIGURE A.IV-5: SCHEMATIC OF THE METHOD OF CHARACTERISTICS FOR A POINT NEAR BOUNDARY.

$$\left[U - (g\Delta h)^{1/2}\right]_C (t_P - t_N) = x_P - x_N \qquad \text{(A.IV-65)}$$

$$U_B (t_N - t_B) = x_N - x_B \qquad \text{(A.IV-66)}$$

2. The x-coordinate of Q, the point of intersection of the characteristic curve I through N and ACB, is found from:

$$\left[U + (g\Delta h)^{1/2}\right]_B (t_N - t_Q) = x_N - x_Q \qquad \text{(A.IV-67)}$$

3. U_Q and h_Q are found from linear interpolation formulas:

$$U_Q = U_C + (U_B - U_C) \frac{x_Q - x_C}{\zeta \Delta x} \qquad \text{(A.IV-68)}$$

$$h_Q = h_C + (h_B - h_C) \frac{x_Q - x_C}{\zeta \Delta x} \qquad \text{(A.IV-69)}$$

4. The values of U_N and h_N can be obtained by solving the following two equations simultaneously:

$$h_B (U_N - U_Q) + (h_B)^{1/2} (h_N - h_Q) + \frac{1}{\rho}\left[\frac{\dot{m} (g\Delta h)^{1/2}}{U + (g\Delta h)^{1/2}}\right]_B (x_N - x_Q) = 0 \qquad \text{(A.IV-70)}$$

$$h_N = \frac{U_N^2}{\lambda g \Delta} \qquad \text{(A.IV-71)}$$

5. Equations (A.IV-45), (A.IV-47) and (A.IV-48) give x_R, U_R, and h_R respectively.

6. U_P and h_P can now be found by using equations (A.IV-43) and (A.IV-72):

$$h_C (U_P - U_R) + (h_C)^{1/2} (h_P - h_R) + \frac{1}{\rho}\left[\frac{\dot{m} (g\Delta h)^{1/2}}{U + (g\Delta h)^{1/2}}\right]_C (x_P - x_R) = 0 \qquad \text{(A.IV-43)}$$

$$h_C (U_P - U_N) - (h_C)^{1/2} (h_P - h_N) + \frac{1}{\rho}\left[\frac{\dot{m} (g\Delta h)^{1/2}}{U - (g\Delta h)^{1/2}}\right]_C (x_P - x_N) = 0 \qquad \text{(A.IV-72)}$$

The formulas for the second-order approximations follow.

7. The equations for finding the x- and t- coordinates of N are:

$$\frac{1}{2}\left\{\left[U - (g\Delta h)^{1/2}\right]_P^{(k)} + \left[U - (g\Delta h)^{1/2}\right]_N^{(k)}\right\}(t_P - t_N^{(k+1)}) = x_P - x_N^{(k+1)} \quad \text{(A.IV-73)}$$

$$\frac{1}{2}(U_B + U_N^{(k)})(t_N^{(k+1)} - t_B) = x_N^{(k+1)} - x_B \quad \text{(A.IV-74)}$$

8. The $x^{(k+1)}$ coordinate of Q can be found from the following equation:

$$\frac{1}{2}\left\{\left[U + (g\Delta h)^{1/2}\right]_N^{(k)} + \left[U + (g\Delta h)^{1/2}\right]_Q^{(k)}\right\}(t_N^{(k+1)} - t_Q) = x_N^{(k+1)} - x_Q^{(k+1)} \quad \text{(A.IV-75)}$$

9. $U_Q^{(k+1)}$ and $h_Q^{(k+1)}$ can be computed from second-order interpolation formulas:

$$U_Q^{(k+1)} = U_C - \frac{\zeta^2 U_A + (1-\zeta^2) U_C - U_B}{\zeta(1+\zeta)\Delta x}(x_Q^{(k+1)} - x_C) + \frac{\zeta U_A - (1+\zeta) U_C + U_B}{\zeta(1+\zeta)(\Delta x)^2}(x_Q^{(k+1)} - x_C)^2 \quad \text{(A.IV-76)}$$

$$h_Q^{(k+1)} = h_C - \frac{\zeta^2 h_A + (1-\zeta^2) h_C - h_B}{\zeta(1+\zeta)\Delta x}(x_Q^{(k+1)} - x_C) + \frac{\zeta h_A - (1+\zeta) h_C + h_B}{\zeta(1+\zeta)(\Delta x)^2}(x_Q^{(k+1)} - x_C)^2 \quad \text{(A.IV-77)}$$

10. The values of $U_N^{(k+1)}$ and $h_N^{(k+1)}$ are obtained by solving the following equations simultaneously:

$$\frac{1}{2}\left(h_N^{(k)} + h_Q^{(k+1)}\right)\left(U_N^{(k+1)} - U_Q^{(k+1)}\right) + \frac{1}{2}\left[\left(h_N^{(k)}\right)^{1/2} + \left(h_Q^{(k+1)}\right)^{1/2}\right]\left(h_N^{(k+1)} - h_Q^{(k+1)}\right)$$

$$+ \frac{1}{2\rho}\left\{\left[\frac{\dot{m}\,(g\Delta h)^{1/2}}{U + (g\Delta h)^{1/2}}\right]_N^{(k)} + \left[\frac{\dot{m}\,(g\Delta h)^{1/2}}{U + (g\Delta h)^{1/2}}\right]_Q^{(k+1)}\right\}\left(x_N^{(k+1)} - x_Q^{(k+1)}\right) = 0 \qquad \text{(A.IV-78)}$$

$$h_N^{(k+1)} = \frac{\left[U_N^{(k+1)}\right]^2}{\lambda g \Delta} \qquad \text{(A.IV-79)}$$

11. $x_R^{(k+1)}$, $U_R^{(k+1)}$, and $h_R^{(k+1)}$ can be calculated using equations (A.IV-45), (A.IV-61) and (A.IV-62).

12. Finally, equation (A.IV-51) and the following equation can be solved for $U_P^{(k+1)}$ and $h_P^{(k+1)}$:

$$\frac{1}{2}\left(h_P^{(k)} + h_N^{(k+1)}\right)\left(U_P^{(k+1)} - U_N^{(k+1)}\right) - \frac{1}{2}\left\{\left[h_P^{(k+1)}\right]^{1/2} + \left[h_N^{(k+1)}\right]^{1/2}\right\}$$

$$\left(h_P^{(k+1)} - h_N^{(k+1)}\right) + \frac{1}{2\rho}\left\{\left[\frac{\dot{m}\,(g\Delta h)^{1/2}}{U - (g\Delta h)^{1/2}}\right]_P^{(k)} + \left[\frac{\dot{m}\,(g\Delta h)^{1/2}}{U - (g\Delta h)^{1/2}}\right]_N^{(k+1)}\right\}$$

$$\left(x_P - x_N^{(k+1)}\right) = 0 \qquad \text{(A.IV-80)}$$

The thickness of the cryogen decreases as it spreads and evaporates. It is necessary to establish an arbitary tolerance for h or else the numerical solution would expand to regions of physical non-relevance. If at any point the value of h becomes less than the convergence criterion of h = 0.005 cm used in the computation procedure, that point is dropped from the calculational scheme outlined above. The physical significance of this step is that the cryogen is assumed to have evaporated completely.

A detailed flow diagram of the computer algorithm for the one-dimensional boiling/spreading model is given in Figure A.IV-6.

E. DERIVATION OF CHARACTERISTIC LENGTH AND TIME FOR ONE-DINEMSIONAL BOILING/SPREADING PROCESS WITH A CONSTANT BOILING RATE PER UNIT AREA

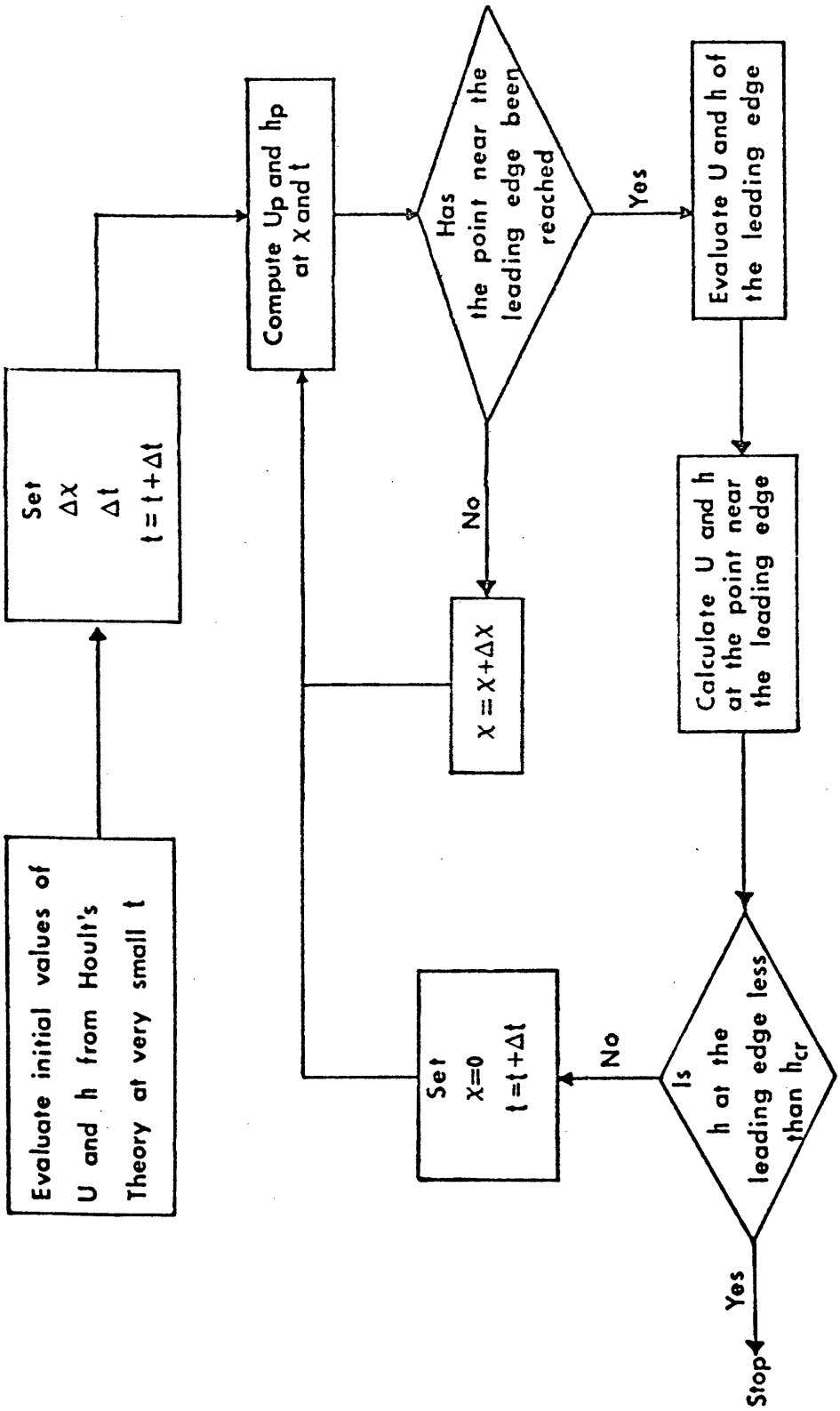

FIGURE A.IV-6: FLOW CHART FOR THE NUMERICAL MODEL

Using an order-of-magnitude analysis, the accelerating force may be taken as

$$F \sim (\Delta\rho g h)\, hw \qquad \text{(A.IV-81)}$$

The inertia of the spill may be characterized as

$$ma \sim \rho h x w\, (x/t^2) \qquad \text{(A.IV-82)}$$

Equating the two expressions:

$$t \sim x/(\Delta g h)^{1/2} \qquad \text{(A.IV-83)}$$

With

$$h \sim V/(xw) \qquad \text{(A.IV-84)}$$

Substituting into equation (A.IV-83), one obtains

$$t \sim \left[x^3 (\Delta g V/w)^{-1}\right]^{1/2} \qquad \text{(A.IV-85)}$$

Furthermore, the characteristic time t_e for the evaporation of the entire spill volume V may be expressed as

$$t_e = \frac{V}{\left[\left(\frac{\dot{m}}{\rho}\right) w x_e\right]} \qquad \text{(A.IV-86)}$$

where x_e is the radius at time t_e, Eliminating x_e from equation (A.IV-86) using equation (A.IV-85) with $x = x_e$ the following expression is obtained:

$$t_e = \left[\left(\frac{\rho}{\dot{m}}\right)^3 \left(\frac{V}{w}\right)^2 (g\Delta)^{-1}\right]^{1/5} \qquad \text{(A.IV-87)}$$

Substituting equation (A.IV-87) into equation (A.IV-83), characteristic length x_e corresponding to t_e is

$$x_e = \left[\left(\frac{\rho}{\dot{m}}\right)^2 \left(\frac{V}{w}\right)^3 (g\Delta)\right]^{1/5} \qquad \text{(A.IV-88)}$$

The physical quantities in dimensionless form are defined as:

$$x^* = \frac{x}{x_e} \quad ; \quad t^* = \frac{t}{t_e}$$

$$U^* = \frac{U}{[x_e/t_e]} \; ; \; h^* = \frac{h}{[V/x_e w]}$$

F. COMPUTER PROGRAM FOR ONE-DIMENSIONAL BOILING/SPREADING MODEL

```
      IMPLICIT REAL*8 (A-H,O-Z)                                          LPG00010
C     ONE-DIMENSIONAL BOILING AND SPREADING MODEL FOR INSTANTANEOUS      LPG00020
C     SPILLS                                                             LPG00030
C     ASSUME  HEAT FLUX PER UNIT AREA ARE FUNCTIONS OF TIME AND POSITION LPG00040
C     INITIAL CONDITIONS                                                 LPG00050
      DIMENSION X(1000),U(1000),H(1000), B(1000),TW(1000)                LPG00060
      ATA=1.72                                                           LPG00070
      COE=4./(9.*(2./27.+1./(ATA**3.)))                                  LPG00080
      CC1=4./COE                                                         LPG00090
      CC2=COE/2.                                                         LPG00100
      T0=0.07                                                            LPG00110
      T00=0.02                                                           LPG00120
      TAA=1.0                                                            LPG00130
      E1=0.0362                                                          LPG00140
      E3=E1/T00**0.5                                                     LPG00150
      E0=0.                                                              LPG00160
      DELTA=1.                                                           LPG00170
      A3=980.                                                            LPG00180
      RHO=0.4                                                            LPG00190
      DELT=1.-RHO                                                        LPG00200
      A1=(980.*DELT)**0.5                                                LPG00210
      A2=A1*A1                                                           LPG00220
      SV=1./RHO                                                          LPG00230
      W=16.5                                                             LPG00240
      V0=582./RHO                                                        LPG00250
      X0=ATA*(A2*V0*T0*T0/W)**(1./3.)                                    LPG00260
      DX=2.                                                              LPG00270
      N=X0/DX                                                            LPG00280
      N=N+2                                                              LPG00290
      NN=N-1                                                             LPG00300
      VEL=2./3.                                                          LPG00310
      CK=ATA*ATA*(4./(9.*COE)-1./9.)                                     LPG00320
      WRITE(6,400)   COE,CK,RHO                                          LPG00330
400   FORMAT(  10X,'COE=',F10.3,5X,'CK=',F10.3,5X,'RHO=',F10.3)          LPG00340
      E4=E3+E0                                                           LPG00350
      BOL1=E4                                                            LPG00360
      TM=(V0/(A1*T0*W))**VEL                                             LPG00370
```

```
      TM1=CK*TM                                                          LPG00380
      DO 2 I=1,NN                                                        LPG00390
      X(I)=DX*(I-1)                                                      LPG00400
      U(I)=X(I)*VEL/T0                                                   LPG00410
2     H(I)=X(I)*X(I)/(9.*A2*T0*T0)+TM1                                   LPG00420
      X(N)=X0                                                            LPG00430
      U(N)=X0*VEL/T0                                                     LPG00440
      H(N)=U(N)*U(N)/(COE*A2)                                            LPG00450
      DO 2009  I=1,N                                                     LPG00460
      B(I)=BOL1                                                          LPG00470
      TW(I)=0.                                                           LPG00480
2009  CONTINUE                                                           LPG00490
      AVH=1./(X0*W)                                                      LPG00500
      V=0.                                                               LPG00510
      DO 301 I=1,NN                                                      LPG00520
301   V=V+H(I)                                                           LPG00530
      V0=W*((V-0.5*(H(1)+H(NN)))*DX+(H(NN)+H(N))*(X(N)-X(NN))*0.5)       LPG00540
      WRITE(6,848)  V0                                                   LPG00550
848   FORMAT(2X,'INITIAL VOLUME=',E11.5)                                 LPG00560
      WRITE(6,999)  T0                                                   LPG00570
      DO 300 I=1,N                                                       LPG00580
      WRITE(6,1001)  I,X(I),U(I),H(I),B(I)                               LPG00590
300   CONTINUE                                                           LPG00600
      DT=0.0005                                                          LPG00610
      THETA=DT/DX                                                        LPG00620
      KX=200                                                             LPG00630
      KX1=KX+1                                                           LPG00640
      XK=0.005                                                           LPG00650
      YK=XK                                                              LPG00660
      J=21                                                               LPG00670
      T1=T00-TAA                                                         LPG00680
      BG=E1/DT**0.5+E0                                                   LPG00690
3     IF(T0 .GE. 30.)  GO TO 27                                          LPG00700
      T=T0+DT                                                            LPG00710
      IF(J.NE. KX)  GO TO 46                                             LPG00720
      WRITE(6,999)  T                                                    LPG00730
999   FORMAT(2X,'T=',E11.5)                                              LPG00740
C       CALCULATE H AT X=0.                                              LPG00750
```

```
46    IF(H(1) .LE. XK)  GO TO 28                                        LPG00760
      SQH1=H(1)**0.5*A1                                                 LPG00770
      XS=SQH1*DT                                                        LPG00780
      IF(XS.GT. X(2))  GO TO 27                                         LPG00790
      DFS=XS/X(2)                                                       LPG00800
      US=U(2)*DFS                                                       LPG00810
      HS=H(1)+(H(2)-H(1))*DFS                                           LPG00820
      BXS=B(1)*DT*SV                                                    LPG00830
      HO=HS-H(1)*US/SQH1-BXS                                            LPG00840
      BO=E4                                                             LPG00850
      IF(T.GT.TAA)    BO=E1/(T+T1)**0.5+E0                              LPG00860
      BS=B(1)                                                           LPG00870
4     SQHO=HO**0.5*A1                                                   LPG00880
      ZAIHO=1./SQHO                                                     LPG00890
      GO=HS**0.5*A1-US                                                  LPG00900
      ZAIHS=1./GO                                                       LPG00910
      XS=2.*DT/(ZAIHO+ZAIHS)                                            LPG00920
      IF(XS.GT. X(2))  GO TO 27                                         LPG00930
      DXS=XS/X(2)                                                       LPG00940
      US=U(2)*DXS                                                       LPG00950
      HS=H(1)+(H(2)-H(1))*DXS                                           LPG00960
      SQHS=HS**0.5*A1                                                   LPG00970
      G1=SQHS-US                                                        LPG00980
      ZHS=SQHS/G1                                                       LPG00990
      HOHS=SQHO+SQHS                                                    LPG01000
      BBXS=SV*XS*(BO+BS*ZHS)                                            LPG01010
      HHO=HS-(US*(HO+HS)+BBXS)/HOHS                                     LPG01020
      DHO=(HHO-HO)/HO                                                   LPG01030
      HO=HHO                                                            LPG01040
      IF(DABS(DHO) .LE. 0.001)    GO TO 5                               LPG01050
      GO TO 4                                                           LPG01060
5     H(1)=HO                                                           LPG01070
      B(1)=BO                                                           LPG01080
      IF(J.NE. KX)  GO TO 28                                            LPG01090
      WRITE(6,1000)   H(1),B(1)                                         LPG01100
1000  FORMAT(2X,'I=   1',5X,'X=0.',17X,'U=0.',17X,'H=',E10.4,9X,'B=',E10LPG01110
     1.4)                                                               LPG01120
```

```
C       CALCULATE U,H,AT X(I) WHERE I FROM 2 TO N-2                    LPG01130
28    IF(N.EQ. 2)  GO TO 791                                           LPG01140
      NNN=N-2                                                          LPG01150
      UA=U(NNN)                                                        LPG01160
      HA=H(NNN)                                                        LPG01170
      BA=B(NNN)                                                        LPG01180
      XA=X(NNN)                                                        LPG01190
      TWA=TW(NNN)                                                      LPG01200
791   UB=U(N-1)                                                        LPG01210
      HB=H(N-1)                                                        LPG01220
      BB=B(N-1)                                                        LPG01230
      XB=X(N-1)                                                        LPG01240
      TWB=TW(N-1)                                                      LPG01250
      UC=U(N)                                                          LPG01260
      HC=H(N)                                                          LPG01270
      BC=B(N)                                                          LPG01280
      XC=X(N)                                                          LPG01290
      TWC=TW(N)                                                        LPG01300
      IF(NN .LE. 2)  GO TO 700                                         LPG01310
      DO 6 I=2,NNN                                                     LPG01320
      IF(H(I) .LE. XK)  GO TO 6                                        LPG01330
      SQHI=H(I)**0.5*A1                                                LPG01340
      ZAIP=SQHI+U(I)                                                   LPG01350
      ZAIN=SQHI-U(I)                                                   LPG01360
      XR=X(I)-DT*ZAIP                                                  LPG01370
      II=I-1                                                           LPG01380
      IF(XR.LT.X(II))  GO TO 27                                        LPG01390
      XS=X(I)+DT*ZAIN                                                  LPG01400
      IJ=I+1                                                           LPG01410
      IF(XS.GT. X(IJ))  GO TO 27                                       LPG01420
      IF(XS .LT. X(I)) GO TO 40                                        LPG01430
C       USE LINEAR INTERPOLATION FOR THE FIRST ESTIMATION OF           LPG01440
C       UR,HR,US,HS                                                    LPG01450
      THEP=THETA*ZAIP                                                  LPG01460
      THEN=THETA*(-ZAIN)                                               LPG01470
      UR=U(I)*(1.-THEP)+U(II)*THEP                                     LPG01480
      HR=H(I)*(1.-THEP)+H(II)*THEP                                     LPG01490
      US=U(I)*(1.-THEN)+U(IJ)*THEN                                     LPG01500
```

```
      HS=H(I)*(1.-THEN)+H(IJ)*THEN                                      LPG01510
      GO TO 41                                                          LPG01520
40    DFXR=(X(I)-XR)/DX                                                 LPG01530
      UD=U(I)-U(II)                                                     LPG01540
      HD=H(I)-H(II)                                                     LPG01550
      UR=U(I)-UD*DFXR                                                   LPG01560
      HR=H(I)-HD*DFXR                                                   LPG01570
      DFXS=(X(I)-XS)/DX                                                 LPG01580
      US=U(I)-UD*DFXS                                                   LPG01590
      HS=H(I)-HD*DFXS                                                   LPG01600
41    UP=0.5*(UR+US)-0.5*(HS-HR)*SQHI/H(I)                              LPG01610
      HP=0.5*(HR+HS)+0.5*H(I)*(UR-US)/SQHI-B(I)*SV*DT                   LPG01620
      BP=E4                                                             LPG01630
      TI=T-TW(I)                                                        LPG01640
      IF(TI.GT.TAA)  BP=E1/(TI+T1)**0.5+E0                              LPG01650
C       SECOND-ORDER PROCESS                                            LPG01660
7     ZAIR=1./(HR**0.5*A1+UR)                                           LPG01670
      G3=HS**0.5*A1-US                                                  LPG01680
      ZAIS=-1./G3                                                       LPG01690
      PT=HP**0.5*A1                                                     LPG01700
      ZAIP=1./(PT+UP)                                                   LPG01710
      G4=PT-UP                                                          LPG01720
      ZAIN=-1./G4                                                       LPG01730
      XR=X(I)-2.*DT/(ZAIR+ZAIP)                                         LPG01740
      IF(XR.LT.X(II))  GO TO 27                                         LPG01750
      XS=X(I)-2.*DT/(ZAIS+ZAIN)                                         LPG01760
      IF(XS.GT.X(IJ))  GO TO 27                                         LPG01770
C       USE QUADRATIC INTERPOLATION TO CALCULATE UR,US,HR,HS            LPG01780
      DXR=(XR-X(I))/DX                                                  LPG01790
      DXS=(XS-X(I))/DX                                                  LPG01800
      DTW1=TW(IJ)-TW(II)                                                LPG01810
      DTW2=TW(IJ)+TW(II)-2.*TW(I)                                       LPG01820
      TWXR=TW(I)+0.5*DTW1*DXR+0.5*DTW2*DXR*DXR                          LPG01830
      TWXS=TW(I)+0.5*DTW1*DXS+0.5*DTW2*DXS*DXS                          LPG01840
      BOLXR=E4                                                          LPG01850
      BOLXS=E4                                                          LPG01860
      TW1=TO-TWXR                                                       LPG01870
      TW2=TO-TWXS                                                       LPG01880
```

```
      IF(TW1.GT.TAA)    BOLXR=E1/(TW1+T1)**0.5+E0                              LPG01890
      IF(TW2.GT.TAA)   BOLXS=E1/(TW2+T1)**0.5+E0                               LPG01900
      DU1=U(IJ)-U(II)                                                          LPG01910
      DH1=H(IJ)-H(II)                                                          LPG01920
      DU2=U(IJ)+U(II)-2.*U(I)                                                  LPG01930
      DH2=H(IJ)+H(II)-2.*H(I)                                                  LPG01940
      UR=U(I)+0.5*DU1*DXR+0.5*DU2*DXR*DXR                                      LPG01950
      HR=H(I)+0.5*DH1*DXR+0.5*DH2*DXR*DXR                                      LPG01960
      US=U(I)+0.5*DU1*DXS+0.5*DU2*DXS*DXS                                      LPG01970
      HS=H(I)+0.5*DH1*DXS+0.5*DH2*DXS*DXS                                      LPG01980
      IF(XS.LE.X(I))   BOLXS=B(I)                                              LPG01990
      RT=HR**0.5*A1                                                            LPG02000
      ST=HS**0.5*A1                                                            LPG02010
      ZR=RT/(RT+UR)                                                            LPG02020
      G5=ST-US                                                                 LPG02030
      ZS=ST/G5                                                                 LPG02040
      ZP=PT*ZAIP                                                               LPG02050
      ZN=PT*(-ZAIN)                                                            LPG02060
      PR=HP+HR                                                                 LPG02070
      SQPR=PT+RT                                                               LPG02080
      PS=HP+HS                                                                 LPG02090
      SQPS=PT+ST                                                               LPG02100
      PRS=PR*SQPS+PS*SQPR                                                      LPG02110
      ZZPR=SV*(BP*ZP+BOLXR*ZR)*(X(I)-XR)                                       LPG02120
      ZZPS=SV*(BP*ZN+BOLXS*ZS)*(X(I)-XS)                                       LPG02130
      UUP=(PR*SQPS*UR+PS*SQPR*US+SQPR*SQPS*(HR-HS)-ZZPR*SQPS-ZZPS              LPG02140
     1*SQPR)/PRS                                                               LPG02150
      HHP=(PR*PS*(UR-US)+SQPR*PS*HR+SQPS*PR*HS-ZZPR*PS+ZZPS*PR)                LPG02160
     1/PRS                                                                     LPG02170
      DUP=(UUP-UP)/UP                                                          LPG02180
      DHP=(HHP-HP)/HP                                                          LPG02190
      UP=UUP                                                                   LPG02200
      HP=HHP                                                                   LPG02210
      IF (DABS(DUP) .LE. 0.001)    GO TO 8                                     LPG02220
      GO TO 7                                                                  LPG02230
8     IF(DABS(DHP) .LE. 0.001)   GO TO 9                                       LPG02240
      GO TO 7                                                                  LPG02250
9     U(I)=UP                                                                  LPG02260
```

```
      H(I)=HP                                                          LPG02270
      B(I)=BP                                                          LPG02280
      IF(U(I).LT. 0.0)  GO TO 27                                       LPG02290
      IF( J .NE. KX)  GO TO 6                                          LPG02300
      WRITE(6,1001)   I,X(I),U(I), H(I),B(I)                           LPG02310
1001  FORMAT(2X,'I=',I4,5X,'X=',E10.4,9X,'U=',E10.4,9X,'H=',E10.4      LPG02320
     1,9X,'B=',E10.4)                                                  LPG02330
6     CONTINUE                                                         LPG02340
C       CALCULATE U AND H AT BOUNDARY POINT                            LPG02350
700   IF(HC .LE. YK)  GO TO 27                                         LPG02360
       XN=UC*DT+XC                                                     LPG02370
      CT=HC**0.5*A1                                                    LPG02380
      ZZC=CT+UC                                                        LPG02390
      XT=XN-DT*ZZC                                                     LPG02400
      IF(XT.LT.XB)  GO TO 27                                           LPG02410
C       USE LINEAR INTERPOLATION FOR THE FIRST ESTIMATION OF           LPG02420
C       UN AND HN                                                      LPG02430
      E=XC-XB                                                          LPG02440
      EF=(XC-XT)/E                                                     LPG02450
      DUC=UC-UB                                                        LPG02460
      DHC=HC-HB                                                        LPG02470
      UT=UC-DUC*EF                                                     LPG02480
      HT=HC-DHC*EF                                                     LPG02490
      ZC=CT/ZZC                                                        LPG02500
      BOIL=DT*BC*SV                                                    LPG02510
      ROOT2=HC+CC1*(HT+CT*UT/A2-BOIL)                                  LPG02520
      IF(ROOT2 .LT. 0.)  GO TO 101                                     LPG02530
      UN=CC2*(ROOT2**0.5*A1-CT)                                        LPG02540
      HN=UN*UN/(COE*A2)                                                LPG02550
       BN=E4                                                           LPG02560
C       SECONDER-ORDER PROCESS                                         LPG02570
10    XN=0.5*(UC+UN)*DT+XC                                             LPG02580
      ZAIT=1./(HT**0.5*A1+UT)                                          LPG02590
      SQN=HN**0.5*A1                                                   LPG02600
      ZAIN=1./(SQN+UN)                                                 LPG02610
      XT=XN-2.*DT/(ZAIT+ZAIN)                                          LPG02620
      IF(XT.LT.XB)  GO TO 27                                           LPG02630
      IF(N.EQ. 2)  GO TO 793                                           LPG02640
```

```
      DXT=XT-XB                                                          LPG02650
      EC=E/DX                                                            LPG02660
      EE=EC*(1.+EC)*DX                                                   LPG02670
      FTW=((EC*EC-1.)*TWB+TWC-EC*EC*TWA)/EE                              LPG02680
      FFTW=(EC*TWA+TWC-(1.+EC)*TWB)/(EE*DX)                              LPG02690
      FU=((EC*EC-1.)*UB+UC-EC*EC*UA)/EE                                  LPG02700
      FH=((EC*EC-1.)*HB+HC-EC*EC*HA)/EE                                  LPG02710
      FFU=(EC*UA+UC-(1.+EC)*UB)/(EE*DX)                                  LPG02720
      FFH=(EC*HA+HC-(1.+EC)*HB)/(EE*DX)                                  LPG02730
      UT=UB+FU*DXT+FFU*DXT*DXT                                           LPG02740
      HT=HB+FH*DXT+FFH*DXT*DXT                                           LPG02750
      TWXT=TWB+FTW*DXT+FFTW*DXT*DXT                                      LPG02760
      BOLXT=E4                                                           LPG02770
      TW3=TO-TWXT                                                        LPG02780
      IF(TW3.GT. TAA)   BOLXT=E1/(TW3+T1)**0.5+EO                        LPG02790
      GO TO 794                                                          LPG02800
793   DXT=(XC-XT)/E                                                      LPG02810
      UT=UC-DUC*DXT                                                      LPG02820
      HT=HC-DHC*DXT                                                      LPG02830
794   TN=HT+HN                                                           LPG02840
      SQT=HT**0.5*A1                                                     LPG02850
      SQTN=SQT+SQN                                                       LPG02860
      ZZT=SQT/(SQT+UT)                                                   LPG02870
      ZZN=SQN*ZAIN                                                       LPG02880
      BZZTN=SV*(BN*ZZN+BOLXT*ZZT)*(XN-XT)                                LPG02890
      RA2=1./A2                                                          LPG02900
      B24AC=TN*TN+CC1*SQTN*(TN*UT+SQTN*HT-BZZTN)*RA2                     LPG02910
      IF(B24AC .LT.0.0)  GO TO 11                                        LPG02920
      UUN=CC2*A2*(B24AC**0.5-TN)/SQTN                                    LPG02930
      HHN=UUN*UUN/(COE*A2)                                               LPG02940
      DUN=(UUN-UN)/UN                                                    LPG02950
      DHN=(HHN-HN)/HN                                                    LPG02960
      UN=UUN                                                             LPG02970
      HN=HHN                                                             LPG02980
      IF(DABS(DUN) .LE. 0.001)  GO TO 12                                 LPG02990
      GO TO 10                                                           LPG03000
12    IF(DABS(DHN) .LE. 0.001)  GO TO 13                                 LPG03010
      GO TO 10                                                           LPG03020
```

```
13      K=(XN-XB)/DX                                                    LPG03030
        DFXN=(XN-XB-K*DX)/DX                                            LPG03040
        IF(DFXN.LE.0.1)  GO TO 2001                                     LPG03050
        NK=N+K                                                          LPG03060
        GO TO 2002                                                      LPG03070
2001     NK=N+K-1                                                       LPG03080
2002    X(NK)=XN                                                        LPG03090
        U(NK)=UN                                                        LPG03100
        H(NK)=HN                                                        LPG03110
        B(NK)=BN                                                        LPG03120
        TW(NK)=TO                                                       LPG03130
        IF(J .NE. KX) GO TO 45                                          LPG03140
        WRITE(6,1001)  NK,X(NK),U(NK),H(NK),B(NK)                       LPG03150
45      IF(U(NK) .LE. 0.)  GO TO 27                                     LPG03160
        IF(N.EQ. 2)  GO TO 792                                          LPG03170
        GO TO 14                                                        LPG03180
101     WRITE(6,997)  ROOT2                                             LPG03190
997     FORMAT(2X,'ROOT2=',E14.8)                                       LPG03200
        GO TO 27                                                        LPG03210
11      WRITE(6,998)  B24AC                                             LPG03220
998     FORMAT(2X,'B24AC=',E14.8)                                       LPG03230
        GO TO 27                                                        LPG03240
14      CONTINUE                                                        LPG03250
C         POINT NEAR BOUNDARY ( U(N-1) AND H(N-1))                      LPG03260
        IF(HB .LE. XK)  GO TO 27                                        LPG03270
        SQB=HB**0.5*A1                                                  LPG03280
        ZAPB=SQB+UB                                                     LPG03290
        ZANB=SQB-UB                                                     LPG03300
        XRR=XB-DT*ZAPB                                                  LPG03310
        IF(XRR.LT.XA)  GO TO 27                                         LPG03320
        BOLXRR=BB                                                       LPG03330
        XSS=XB+DT*ZANB                                                  LPG03340
        DU3=UB-UA                                                       LPG03350
        DH3=HB-HA                                                       LPG03360
        BR=(XB-XRR)/DX                                                  LPG03370
        URR=UB-DU3*BR                                                   LPG03380
        HRR=HB-DH3*BR                                                   LPG03390
        IF(XSS .GT. XC)   GO TO 15                                      LPG03400
```

```
      IF(XSS .LT. XB)  GO TO 50                                          LPG03410
      SC=(XC-XSS)/E                                                      LPG03420
      USS=UC-DUC*SC                                                      LPG03430
      HSS=HC-DHC*SC                                                      LPG03440
      GO TO 51                                                           LPG03450
50    SC=(XB-XSS)/DX                                                     LPG03460
      USS=UB-DU3*SC                                                      LPG03470
      HSS=HB-DH3*SC                                                      LPG03480
51    UPP=0.5*(URR+USS)-0.5*(HSS-HRR)*SQB/HB                             LPG03490
      HPP=0.5*(HRR+HSS)+0.5*HB*(URR-USS)/SQB-BB*SV*DT                    LPG03500
      BPP=E4                                                             LPG03510
      TB=T-TWB                                                           LPG03520
      IF(TB.GT. TAA)  BPP=E1/(TB+T1)**0.5+E0                             LPG03530
C       SECONDER-ORDER PROCESS                                           LPG03540
16    SQP=HPP**0.5*A1                                                    LPG03550
      ZAPP=1./(SQP+UPP)                                                  LPG03560
      G8=SQP-UPP                                                         LPG03570
      ZAPN=-1./G8                                                        LPG03580
      ZAR=1./(HRR**0.5*A1+URR)                                           LPG03590
      G9=HSS**0.5*A1-USS                                                 LPG03600
      ZAS=-1./G9                                                         LPG03610
      XRR=XB-2.*DT/(ZAPP+ZAR)                                            LPG03620
      IF(XRR.LT. XA)  GO TO 27                                           LPG03630
      XSS=XB-2.*DT/(ZAPN+ZAS)                                            LPG03640
      IF(XSS.GT.XC)  GO TO 102                                           LPG03650
      DXRR=XRR-XB                                                        LPG03660
      TWXRR=TWB+FTW*DXRR+FFTW*DXRR*DXRR                                  LPG03670
      URR=UB+FU*DXRR+FFU*DXRR*DXRR                                       LPG03680
      HRR=HB+FH*DXRR+FFH*DXRR*DXRR                                       LPG03690
      DXSS=XSS-XB                                                        LPG03700
      TWXSS=TWB+FTW*DXSS+FFTW*DXSS*DXSS                                  LPG03710
      BOLXRR=E4                                                          LPG03720
      BOLXSS=E4                                                          LPG03730
      TW4=T0-TWXRR                                                       LPG03740
      TW5=T0-TWXSS                                                       LPG03750
      IF(TW4.GT.TAA)   BOLXRR=E1/(TW4+T1)**0.5+E0                        LPG03760
      IF(TW5.GT.TAA)  BOLXSS=E1/(TW5+T1)**0.5+E0                         LPG03770
      USS=UB+FU*DXSS+FFU*DXSS*DXSS                                       LPG03780
```

```
      HSS=HB+FH*DXSS+FFH*DXSS*DXSS                                          LPG03790
      SQR=HRR**0.5*A1                                                       LPG03800
      SQS=HSS**0.5*A1                                                       LPG03810
      ZZR=SQR/(SQR+URR)                                                     LPG03820
      G10=SQS-USS                                                           LPG03830
      ZZS=SQS/G10                                                           LPG03840
      ZZP=SQP*ZAPP                                                          LPG03850
      ZZN=SQP*(-ZAPN)                                                       LPG03860
      PRR=HPP+HRR                                                           LPG03870
      SQPRR=SQP+SQR                                                         LPG03880
      PSS=HPP+HSS                                                           LPG03890
      SQPSS=SQP+SQS                                                         LPG03900
      AV1=SV*(ZZP*BPP+ZZR*BOLXRR)*(XB-XRR)                                  LPG03910
      AV2=SV*(ZZN*BPP+ZZS*BOLXSS)*(XB-XSS)                                  LPG03920
      DPRS=PRR*SQPSS+PSS*SQPRR                                              LPG03930
      UPP1=(PRR*SQPSS*URR+PSS*SQPRR*USS+SQPRR*SQPSS*(HRR-HSS)-AV1           LPG03940
     1*SQPSS-AV2*SQPRR)/DPRS                                                LPG03950
      HPP1=(PRR*PSS*(URR-USS)+SQPRR*PSS*HRR+SQPSS*PRR*HSS-AV1*PSS           LPG03960
     1+AV2*PRR)/DPRS                                                        LPG03970
      DUPP=(UPP1-UPP)/UPP                                                   LPG03980
      DHPP=(HPP1-HPP)/HPP                                                   LPG03990
      UPP=UPP1                                                              LPG04000
      HPP=HPP1                                                              LPG04010
      IF(DABS(DUPP) .LE. 0.001)   GO TO 17                                  LPG04020
      GO TO 16                                                              LPG04030
17    IF(DABS(DHPP) .LE. 0.001)    GO TO 18                                 LPG04040
      GO TO 16                                                              LPG04050
18    U(N-1)=UPP                                                            LPG04060
      H(N-1)=HPP                                                            LPG04070
      X(N-1)=XB                                                             LPG04080
      B(N-1)=BPP                                                            LPG04090
      NN=N-1                                                                LPG04100
      IF(U(NN).LT. 0.0) GO TO 27                                            LPG04110
      IF(J .NE. KX)  GO TO 19                                               LPG04120
      WRITE(6,1001)   NN,X(NN),U(NN),H(NN),B(NN)                            LPG04130
      GO TO 19                                                              LPG04140
102   WRITE(6,996)  XSS                                                     LPG04150
996   FORMAT(2X,'XSS=',E14.8)                                               LPG04160
```

```
      GO TO 27                                                          LPG04170
C       PROCEDURE FOR ESTIMATIOM OF U(N-1) AND H(N-1) WITH XSS          LPG04180
C       GREATER THAN XC                                                 LPG04190
15    ZBB=-1./ZANB                                                      LPG04200
      TSS=(ZBB*(XB-XC+UC*TO)-T)/(ZBB*UC-1.)                             LPG04210
      DDT=TSS-TO                                                        LPG04220
      XSS=XC+UC*DDT                                                     LPG04230
      BOLXSS=E4                                                         LPG04240
      XSO=XSS-DDT*ZZC                                                   LPG04250
      IF(XSO.LT.XB)  GO TO 27                                           LPG04260
      DF=(XC-XSO)/E                                                     LPG04270
      USO=UC-DUC*DF                                                     LPG04280
      HSO=HC-DHC*DF                                                     LPG04290
      BZXSO=DDT*BC*SV                                                   LPG04300
      ROOT3=HC+CC1*(CT*USO*RA2+HSO-BZXSO)                               LPG04310
      IF(ROOT3 .LT. 0.)  GO TO 103                                      LPG04320
      USS=(ROOT3**0.5*A1-CT)*CC2                                        LPG04330
      HSS=USS*USS/(COE*A2)                                              LPG04340
      UPP=0.5*(URR+USS)+0.5*(HRR-HSS-DDT*SV*BB)*SQB/HB                  LPG04350
      HPP=0.5*HB*(URR-USS)/SQB+0.5*(HRR+HSS+(DDT-2.*DT)*SV*BB)          LPG04360
      BPP=E4                                                            LPG04370
      TB=T-TWB                                                          LPG04380
      IF(TB.GT.TAA)  BPP=E1/(TB+T1)**0.5+E0                             LPG04390
C       SECONDER-ORDER PROCESS                                          LPG04400
20    SQP=HPP**0.5*A1                                                   LPG04410
      ZAPP=1./(SQP+UPP)                                                 LPG04420
      G12=SQP-UPP                                                       LPG04430
      ZAPN=-1./G12                                                      LPG04440
619   ZAR=1./(HRR**0.5*A1+URR)                                          LPG04450
      G13=HSS**0.5*A1-USS                                               LPG04460
      ZAS=-1./G13                                                       LPG04470
      XRR=XB-2.*DT/(ZAPP+ZAR)                                           LPG04480
      IF(XRR.LT.XA)  GO TO 27                                           LPG04490
      DXRR=XRR-XB                                                       LPG04500
      TWXRR=TWB+FTW*DXRR+FFTW*DXRR*DXRR                                 LPG04510
      BOLXRR=E4                                                         LPG04520
      TW6=TO-TWXRR                                                      LPG04530
      IF(TW6.GT.TAA)    BOLXRR=E1/(TW6+T1)**0.5+E0                      LPG04540
```

```
URR=UB+FU*DXRR+FFU*DXRR*DXRR                                          LPG04550
HRR=HB+FH*DXRR+FFH*DXRR*DXRR                                          LPG04560
AVCS=0.5*(UC+USS)                                                     LPG04570
ZAV=0.5*(ZAPN+ZAS)                                                    LPG04580
TSS=(ZAV*(XB-XC+AVCS*TO)-T)/(ZAV*AVCS-1.)                             LPG04590
DDT=TSS-TO                                                            LPG04600
XSS=XC+AVCS*DDT                                                       LPG04610
IF(XSS .LE. XC)  GO TO 104                                            LPG04620
SQS=HSS**0.5*A1                                                       LPG04630
ZSS=1./(SQS+USS)                                                      LPG04640
ZSO=1./(HSO**0.5*A1+USO)                                              LPG04650
ZAVSO=0.5*(ZSS+ZSO)                                                   LPG04660
XSO=XSS-ZAVSO*DDT                                                     LPG04670
IF(XSO.LT.XB)  GO TO 27                                               LPG04680
DXSO=XSO-XB                                                           LPG04690
TWXSO=TWB+FTW*DXSO+FFTW*DXSO*DXSO                                     LPG04700
BOLXSO=E4                                                             LPG04710
TW7=TO-TWXSO                                                          LPG04720
IF(TW7.GT.TAA)    BOLXSO=E1/(TW7+T1)**0.5+E0                          LPG04730
USO=UB+FU*DXSO+FFU*DXSO*DXSO                                          LPG04740
HSO=HB+FH*DXSO+FFH*DXSO*DXSO                                          LPG04750
SO=HSS+HSO                                                            LPG04760
SQSO=HSO**0.5*A1                                                      LPG04770
SOT=SQS+SQSO                                                          LPG04780
ZZSS=SQS/(SQS+USS)                                                    LPG04790
ZZSO=SQSO/(SQSO+USO)                                                  LPG04800
BBZXSO=SV*(ZZSS*BOLXSS+ZZSO*BOLXSO)*(XSS-XSO)                         LPG04810
SSO2=SO*SO+CC1*SOT*(SO*USO+SOT*HSO-BBZXSO)*RA2                        LPG04820
IF(SSO2 .LT. 0.)  GO TO 105                                           LPG04830
USS=CC2*A2*(SSO2**0.5-SO)/SOT                                         LPG04840
HSS=USS*USS/(COE*A2)                                                  LPG04850
SQHRR=HRR**0.5*A1                                                     LPG04860
SQHSS=HSS**0.5*A1                                                     LPG04870
ZZR=SQHRR/(SQHRR+URR)                                                 LPG04880
G14=SQHSS-USS                                                         LPG04890
ZZS=SQHSS/G14                                                         LPG04900
ZPP=SQP*ZAPP                                                          LPG04910
ZPN=SQP*(-ZAPN)                                                       LPG04920
```

```
      PRR=HPP+HRR                                                        LPG04930
      SQPRR=SQP+SQHRR                                                    LPG04940
      PSS=HPP+HSS                                                        LPG04950
      SQPSS=SQP+SQHSS                                                    LPG04960
      AV1=SV*(ZPP*BPP+ZRR*BOLXRR)*(XB-XRR)                               LPG04970
      AV2=SV*(ZPN*BPP+ZSS*BOLXSS)*(XB-XSS)                               LPG04980
      DPRS=PRR*SQPSS+PSS*SQPRR                                           LPG04990
      UPP1=(PRR*SQPSS*URR+PSS*SQPRR*USS+SQPRR*SQPSS*(HRR-HSS)-AV1        LPG05000
     1*SQPSS-AV2*SQPRR)/DPRS                                             LPG05010
      HPP1=(PRR*PSS*(URR-USS)+SQPRR*PSS*HRR+SQPSS*PRR*HSS-AV1*PSS        LPG05020
     1+AV2*PRR)/DPRS                                                     LPG05030
      DUPP=(UPP1-UPP)/UPP                                                LPG05040
      DHPP=(HPP1-HPP)/HPP                                                LPG05050
      UPP=UPP1                                                           LPG05060
      HPP=HPP1                                                           LPG05070
      IF(DABS(DUPP) .LE. 0.001)  GO TO 21                                LPG05080
      GO TO 20                                                           LPG05090
21    IF(DABS(DHPP) .LE. 0.001)  GO TO 22                                LPG05100
      GO TO 20                                                           LPG05110
22    U(N-1)=UPP                                                         LPG05120
      H(N-1)=HPP                                                         LPG05130
      X(N-1)=XB                                                          LPG05140
      B(N-1)=BPP                                                         LPG05150
      NN=N-1                                                             LPG05160
      IF(U(NN).LT.0.0)  GO TO 27                                         LPG05170
      IF(  J.NE. KX)  GO TO 19                                           LPG05180
      WRITE(6,1001)   NN,X(NN),U(NN),H(NN),B(NN)                         LPG05190
      GO TO 19                                                           LPG05200
103   WRITE(6,995)  ROOT3                                                LPG05210
995   FORMAT(2X,'ROOT3=',E14.8)                                          LPG05220
      GO TO 27                                                           LPG05230
104   WRITE(6,994)  XC,XSS                                               LPG05240
994   FORMAT(2X,'XC=',E14.8,5X,'XSS=',E14.8)                             LPG05250
      GO TO 27                                                           LPG05260
105   WRITE(6,993) SSO2                                                  LPG05270
993   FORMAT(2X,'SSO2=',E14.8)                                           LPG05280
      GO TO 27                                                           LPG05290
19    CONTINUE                                                           LPG05300
```

```
C       POINTS BETWEEN XB AND X(NK)                                          LPG05310
792   NK1=NK-1                                                               LPG05320
      IF(NK .EQ. N)  GO TO 29                                                LPG05330
      DO 23 I=N,NK1                                                          LPG05340
      X(I)=XB+(I-N+1)*DX                                                     LPG05350
      TW(I)=TO-(TO-TWB)*(X(NK)-X(I))/(X(NK)-XB)                              LPG05360
      BNP=E4                                                                 LPG05370
      TWB=T-TW(I)                                                            LPG05380
      IF(TWB.GT.TAA)    BNP=E1/(TWB+T1)**0.5+E0                              LPG05390
      XTT=X(I)-DT*ZZC                                                        LPG05400
      IF(XTT.LT.XB)  GO TO 27                                                LPG05410
      DXTT=(XC-XTT)/E                                                        LPG05420
      UTT=UC-DUC*DXTT                                                        LPG05430
      HTT=HC-DHC*DXTT                                                        LPG05440
      G16=CT-UC                                                              LPG05450
      XTO=X(I)+DT*G16                                                        LPG05460
      IF(XTO .GT. XC)  GO TO 70                                              LPG05470
      TOC=(XC-XTO)/E                                                         LPG05480
      UTO=UC-DUC*TOC                                                         LPG05490
      HTO=HC-DHC*TOC                                                         LPG05500
      UNP=0.5*(UTT+UTO)+0.5*CT*(HTT-HTO)/HC                                  LPG05510
      HNP=0.5*HC*(UTT-UTO)/CT+0.5*(HTT+HTO)-DT*SV*BC                         LPG05520
C       SECONDER-ORDER PROCESS                                               LPG05530
69    SQNP=HNP**0.5*A1                                                       LPG05540
      ZNPP=1./(SQNP+UNP)                                                     LPG05550
      G40=SQNP-UNP                                                           LPG05560
      ZNPN=-1./G40                                                           LPG05570
      ZATT=1./(HTT**0.5*A1+UTT)                                              LPG05580
      G41=HTO**0.5*A1-UTO                                                    LPG05590
      ZATO=-1./G41                                                           LPG05600
      XTT=X(I)-2.*DT/(ZATT+ZNPP)                                             LPG05610
      IF(XTT.LT.XB)  GO TO 27                                                LPG05620
      XTO=X(I)-2.*DT/(ZATO+ZNPN)                                             LPG05630
      IF(XTO.GT. XC)   GO TO 27                                              LPG05640
      IF(N.EQ. 2)  GO TO 795                                                 LPG05650
      DXTT=XTT-XB                                                            LPG05660
      TWXTT=TWB+FTW*DXTT+FFTW*DXTT*DXTT                                      LPG05670
      UTT=UB+FU*DXTT+FFU*DXTT*DXTT                                           LPG05680
```

```
      HTT=HB+FH*DXTT+FFH*DXTT*DXTT                                          LPG05690
      DXTO=XTO-XB                                                           LPG05700
      TWXTO=TWB+FTW*DXTO+FFTW*DXTO*DXTO                                     LPG05710
      BOLXTT=E4                                                             LPG05720
      BOLXTO=E4                                                             LPG05730
      TW9=TO-TWXTT                                                          LPG05740
      TW10=TO-TWXTO                                                         LPG05750
      IF(TW9.GT.TAA)    BOLXTT=E1/(TW9+T1)**0.5+E0                          LPG05760
      IF(TW10.GT.TAA)   BOLTXO=E1/(TW10+T1)**0.5+E0                         LPG05770
      UTO=UB+FU*DXTO+FFU*DXTO*DXTO                                          LPG05780
      HTO=HB+FH*DXTO+FFH*DXTO*DXTO                                          LPG05790
      GO TO 796                                                             LPG05800
  795 DXTT=(XC-XTT)/E                                                       LPG05810
      DXTO=(XC-XTO)/E                                                       LPG05820
      UTT=UC-DUC*DXTT                                                       LPG05830
      HTT=HC-DHC*DXTT                                                       LPG05840
      HTO=HC-DHC*DXTO                                                       LPG05850
      UTO=UC-DUC*DXTO                                                       LPG05860
  796 SQTT=HTT**0.5*A1                                                      LPG05870
      SQTO=HTO**0.5*A1                                                      LPG05880
      ZZTT=SQTT/(SQTT+UTT)                                                  LPG05890
      G17=SQTO-UTO                                                          LPG05900
      ZZTO=SQTO/G17                                                         LPG05910
      Z1PN=SQNP*ZNPP                                                        LPG05920
      Z2PN=SQNP*(-ZNPN)                                                     LPG05930
      RNPTT=HNP+HTT                                                         LPG05940
      SQNPT=SQNP+SQTT                                                       LPG05950
      RNPTO=HNP+HTO                                                         LPG05960
      SQNPO=SQNP+SQTO                                                       LPG05970
      AV4=SV*(Z1PN*BNP+ZZTT*BOLXTT)*(X(I)-XTT)                              LPG05980
      AV5=SV*(Z2PN*BNP+ZZTO*BOLXTO)*(X(I)-XTO)                              LPG05990
      DPTO=RNPTT*SQNPO+RNPTO*SQNPT                                          LPG06000
      UNP1=(RNPTT*SQNPO*UTT+RNPTO*SQNPT*UTO+SQNPT*SQNPO*(HTT-HTO)           LPG06010
     1-AV4*SQNPO-AV5*SQNPT)/DPTO                                            LPG06020
      HNP1=(RNPTO*RNPTT*(UTT-UTO)+SQNPT*RNPTO*HTT+SQNPO*RNPTT*HTO-          LPG06030
     1AV4*RNPTO+AV5*RNPTT)/DPTO                                             LPG06040
      DUNP=(UNP1-UNP)/UNP                                                   LPG06050
      DHNP=(HNP1-HNP)/HNP                                                   LPG06060
```

```
      UNP=UNP1                                                          LPG06070
      HNP=HNP1                                                          LPG06080
      IF(DABS(DUNP) .LE. 0.001) GO TO 68                                LPG06090
      GO TO 69                                                          LPG06100
 68   IF(DABS(DHNP) .LE. 0.001)  GO TO 67                               LPG06110
      GO TO 69                                                          LPG06120
 67   U(I)=UNP                                                          LPG06130
      H(I)=HNP                                                          LPG06140
      B(I)=BNP                                                          LPG06150
      IF(U(I).LT. 0.0) GO TO 27                                         LPG06160
      IF(J.NE. KX)  GO TO 23                                            LPG06170
      WRITE(6,1001)  I,X(I),U(I),H(I),B(I)                              LPG06180
      GO TO 23                                                          LPG06190
 70   TTO=(X(I)-XC+UC*T0+T*G16)/CT                                      LPG06200
      DDTO=TTO-T0                                                       LPG06210
      XTO=XC+UC*DDTO                                                    LPG06220
      BOLXTO=E4                                                         LPG06230
      XTP=XTO-ZZC*DDTO                                                  LPG06240
      IF(XTP.LT.XB)  GO TO 27                                           LPG06250
      DFP=(XC-XTP)/E                                                    LPG06260
      UTP=UC-DUC*DFP                                                    LPG06270
      HTP=HC-DHC*DFP                                                    LPG06280
      BZXTO=BC*SV*DDTO                                                  LPG06290
      ROOT4=HC+CC1*(RA2*CT*UTP+HTP-BZXTO)                               LPG06300
      IF(ROOT4 .LT. 0.) GO TO 106                                       LPG06310
      UTO=(ROOT4**0.5*A1-CT)*CC2                                        LPG06320
      HTO=UTO*UTO/(COE*A2)                                              LPG06330
      UNP=0.5*(UTT+UTO)+0.5*(HTT-HTO-DDTO*SV*BC)*CT/HC                  LPG06340
      HNP=0.5*HC*(UTT-UTO)/CT+0.5*(HTT+HTO+(DDTO-2.*DT)*SV*BC)          LPG06350
 C    SECONDER-ORDER PROCESS                                            LPG06360
 24   ZTT=1./(HTT**0.5*A1+UTT)                                          LPG06370
      SQNP=HNP**0.5*A1                                                  LPG06380
      ZNPP=1./(SQNP+UNP)                                                LPG06390
      XTT=X(I)-2.*DT/(ZTT+ZNPP)                                         LPG06400
      IF(XTT.LT.XB)  GO TO 27                                           LPG06410
      IF(N.EQ.2)  GO TO 797                                             LPG06420
      DXTT=XTT-XB                                                       LPG06430
      TWXTT=TWB+FTW*DXTT+FFTW*DXTT*DXTT                                 LPG06440
```

```
      BOLXTT=E4                                                          LPG06450
      TW11=TO-TWXTT                                                      LPG06460
       IF(TW11.GT.TAA)  BOLXTT=E1/(TW11+T1)**0.5+EO                      LPG06470
      UTT=UB+FU*DXTT+FFU*DXTT*DXTT                                       LPG06480
      HTT=HB+FH*DXTT+FFH*DXTT*DXTT                                       LPG06490
      GO TO 798                                                          LPG06500
797   DXTT=(XC-XTT)/E                                                    LPG06510
      UTT=UC-DUC*DXTT                                                    LPG06520
      HTT=HC-DHC*DXTT                                                    LPG06530
798   G19=SQNP-UNP                                                       LPG06540
      ZNPN=-1./G19                                                       LPG06550
      G20=HTO**0.5*A1-UTO                                                LPG06560
      ZATO=-1./G20                                                       LPG06570
      AVTO=0.5*(UC+UTO)                                                  LPG06580
      AV3=0.5*(ZNPN+ZATO)                                                LPG06590
      TTO=(AV3*(X(I)-XC+AVTO*TO)-T)/(AV3*AVTO-1.)                        LPG06600
      DDTO=TTO-TO                                                        LPG06610
      XTO=XC+AVTO*DDTO                                                   LPG06620
      SQTO=HTO**0.5*A1                                                   LPG06630
      ZTO=1./(SQTO+UTO)                                                  LPG06640
      ZTP=1./(HTP**0.5*A1+UTP)                                           LPG06650
      ZAVPO=0.5*(ZTO+ZTP)                                                LPG06660
      XTP=XTO-ZAVPO*DDTO                                                 LPG06670
      IF(XTP.LT.XB) GO TO 27                                             LPG06680
       IF(N.EQ. 2)  GO TO 799                                            LPG06690
      DXTP=XTP-XB                                                        LPG06700
      TWXTP=TWB+FTW*DXTP+FFTW*DXTP*DXTP                                  LPG06710
      BOLXTP=E4                                                          LPG06720
      TW12=TO-TWXTP                                                      LPG06730
      IF(TW12.GT.TAA)  BOLXTP=E1/(TW12+T1)**0.5+EO                       LPG06740
      UTP=UB+FU*DXTP+FFU*DXTP*DXTP                                       LPG06750
      HTP=HB+FH*DXTP+FFH*DXTP*DXTP                                       LPG06760
      GO TO 780                                                          LPG06770
799   DXTP=(XC-XTP)/E                                                    LPG06780
      UTP=UC-DUC*DXTP                                                    LPG06790
       HTP=HC-DHC*DXTP                                                   LPG06800
780   TPTO=HTO+HTP                                                       LPG06810
      SQTP=HTP**0.5*A1                                                   LPG06820
```

```
      SQTPO=SQTP+SQTO                                                    LPG06830
      ZZTP=SQTP/(SQTP+UTP)                                               LPG06840
      ZZTO=SQTO/(SQTO+UTO)                                               LPG06850
      BZTPO=SV*(ZZTP*BOLXTP+ZZTO*BOLXTO)*(XTO-XTP)                       LPG06860
      TPO2=TPTO*TPTO+CC1*RA2*SQTPO*(TPTO*UTP+SQTPO*HTP-BZTPO)            LPG06870
      IF( TPO2 .LT. 0.)  GO TO 107                                       LPG06880
      UTO=CC2*A2*(TPO2**0.5-TPTO)/SQTPO                                  LPG06890
      HTO=UTO*UTO/(COE*A2)                                               LPG06900
      SQTT=HTT**0.5*A1                                                   LPG06910
      RTTO=HTO**0.5*A1                                                   LPG06920
      ZATT=SQTT/(SQTT+UTT)                                               LPG06930
      G21=RTTO-UTO                                                       LPG06940
      ZATO=RTTO/G21                                                      LPG06950
      Z1PN=SQNP*ZNPP                                                     LPG06960
      Z2PN=SQNP*(-ZNPN)                                                  LPG06970
      RNPTT=HNP+HTT                                                      LPG06980
      SQNPT=SQTT+SQNP                                                    LPG06990
      RNPTO=HTO+HNP                                                      LPG07000
      SQNPO=SQNP+RTTO                                                    LPG07010
      AV4=SV*(Z1PN*BNP+ZATT*BOLXTT)*(X(I)-XTT)                           LPG07020
      AV5=SV*(Z2PN*BNP+ZATO*BOLXTO)*(X(I)-XTO)                           LPG07030
      DNPTO=RNPTT*SQNPO+RNPTO*SQNPT                                      LPG07040
      UNP1=(RNPTT*SQNPO*UTT+RNPTO*SQNPT*UTO+SQNPT*SQNPO*(HTT-HTO)        LPG07050
     1-AV4*SQNPO-AV5*SQNPT)/DNPTO                                        LPG07060
      HNP1=(RNPTT*RNPTO*(UTT-UTO)+SQNPT*RNPTO*HTT+SQNPO*RNPTT*HTO-AV4    LPG07070
     1*RNPTO+AV5*RNPTT)/DNPTO                                            LPG07080
      DUNP=(UNP1-UNP)/UNP                                                LPG07090
      DHNP=(HNP1-HNP)/HNP                                                LPG07100
      UNP=UNP1                                                           LPG07110
      HNP=HNP1                                                           LPG07120
      IF(DABS(DUNP) .LE. 0.001)  GO TO 25                                LPG07130
      GO TO 24                                                           LPG07140
25    IF(DABS(DHNP) .LE. 0.001) GO TO 26                                 LPG07150
      GO TO 24                                                           LPG07160
26    U(I)=UNP                                                           LPG07170
      H(I)=HNP                                                           LPG07180
      B(I)=BNP                                                           LPG07190
      IF(U(I).LT. 0.0) GO TO 27                                          LPG07200
```

```
      IF(J.NE. KX) GO TO 23                                                    LPG07210
      WRITE(6,1001)  I,X(I),U(I),H(I),B(I)                                     LPG07220
      GO TO 23                                                                 LPG07230
106   WRITE(6,992)  ROOT4                                                      LPG07240
992   FORMAT(2X,'ROOT4=',E14.8)                                                LPG07250
      GO TO 27                                                                 LPG07260
107   WRITE(6,991)  TP02                                                       LPG07270
991   FORMAT(2X,'TP02=',E14.8)                                                 LPG07280
      GO TO 27                                                                 LPG07290
23    CONTINUE                                                                 LPG07300
29    T0=T                                                                     LPG07310
      V=0.                                                                     LPG07320
      IJK1=0                                                                   LPG07330
      DO 750 I=1,NK1                                                           LPG07340
      IF(H(I).LE. 0.01)  GO TO 751                                             LPG07350
      V=V+H(I)                                                                 LPG07360
      GO TO 750                                                                LPG07370
751   IJK1=I                                                                   LPG07380
750   CONTINUE                                                                 LPG07390
      IF(IJK1 .NE.0)  GO TO 752                                                LPG07400
      IJK=1                                                                    LPG07410
      GO TO 753                                                                LPG07420
752   IJK=IJK1                                                                 LPG07430
753   V=W*((V-0.5*(H(NK1)+H(IJK)))*DX+(H(NK1)+H(NK))*(X(NK)-X(NK1))*0.5)LPG07440
      N=NK                                                                     LPG07450
      J=J+1                                                                    LPG07460
      IF(J.NE. KX1) GO TO 3                                                    LPG07470
      IF(T0.GE. 0.1)  KX=500                                                   LPG07480
      IF(T0.GE.2.5)  KX=200                                                    LPG07490
      WRITE(6,849)  T,V                                                        LPG07500
849   FORMAT(2X,'T=',E11.5,5X,'VOLUME=',E11.5)                                 LPG07510
      KX1=KX+1                                                                 LPG07520
      J=1                                                                      LPG07530
      GO TO 3                                                                  LPG07540
27    STOP                                                                     LPG07550
      END                                                                      LPG07560
```

BIBLIOGRAPHY

Ackermann, H., L. Bewilogua, A.Jahn, R. Knöner, and H. Vinzelberg, "Heat Transfer in Nitrogen - Methane Mixtures Under Pressure with Film Boiling", Cryogenics, 16, 497 (1976).

Benjamin, T.B., "Gravity Currents and Related Phenomena", J. Fluid Mech., 31, 209 (1968).

Berenson, P.J., "Experiments on Pool-Boiling Heat Transfer", Int. J. Heat Mass Trans., 5, 985 (1962).

Bewilogua, L., R. Knöner and H. Vinzelberg, "Heat Transfer in Cryogenic Liquids Under Pressure", Cryogenics, 15, 121 (1975).

Bird, R.B., W.E. Stewart and E.N. Lightfoot, Transport Phenomena, Wiley, New York (1960).

Boyle, G.I. and A. Kneebone, "Laboratory Investigations into the Characteristics of LNG Spills on Water. Evaporation, Spreading, and Vapor Dispersion", API Report 6732, Shell Research Ltd., Thornton Research Center, Chester, England (1973).

Brown, L.E., "Pool Boiling Heat Transfer to Liquefied Natural Gas and Liquefied Petroleum Gas", M.S. Thesis, University of Oklahoma, Norman, Oklahoma (1967).

Burgess, D.S., J.N. Murphy and M.G. Zabetakis, "Hazards Associated with the Spillage of LNG on Water", Bureau of Mines Report on Investigations RI-7448, U.S. Dept. of Interior (1970).

Burgess, D.S., J. Biordi and J.N. Murphy, "Hazards of Spillage of LNG into Water", MIPR No. Z-70099-9-12395, Bureau of Mines, U.S. Dept. of Interior (1972).

Carslaw, H.S. and J.C. Jaeger, Conduction of Heat in Solids, Clarendon Press, Oxford (1959).

Corty, C. and A.S. Foust "Surface Variables in Nucleate Boiling", Chem. Eng. Prog. Symp. Ser., 17 (51), 1 (1955).

Davies, R.M. and G.I. Taylor, "The Mechanics of Large Bubbles Rising through Extended Liquids and Through Liquids in Tubes", Proc. Roy. Soc. (London), A200, 375 (1950).

Davenport, W.G., F.D. Richardson and A.V. Bradshaw "Spherical Cap Bubbles in Low Density Liquids", Chem. Eng. Sci., 22, 1221 (1967).

Dincer, A.K., E.M. Drake and R.C. Reid, "Boiling of Liquid Nitrogen and Methane on Water. The Effect of Initial water Temerpature", Int. J. Heat Mass Trans., 20, 197 (1977).

Drake, E.M., A.A. Jeje and R.C. Reid, "Transient Boiling of Cryogens on a Water Surface. I. Nitrogen, Methane, and Ethane. II. Light Hydrocarbon Mixtures", Int. J. Heat Mass Trans., 18, 1361 (1975).

Eckert, E.R. G. and R.M. Drake, Analysis of Heat and Mass Transfer, McGraw-Hill, New York (1975).

Fannelop, T.K. and G.D. Waldman, "Dynamics of Oil Slicks", A.I.A.A.J., 10 (4), 506 (1972).

Fay, J.A., "The Spread of Oil Slicks on a Calm Sea", Oil on the Sea (ed. by Hoult), pp. 53-64, Plenum, New York (1969).

Fay, J.A., "Physical Processes in the Spread of Oil on a Water Surface", Conference on Prevention and Control of Oil Spills, American Petroleum Institute, Washington, D.C. (1971).

Fay, J.A. "Unusual Fire Hazard of LNG Tanker Spills", Combustion Sci. and Tech., 7, 47 (1973).

Georgakis, C., J. Congalidis and G.C. Williams, "Model for Non-Instantaneous LNG and Gasoline Spills", Fuel, 58, 113 (1979).

Haberman, W.L. and R.K. Morton, "David Taylor Model Basin" Report No. 802, U.S. Dept. of Naval Research (1953).

Hoult, D.P., "Oil Spreading on the Sea", Annual Review of Fluid Mechanics, 4, 341 (1972a).

Hoult, D.P., "The Fire Hazard of LNG Spilled on Water", Proc. Conference on LNG Improtation and Safety, Boston, Massachusetts, 87 (1972b).

Kosky, P.G. and D.N. Lyon, "Pool Boling Heat Transfer to Cryogenic Liquids", A.I.CH.E.J., 14, 372 (1968).

Levenspiel, O., Chemical Reaction Engineering, John Wiley & Sons, Inc., New York (1972).

May, W.G. and P. Perumal, "The Spreading and Evaporation of LNG on Water", Process Ind. Div. Annual ASME Meeting, November (1974).

Merte, H., and J.A. Clark, "Boiling Heat Transfer with Cryogenic Fluids at Standard, Fractured, and Near-Zero Gravity", Trans. ASME, C-96, 351 (1964).

Muscari, C.C., "The Evolution of Liquid Natural Gas on Water," M.S. Thesis, Massachusetts Institute of Technology, Cambridge, Massachusetts (1974).

Opschoor, G. "Investigations Into the Spreading and Evaporation of LNG Spilled on Water", Cryogenics, 17, 629 (1977).

Otterman, B., "Analysis of Large LNG Spills on Water -- Part I: Liquid Spread and Evaporation", Cryogenics, 15, 455 (1975).

Park, E.L., C.P. Colver and C.M. Sliepcevich, "Nucleate and Film Boiling Heat Transfer to Nitrogen and Methane at Elevated Pressures and Large Temperature Differences", Advances in Cryogenic Eng., Vol. 11, pp. 516, Plenum Press, New York (1966).

Perry, R.H. and C.H. Chilton, Chemical Engineers' Handbook, McGraw-Hill, New York (1973).

Porteous, W.M. and R.C. Reid, "Light Hydrocarbon Vapor Explosions", Chem. Eng. Prog., pp. 83, May (1976).

Raj, P., "Simultaneous Boiling and Spreading of LNG on Water", Proposal to GRI, Dept. of Chem. Eng., Massachusetts Institue of Technology (1978).

Raj, P. and A. Kalelkar, "Fire Hazard Presented by a Spreading Burning Pool of Liquefied Natural Gas on Water", Presented at Combustion Institute (USA) Western Section Meeting (1973).

Reid, R.C., J.M. Prausnitz and T.K. Sherwood, The Properties of Gases and Liquids, McGraw-Hill, New York (1977).

Reid, R.C. and K.A. Smith, "Behavior of LPG on Water", Hydrocarbon Processing, pp. 117, April (1978).

Reid, R.C. and R. Wang, "The Boiling Rates of LNG on Typical Dike Floor Materials", Cryogenics, pp. 408, July (1978).

Rohsenow, W.M. and H.V. Choi, Heat, Mass and Momentum Transfer, Prentice-Hall, Inc., New Jersey (1961).

Sciance, C.T., C.P. Colver and C.M. Sliepcevich, "Pool Boiling of Methane Between Atmospheric Pressure and the Critical Pressure", Advances in Cryogenic Eng., Vol. 12, pp. 395, Plenum Press, New York (1967a).

Sciance, C.T., C.P. Colver and C.M. Sliepcevich, "Nucleate Pool Boiling and Burnout of Liquefied Hydrocarbon Gases", Chem. Eng. Prog. Sym. Ser., 63, 109 (1967b).

Shapiro, A.H., The Dynamics and Thermodynamics of Compressible Fluid Flow, Vol.1, Ronald Press, New York (1953).

Sliepcevich, C.M., H.T. Hashemi and C.P. Colver, "Heat Transfer Problems in LNG Technology", Chem. Eng. Prog. Sym. Ser., 64, 120 (1968).

Suchon, W., "An Experimental Investigation of Oil Spreading Over Water", M.S. Thesis, Massachusetts Institute of Technology Cambridge, Massachusetts (1970).

Szekely, J. and N.J. Themelis, Rate Phenomena in Process Metallurgy, John Wiley & Sons, Inc., New York (1971).

Thompson, P.A., Compressible - Fluid Dynamics, McGraw-Hill, New York (1972).

Valencia, J.A., "The Effect of Composition on the Boiling Rates of Liquefied Natural Gas for Confined Spills on Water", Sc.D. Thesis, Massachusetts Institute of Technology, Cambridge, Massachusetts, (1978).

Valencia, J.A. and R.C. Reid, "The Effect of Composition on the Boiling Rates of Liquefied Natural Gas for Confined Spills on Water", Int. J. Heat Mass Trans., 22, 831 (1979).

Van Krevelen, D.W. and P.J. Hoftijzer, "Studies of Gas - Bubble Formation. Calculation of Interfacial Area in Bubble Contactors", Chem. Eng. Prog., 46, 29 (1950).

Von Karman, T., "The Engineer Grapples with Nonlinear Problems", Bull. Am. Math. Soc., 46,615 (1940)

Wilke, C.R., "A Viscosity Equation for Gas Mixtures", J. Chem. Phys., 18, 517 (1950).

Wright, R.D. and C.P. Colver, "Saturated Pool Boiling Burnout of Ethane, Ethylene Mictures", Chem. Eng. Prog. Sym. Ser., 65, 204 (1965).